Analysis and prediction of rainfall-induced shallow landslides along the road corridors in northern New South Wales, Australia

Sinnappoo Ravindran
BScEng, MEngSc, CPEng

Griffith School of Engineering and Built Environment
Gold Coast Campus, Griffith University

Submitted in fulfilment of the requirements of the degree of
Doctor of Philosophy

November 2020

Abstract

Globally, landslides have occurred regularly and caused massive destruction with numerous loss of life. Although they may result from earthquakes, geological factors and human activities, landslides are mostly caused by heavy or prolonged rainfall. Furthermore, research indicates that rainfall-induced landslides are primarily responsible for landslides that occur on mountainous terrains. Some of the worst rainfall-induced landslides across the world which caused loss of life and destruction of property and infrastructure, occurred in Nepal in 1926, 1988 and 2009; in Thailand in 2008; in India in 2009 and in Japan in 2012. Thredbo landslide occurred in southern region of New South Wales (NSW), Australia in 1997, killed 18 people, destroyed two lodges and moved over 1000 tonnes of liquefied earth and debris over slope. The cause of this landslide was heavy rainfall, melting snow and leaking water pipeline.

In northern NSW, many roads were closed for weeks and months due to rainfall-induced landslides from 2009 till 2019. Waterfall Way leading to Dorrigo Mountain from Raleigh was closed in 2009 (3 times), 2011, 2013, 2015, 2017 & 2019 and the road users have to travel more than three hours on alternative routes to reach the other side of the Dorrigo Mountain. Gwydir Highway at Gibraltar Range was closed in 2011 and 2013; Oxley Highway at Mt Seaview was closed in 2011 and 2013. Summerland Way at Mt Lindesay was closed in 2011 and 2017 and Bruxner Highway at Mallanganee Range was closed in 2011, 2013 and 2015. Road closures make inconvenience to the road users impacting access, work travel, school travel, medical travel and long-distance travel and there are economic consequences as well.

There were over 100 landslides occurred along the state road corridors in northern region of NSW, Australia, since 2009 till 2019. Rainfall events triggered about 80% of landslides in northern NSW. Rainfall-induced landslides occur in this region in every two years according to historical records from 2009. Mountain passes such as Mt Seaview, Dorrigo Mountain, Gibraltar Range, Ramornie – Cangai Bluff, Mallanganee Range and Mt Lindesay are adversely affected by rainfall-induced landslides.

Therefore, there are economic and social needs to address root causes of rainfall-induced landslides along the road corridors. Despite the common occurrences of rainfall-induced landslides in the Australian region of northern New South Wales (NSW), there has been no

study conducted on this phenomenon for this region. This thesis conducts a comprehensive analysis of shallow landslide events that occurred along the road corridors in northern New South Wales (NSW) throughout the period of 2009 - 2019.

Furthermore, this thesis employs the analysis to prognosticate future patterns of rainfall-induced shallow landslides for this region. The scope of this thesis includes analysis of rainfall-induced shallow landslides occurred in coarse-grained soils, prediction of shear strength of coarse-grained soils using soil suction and prediction of rainfall-induced shallow landslides using different approaches such as rainfall threshold, rainfall index and limit equilibrium method in northern NSW. It involves developing a relationship among rainfall characteristics, soil characteristics and slope characteristics.

The study found out that when moisture content of soil is increased, there is a reduction in matric suction and thereby a decrease in shear strength. It also revealed that slopes consist of coarse-grained soils are vulnerable to rainfall-induced landslides. The slopes consist of sedimentary rocks and igneous rocks at mountain passes are vulnerable to landslides. The slopes are susceptible to rainfall-induced shallow landsides when the slope angle is greater than 25 degrees.

The key benefit of this thesis is that government, road authorities and industry can use the simple tools that can predict rainfall-induced shallow landslides in northern NSW. These simple tools include rainfall threshold, rainfall index and the SLIP model that are specifically developed for northern NSW. The findings are also useful for management of road corridor and slopes in the mountain passes.

This study presents the major factors that lead to shallow rainfall-induced landslides in northern NSW and proposes simple tools that can be used to predict this natural disaster. It is believed that these findings will be useful for the relevant industry including decision-makers who manage the slope assets and landslide hazard along the road corridors in northern NSW, Australia. These findings are also applicable to other parts of the world.

Statement of Originality

This work has not previously been submitted for a degree or diploma in any university. To the best of my knowledge and belief, the thesis contains no material previously published or written by another person except where due reference is made in the thesis itself.

(Signed)_  _

Sinnappoo Ravindran

Contents

Abstract ii

Statement of Originality iv

Contents v

List of Figures x

List of Tables xii

List of Abbreviations xiii

List of Symbols xv

Acknowledgements xviii

Acknowledgement of research papers included in this thesis xix

Chapter 1: Introduction 20

1.1 Landslides in the northern region of NSW 21

1.2 Prediction of rainfall-induced shallow landslides 24

1.3 Research gap 25

1.4 Objectives of this research 25

1.5 Scope of thesis 26

1.6 Layout of thesis 26

Chapter 2: Literature review and research significance 29

2.1 Landslides in general 29

2.1.1 Common causes of landslides 29

2.1.2 Types of rainfall-induced landslides 31

2.1.3 Geological characteristics of rainfall-induced landslides 32

2.2 Rainfall characteristics 33

2.3 Mechanisms of shallow landslides and factors affecting them 43

2.3.1 Types of slopes and materials 44

2.3.2 Infiltration process, matric suction and shear strength 45

2.3.3 Unsaturated soils 47

2.3.4 Soil water characteristics curve 48

2.3.5 Hydraulic conductivity 53

2.3.6 Shear strength characteristics of unsaturated soils 53

2.3.7 Shear strength equations of unsaturated soils 56
2.3.7.1 Apparent cohesion and friction angle of unsaturated soils 58
2.3.7.2 Friction angle due to matric suction 59
2.3.7.3 Apparent friction angle 61
2.4 Prediction of shear strength and shallow landslides 64
2.4.1 Analysis of rainfall-induced landslides 66
2.4.1.1 Soil characteristics 68
2.4.1.2 Slope characteristics 69
2.4.1.3 Findings from previous studies on rainfall-induced slope failures 70
2.4.1.4 Stability analysis 71
2.4.2 Prediction of rainfall-induced shallow landslides 73
2.4.2.1 Key variables in the prediction models 73
2.4.2.2 Types of models 74
2.4.2.3 Physical models 75
2.4.3 Risk reduction of rainfall-induced landslides 79
2.4.4 Summary of literature review 79
2.4.5 Gaps in the previous research 82
Chapter 3: Methodology, Materials and Testing Methods 85
3.1 Testing plan 85
3.2 Direct shear test 86
3.3 Suction tests using filter paper 87
3.4 Consolidated undrained triaxial tests 88
3.5 Hydraulic conductivity test 90
3.6 Summary of properties of soils from landslide sites 90
Chapter 4: Analysis of rainfall-induced landslides in northern New South Wales, Australia 95
4.1 Abstract 95
4.2 Introduction 95
4.3. Characteristics of shallow landslides in the studied area 97
4.3.1 Geological context 100
4.3.2 Slope characteristics 102
4.4 Rainfall characteristics 103
4.4.1 Rainfall threshold 104
4.4.2 Rainfall index 106

4.5 Soil characteristics 109
4.5.1 Direct shear test 110
4.5.2 Shear strength of soil from landslide sites 111
4.6 Conclusions 113
4.7 Acknowledgements 114
Chapter 5: Estimation of shear strength of gravelly and sandy soils from shallow landslides 116
5.1 Abstract 116
5.2 Introduction 116
5.3 Theoretical considerations 118
5.3.1 Soil-Water Characteristic Curves 118
5.3.2 Shear Strength of Unsaturated Soils 118
5.3.2.1 Khalili and Khabbaz's (1998) method 119
5.3.2.2 Naghadeh and Toker (2019) method 119
5.3.2.3 A new model to estimate the shear strength of unsaturated 120
5.4 Experimental Program 121
5.4.1 Direct Shear Tests 122
5.4.2 Suction Test using Filter Paper Technique 122
5.5 Results of Laboratory Tests 123
5.5.1 Shear Strength of Unsaturated Soils 123
5.5.2 SWCC of Tested Soils 126
5.6 Estimation of Shear Strength 128
5.7 Conclusion 131
5.8 Acknowledgements 132
5.9 References 132
Chapter 6: Prediction of shallow rainfall-induced landslides using shear strength of unsaturated soil 136
6.1 Abstract 136
6.2 Introduction 136
6.3 Theoretical background 138
6.3.1 SLIP model to estimate the stability of unsaturated soil mass 138
6.3.2 New procedure to estimate the parameter A 140
6.4 Experimental program 142
6.4.1 Direct shear tests 144

6.4.2 Undrained triaxial tests 144
6.4.3 Hydraulic conductivity test 145
6.5 Results and discussion 145
6.6 Numerical analysis 150
6.7 Conclusions 156
6.8 Acknowledgements 156
6.9 Declarations 156
6.10 Appendix 6A 157
6.11 Appendix 6B 158
Chapter 7: Concluding remarks 160
7.1 Concluding remarks 160
7.2 Future works 162
Appendix A: Conference Paper published at UNSAT 2018, Hong Kong - Prediction of shear strength of unsaturated soils in landslide-prone areas using direct shear and suction tests under low normal stress condition 164
A.1 Abstract 164
A.2 Introduction 164
A.3 Materials and methods 166
A.3.1 Test setup and arrangement of instruments 166
A.3.1.1 Direct shear test 166
A.3.1.2 Suction test using filter paper technique 167
A.3.2 Soil type and index properties 168
A.4 Test results and analysis 169
A.5 Prediction of shear strength 171
A.5.1 SWCC equation 171
A.5.2 Shear strength equation 173
A.6 Conclusions 177
Appendix B: Inventory of landslides in northern region 178
Appendix C: Rainfall characteristics of rainfall-induced landslides in northern NSW 183
Appendix D: Slope characteristics of rainfall-induced landslides in northern NSW 188
Appendix E: Test results 192

E.1 Direct shear test results 192
E.2 Suction test results 196
E.3 Consolidated undrained (CU) triaxial test results 198
E.4 Hydraulic conductivity test results 200
References 201

List of Figures

Figure 1.1: Study area in northern region of NSW, Australia (Source: Office of Environment & Heritage) 22

Figure 1.2: Gibraltar Range landslides occurred in January 2011 by natural disaster rainfall event 23

Figure 1.3: Glen Road landslide occurred in January 2011 by natural disaster rainfall event 23

Figure 2.1: Worldwide landslide triggering threshold (mm/h) (Source: Caine 1980) 36

Figure 2.2: Rainfall intensity – duration thresholds (legend or numbers are shown in Table 2. 1) (Source: Guzzetti et al. 2007) 37

Figure 2.3: Typical SWCC showing main zones (source: Fredlund et al. 2012) 49

Figure 2.4a: Shear strength variation with matric suction at different net normal stress for specimens at dry of optimum moisture conditions (Source: Vanapalli et al. 1996) 54

Figure 2.4b: Shear strength variation with matric suction at different net normal stress for specimens at wet of optimum moisture conditions (Source: Vanapalli et al. 1996) 55

Figure 2.4c: Relationship of shear stress with matric suction under low applied matric suctions (Source: after Donald 1956; Fredlund, Rahardjo & Fredlund 2012) 55

Figure 2.5: Demonstration of two-layer structure of landslide mass (Source: Wang & Sassa 2000) 62

Figure 2.6: Change model of apparent friction coefficient, $tan\emptyset_a$ (Source: Wang & Sassa 2000) 63

Figure 2.7: Failure mechanism of rainfall-induced landslide (Source: Rahardjo et al. 2007) 67

Figure 3.1: Direct shear test equipment 87

Figure 3.2: Membrane stretcher used to prepare specimen for triaxial test 89

Figure 3.3: Specimen prepared for triaxial test 89

Figure 3.4: Specimen after shearing on the triaxial chamber 90

Figure 4.1: Mountain passes in northern NSW 97

Figure 4.2: Typical landslides in northern NSW 98

Figure 4.3: Schematic cross-sections of landslides from Figure 4.2 98

Figure 4.4: Timeline of landslides in the studied area 99

Figure 4.5: Mt Lindesay & Mallanganee Range 100

Figure 4.6: Ramornie – Cangai Bluff & Gibraltar Range 101

Figure 4.7: Dorrigo Mountain 101

Figure 4.8: Mt Seaview 102

Figure 4.9: Slope angles of rainfall-induced landslides (2009 – 2017) in northern NSW 103

Figure 4.10: Rainfall data preceding landslide occurrence 104

Figure 4.11: Landslide-triggering rainfall threshold for northern NSW 105

Figure 4.12: Modified rainfall index (R') concept (Source: Nakai et al. 2006) 106

Figure 4.13: Rainfall index obtained for Mt Lindesay 107

Figure 4.14: Rainfall index obtained for Dorrigo Mountain 108

Figure 4.15: Typical shear stress-displacement behaviour observed for Soil 7 at 10%, 20% & 30% moisture content 112

Figure 4.16: Shear strength against moisture content for all tested soils 112

Figure 4.17: Shear strength reduction due to changes in moisture content 113

Figure 5.1: Shear stress vs. shear displacement at different normal stresses and moisture content (mc, in %) 124

Figure 5.2: Test results from shear box test plotted as the apparent cohesion vs. volumetric moisture content 124

Figure 5.3: Test results from shear box tests plotted as the friction angle vs. volumetric moisture content 125

Figure 5.4: Volumetric moisture content vs. matric suction (measured SWCC) 126

Figure 5.5: Comparison of the best fit SWCC models with the measured lab data – Soil 1 127

Figure 5.6: Comparison of the best fit SWCC models with the measured lab data – Soil 2 128

Figure 5.7: Comparison of the best fit SWCC models with the measured lab data – Soil 6 128

Figure 5.8: Comparison of predicted shear strength with measured shear strength of Soil 1 129

Figure 5.9: Comparison of predicted shear strength with measured shear strength of Soil 2 129

Figure 5.10: Comparison of predicted shear strength with measured shear strength of Soil 3 130

Figure 5.11: Comparison of predicted shear strength with measured shear strength of Soil 4 130

Figure 5.12: Comparison of predicted shear strength with measured shear strength of Soil 5 130

Figure 5.13: Comparison of predicted shear strength with measured shear strength of Soil 6 131

Figure 6.1: Forces acting on soil mass in an infinite slope (after Montrasio and Valentino, 2016) 138

Figure 6.2: Cross-sections of the studied landslides 143

Figure 6.3: Results of shear box tests on soils from landslide sites (1 - 3) at different water content (given in %) 146

Figure 6.4: Results of undrained triaxial tests on three soils from landslide sites (1 - 3) 148-149

Figure 6.5: Difference between the unsaturated and saturated shear strength and the variation of apparent cohesion against the degree of saturation 149-150

Figure 6.6: Estimation of the Factor of Safety (*FS*) during rainfall events at Site 1 151-152

Figure 6.7: Estimation of the Factor of Safety (*FS*) during rainfall events at Site 2 152-153

Figure 6.8: Estimation of the Factor of Safety (*FS*) during rainfall events at Site 3 154

List of Tables

Table 2.1: Intensity – duration thresholds for the initiation of landslides of the curves shown in Figure 2.2 (Source: Guzzetti et al. 2007) 38-43

Table 2.2: Shear strength equations for unsaturated soils 60-61

Table 2.3: Description of shear behaviour types in the sliding zone and suggested values for B_{ss} (Source: Wang & Sassa 2000) 62-63

Table 2.4: Some examples of physical models 75-76

Table 3.1: Testing program 86

Table 3.2: Summary of properties of soils from landslide sites 91-93

Table 4.1: Geometry of landslide sites from Figure 4.2 99

Table 4.2: Rainfall-induced landslides (2009 – 2017) by rock type 102

Table 4.3: Characteristics of rainfall-induced landslides sites at mountain passes 103-104

Table 4.4: Calculation of rainfall index for Mt Lindesay and Dorrigo Mountain 108

Table 4.5: Highest historical rainfall data for Mt Lindesay and Dorrigo Mountain 108

Table 4.6: Grading of soil samples from landslides 109-110

Table 4.7: Landslide sites vs. soil samples taken and used in the direct shear tests 111

Table 5.1: Particle size distribution and classification of tested soils 121-122

Table 5.2: Model parameters used to estimate used to estimate shear strength 127

Table 6.1: Properties of soil samples collected from landslide sites 144

Table 6.2: Results of shear box and triaxial tests 147

Table 6.3: Input data and numerical analysis outcome 151

List of Abbreviations

AEV	Air-Entry Value
AS	Standards Australia
ASTM	American Society for Testing and Materials
BOM	Bureau of Metrology
COV	Coefficient of Variation
CU	Consolidated Undrained
dSLAM	Distributed, physically based stability model
Eq.	Equation
Fig.	Figure
FS	Factor of Safety
GDS	Global Digital Systems Ltd
GP	Poorly-graded Gravel
GW	Well-graded Gravel
HCF	Hydraulic Conductivity Function or K function
HIRESSS	High Resolution Slope Stability Simulator
ICL	International Consortium on Landslides
ID	Identification Number
IQS	Initial quasi-saturated volumetric water content
LL	Liquid Limit
NDVI	Normalised Difference Vegetation Index
NSW	New South Wales
mc	Moisture Content
OCR	Over-consolidated Ratio
PDF	Probability Density Function
PG_TRIGRS	Probabilistic physically-based model
PI	Plasticity Index
PL	Plastic Limit
PoF	Probability of Failure
SHALSTAB	SHAllow Landsliding STABility model
SHE-TRAN	Systeme Hydrologique European with water flow, sediment & solute transport modules
SHIA_Landslide	SHIA (open hydrological simulation in Spanish)

SINMAP	Stability Index Mapping
SINTOP	Shallow landslide prediction based on Infinite slope Model and TOPMODEL
SLIDE	Slope-Infiltration-Distributed Equilibrium
SLIP	Shallow Landslide Instability Prediction Model
SP	Poorly-graded Sand
SSCC	Suction Stress Characteristic Curve
SSNR	Squared Sum of Normalised Residuals
SW	Well-graded Sand
SWCC	Soil-Water Characteristics Curve
SWRC	Soil-Water Retention Curve
TOPMODEL	a TOPography based hydrological MODEL
TRIGRS	Transient Rainfall Infiltration and Grid-based Regional Slope Stability Model
USCS	Unified Soil Classification System
USPF	Unsaturated Soil Property Function

List of Symbols

A: model parameter in Eqs. (12) & (38) (dimensionless)

a: model parameter in SWCC Eqs. (1), (24), (25) & (A1) (dimensionless)

B_{ss}: Accumulation possibility of excess pore pressure (dimensionless)

C: maximum cohesion or ultimate cohesion in Eqs. (13) & (A5) (kPa)

C: cohesion in Eqs. (37a) & (37b) (kPa)

C(ψ): correction factor in Eqs. (2) & (A2) (dimensionless)

C': representing Eq. (42)

C_c: coefficient of curvature (dimensionless)

C_u: coefficient of uniformity in Eq. (A7) (dimensionless)

C_ψ: apparent cohesion (kPa)

C^*_ψ: ancillary parameter in Eqs. (38) & (39) (kPa)

c: cohesion in Eq. (34) (kPa)

c': effective cohesion (kPa)

c": capillary cohesion in Eq. (32) (kPa)

c_a: apparent cohesion in Eq. (32) (kPa)

c_o: cohesion at zero moisture content in Eq. (34) (kPa)

$c"_{max}$: maximum capillary cohesion in Eq. (31) (kPa)

D: duration in Eq. (21) (hr)

D_{50}: 50% particle are finer than this size (mm)

D_{60}: 60% particle are finer than this size (m)

H: Thickness of soil layer in Eq. (36) (m)

h: rainfall amount as a function of time (mm) in Eq. (36)

h: thickness of sliding mass in Eq. (15) (m)

I: rainfall intensity in Eq. (21) (mm/hr)

I_{max}: peak daily rainfall intensity (mm/d)

I_{mean}: mean daily rainfall intensity (mm/d)

K: model parameter in Eqs. (16), (17) & (A4) (dimensionless)

k_{iqs}: unsaturated hydraulic conductivity (mm/hr)

k_t: hydraulic conductivity (m/s)

M: model parameter in Eqs. (33) & (A7) (dimensionless)

m: model parameter in SWCC Eqs. (1), (24), (25) & (A1) (dimensionless)

m: portion of saturated layer of H in Eq. (36) (dimensionless)

m: model parameter Eqs (12) & (39) (dimensionless)

m: representing Eq. (43)

n: model parameter in SWCC Eqs. (1), (24), (25) & (A1) (dimensionless)

n: soil porosity in Eq. (36) (dimensionless)

n_w: representing Eq. (44)

P: parameter varies from 0 to 1 in Eq. (5) (dimensionless)

R: model parameter in Eq. (29) (dimensionless)

R': newly modified rainfall index in Eq. (22) (mm)

R_1: highest long-term effective rainfall in Eq. (23) (mm)

R_w: long-term effective rainfall in Eq. (23) (mm)

R_{fwo}: distance from origin (0,0) to reference point (R_1, r_1) in Eq. (22) (mm)

R_{fw}: distance from reference point (R_1, r_1) to elliptic arc in Eq. (22) (mm)

RI: rainfall intensity/infiltration (mm/hr)

r_1: highest short-term effective rainfall in Eq. (23) (mm)

r_w: short-term effective rainfall in Eq. (23) (mm)

S_e: effective degree of saturation in Eq. (4) (dimensionless)

S_r: degree of saturation (dimensionless)

S_{res}: residual degree of saturation in Eq. (4) (dimensionless)

t: model fitting parameter in Eq. (10b) (dimensionless)

u_a: pore air pressure (kPa)

u_w: pore water pressure (kPa)

$(u_a - u_w)$: matric suction in Eqs. (26), (27) & (28) (kPa)

$(u_a - u_w)_b$: air-entry value in Eqs. (20), (27) & (28) (kPa)

$(u_a - u_w)_f$: matric suction at failure condition in Eq. (20) (kPa)

v: model fitting parameter in Eq. (10b) (dimensionless)

w: volumetric water content (dimensionless)

α: model parameter Eqs. (12) & (39) (dimensionless)

α: constant in Eq. (23) (dimensionless)

β*: percentage of rainfall that infiltrates into the soil (dimensionless)

χ: representing Eqs. (20) & (27)

Δu_{ss}: change in pore pressure (kN/m^2)

γ: unit weight of water (kN/m3)

Γ: representing Eq. (41)

λ: model parameter Eqs. (12) & (38) (dimensionless)

μ: susceptibility coefficient in Eqs. (13) & (A5) (dimensionless)

Ω: representing Eq. (45)

∅: friction angle (degrees)

$\emptyset'$: effective friction angle (degrees)

$\emptyset^b$: friction angle due to matric suction (degrees)

$\emptyset_0$: friction angle at zero moisture content in Eq. (35) (degrees)

$\emptyset_a$: apparent friction angle in Eq. (15) (degrees)

ψ: matric suction in Eqs. (1), (24), (25), (30), (A1), (A2) & (A7) (kPa)

ψ_r: matric suction at residual water content in SWCC Eqs. (1), (24), (25) & (A2) (kPa)

ψ_t: transition suction Eq. (30) (kPa)

ρ: prediction accuracy (dimensionless)

σ: normal stress (kPa)

σ_n: normal stress in Eqs. (26), (32), (A4) & (A7) (kPa)

σ': effective normal stress (kPa)

σ^s: suction stress (kPa)

σ_n: normal stress in Eqs. (26), (33), (A4) & (A7) (kPa)

τ: shear stress (kPa)

τ_e: measured shear strength in Eq. (A6) (kPa)

τ_f: shear stress at failure (kPa)

τ_m: measured shear strength in Eq. (A6) (kPa)

τ_{sat}: saturated shear strength (kPa)

τ_{ss}: shear resistance at the steady state in the completely undrained condition (kN/m^2)

τ_{unsat}: unsaturated saturated shear strength (kPa)

Θ: representing Eq. (25)

θ: volumetric water content in SWCC Eqs. (1), (24), (25) & (A1) (dimensionless)

θ: moisture content (dimensionless)

θ_e: estimated water content in Eqs. (3) & (A3) (dimensionless)

θ_m: measured water content in Eqs. (3) & (A3) (dimensionless)

θ_r: residual water content in SWCC Eq. (1) (dimensionless)

θ_s: saturated water content in SWCC Eqs. (1), (24), (25) & (A1) (dimensionless)

Acknowledgements

I would like to express my sincere appreciation to my principal supervisor Dr Ivan Gratchev for his relentless guidance, insightful suggestions, encouragement, critical review and support throughout my study. I also would like to thank my co-supervisor Prof Dong-Sheng Jeng for continuous encouragement, providing advice, assistance, critical review of my work and support throughout my study. I also would like to thank Geotechnical Laboratory staff, in particular Chuen Yiu Lo for demonstrating experiments. I would like to thank Griffith University for providing me a continuous learning opportunity and grant permission to carry out this doctoral study. I would like to thank Griffith University library staff as well.

I would like to thank many public authorities including Bureau of Metrology; NSW Department of Planning and Environment Division of Resources and Geoscience and Disaster Assist Unit of Department of Home Affairs, Australia for providing data. I would like to thank public authorities based in Grafton for providing details of landslides including site information and granting permission to obtain soil samples from landslide sites in northern NSW.

In addition, I would like to thank my wife and two sons for their tolerance and continuous support. I also present this work to my late devoted parents. Finally, I thank God for everything to complete my study.

Acknowledgement of research papers included in this thesis

Research papers included in this thesis are Chapters 4 to 6 which were co-authored with my supervisors. A conference paper presented at UNSAT 2018 Conference in Hong Kong is also attached in Appendix A. My contribution in these research papers include concept, design, lab testing, data analysis, findings and drafting the article. My supervisors have critically reviewed these research papers, provided constructive feedback and final approval. I would like to appreciate my supervisors for critical review.

Chapter 4

Technical Note:

Ravindran, S, Gratchev, I and Jeng, D-S 2019, 'Analysis of rainfall-induced landslides in northern New South Wales, Australia', *Australian Geomechanics*, vol. 54, no. 4, pp. 83-97.

Chapter 5

Journal Paper:

Ravindran, S and Gratchev, I 2020, 'Estimation of shear strength of gravelly and sandy soils from shallow landslides', *International Journal of GEOMATE*, vol. 18, no. 70, pp. 130-137.

Chapter 6

Journal Paper:

Ravindran, S and Gratchev, I 2021, 'Prediction of shallow rainfall-induced landslides using shear strength of unsaturated soil', *Indian Geotechnical Journal*, pp. 1-12.

Appropriate acknowledgements of those who contributed to the research, yet did not qualify are authors, are included in each research paper.

(Signed)_____ Date:

Sinnappoo Ravindran

(Counter-signed)_____ Date:

Supervisor: Dr Ivan Gratchev

Chapter 1: Introduction

Landslides regularly occur in parts of many regions globally. They have caused massive destruction and the loss of numerous lives for centuries. Landslides may be caused by rainfall, earthquakes, melting of ice, abrupt changes in groundwater level and human activities, but most are triggered by heavy or prolonged rainfall.

Some devastating rainfall-induced landslides have happened recently in disparate locations. For instance, such landslides by intense rainfall caused the loss of many lives and massive damage to infrastructure in the coastal area of Messina province, Sicily, southern Italy in 2009 and prolonged rainfall triggered significant damage to infrastructure in two mountainous municipalities, Acquasanta Terme and Roccafluvione, in the Marche Region, central Italy in 2013 (Donnini et al. 2017). High intensity rainfall on the northeastern rim of Aso Caldera, in northern Kyushu, Japan (where there are high volumes of basaltic to rhyolitic lavas and pyroclastic fall and flows are distributed by past eruptive events) from 11 to 14 July 2012, destroyed extensive housing and transport routes (Yang et al. 2015). Oh et al. (2008) and Ono, Kazama and Ekkawatpanit (2014) reported that south-eastern Asian monsoons consistently induced landslides and mudflows in the hilly regions of northern and southern Thailand. Crosta (1998), Iverson (2000), Catani et al. (2005), Hong, Adler and Huffman (2006), Kirschbaum et al. (2009) and Ono, Kazama and Ekkawatpanit (2014) all noted that rainfall-induced landslides significantly impact infrastructure and thereby society and the economy. In Nepal (which is part of Himalayan region where rugged topography, unstable geological structures, soft and fragile rocks are present), rainfall-induced landslides by heavy and concentrated rainfall caused major disasters, including the loss of many lives and significant damage to property, infrastructure and the environment in 1926, 1988 and 2009. In 1998, such a landslide wiped out an entire village, killing 380 people in Uttarakhand, India (which is also a part of Himalaya region) (Dahal 2012). In 2009, many lives were lost and considerable damage to infrastructure was caused by rainfall-induced landslides (which was created by intense rainfall during monsoon) in the hilly district of Nilgiris (which is situated in the seismic zone) in the state of Tamilnadu, India (Chandrasekaran et al. 2013).

Australia, too, suffers from rainfall-induced landslides. More than 160 landslides caused the loss of many lives and significant damage to infrastructure including roads from 1842 to 1996

(Michael-Leiba, Andrews & Blong 1997). In Wollongong in the state of New South Wales (NSW), 142 landslides were triggered by rainfall events in 1998 (Flentje et al. 2005). Several landslides occurred on the Gold Coast and in northern NSW due to ex-tropical cyclone Debbie in March 2017 (Cogan, Gratchev & Wang 2018).

Rainfall-induced landslides can be sub-divided into two categories: shallow (up to 3 m in depth) and deep-seated (more than 3 m in depth). A loss of suction and consequent reduction of shear strength can cause shallow landslides (Yoshida, Kuwano & Kuwano 1991; Ching-Chuan et al. 2014; Suradi et al. 2014). Deep-seated rainfall-induced landslides occur when groundwater rises after prolonged rainfall, which increases pore pressure and reduces shear strength (Van Asch, Buma & Van Beek 1999; Hong & Wan 2011). Climate change has exacerbated vulnerability in some parts of the world due to rainfall-induced landslides (Gariano & Guzzetti 2016).

Rainfall-induced landslides are common in northern NSW, Australia, but no study has been conducted on this phenomenon in that region. This thesis focuses on the analysis and prediction of rainfall-induced shallow landslides along the road corridors in northern NSW, Australia such as Summerland Way, Bruxner Highway, Gwydir Highway, Waterfall Way, Oxley Highway, Lismore – Bangalow Road, New England Highway and Pacific Highway.

1.1 Landslides in the northern region of NSW

From January 2009 till the end of December 2019, 108 landslides occurred along the state road corridors in northern NSW, Australia, according to local authorities based in Grafton. Rainfall events caused about 80% of landslides (86) in this area whereas 20% (22) were due to loose fill, seepage and human activities such as excavation at the toe of a cut slope and impact from vehicles hitting guardrails at a downslope. The region is characterised by rolling hills, (embankments and riverbanks) and mountainous terrain. Mountainous ground is more prone to landslides, with 64% (69) of all landslides. Of the rainfall-induced landslides, all were shallow, with depths below 3 m.

In regard to these rainfall-induced landslides, 62% (53) occurred in mountainous terrain whereas 38% (33) happened in lower hills, embankments and riverbanks. Mountain passes in

the northern NSW such as those at Mt Seaview, Dorrigo Mountain, Gibraltar Range, Cangai-Ramornie Range, Mallanganee Range and Mt Lindesay are adversely affected by rainfall-induced landslides. The highest annual rainfall in this period was recorded in 2009 at Mt Seaview: 3671 mm. The average annual rainfall varies from 1096 mm to 2825 mm in the mountain ranges in northern NSW. The length of mountain passes varies from approximately 5 km to 35 km. Rainfall-induced landslides along these road corridors often result in road closures which not only prevent access to emergency services but also impact negatively on work, schooling and the supply of goods and services.

It is pertinent to address root causes of rainfall-induced landslides along the road corridors. It is also better to plan for landslide risk management proactively so that cost of remediation, destruction and impacts can be minimised. Particularly, mountain passes can be made available for travel within few weeks after the occurrence of landslides if the failure mechanism of landslide is known and remedial actions are implemented. In addition, preventive measures in slope risk management such as clearing root-jacking trees on the slopes, scaling and drainage management will also reduce the impact of rainfall-induced landslides. Figure 1.1 shows the study area in the northern region of NSW state of Australia. There are six major mountain passes, at Mount Seaview, Dorrigo Mountain, Gibraltar Range, Mallanganee Range, Ramornie-Cangai Bluff and Mount Lindesay, where landslides frequently occur.

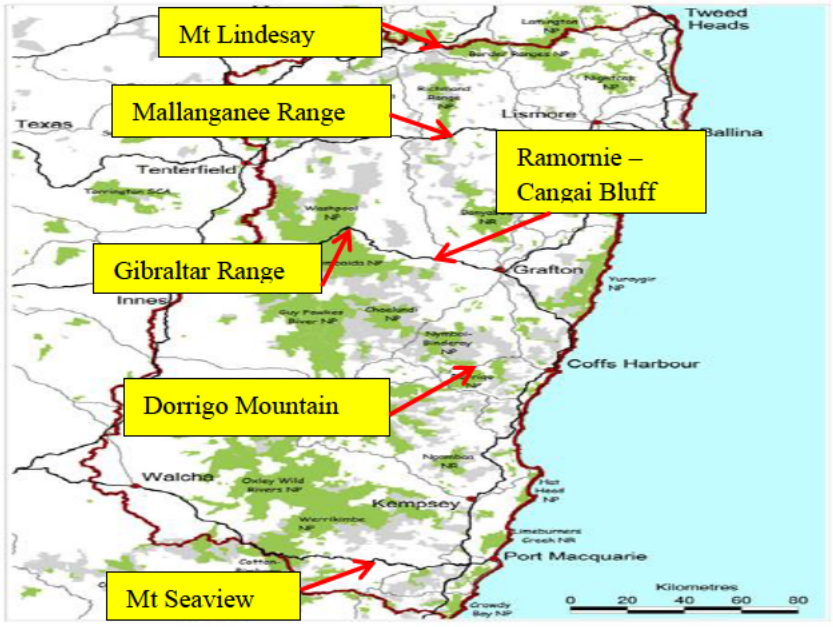

Figure 1.1: Study area in northern region of NSW, Australia (Source: Office of Environment & Heritage)

Over 150 km of roads pass through these landslide-prone mountains whose elevation varies from 219 m to 729 m from the mean sea level, as portrayed by Google Earth. Major rainfall events occurred in 2009, 2011, 2013 and 2017 and minor ones in 2015, 2016, 2018 and 2019. Figures 1.2 and 1.3 illustrate examples of landslides occurring in the vicinity of these road corridors.

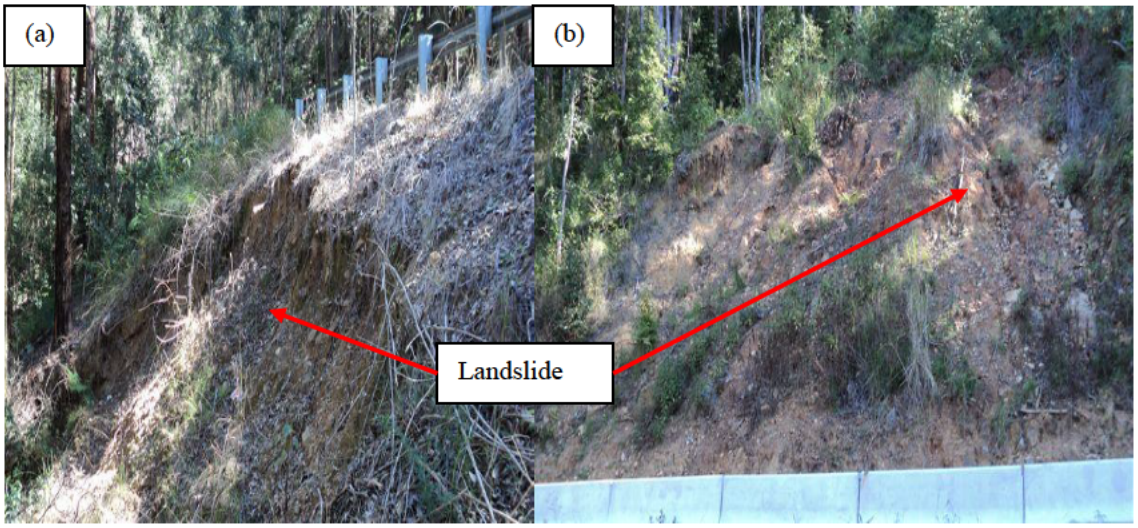

Figure 1.2: Gibraltar Range landslides occurring in January 2011 by natural disaster rainfall event

Figure 1.2a shows a downslope failure below the road and an upslope failure is seen above the road in Figure 1.2b at the Gibraltar Range section of the Gwydir Highway between Grafton and Glen Innes. A downslope failure which occurred at Summerland Way between Kyogle and Woodenbong is depicted in Figure 1.3.

Figure 1.3: Glen Road landslide occurring in January 2011 by natural disaster rainfall event

Out of the108 landslides between 2009 and 2019, about 72% were failures downslope of the road corridors whereas 28% were upslope failures. Appendix B provides the inventory of these 108 landslides.

1.2 Prediction of rainfall-induced shallow landslides

Prediction of rainfall-induced shallow landslides is required to manage their associated risks and consequences. Bordoni et al. (2015a) discovered that shallow rainfall-induced landsides can be predicted by one of two methods: a rainfall threshold, based on the rainfall intensity – duration relationship or stability models, by monitoring the hydrological and mechanical properties of the soil. The most widely used method is the former. Stability models are of various types: closed form equations, physical models and finite element methods. Ono, Kazama and Ekkawatpanit (2014) highlighted many physical models, some examples of which are shallow landslide instability prediction (SLIP) and transient rainfall infiltration and grid-based regional slope stability (TRIGRS).

According to Rahardjo, Satyanaga and Leong (2012), to comprehend the mechanism of rainfall-induced slope failures, unsaturated soil mechanics is required.

Shear strength is a key engineering property, while unsaturated soil strength is affected by matric suction. Measuring the shear strength of unsaturated soils is very difficult, which is why predicting the shear strength of unsaturated soils is important for practical applications in the analysis and forecasting of rainfall-induced landslides.

Garven (2009) discovered 25 empirical equations available to predict the shear strength of unsaturated soil, with certain equations suitable for particular types of soils.

1.3 Research gap

Based on the obtained information and the literature review which is discussed in detail in Chapter 2, the following major research gaps can be identified.

- Up to now, there has not been any systematic study on the mechanism rainfall-induced shallow landslides and factors affecting it in the study area. Such a study is required to better manage the landslide hazard along the road corridors in northern NSW's mountain ranges.
- There is insufficient laboratory data on the strength characteristics of soils from the rainfall-induced shallow landsides that regularly occur in northern NSW. No methods for strength prediction have been developed and applied for the slope and soil conditions of common landslide types from this area.
- No prediction models of shallow rainfall-induced landslides have been adopted for common site conditions in northern NSW and validated against real-life landslide records. Such prediction methods will provide engineers and decision-makers with an important tool to identify areas prone to rainfall-induced landslides.

1.4 Objectives of this research

The aim of this research is to better understand the failure mechanism of rainfall-induced shallow landsides in northern NSW; identify the major factors that lead to the occurrence of such landslides, and modify the existing methods for the prediction of both soil shear strength and landslide occurrence, based on field and laboratory data from common types of landslides in northern NSW. The objectives of this study are:

1. To investigate common types of rainfall-induced shallow landslides and better understand the effect of rainfall characteristics, slope conditions and soil properties on the occurrence of such landslides.
2. To study the effect of water on the shear strength characteristics of soils from several landslide sites in northern NSW and to establish empirical correlations and numerical relationships between the soil strength and its water content.

3. To modify the existing methods of landslide prediction so that they can be applied to site conditions in northern NSW as well as being easily adapted to local conditions in other countries.

The outcomes of this study comprise:

1. a detailed analysis of major factors that lead to landslide occurrences in northern NSW;
2. constitutive models to estimate the shear strength of soil in regard to soil's water content;
3. a validated model to predict the occurrence of landslides during a rainfall event adapted to common site conditions in northern NSW.

1.5 Scope of thesis

As a large number of landslides occur annually in NSW and it is impossible to study each one, it is important to clearly define this research's scope:

- This study focuses on rainfall-induced shallow landslides that occur in coarse-grained material as this is the most common type of landslide in northern NSW.
- The effect is investigated of water on the suction and shear strength of coarse-grained material, this being the common type of soil found at landslide sites.
- Different methods are examined to predict the occurrence of landslides: rainfall threshold, rainfall index, and stability models based on the limit equilibrium.

1.6 Layout of thesis

This thesis has been prepared in accordance with Griffith University requirements for which journal papers (both published or accepted) are included as separate chapters. The thesis consists of seven chapters, five appendices and references. Published journal papers form the major part of this work and they are presented in Chapters 4, 5 and 6 in the form in which they were accepted for publication.

Chapter 1 provides the introduction. In it are highlighted global issues in rainfall-induced landslides, the damage caused by rainfall-induced landslides worldwide, features of shallow

landslides in northern NSW, especially in terms of terrain, rainfall characteristics, slope characteristics and frequency of landslides, prediction of shear strength, prediction of rainfall-induced shallow landslides, the research gap, research objective, scope and layout of the thesis.

Chapter 2 comprises the literature review and includes the research significance for types of landsides, rainfall-induced landslides, shallow landslides, rainfall characteristics, unsaturated soils, shear strength, suction, and prediction models of shear strength and rainfall-induced shallow landslides.

Chapter 3 is a discussion about materials and methods involved in this study, including test procedures.

Chapter 4 includes the following technical note on the analysis of rainfall-induced landslides in northern NSW, Australia, published in 2019:

- Ravindran, S, Gratchev, I and Jeng, D-S 2019, 'Analysis of rainfall-induced landslides in northern New South Wales, Australia', *Australian Geomechanics*, vol. 54 (4), pp. 83-97.

It provides details of some landslides, details of the surface geology where landslides occurred, slope angles of landslides, rainfall characteristics causing landslides, the rainfall threshold and rainfall index for predicting rainfall-induced landslides in northern NSW and particle size distribution of soil samples collected from past landslide sites, and shear strength reduction with increasing moisture content.

Chapter 5 includes a journal paper on shear strength estimations for particular soils in shallow landslides, published in 2020:

- Ravindran, S and Gratchev, I 2020, 'Estimation of shear strength of gravelly and sandy soils from shallow landslides', *International Journal of GEOMATE*, vol. 18 (70), pp. 130-137.

It provides a new method of predicting the shear strength of gravelly and sandy soils using the coefficient of uniformity and matric suction and a comparison of two published methods for predicting shear strength, the estimation of air entry value (AEV), the cohesion and the friction angle of gravelly and sandy soils.

Chapter 6 includes a journal paper on the prediction of shallow rainfall-induced landslides:

- Ravindran, S and Gratchev, I 2021, 'Prediction of shallow rainfall-induced landslides using shear strength of unsaturated soil', *Indian Geotechnical Journal*, pp. 1-12.

It provides shear box test results, consolidated undrained triaxial test results, a site-specific SLIP model for predicting rainfall-induced shallow landslides and a method of estimating a model parameter using unsaturated shear strengths of soils collected from the past landslide sites.

Chapter 7 comprises the conclusions and recommendations from this research.

Appendix A includes the conference paper presented at the UNSAT 2018 Conference held in Hong Kong in 2018 on the prediction of shear strength of unsaturated soils in landslide-prone areas using direct shear and suction tests under low normal stress conditions.

Appendix B lists the landslide inventory, including the road name where landslide occurred, the name of landslide sites, types of terrain, the cause of failure and details such as if it was an upslope or downslope failure.

Appendix C illustrates rainfall characteristics such as the nearest rain gauge station number, rainfall event details and cumulative rainfall by rainfall-induced landslide sites in northern NSW.

Appendix D provides slope characteristics such as the slope angle, surface geology and major rock group by rainfall-induced landslide sites in northern NSW.

Appendix E incorporates significant test results of direct shear test, suction test, consolidated undrained triaxial test and hydraulic conductivity test.

References are provided at the end of this thesis.

Chapter 2: Literature review and research significance

Many prior studies have been undertaken on rainfall-induced landslides. As research into rainfall-induced landsides involves shear strength of soils and unsaturated soil mechanics, this chapter includes a variety of research into these topics.

This literature review consists of four major research areas: 1) landslides in general, 2) rainfall characteristics, 3) mechanisms of shallow landslides and factors affecting them and 4) prediction of shear strength and shallow landslides. In the first section, a landslide is defined and an outline is given of common causes of landslides, types of rainfall-induced landslides and geological characteristics of landslides. Rainfall characteristics are described in the second section whereas the third section gives a description of the mechanism of shallow landslides, types of slopes and materials, infiltration process, matric suction and shear strength, unsaturated soils, soil water characteristics curve (SWCC), hydraulic conductivity, shear strength of unsaturated soils and shear strength equations for unsaturated soils. In the last section, the prediction of shear strength, analysis of rainfall-induced shallow landslides and prediction of rainfall-induced shallow landslides and risk mitigation measures of rainfall-induced landslides are provided, followed by a summary of the literature review and gaps in the previous research.

2.1 Landslides in general

2.1.1 Common causes of landslides

Prior to discussing landslides, it is pertinent to define what a landslide is. Highland and Bobrowsky (2008) defined a landslide as a downslope movement of soil, rock, organic materials and landform under the gravitational force. Based on the rupture of the surface, it can be classified as a rotational or translational slide.

Norris et al. (2008) advised that rotational failure usually occurs when there is a thick cohesive deposit that may or may not have stratification and also with heavily fractured rock masses while Highland and Bobrowsky (2008) reported that rotational landslides are caused by intense and/or sustained rainfall or base erosion by flood.

On the other hand, translational slides take place when there are layers of soils (Norris et al. 2008). Ghiassian and Ghareh (2008) and Highland and Bobrowsky (2008) revealed that translational slides are usually due to the surface weaknesses such as faults, joints, bedding planes and variations in shear strengths between layers of bedding deposits. Translational slides can happen in homogenous coarse-grained, cohesionless soils as well. Concurrently, Highland and Bobrowsky (2008) reported that translational landslides are activated by intense rainfall or a rise in groundwater level. Igwe (2015a) revealed that landslides in metamorphic zones were very complex translational and rotational slides and mudslides on the steep slopes. It involves a combination of slide and flow with headscarps and slickensided shear surfaces sometimes. On the sedimentary zones, looseness of materials and relatively low strength are the factors affecting landslides. Due to their potential for disastrous consequences, it is paramount to investigate the origins of landslides.

Bell (1993) reported a number of landslide causes, grouped as external and internal:

- External causes include an increase in the weight of the slope, removal of the toe support of the slope, overloading on the top of the slope and earthquakes.
- Internal causes are the mechanisms which reduce shear strength such as an increase in pore water pressure, seepage in granular soils, an increase in water content, weathering and swelling in impermeable cohesive soils.

Various research studies on landslides have been conducted in the past, with some of the highlights noted below. The general topic has been approached from a range of perspectives. Jotisankasa et al. (2008) reported that rainfall is the dominant trigger for landslides whereas Parriaux (2009) advised that slope failures occur during the rainy season because surface water and ground water play key roles in the mechanics of slope instability. Aydilek and Ramanathan (2013) also showed that rainfall and poor surface and/or subsurface drainage are the key factors influencing slope stability along highways. Dahal (2012) discovered that soil characteristics, low internal friction angle of fines, the presence of clay minerals, bedrock hydrology and human intervention are key contributing factors for landslides.

Gue and Liong (2007) analysed the landslides in Hulu Kelang, Malaysia and determined that the poor design and construction methods of retaining walls and slopes cause the majority of these landslides while Farisham (2007) also added that a lack of maintenance of the internal

drainage system of slopes and retaining structures in this area are also influential factors leading to landslides (Lee et al. 2014).

Delayed slope failure can also occur. Cornforth (2005) advised that delayed failure can occur after months or decades due to pore pressure changes triggered by causative factors. This occurs because of an initial drop in pore pressure and a subsequent rise to reach equilibrium conditions. The following three conditions should occur to cause a delayed failure:

- The soil is an over-consolidated clay or clayey silt.
- The shear stress increases due to an event such as erosion at the base or construction of fill.
- The rate of shear movement increases with time.

Major catastrophic failure can occur if the above conditions are met (Cornforth 2005).

This research focuses on rainfall-induced landslides only and not on delayed slope failures. To round out this background, it is important to set out how rainfall-induced landslides affect people's lives, infrastructure and economy.

2.1.2 Types of rainfall-induced landslides

Based on their failure mechanism, rainfall-induced landslides can be either deep-seated (activated by the rise of groundwater) or shallow (caused by a loss of suction). Deep-seated landslides are generally considered to be greater than 3 m in depth whereas shallow ones are less than 3 m deep. First some research into deep-seated rainfall-induced landslides will be presented. Various causes have been posited, depending on the focus of the research and the conditions of the particular study area. Section 2.2 and following subsections offer insight into rainfall characteristics which affect both shallow and deeper landslides.

Van Asch, Buma and Van Beek (1999) reported that the deeper landslides (5 – 20 m depth) are caused by positive pore water pressure on the slip surface induced by the rising groundwater level (Hong & Wan 2011). According to Garland and Olivier (1993), deeper and larger landslides are caused not necessarily by intense rainfall, but by continuous rainfall over a long period of time (Matsuura, Asano & Okamoto 2008). Caris and Van Asch (1991) found that a groundwater level of 4 m below the ground surface is the critical threshold for reactivating a deep-seated landslide.

From the case study of a landslide at Lushan, Taiwan, Liming Engineering Consultants Co. (2006) found that the rising groundwater table produced by torrential rainfall was the major cause of the deep-seated landslide. The material in the landslide area is Miocene sediment consisting of dark grey slate mixed with hard slaty sand. The depth of groundwater is 25 m to 40 m during the dry season and this rises to 10 to 15 m after rainfall of 400 mm/day. The return period of a daily rainfall of 400 mm is estimated to be 5 to 10 years (Lee & Chi 2011).

To understand the slope characteristics of rainfall-induced landslides, it is important to establish the vulnerable rock types that are subject to these landslides.

2.1.3 Geological characteristics of rainfall-induced landslides

Deep rock weathering, faults, joints and fractures contribute to large and complex landslides. Gerrard (1994) revealed that phyllite rocks are vulnerable to landslides. Shales, schists, poorly cemented sandstones, gneiss, granites and quartzite are also susceptible to landslides (Regmi et al. 2013).

Pradhan, Lee and Kim (2019) studied 260 rainfall-induced landslides in Busan, Korea and found that 50% were activated in volcanic rocks; 20% in plutonic rocks and the rest in sedimentary and recent deposits. Water can infiltrate into slopes through weathered, fractured or permeable rocks and thus destabilise slopes. Bhandary et al. (2011) reported that slate and phyllite formations in the Himalayan zone of central Nepal have the highest percentage of deep-seated landslides compared to similar tectonically active topographies in the world.

Terrains consisting of phyllites, slates and the intercalation of phyllites and quartzites are heavily prone to landslides. Riverbanks consisting of alluvial and glacial moraines are also susceptible (Dahal 2012).

Highly permeable rock types exist such as rhyolite, trachyte, quartz, dacite, andesite, basalt, pumice, scoria, vesicular basalt, sandstone with partial filling of voids by cement coatings and limestone in caverns (Look 2007). These rocks may be susceptible to rainfall-induced landslides.

Suradi, Fourie and Saynor (2016) studied a landslide occurring in the Jabiru region of the Northern Territory, Australia and drew the inference that this natural slope failed due to 2 m thick highly weathered residual dolerite overlying sandstone material and pore pressure development, even though this slope consists of soils with an internal friction angle of 25 degrees and a slope angle of 19 degrees.

Igwe (2015a) divulged from the study of geotechnical characteristics of landslides from southeast Nigeria that sedimentary zones are more vulnerable to landslides as opposed to metamorphic zones. On the sedimentary terrain, landslides are in the form of slumps and short runout debris slides with limited volume. On the contrary, they are mudflows/slides and continue for long distance.

A study of fatal slope failures in metamorphic zones of Obudu tourist area, Nigeria revealed that failures occurred in the slopes consisting of schist rather than gneiss or granite (Igwe 2015b).

Having highlighted the relevant geology, it is important to examine how rainfall characteristics such as the rainfall pattern, rainfall intensity and duration cause shallow landslides.

2.2 Rainfall characteristics

Tsai (2007) and Tsai and Wang (2011) studied rainfall-induced landslides using physical modelling, which showed that the failure time and depth of landslides are influenced by rainfall characteristics (Ran et al. 2018).

Cilmate change has an influence in activating rainfall-induced landslides. Chou et al. (2013) are some among many researchers who have established that understanding the risk and disaster potential due to extreme and complex climate change is important in the current era. Kristo, Rahardjo and Satyanaga (2017) studied the rainfall pattern in Singapore from 1985 to 2009, revealing that the rainfall intensity for most durations is on the rise and rainfall duration itself may also increase in the future.

Research results have varied due to the particular characteristics of the regions in which studies have taken place. Jemec and Komac (2013) found that rainfalls of both short and long durations

activate landslides in Slovenia. Howard, Baldwin and Donley (1982) and Montrasio and Valentino (2008) reported that shallow landslides are activated by intense rainfall (Bordoni et al. 2015a). A longitudinal study conducted on landslide erosion in three mountainous watersheds in Taiwan showed that shallow landslides are caused by short duration rainfall whereas deeper landslides are triggered by long duration rainfall (Chen et al. 2014).

Campbell (1975), Costa (1984), Crozier (1986) and Wilson and Wieczorek (1995) have discovered that antecedent rainfall and a critical intensity of rainfall are equally influential in activating rainfall-induced landslides (Dai & Lee 2001). However Brand (1995) discovered that antecedent rainfall is not important in the case of highly permeable soils in tropical countries where shallow landslides occur (Dai & Lee 2001). Jan et al. (2016) reported that the amount of rain and its intensity both influence rainfall-induced shallow landslides.

According to Wieczorek (1987), antecedent rainfall is a deciding factor for whether a landslide would begin, whereas rainfall intensity and duration would influence where landslides take place. On the other hand, Low, Ali and Ibrahim (2012) studied one of the major landslides in Hulu Kelang and found that prolonged rainfall during the monsoon season is a major factor activating the landslide (Lee et al. 2014).

Li et al. (2011) studied the influence of rainfall event duration by analysing 1414 landslides and revealed that the majority of rainfall-induced landslides (71.3%) were caused by an intraday event (Ma et al. 2015). Trigo et al. (2005) advocated that high intensity short duration rainfall (greater than 130 mm per day) and medium intensity medium duration rainfall (174 mm in 5 days to 217 mm in 15 days) cause shallow landslides whereas low intensity prolonged rainfall (333 mm in 30 days to 793 mm in 90 days) triggers deep-seated landslides (Lee et al. 2014).

Centrifuge simulation modelling reveals that when the incrementally accumulated rainfall is around 200 mm, local failure occurs and when the accumulated rainfall reaches 400 mm, global failure is initiated (Ling & Ling 2012) while Toll (2001) by observation advises that cumulative rainfall up to 100 mm over a period of six days is enough to create minor landslides in Singapore.

According to a study conducted on 677 rainfall-induced landslides in the Himalayan area of Nepal, continuous rainfall of 5, 7 or 10 days activates landslides. There is a clear correlation between progressive monsoon rainfall and the frequency of landslides. Monsoon rainfalls are usually of low intensity and long duration and occur with interruptions (Dahal 2012).

Chen et al. (2017) discovered from the study of 172 landslides in Taiwan from 2006 to 2012 that large and deep landslides happen due to prolonged and medium intensity rainfall and the rise of the groundwater table while small and shallow landslides occur in a variety of rainfall conditions. Even short duration rainfall can create shallow landslides.

A 25-year study of rainfall-induced landslides in Hong Kong indicated that landslides are caused by localised short duration rainfall of high intensity and occur when the rainfall intensity threshold reaches 70mm/hr (Brand et al. 1984).

One concept that has arisen from the research is critical duration of prolonged rainfall, which is defined as the duration of rainfall that produces the highest amount of rainfall on the day of landslide occurrence. The critical duration is, of course, influenced by factors separate to the actual rainfall features themselves: hydraulic conductivity, slope terrain, soil strength properties and initial moisture content (Lee et al. 2014).

In an experiment on an instrumented slope of saprolite material, Li et al. (2005) revealed that 70% of total rainfall infiltrates to a shallow depth and this increases the soil moisture content but the infiltration has no effect on groundwater.

A study conducted at an experimental slope gully site in Taiwan with instrumentation showed that during rainfall, the arrival time of the wetting front and the time taken to decrease shear strength to the lowest reduced at lower elevations as opposed to upper elevations. The arrival time of the wetting front, the time taken to decrease shear strength to the lowest and their distribution with depth are dependent on the rainfall characteristics. The onset of slope failure at lower elevations of a slope gully is faster than that at upper elevations (Fan & Wang 2014).

Tsai and Wang (2011) analysed the influence of four different rainfall patterns, uniform, advanced, intermediated and delayed. Results disclosed that the occurrence of landslide, failure depth and time of failure are affected by the rainfall pattern.

Rainfall distribution also plays a key role in activating landslides. In a case study conducted in the Piedmont area in Taiwan, the correlations between the factor of safety of the slope and various rainfall distributions (advanced, delayed, central, doubled and uniform) were analysed. The delayed distribution of rainfall drastically reduces the factor of safety, compared to other distributions. The factor of safety decreased when the rainfall intensity increased according to this numerical modelling (Lo et al. 2010).

Another fruitful approach in landslide prediction using rainfall consists of studies of the rainfall threshold which triggers landslides. Guzzetti et al. (2008) reported that the daily rainfall is a key parameter in predicting landslides. Caine (1980) has developed a worldwide landslide triggering rainfall threshold (mm/h) using data from 73 landslide sites all over the world. The relationship between rainfall intensity and duration is shown in Figure 2.1 (Pando, Ruiz & Larsen 2005). This line shows the minimum rainfall threshold; when the rainfall exceeds the intensity-duration level, a landslide can be activated (Jan et al. 2016). Nevertheless, the rainfall threshold causing a landslide for a region is not a fixed value. It changes according to environmental factors (Wu et al. 2015b). More rainfall intensity – duration threshold curves are included on Figure 2.2 and their relationships are expressed in Table 2.1 respectively (Guzzetti et al. 2007).

Leonarduzzi, Molnar and McArdell (2017) identified three issues in using intensity-duration thresholds and addressed them in their study which consists of a landslides database of 2000 events with high resolution gridded daily rainfall data in Switzerland:

- Methodological confusion in defining intensity-duration thresholds
- Inconsistency in rainfall and landslide data
- Improper validation of intensity-duration curves.

Leonarduzzi, Molnar and McArdell (2017) revealed that shallow landslides can be best predicted by an intensity-duration threshold curve, followed by peak daily intensity (I_{max}) and mean event intensity (I_{mean}).

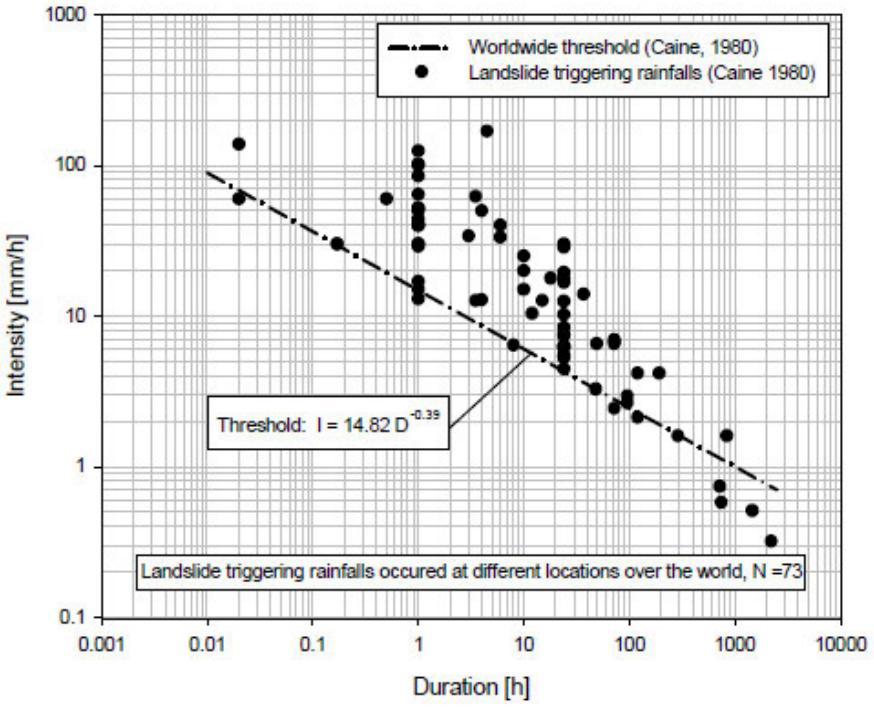

Figure 2.1: Worldwide landslide triggering threshold (mm/h) (Source: Caine 1980)

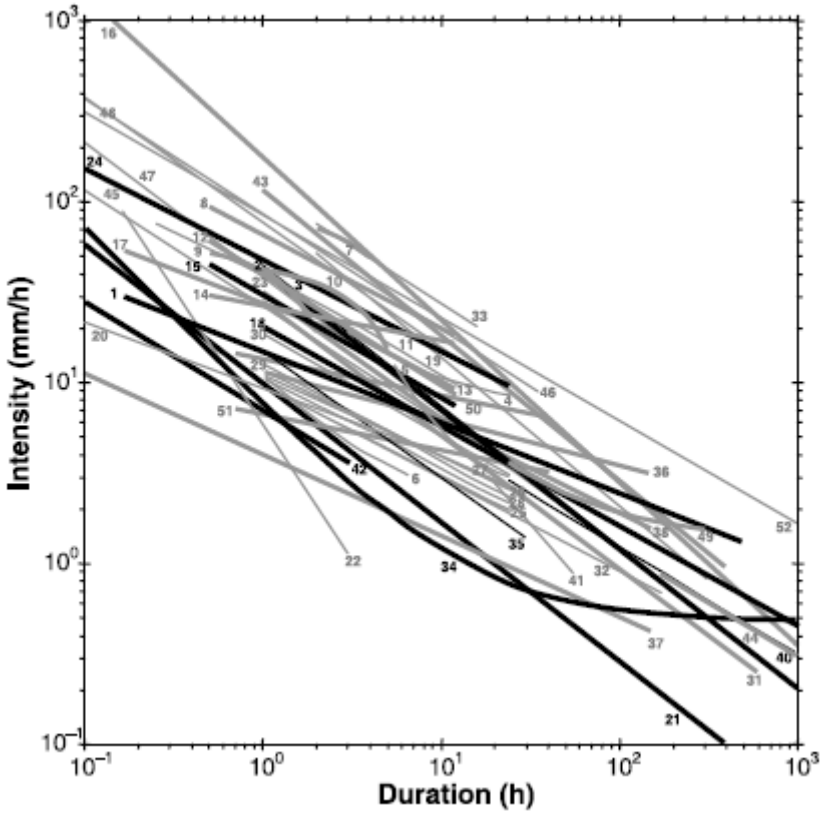

Figure 2.2: Rainfall intensity – duration thresholds (legend or numbers are shown in Table 2. 1) (Source: Guzzetti et al. 2007)

In Figure 2.2, very thick line indicates global threshold; thick line represents regional threshold and thin line specifies local threshold.

Table 2.1: Intensity – duration thresholds for the initiation of landslides of the curves shown in Figure 2.2 (Source: Guzzetti et al. 2007)

No.	Threshold	Area	Landslide type	Equation (Rainfall, I – mm/hr; Duration, D – hr)	Range (hours)
1	Global	World	Shallow landslide, Debris flow	$I = 14.82\ x\ D^{-0.39}$	0.167<D<500
2	Regional	Carinthia and E Tyrol, Austria	Soil slip	$I = 41.66\ x\ D^{-0.77}$	1<D<1000
3	Local	Valtellina, Lombardy, N Italy	Soil slip	$I = 44.668\ x\ D^{-0.78}$	1<D<1000
4	Local	San Francisco Bay Region, California (high mean annual precipitation)	Debris flow	$I = 6.9 + 38\ x\ D^{-1.00}$	2<D<24
5	Local	San Francisco Bay Region, California (low mean annual precipitation)	Debris flow	$I = 2.5 + 300\ x\ D^{-2.00}$	5.5<D<24
6	Local	Central Santa Cruz Mountains, California	Debris flow	$I = 1.7 + 9\ x\ D^{-1.00}$	1<D<6.5

7	Regional	Indonesia	Debris flow	$I = 92.06 - 10.68\, x\, D^{1.00}$	2<D<4
8	Regional	Puerto Rico	Debris flow	$I = 66.18\, x\, D^{-0.52}$	0.5<D<12
9	Regional	Brazil	Debris flow	$I = 63.38 - 22.19\, x\, D^{1.00}$	0.5<D<2
10	Regional	China	Debris flow	$I = 49.11 - 6.81\, x\, D^{1.00}$	1<D<5
11	Local	Hong Kong	Debris flow	$I = 41.83\, x\, D^{-0.58}$	1<D<12
12	Regional	Japan	Debris flow	$I = 39.71\, x\, D^{-0.62}$	0.5<D<12
13	Regional	California	Debris flow	$I = 35.23\, x\, D^{-0.54}$	3<D<12
14	Regional	California	Debris flow	$I = 26.51\, x\, D^{-0.19}$	0.5<D<12
15	Global	World (lower envelope)	Debris flow	$I = 30.53\, x\, D^{-0.57}$	0.5<D<12
16	Regional	Peri-Vesuvian area, Campania Region, S Italy (volcanic soils)	Debris flow	$I = 176.40\, x\, D^{-0.90}$	0.5<D<12
17	Local	Mayon, Philippines	Lahar	$I = 27.3\, x\, D^{-0.38}$	0.167<D<3
18	Regional	Lombardy, N Italy	All types	$I = 20.1\, x\, D^{-0.55}$	1<D<1000
19	Regional	Puerto Rico	All types	$I = 91.46\, x\, D^{-0.82}$	2<D<312
20	Local	Pasig-Potrero River, Philippines	Lahar	$I = 9.23\, x\, D^{-0.37}$	0.08<D<7.92
21	Global	World	Soil slip	$I = 10\, x\, D^{-0.77}$	0.1<D<1000

22	Local	Sacobia River, Philippines	Lahar	$I = 5.94\ x\ D^{-1.50}$	0.167<D<3
23	Regional	Switzerland	All types	$I = 32\ x\ D^{-0.70}$	1<D<45
24	Regional	NE Alps, Italy	Debris flow	$I = 47.742\ x\ D^{-0.507}$	0.1<D<24
25	Local	Rho Basin, Susa Valley, Piedmont NW Italy (antecedent rainfall > 14% mean annual precipitation)	Debris flow	$I = 9.521\ x\ D^{-0.4955}$	1<D<24
26	Local	Rho Basin, Susa Valley, Piedmont NW Italy (antecedent rainfall < 14% mean annual precipitation)	Debris flow	$I = 11.698\ x\ D^{-0.4783}$	1<D<24
27	Local	Perilleux Basin, Piedmont, NW Italy (antecedent rainfall > 9% mean annual precipitation)	Debris flow	$I = 11.00\ x\ D^{-0.4459}$	1<D<24
28	Local	Perilleux Basin, Piedmont, NW Italy (Antecedent rainfall < 9%	Debris flow	$I = 10.67\ x\ D^{-0.5043}$	1<D<24

		mean annual precipitation)			
29	Local	Champeyron Basin, Piedmont, NW Italy (antecedent rainfall > 14% mean annual precipitation)	Debris flow	$I = 12.649\ x\ D^{-0.5324}$	1<D<24
30	Local	Champeyron Basin, Piedmont, NW Italy (antecedent rainfall > 14% mean annual precipitation)	Debris flow	$I = 18.675\ x\ D^{-0.565}$	1<D<24
31	Regional	Campania, S Italy	All types	$I = 28.10\ x\ D^{-0.74}$	1<D<600
32	Local	Mettman Ridge, Oregon	All types	$I = 9.9\ x\ D^{-0.52}$	1<D<170
33	Local	Blue Ridge, Madison County, Virginia	Debris flow	$I = 116.48\ x\ D^{-0.63}$	2<D<16
34	Global	World	Shallow landslide	$I = 0.48 + 7.2\ x\ D^{-1.00}$	0.1<D<1000
35	Local	Moscardo Torrent, NE Italy	All types	$I = 15.00\ x\ D^{-0.70}$	1<D<30
36	Regional	E Jamaica	Shallow landslide	$I = 11.50\ x\ D^{-0.26}$	1<D<150

37	Regional	North Shore Mountains, Vancouver, Canada	Shallow landslide	$I = 4.00\ x\ D^{-0.45}$	0.1<D<150
38	Regional	Piedmont, NW Italy	Shallow landslide	$I = 19.00\ x\ D^{-0.50}$	4<D<150
39	Local	Piedmont, NW Italy	All types	$I = 44.668\ x\ D^{-0.78}\ x\ N$ (N = Ratios of mean annual precipitation)	1<D<1000
40	Local	Valzangona, N Apennines, Italy	All types	$I = 18.83\ x\ D^{-0.59}$	24<D<3360
41	Local	Seattle, Washington	Soil slip	$I = 82.73\ x\ D^{-1.13}$	20<D<55
42	Global	World (for burnt areas)	Debris flow	$I = 7.00\ x\ D^{-0.60}$	0.1<D<3
43	Regional	Taiwan	All types	$I = 115.47\ x\ D^{-0.80}$	1<D<400
44	Regional	Pyrenees, Spain	All types	$I = 17.96\ x\ D^{-0.59}$	D>168
45	Local	Apuane, Alps, Tuscany, Italy (lower threshold)	Shallow landslide	$I = 26.871\ x\ D^{-0.638}$	0.1<D<35
46	Local	Apuane, Alps, Tuscany, Italy (upper threshold)	Shallow landslide	$I = 85.584\ x\ D^{-0.781}$	0.1<D<35
47	Local	Apuane, Alps, Tuscany, Italy (lower threshold)	Shallow landslide	$I = 38.363\ x\ D^{-0.743}$	$0.1 < D \leq 12$

48	Local	Apuane, Alps, Tuscany, Italy (upper threshold)	Shallow landslide	$I = 76.199\ x\ D^{-0.692}$	$0.1 < D \leq 12$
49	Regional	Shikoku Island, Japan	All types	$I = 1.35 + 55.0\ x\ D^{-1.00}$	24<D<300
50	Regional	Central Taiwan (before Chi-Chi earthquake)	Debris flow	$I = 13.5\ x\ D^{-0.20}$	0.7<D<40
51	Regional	Central Taiwan (after Chi-Chi earthquake)	Debris flow	$I = 6.7\ x\ D^{-0.20}$	0.7<D<40
52	Local	N of Lisbon, Portugal	All types	$I = 84.3\ x\ D^{-0.57}$	0.1<D<2000

2.3 Mechanisms of shallow landslides and factors affecting them

In this research, the focus is on shallow rainfall-induced landslides. For prediction and assessment purposes, it is vital to note what factors influence shallow rainfall-induced landslides (0.5 m to 3 m depth) and understand their failure mechanisms. During rainfall, infiltration occurs in the slopes, which leads to an increase in moisture content and reduction of shear strength. Yoshida et al. (1991), Ching-Chuan et al. (2009) and Suradi et al. (2014) noted a drastic reduction in shear strength during infiltration. Shallow landslides can happen during rainfall of short duration (Chen et al. 2017). Other factors such as geomorphology, soil thickness, slope aspect and slope protection are also crucial in influencing the occurrence of shallow landslides (Dai & Lee 2001).

Prior to analysing rainfall-induced shallow landslides, it is pertinent to determine in detail such influencing factors, the types of slopes and materials where these shallow landslides occur, the infiltration process and how matric suction and shear strength changes contribute to failure of slopes.

Rainfall intensity and duration, slope angle, soil initial conditions and the hydraulic and mechanical properties of soil affect slope stability (Cuomo & Della Sala 2015). The

vulnerability of a slope to rainfall-induced landslides is highly dependent on hydraulic properties. In the following discussion, these factors will be explored in more detail.

2.3.1 Types of slopes and materials

Maharaj (1993), Zhu and Anderson (1998), Fuchu, Lee and Sijing (1999), Dai and Lee (2002), Capra, Lugo-Hubp and Borselli (2003), Dai et al. (2004), Yu et al. (2006), Dahal et al. (2009), Giannecchini, Galanti and Avanzi (2012) and Wang et al. (2015) noted that shallow landslides occur in weathered debris or loose soils in steep slopes during heavy rain (Yang et al. 2015). Brand, Premchitt and Phillipson (1984) reported that steep slopes in Hong Kong with deeply weathered rocks are vulnerable to landslides during heavy rain.

Cho (2009), Godt, Baum and Lu (2009), Springman et al. (2009), Zhang et al. (2011), Chae and Kim (2012), Bhandary et al. (2013), Guns and Vanacker (2014) and Chen and Zhang (2014) ascertained that in mountainous terrains, rainfall is the primary factor triggering shallow landslides (Wu et al. 2015a). Li (2004) reported that mountainous terrains are mostly affected by intense rainfall events and are likely to have landslides (Ma et al. 2015).

Rainfall-induced landslides normally occur in steep slopes due to water infiltration, resulting in change in the pore water pressure and shear strength of soil (Conte & Troncone 2012). The Government of Hong Kong (1977) found that loosely compacted soils slopes in Hong Kong fail abruptly during intense rainfall. This may occur although the fill material may not be saturated (Chen, Lee & Law 2004).

A study of 120 rainfall-induced landslides in Nanka area, southeast Nigeria divulged that most of them are of shallow depth varying from 0.2 m to 1.8 m, slope angle ranging from 36 to 65 degrees and on the slopes consisting of poorly consolidated sands overlying less permeable silty caly material (Igwe & Una, 2019).

Rahardjo et al. (1995) advised that shallow landslides occur in slopes consisting of residual or colluvial soil over bedrock (Collins & Znidarcic 2004). Matsushi and Matsukura (2006) compared failure mechanisms of hillslopes consisting of sandstone with those of mudstone and reported that failure occurs at steep lower parts of sandstone hillslopes whereas failure

happened at the soil-bedrock interface of mudstone hillslopes. In residual soils with steep angles and deep groundwater tables, shallow failures normally happen (Suradi et al. 2014).

For a particular rainfall intensity, when the slope consists of fine-grained soils, the time taken for slope failure increases. Slopes with finer soils have more surface runoff and less infiltration. High suction is present in the slopes of finer material and, as a result, these slopes fail much later. On the other hand, infiltration is faster on slopes comprising coarser material. A high intensity rainfall can activate landslides with coarser material sooner than with finer material. But low intensity rainfalls of similar durations can trigger landslides in both coarser and finer material (Ahmadi-Adli, Huvaj & Toker 2014).

Shallow landslides will not happen if the slope angle is less than the internal friction angle (Ran et al. 2018). Slope instability during rainfall at lower elevations occurs much faster than at upper elevations in a slope gully (Fan & Wang 2014). Dai et al. (2001) revealed from a study of landslides at Lantau Island, Hong Kong that landslide frequency reduces when the site is located away from the drainage line (Fan & Wang 2014). Having highlighted some reseaerch into types of slopes and slope materials, a closer look at infiltration follows.

2.3.2 Infiltration process, matric suction and shear strength

The upper layer of soil gets wet during the infiltration process and the moisture content increases as a result. Nishigaki, Tohari and Komatsu (1999) carried out rainfall tests on sandy slope models and identified two phases in the soil moisture content change. These are wetting front progress in a downward direction and groundwater rise in an upward direction by rainfall infiltration. They concluded that the in-soil moisture content is a better predictor of slope failure initiation than the pore water pressure (Ching-Chuan et al. 2009).

Gavin and Xue (2008) used the Green-Ampt Model to explain the infiltration process. It was assumed that the soil layer between the ground surface and wetting front was saturated and the soil layer below the wetting front was unsaturated. They discovered a landslide occurs along the bedrock when the matric suction is low. On the other hand, a landslide happens along the wetting front when the matric suction is high. The factor of safety reduces with increasing infiltration time. The depth of the wetting front increases during prolonged rain (Wang et al. 2017). To develop the wetting front, a minimum intensity and duration of rainfall is required

(Suradi et al. 2014). Key features triggering shallow landslides after infiltratoin include matric suction and shear strength.

The shallow failures are triggered by a reduction of matric suction due to rainwater infiltration associated with prolonged periods of heavy rain (Ching-Chuan et al. 2009). When the soil is unsaturated, suction provides additional strength which disappears during the infiltration. An analysis of rainfall-induced shallow landslides (0.5 m to 3 m) in Singapore and Thailand showed that a reduction of suction is caused by rainfall infiltration and thereby the shear strength is decreased (Jotisankasa et al. 2008).

Bishop and Morgenstern (1960), Bishop and Blight (1963), Blight (2002), Springman, Jommi and Teysseire (2003) and Rahardjo et al. (2005) noted that infiltration of rainfall increases saturation, reduces suction and decreases shear strength as a result in steep slopes (Springman et al. 2013). Tsai, Chen and Yang (2008) and Tsai and Chen (2010) also revealed that slope instability is caused by the loss of matric suction due to infiltration during rainfall (Tsai 2010). Suction can be lost at a depth of 1 to 2 m from the surface level even with a small amount of rainfall (Karthikeyan, Toll & Phoon 2008).

Gofar, Lee and Kassim (2008) and Yeh, Lee and Lee (2008) advised that at the onset of rainfall-induced landslides, a low suction range (0 to 50 kPa) or positive pore pressure is anticipated (Gallage & Uchimura 2016). The shear strength under the wetting process is vital in terms of slope stability. During rainfall, water content increases, matric suction decreases and the soil state changes from a drying path to a wetting path. During wetting, the reduction of shear strength occurs. Thus wetting shear strength triggers shear deformation (Guan, Rahardjo & Choon 2010). A study conducted on remoulded samples from rainfall-induced landslides at Salt Range, Pakistan revealed that the shear strength decreases with the increasing degree of saturation (Farooq, Rogers & Ahmed 2015). The shear strength of soil is greatly reduced when it is saturated (Cogan, Gratchev & Wang 2018).

Springman et al. (2013) found from a test site experiment that the changes in suction in unsaturated soils layers for small rainfall events during summer months are minimal. On the other hand, the reduction of suction is very high during winter months, even for the same amount of rainfall. Moreover, Zhang, Jiao and Yang (2000) reported that suction changes due

to precipitation depend on the permeability, water content and degree of satuation of soil (Springman et al. 2013).

Research reveals that unsaturated soil mechanics play a key role in the soil characteristics of rainfall-induced landslides.

2.3.3 Unsaturated soils

As indicated above, to understand the failure mechanism of rainfall-induced landslides, the study of unsaturated soils mechanics is pertinent (Rahardjo, Satyanaga & Leong 2012). There are three types of unsaturated soils which have challenging characteristics: collapsible soils, expansive soils and residual soils (Fredlund, Rahardjo and Fredlund, 2012). The slopes consisting of residual soils are subject to shallow landslides.

Residual soils, alluvium, colluvium and filled material which are above groundwater level are some examples of unsaturated soils. Regmi et al. (2013) reported from the study of 275 landslides in Central Nepal Himalaya that shallow landslides occur in residual soils and colluvium. Rahardjo, Satyanaga and Leong (2012) also found that in many steep residual soil slopes, rainfall-induced landslides occur. Karthikeyan, Toll and Phoon (2008) discovered that shallow landslides normally occur in residual soils slopes during severe rainfall event.

Type of soil materials is also a contributing factor. Gul (2015) conducted a study of colluvium properties and related environmental issues in Turkey. This revealed that the grading of colluvium from fourteen samples showed it is comprised of 68% to 98.5% gravel, 1.5% to 31% sand and 0% to 4% fines. It means colluvium consists of coarse-grained soils

Clay minerology within the slopes is also a contributing factor for rainfall-induced landslides in the Nepalese Himalayas (Dahal 2012). Admadi-Adli, Huvaj and Toker (2014) reported that slopes consisting of finer soil takes longer to fail during rainfall due to higher suction. To fail, they need a longer duration of rainfall of the same intensity.

Higher intensity rainfall of short duration a may trigger a landslide in coarser soils as opposed to finer soils. However, low intensity rainfall of similar durations may trigger a landslide in both coarser and finer soils (Admadi-Adli, Huvaj & Toker 2014).

Houston (2014) found that unsaturated soils have lower compressibility and higher shear strength compared to saturated soils while Fredlund, Rahardjo and Fredlund (2012) revealed that suction is the key property of unsaturated soil.

A better indicator of the moisture state of unsaturated soil is matric suction (Houston 2014). In a study conducted by the University of Malaya, it was found that matric suction increases in soils of high plasticity and also with increasing silt content. Vegetation increases matric suction by protecting a slope (Khalilnejad et al. 2013). The functions of suction are hydraulic conductivity, shear strength, compressibility and swelling potential of unsaturated soil. Total suction is the sum of matric suction and osmotic suction. The presence of salt or contaminants affects the osmotic suction (Sreedeep & Singh 2011).

Clayey soil will have higher matric suction compared to silt and sand at a particular degree of saturation. This is because clay soil can hold more moisture than other types (Houston 2014). Field observations show that significant suction in excess of 80 kPa can appear during dry periods in Singapore. But, with minor rainfall, suction can be lost and positive pore water pressure up to 5 kPa can develop to a depth of 1 to 2 m (Karthikeyan, Toll & Phoon 2008).

It is interesting to note the behaviour of unsaturated soils under the influence of water. Brooks and Corey (1964) and Fredlund and Rahardjo (1993) reported that the hydraulic function of unsaturated soils varies with moisture content in unsaturated conditions (Tofani et al. 2006).

As the key properties of unsaturated soils are the soil water characteristics curve and hydraulic conductivity, it is vital to investigate them in more detail.

2.3.4 Soil water characteristics curve

Matric suction, which was explored in some detail in Section 2.3.2, is the key variable in unsaturated soil mechanics (Lu 2008). The SWCC shows the relationship between the suction and water content of a soil (Guan, Rahardjo & Choon 2010). The SWCC is the main fundamental property of unsaturated soil mechanics and is influenced by the initial moisture content and stress state such as the net normal stress (Heshmati & Motahari 2012). The SWCC

is related to pore water pressure and moisture content (Bordoni et al. 2015a). A typical SWCC is illustrated in Figure 2.3.

Unsaturated soil properties such as the SWCC and hydraulic conductivity function play a crucial role in the performance of unsaturated slopes. The SWCC can be defined in terms of the saturated and residual volumetric water contents, AEV and desaturation rate as shown in Figure 2.3. The AEV, which represents the size of the particles, is the most important parameter influencing the SWCC and instability. Coarser soils have a smaller AEV whereas finer soils have a higher AEV (Admadi-Adli, Huvaj & Toker 2014).

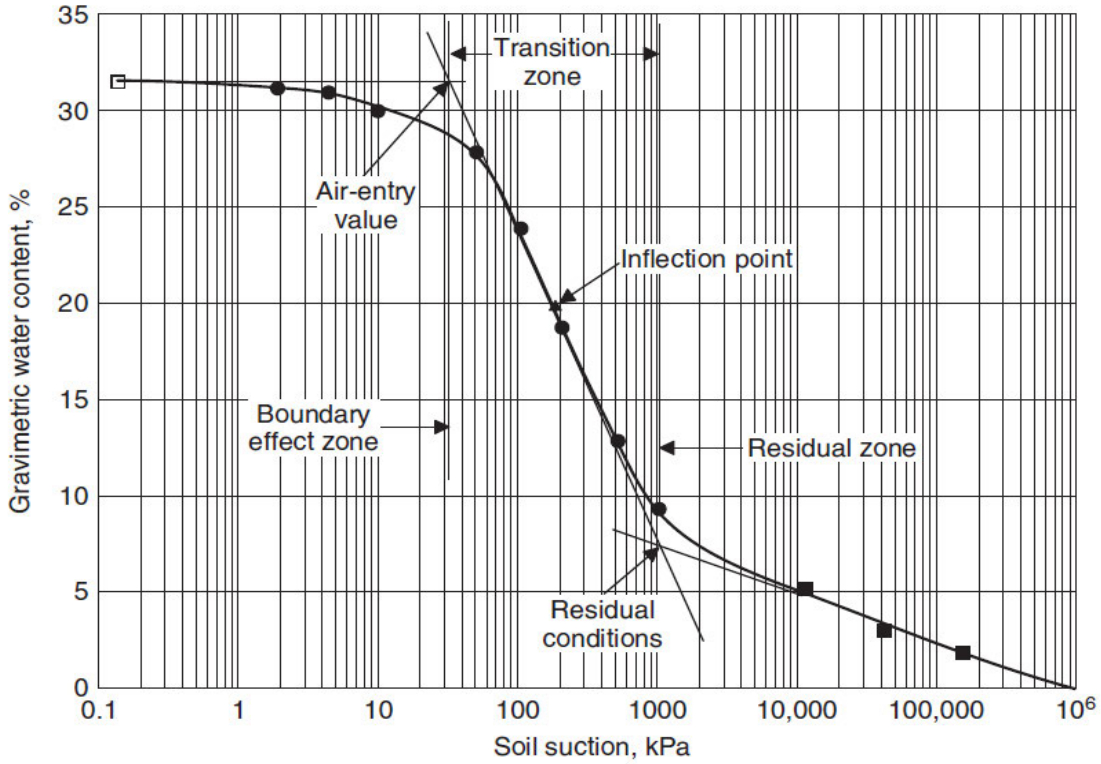

Figure 2.3: Typical SWCC showing main zones (source: Fredlund et al. 2012)

The factors influencing the SWCC are the type of soil, measurement range, equilibration time and amount of salt or contaminants. Prior to measuring total suction, an initial chemical analysis is required as the presence of salt or contaminants considerably influences suction (Sreedeep & Singh 2011). It has been found that initial dry density has a great influence in the SWCC (Zhou, Yuen & Tan 2014). According to Yang et al. (2004), the shape of the SWCC is similar to the particle size distribution (Zhou, Yuen & Tan 2014).

Fredlund and Rahardjo (1993) discovered that the water content of soil in a drying path is higher than that of a wetting path at a given matric suction. The difference between the drying SWCC and wetting SWCC is called hysteresis (Guan, Rahardjo & Choon 2010). Gofar, Lee and Kassim (2008) and Yeh, Lee and Lee (2008) advised that at the onset of rainfall-induced landslides, a low suction range (0 to 50 kPa) or positive pore pressure is anticipated. Gallage and Uchimura (2010) concluded that at a low suction range, fine-grained soils show substantial hysteresis. Unsaturated shear strength is affected by hysteresis (Gallage & Uchimura 2016). Thus hysteretic response is important in analysing rainfall-induced landslides (Likos, Lu & Godt 2014). The degree of saturation is a better parameter than the moisture content to indicate the wetting process (Houston 2014).

Matric suction test results using a filter paper method are affected by various factors such as the quality and type of filter paper, hysteresis on wetting and drying and equilibration time. With increasing moisture content, matric suction decreases. But the rate of decrease in matric suction up to an optimum moisture content is much greater that the rate of decrease after the optimum moisture content (Kim et al. 2015).

Lu and Likos (2006) and Khalili and Zarbargashi (2010) highlighted the relationship between effective stress and suction as a suction stress characteristic curve (SSCC) (Likos, Lu & Godt 2014).

Various methods have been proposed to estimate the SWCC. Chin, Leong and Rahardjo (2010) studied 31 coarse-grained and 31 fine-grained soils and developed a method of estimating SWCC using one measured point involving D_{50} and an adjustable parameter related to Fredlund and Xing's (1994) equation for the range of suctions from 10 kPa to 500 kPa. This method is simpler and better than other one-point estimating methods for the SWCC.

However, Phoon and Kulhawy (1999a and 1999b) indicated uncertainties in estimating the curve-fitting parameters of the SWCC due to inherent variability, measurement error and transformation uncertainty (Zhou, Yuen & Tan 2014). According to Sillers and Fredlund (2004), the residual suction is presumed to be of 3000 kPa regardless of the soil types (Zhou, Yuen & Tan 2014).

Fredlund, Sheng and Zhao (2011) reported that the use of the SWCC to estimate in-situ suction by geotechnical engineers was discouraged due to the fact that the SWCC is affected by hysteresis and proposed a method of estimating the wetting SWCC from the drying SWCC. The drying SWCC is usually measured in the lab while the wetting SWCC can be calculated using soil classification. For most empirical SWCCs, the changing variable between drying and wetting is parameter "a" in Equation (1). Maximum, minimum and median suction can be estimated. If measured values are not available to estimate the wetting SWCC from the drying SWCC, a shift is suggested of 25% for sands; 50% for silts and 100% for clays.

Fredlund and Xing (1994) developed the following Equations (1) and (2) for the SWCC for the full range of matric suction from zero to 10^6 kPa (Vanapalli et al. 1996):

$$\theta = C(\psi) x \theta_s [1/ln(e + (\psi/a)^n]^m \quad (1)$$

$$C(\psi) = ln\,[1 + (\frac{\psi}{\psi_r})]/\ln\,[1+(\frac{1000000}{\psi_r})] \quad (2)$$

where θ is the volumetric water content; θ_s is the saturated volumetric content; ψ is the matric suction; and a n and m are model parameters. Model parameter a is in kPa whereas n and m are dimensionless. $C(\psi)$ is the correction factor; ψ_r is the matric suction at the residual volumetric content θ_r.

When the parameters n and m are fixed, parameter a with a unit of kPa is related to AEV. Parameter a is normally higher than AEV. In the case of small values for parameter m, parameter a can be assumed to be equal to AEV. Parameter n rules the slope of the SWCC. The correction factor $C(\psi)$ becomes 1 at low suctions. Matric suction at residual water content (ψ_r) is usually in the range of 1500 to 3000 kPa (Fredlund & Xing 1994). But the suction value at residual water content Ψ_r can be assumed to be 3000 kPa as this produces a realistic shear strength according to Vanapalli et al. (1996).

After reviewing many equations for the SWCC, Leong and Rahardjo (1997) recommended the empirical model proposed by Fredlund and Xing (1994) which includes Equations (1) and (2) as it provided the best fit to the measured values.

The soil parameters of Equation (1) such as a, n and m for the tested soils can be estimated using EXCEL SOLVER by applying an optimisation technique. The squared sum of normalised residuals (SSNR) as noted below in Equation (3) is minimised:

$$\text{SSNR} = \sum_1^n((\theta_m - \theta_e)/\theta_m)^2 \quad (3)$$

where θ_m is the measured water content and θ_e is the estimated water content.

Chin, Leong and Rahardjo (2010) published the results of a, n and m for 30 coarse-grained soil samples. Based on these results, the following range for a, n and m can be assumed for any study: a from 0.1 to 5; n from 0.1 to 15 and m from 0.1 to 2.

Schnellman, Rahardjo and Schneider (2015) discovered that the effective degree of saturation (S_e) is the key factor of the unsaturated soil property function (USPF) of coarse-grained soils. The effective degree of saturation is shown below in Equation (4):

$$S_e = (S_r - S_{res})/(1 - S_{res}), \text{ where } S_e > 0 \quad (4)$$

where S_e is the effective degree of saturation; S_r is the degree of saturation and S_{res} is the residual degree of saturation.

Brooks and Corey (1964) and Van Genuchten (1980) used the effective degree of saturation as the controlling parameter of the USPF. However, the effective degree of saturation is influenced by the residual degree of saturation. Vanapalli et al. (1996) suggested that the residual state for gravels, sands and silts occur when the suction range is between 0 and 200 kPa whereas it occurs between 500 and 1500 kPa for clays (Schnellman, Rahardjo & Schneider 2015).

It has been emphasised in earlier sections that the vulnerability of a slope to rainfall-induced landslides is highly dependent on hydraulic properties. Further literature investigating this aspect is highlighted below.

2.3.5 Hydraulic conductivity

Suradi et al. (2014) reported that normally, rainfall is unlikely to trigger slope failure in soils with high hydraulic conductivity (k_t >80 mm/h) because no rainfall event can develop a wetting front in these slopes.

At the other end of the spectrum, rainfall events may not trigger instability in slopes with very low hydraulic conductivity (k_t < 0.8 mm/h) due to very small infiltration into the slopes, with most of the rainfall becoming runoff (Suradi et al. 2014).

Antecedent rainfall affects the stability of both high conductivity soils (e.g. k_t is 10^{-4}m/s or 360mm/h) and low conductivity soils (k_t is 10^{-6}m/s or 3.6mm/h). However, the stability of a low conductivity soil slope is more significantly affected than the stability of a high conductivity soil slope (Rahimi, Rahardjo & Leong 2011). Lee, Gofar and Rahardjo (2009) suggested that a long duration of rainfall affects the slope of soils with low permeability and vice versa.

The saturated permeability of soil which is its infiltration capacity plays a key role in the stability of shallow landslides (Yubonchit et al. 2017). To understand the hydrological response of soil slopes to a rainfall event, the pore water pressure was measured in most studies while the moisture content was measured in some others (Tohari 2018). The relationship between hydraulic conductivity and suction is termed the hydraulic conductivity function or K function (Dominguez 2007). In unsaturated soils, the volumetric water content and coefficient of permeability are affected by the combined changes in void ratio and matric suction (Fredlund, Rahardjo & Fredlund 2012; Zhang et al. 2016).

2.3.6 Shear strength characteristics of unsaturated soils

The shear strength of unsaturated soils is affected by moisture content. Farooq, Rogers and Ahmed (2015) conducted a study on remoulded samples from rainfall-induced landslides at Salt Range, Pakistan, finding that the shear strength decreases with an increasing degree of saturation whereas Cogan, Gratchev and Wang (2018) revealed that the shear strength of soil is greatly reduced when it is saturated.

Krahn, Fredlund and Klassen (1989), Rahardjo et al. (1995) and Kim et al. (2004) discovered that the shear strengths of soil under a drying process (during a hot and dry climate) and a wetting process (during rainy weather) are different. The shear strength under a wetting process is vital in terms of slope stability. During rainfall, the water content increases and matric suction decreases. The soil state changes from a drying path to a wetting path and during wetting, the shear strength reduces. Thus, the wetting shear strength triggers shear deformation (Guan, Rahardjo & Choon 2010).

A study performed in Malaysia using a consolidated drained triaxial test on unsaturated samples revealed a liner relationship between shear strength and matric suction (Taha, Hossain & Mofiz 2000). Key findings of past research by Escario and Saez (1986), Fredlund and Rahardjo (1993), Vanapalli et al. (1996), Wheeler and Sivakumar (2000) and Cunningham et al. (2003) on unsaturated soils are as follows (Sheng, Zhou & Fredlund 2011):

- Higher matric suction results in higher shear strength under the same vertical pressure and confining pressure.
- Higher vertical pressure or confining pressure results in higher shear strength under the same matric suction.
- There is a non-linear relationship between shear strength and matric suction.
- At low matric suction, shear strength rises promptly and then evens out or decreases.

Graphical representation of above four key findings is demonstrated in Figures 2.4a to 2.4c.

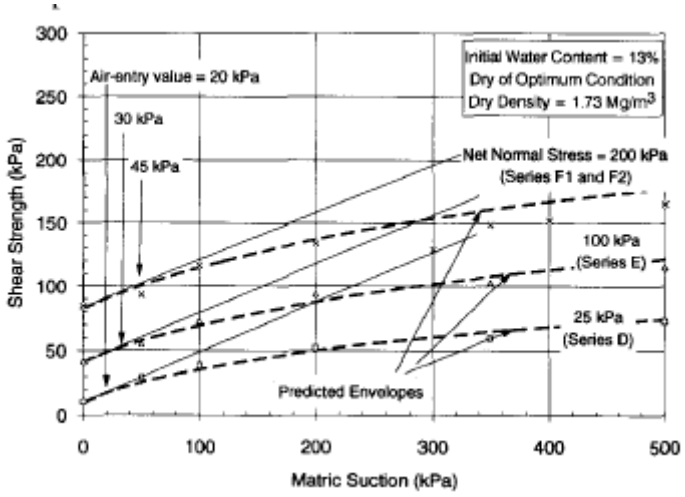

Figure 2.4a: Shear strength variation with matric suction at different net normal stress for specimens at dry of optimum moisture conditions (Source: Vanapalli et al. 1996)

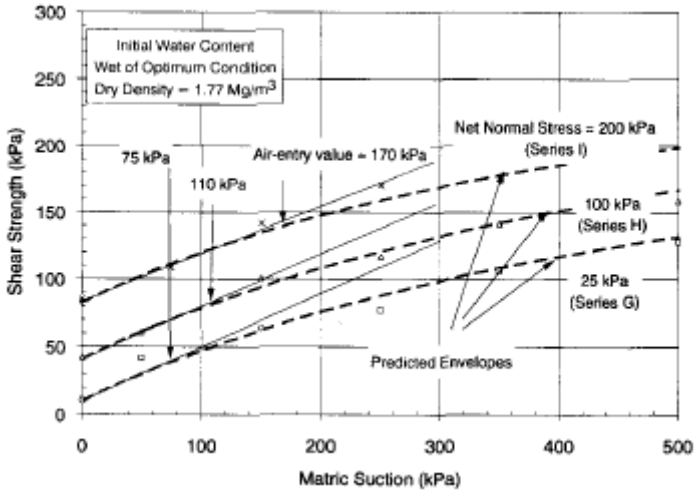

Figure 2.4b: Shear strength variation with matric suction at different net normal stress for specimens at wet of optimum moisture conditions (Source: Vanapalli et al. 1996)

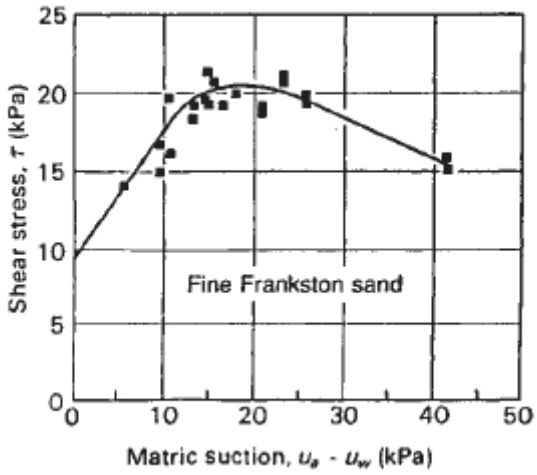

Figure 2.4c: Relationship of shear stress with matric suction under low applied matric suctions (Source: after Donald 1956; Fredlund, Rahardjo & Fredlund 2012)

Vanapalli et al. (1996) revealed that the shear strength of unsaturated soil depends on the amount of water present in the soil pores and thereby the matric suction while Vilar (2006) advised that the shear strength envelope of unsaturated soils with suction varies in a non-linear form.

Skempton (1964), Kenney (1967) and Townsend and Gilbert (1973) showed that the following factors are significant in shear behaviour (Li et al. 2013):

- Liquid limit and plastic index
- Particle shape (symmetry and smoothness)

- Stress history (over-consolidated ratio (OCR))
- Testing methods (triaxial, ring shear or direct shear)
- Testing conditions (normal stress level, shearing rate)

2.3.7 Shear strength equations of unsaturated soils

It is important to note the shear strength equations developed for unsaturated soils over the recent years. Fredlund (2000) has devised the following shear strength Equation (5) for unsaturated soil (Conte & Troncone 2012):

$$\tau_f = c' + (\sigma - u_a)tan\emptyset + P\,(u_a - u_w)tan\emptyset \quad (5)$$

where τ_f is the failure shear stress; c' is the effective cohesion; σ is the total normal stress; u_a is the pore air pressure; $\emptyset$ is the angle of shearing resistance; u_w is the pore water pressure; P is a parameter from 0 to 1 and $(u_a - u_w)$ is the matric suction.

On the other hand, Lu and Likos (2006) introduced suction stress σ^s as follows in Equations (6) and (7):

$$\tau_f = c' + (\sigma - u_a)tan\emptyset + C_\psi \quad (6)$$

$$\sigma^s = C_\psi / tan\emptyset' \quad (7)$$

where C_ψ is the apparent cohesion in unsaturated soils. Apparent cohesion C_ψ is controlled by interparticle bonding from capillarity and physiochemical forces and water distribution in the pores of soil (Jotisankasa & Mairaing 2010).

Futhermore, Bordoni et al. (2015a) defined suction stress as follows in Equation (8):

$$\sigma^s = -(u_a - u_w)\,S_e \quad (8)$$

where σ^s is the suction stress; u_a is the pore air pressure; u_w is the pore water pressure and S_e is the degree of saturation.

The effective stress σ' is provided by Equation (9) (Bordoni et al. 2015a):

$$\sigma' = (\sigma - u_a) - \sigma^s \quad (9)$$

The suction stress is paramount in slope stability analysis of steep unsaturated slopes with a deep groundwater table (Jotisankasa & Mairaing 2010). Suction stress increases with matric suction and vertical stress (Kim, B-S et al. 2010).

Lu, Godt and Wu (2010) introduced a closed form equation for effective stress in unsaturated soil which is related to the SWCC by two pore parameters, air entry pressure and pore spectrum number, as shown in Equations (10a) and (10b). These equations were validated for a range of materials from sands to clays. Equation (10a) is for saturated soil and Equation (10b) is for unsaturated soil.

$$\sigma' = \sigma - u_a + (u_a - u_w) \text{ when } (u_a - u_w) \leq 0 \quad (10a)$$

$$\sigma' = \sigma - u_a + \frac{(u_a - u_w)}{(1+[v(u_a - u_w)]^t)^{\frac{(t-1)}{t}}} \quad \text{when } (u_a - u_w) \geq 0 \quad (10b)$$

where v and t are empirical fitting parameters; v is the inverse of air entry pressure and t is the pore size distribution parameter. A new shear strength criterion for unsaturated soils is not required because of Equations (10a) and (10b) according to Lu, Godt and Wu (2010).

Moreover, the extended Mohr-Coulomb shear strength equation for unsaturated soils can be written in Equations (11) and (12) as follows (Montrasio, Valentino & Terrone 2014):

$$\tau = c' + \sigma' tan\emptyset + C_\psi \quad (11)$$

where C_ψ is the apparent cohesion which is a function of the matric suction.

$$C_\psi = A\, S_r(1 - S_r)^\lambda \text{ x } (1 - m)^\alpha \quad (12)$$

where A, α and m are model parameters. Model parameter A depends on the type of soil whereas α and m are constant for a wide range of soils; S_r is the degree of saturation and λ is constant for a wide range of soils.

Interestingly, there are two parameters controlling the behaviour of unsaturated soils as follows (Houston 2014):

- Net normal stress $(\sigma - u_a)$
- Matric suction $(u_a - u_w)$

Matshusi and Matsukra (2006) introduced a way to estimate cohesion from the volumetric water content of unsaturated soil as shown in Equation (13).

$$\tau = \sigma' tan\emptyset' + C\ x\ e^{-\mu\theta} \quad (13)$$

where C is the maximum cohesion when the water content, θ is zero; θ is the volumetric water content of soil and μ is the susceptibility coefficient.

Dev, Pillai and Robinson (2016) identified that the friction angle obtained from a triaxial test is higher than that from a shear box test for fine soils due to the larger clay content whereas the friction angle for sand obtained from a triaxial test is lower than that from a shear box test. The undrained shear strength is lower than the drained shear strength for normally consolidated clays. On the flip side, for over-consolidated clays, the undrained strength is higher than the drained shear strength (Duncan & Wright 2005).

2.3.7.1 Apparent cohesion and friction angle of unsaturated soils

Michaels (1959) reported that in unsaturated compacted clay, cohesion decreases with a reduction of moisture content when the moisture content is below the optimum moisture content (Tilgen 2003). Kong and Tan (2000) revealed that in expansive soil, cohesion reduces with increasing moisture content whereas internal friction angle reduces drastically with an increasing moisture content when it is within the plastic limit. But it remains the same after the moisture content passes the plastic limit (Tilgen 2003).

Direct shear tests and suction tests were carried out on clayey samples at different moisture contents at the Middle East Technical University, Turkey. These showed that the angle of internal friction decreases with an increasing moisture content. On the other hand, cohesion increases when the moisture content increases up to the optimum moisture content and then reduces afterwards. The suction test results indicated that the shear strength increases when the suction increases (Tilgen 2003).

Tests were conducted on two silty samples using modified direct shear test equipment to understand the effects of wetting and drying on the shear strength at low suction. It was discovered that the apparent cohesion increases with increasing suction. However, the internal friction angle of friction is not affected by suction and hysteresis (Gallage & Uchimura 2016).

Depending on whether the clay is normally consolidated or over-consolidated, the effective shear strength parameters will vary. The cohesion (c') will be zero and angle of internal friction ($\emptyset'$) will be constant for normally consolidated clays. On the other hand, in the case of over-consolidated clays, the cohesion will be greater than zero and the angle of internal friction will be smaller than that of normally consolidated soil (Duncan & Wright 2005).

Shen, Jiang and Thornton (2016) revealed that the peak friction angle is independent of matric suction but is affected by packing density whereas apparent cohesion increases with matric suction in a non-linear fashion at a decreasing rate.

2.3.7.2 Friction angle due to matric suction

Fredlund, Rahardjo and Gan (1987) identified a non-linear relationship between matric suction and shear strength. Equation (14) with friction angle due to matric suction $\emptyset^b$ was proposed by Fredlund, Morgenstern and Widger (1978):

$$\tau_f = c' + (\sigma - u_a)tan\emptyset' + (u_a - u_w)tan\emptyset^b \quad (14)$$

Fredlund, Rahardjo and Gan (1987) found that $\emptyset^b$ approaches $\emptyset$ when matric suction is low (Ran et al. 2018). Ahmad-Adli, Huvaj and Toker (2014) discovered from back analysis that $\emptyset^b = 0.5\emptyset'$ which is also a rule of thumb.

Studies on granite residual soils in Malaysia proved that the shear strength is affected by the change in confining pressure rather than the change in matric suction. It was found from consolidated drained triaxial tests on residual soils that the effective friction angle is not affected by saturated or unsaturated conditions. The rate of change in shear strength due to matric suction is described by $\emptyset^b$ which is found to be 17.8 degrees for residual soils (Taha, Hossain & Mofiz 2000). Ho and Fredlund (1982) revealed that $\emptyset^b$ is 15.3 degrees for undisturbed decomposed granite from Hong Kong (Taha, Hossain & Mofiz 2000).

Abdullah et al. (2013) tested Malaysian residual soils and revealed that $\emptyset^b$ is 11.7 degrees for fine-grained soil (c'= 20; $\emptyset'$ =27, PI=20) whereas $\emptyset^b$ is 17.9 degrees for coarse-grained soil (c'= 22; $\emptyset'$ =33, PI=27.4).

Zhang et al. (2014) recommended an approach to analyse slope stability using the friction angle due to matric suction of $\emptyset^b$ in an extended Mohr-Coulomb Equation. When the AEV is less than 1 kPa, $\emptyset^b$ is considered to be zero. When the AEV is between 1 and 10 kPa, a non-linear equation for estimating $\emptyset^b$ can be used. On the other side of the spectrum, $\emptyset^b$ is assumed to be 15 degrees when the AEV is between 10 and 100 kPa. It is equal to the effective friction angle, $\emptyset'$ when AEV is greater than 200 kPa where the matric suction is around 100 kPa around geotechnical structures.

Table 2.2 summarises equations for shear strength and suction stress or matric suction with cited reference for unsaturated soils.

Table 2.2: Shear strength equations for unsaturated soils

No.	Equation No.	Equation	Reference
1	(5)	$\tau_f = c' + (\sigma - u_a)tan\emptyset + P\,(u_a - u_w)tan\emptyset$	Fredlund (2000)
2	(6)	$\tau_f = c' + (\sigma - u_a)tan\emptyset + C_\psi$	Lu and Likos (2006)
3	(7)	$\sigma^s = C_\psi / tan\emptyset'$	Lu and Likos (2006)
4	(8)	$\sigma^s = -(u_a - u_w)\,S_e$	Bordoni et al. (2015a)

5	(9)	$\sigma' = (\sigma - u_a) - \sigma^s$	Bordoni et al. (2015a)
6	(10a)	$\sigma' = \sigma - u_a + (u_a - u_w)$ when $(u_a - u_w) \leq 0$	Lu, Godt and Wu (2010)
7	(10b)	$\sigma' = \sigma - u_a + \frac{(u_a - u_w)}{(1+[v(u_a - u_w)]^t)^{\frac{(t-1)}{t}}}$ when $(u_a - u_w) \geq 0$	Lu, Godt and Wu (2010)
8	(11)	$\tau = c' + \sigma' tan\emptyset + C_\psi$	Montrasio, Valentino & Terrone (2014)
9	(12)	$C_\psi = A\, S_r(1 - S_r)^\lambda$ x $(1 - m)^\alpha$	Montrasio, Valentino & Terrone (2014)
10	(13)	$\tau = \sigma' tan\emptyset' + C\ x\ e^{-\mu\theta}$	Matshusi and Matsukra (2006)
11	(14)	$\tau_f = c' + (\sigma - u_a) tan\emptyset' + (u_a - u_w) tan\emptyset^b$	Fredlund, Morgenstern and Widger (1978)

2.3.7.3 Apparent friction angle

Sassa (1988) proposed a geotechnical model for the motion of landslide using the concept of apparent friction angle ($\emptyset_a$). A model for change of the apparent friction angle, ($\emptyset_a$) using the concept that landslide is a two-layer structure such as debris layer and sliding zone as shown in Figure 2.5 was suggested by Wang and Sassa (2000).

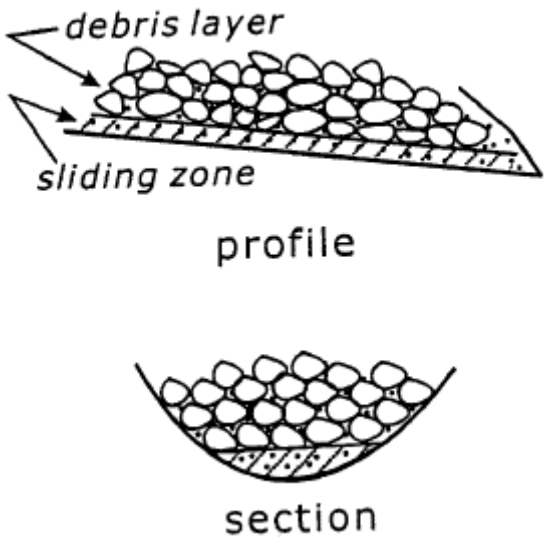

Figure 2.5: Demonstration of two-layer structure of landslide mass (Source: Wang & Sassa 2000)

Wang and Sassa (2000) introduced a new factor called "accumulation possibility of excess pore pressure (B_{ss})" which is an empirical index depends on many factors such as soil properties in the sliding zone, existing ground water level, drainage condition, etc. The reason for B_{ss} is to quantify various types in the travelling path of an actual landslide. There are three types of shear behaviour of soils in the sliding zone such as A-type, B-type and C-type as described in Table 2.3.

Table 2.3: Description of shear behaviour types in the sliding zone and suggested values for B_{ss} (Source: Wang & Sassa 2000)

Shear behaviour type	Suggested range of B_{ss}	Description
A-type	0 - 0.1	Unsaturated sliding mass moving on dry surface; There is no pore pressure built-up; It is case of dry soil landslide; The shear resistance at the steady state is the drained residual shear strength; The apparent friction angle is the residual friction angle.
B-type	0.9 – 1.0	Saturated or unsaturated sliding mass moving on fully saturated surface; Saturated sliding mass moving on

		impermeable surface; It is an ideal saturated undrained condition equivalent to rapid long distance run-out landslides.
C-type	0.1 – 0.9	Saturated sliding mass moving dry and permeable surface; Many actual landslides fit into this type.

The apparent friction coefficient, $tan\emptyset_a$ can be calculated by using Equation (15) as shown below (Wang & Sassa 2000):

$$tan\emptyset_a = (\tau_{ss}(h, B_{ss}))/\sigma(h) \quad (15)$$

where $\tau_{ss}(h, B_{ss})$ is the shear resistance at the steady state in the completely undrained condition; h is the thickness of the sliding mass; $\sigma(h)$ is the normal stress. Figure 2.6 illustrates apparent friction coefficient, $tan\emptyset_a$ where important parameters such as τ_{ss} and $\emptyset$, effective residual friction angle can be measured using ring shear test and Δu_{ss} is the change in pore pressure.

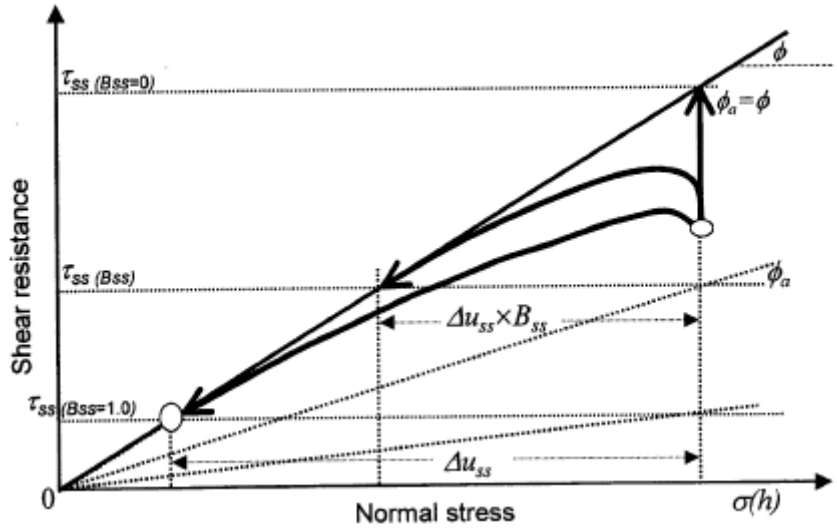

Figure 2.6: Change model of apparent friction coefficient, $tan\emptyset_a$ (Source: Wang & Sassa 2000)

As measuring the shear strength of unsaturated soils is cumbersome, the prediction of shear strength is an important and useful alternative.

2.4 Prediction of shear strength and shallow landslides

Many shear strength prediction models have been developed over the years for different types of soils. Garven and Vanapalli (2006) analysed nineteen empirical equations (of which six used the SWRC (soil-water retention curve) and others used mathematical formulations) to predict the shear strength of twenty different soils such as natural soils, expansive soils, tailings and residual soils (most being clayey material) and found none to predict shear strength reliably.

Garven (2009) discovered that there are 25 empirical equations available to predict the shear strength of unsaturated soil. Thirteen equations used the SWCC and saturated shear strength parameters while other equations were developed using mathematical fitting models and empirical relationships. Certain equations are suitable for particular type of soils. For example, Oberg and Sallfors's approach (1995) is reasonable for silt and sands while Tekinsoy, Kayayadelen, Keskin and Soylemez's approach (2006) is preferred for fine-grained soils.

Vilar (2006) formulated a method to obtain preliminary estimates of the shear strength of unsaturated soils using saturated shear strength parameters and either one set of test results carried out on air-dried samples or results from the controlled suction scenario where suction larger than the maximum suction is expected.

Vanapalli et al. (1999) and Kim et al. (2010) advised that the effect of vertical stress on the SWCC is minimal under low confining pressure conditions. Fine content and the structural retention of soils have a more significant effect on the SWCC at low confining pressure conditions.

Kim and Borden (2011) have used models via Fredlund et al.'s approach, Vanapalli et al.'s approach and Khalili and Khabbaz's approach, which are described below. The first model, from Fredlund et al.'s approach (1996), is shown in Equations (16) and (17):

$$\tau_f = c' + (\sigma_n - u_a)tan\emptyset' + (u_a - u_w)[(\Theta^K)(tan\emptyset')] \quad (16)$$

$$K = -0.0016I_P^2 + 0.0975I_P + 1 \quad (17)$$

where τ_f= shear strength of unsaturated soil; *c'* = effective cohesion; Ø' = effective internal friction angle; σ_n= normal stress; u_a= pore air pressure; u_w= pore water pressure; Θ = normalised water content; K = model parameter; I_P =plasticity index.

The second model comes from Vanapalli et al.'s approach (1996) as highlighted in Equation (18):

$$\tau_f = c' + (\sigma - u_a)tan\emptyset' + (u_a - u_w)[(tan\emptyset')(\Theta_w - \Theta_r)/(\Theta_s - \Theta_r)] \quad (18)$$

where τ_f= shear strength of unsaturated soil; *c'* = effective cohesion; Ø' = effective internal friction angle; σ = normal stress; u_a= pore air pressure; u_w= pore water pressure; Θ_w= volumetric water content; Θ_r= residual volumetric water content; Θ_s = volumetric saturated water content.

The last model, introduced by Khalili and Khabbaz (1998), is presented in Equations (19) and (20):

$$\tau_f = c' + (\sigma - u_a)tan\emptyset' + (u_a - u_w)_f[\chi(tan\emptyset')] \quad (19)$$

where $\chi = [(u_a - u_w)_f/(u_a - u_w)_b]^{0.55}$ for $(u_a - u_w) > (u_a - u_w)_b$.

$\chi = 1$ for $(u_a - u_w) < (u_a - u_w)_b$ (20)

where $(u_a - u_w)_f$ = matric suction of specimen at failure condition

$(u_a - u_w)_b$= air entry value.

Kim and Borden (2011) tested the above three models for fifteen soils including low plastic clays, silts, sandy soils and soils that desaturate faster (n value of the SWCC is greater than 2) in the range of 0 to 200 kPa for the shear strength. The prediction by all three models was good for low plasticity clays whereas it was poor for silts. On the other hand, models tend to overestimate the shear strength for sandy soils. However, the prediction from Khalili and Khabbaz's model was better for low plasticity clays, sandy soils and soils that desaturate faster.

Vanapalli et al. (1996) suggested two approaches to predict the shear strength of unsaturated soils: one using saturated strength parameters, matric suction, normalised water content and model parameter K as described in Equation (16) and the other using saturated shear strength parameters, matric suction, and residual water content as highlighted in Equation (18). Both models were tested with glacial till and a good correlation was found between the predicted and measured values of the shear strength. Fredlund et al. (1996) also tested the model using saturated strength parameters, matric suction, normalised water content and model parameter K as shown in Equation (16) with tuff soil from Hong Kong and it displayed a good agreement with the measured shear strengths.

In the next section, rainfall-induced landslides will be analysed and the influence of soil characteristics, slope characteristics and rainfall characteristics will be explored.

2.4.1 Analysis of rainfall-induced landslides

Figure 2.7 provides the failure mechanism of rainfall-induced landslides. Generally, such landslides are caused by the changes in the pore water pressure and seepage forces (Zhu & Anderson 1998; Gerscovich, Vargas Jr & de Campos 2006; Kitamura & Sako 2010; Zhang et al. 2011; Fredlund, Rahardjo & Fredlund 2012; Lu & Godt 2013; Zhang et al. 2016). Regmi et al. (2012) also identified key factors generally influencing rainfall-induced slope failures during periods of intense rainfall:

- Pore pressure
- Seepage force

The necessary condition for a landslide is the reduction in soil suction and increase in pore water pressure due to antecedent rainfall. Variation in pore water pressures during an intense rainfall event is distributed within the soil depending on the following (Tofani et al. 2006):

- Hydraulic conductivity
- Topography
- Degree of weathering and fracturing of soil
- Soil permeability and thickness, influencing the slope instability

Moreover, Lepore et al. (2012) studied the susceptibility of rainfall-induced landslides and identified landslide-inducing factors to be the aspect, slope, elevation, geological

discontinuities and geology. Further, Hsu et al. (2013) reported that the geology, landform, soil water content, degree of saturation, soil characteristics and groundwater table contribute to the risk of landslides while continuous rainfall may trigger them. Cuomo and Della Sala (2013, 2015) described how rainfall infiltration and surface runoff are key processes affecting instability which are strongly influenced by the rainfall intensity and duration, slope angle, initial soil conditions and the hydraulic and mechanical properties of the soil.

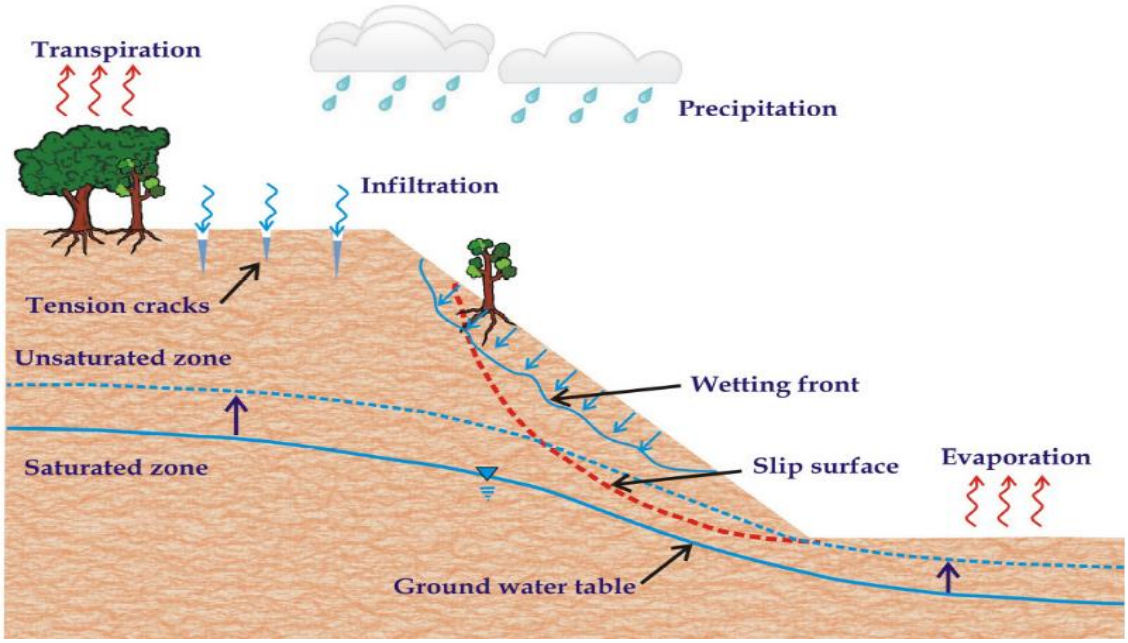

Figure 2.7: Failure mechanism of rainfall-induced landslide (Source: Rahardjo et al. 2007)

Tsaparas et al. (2002) reported that climatic conditions, soil properties and infiltration characteristics affect the stability of a slope while the key factors influencing rainfall-induced landslides include the mechanical and hydraulic properties of the slope, slope morphology, the presence of vegetation and rainfall intensity and duration (Bernardie et al. 2015). The non-dissipated pore pressure at the furthest point of the drainage boundary also influences the occurrence of a landslide (Cornforth 2005).

Rainfall infiltration drastically affects the soil suction which may trigger landslides (Chen, Lee & Law 2004). In a study in Singapore, Rahardjo et al. (1995) discovered that antecedent rainfall plays a more important role in soils with lower permeability in the slopes involving residual soils. A period of 5 days of antecedent rainfall has a major influence in the stability of slopes involving residual soils (Crosta & Frattini 2008).

Saito, Nakayama and Matsuyama (2010) identified that the reason for rainfall-induced landslides in Japan occurring with a low threshold (rainfall intensities of 1.64 to 0.42 mm/h with rainfall duration of 3 to 537 hr) compared to the previously published threshold are high relief topography, geological conditions, human interference, short and heavy rainfall and gentle and long rainfall during the East Asian summer monsoon season.

Furthermore, Godt, Baum and Chleborad (2006) advised that antecedent rainfall should be considered as it directly changes the soil moisture content in initiating landslides. For example, heavy rainfall during a dry period does not necessarily activate a landslide. On the other hand, it will create a landslide during wet periods (Ren et al. 2011).

Koizumi et al. (2019) developed a structural health monitoring system for slopes to predict rainfall-induced shallow landslides, using the initial quasi-saturated volumetric water content (IQS) where the rainfall infiltration (RI in mm/hr) and drainage, which is the unsaturated hydraulic conductivity (k_{iqs} in mm/hr), are balanced and no deformation occurs. When the RI exceeds the k_{iqs} deformation occurs and the slope fails.

Having explored in some depth the physics of landslides, the following section deals with some further highlights of detailed research into soil characteristics and types and their relationship to rainfall-induced landslides.

2.4.1.1 Soil characteristics

The Government of Hong Kong (1977) reported that loosely compacted soil slopes in Hong Kong fail abruptly during intense rainfall while the fill material may not be saturated. The reason is the loss of shear strength due to an induced high pore water pressure. It also discovered that rainfall-induced fill slope failures occur along the impermeable surface which is overlain by highly permeable soils (Chen, Lee & Law 2004).

Further, Michiue (1985) advised that the amount of water penetrating into soil from rainfall influences slope failure. Collins and Znidarcic (2004) explained that with respect to soil types, the mechanism of rainfall-induced slope failures is as follows:

Coarse-grained soils

- High infiltration rates lead to the development of positive pore water pressure and seepage forces cause the failure.

Fine-grained soils

- Low infiltration rates do not lead to the development of positive pore pressure, but loss of suction causes a decrease in the shear strength and thereby failure.

2.4.1.2 Slope characteristics

Groundwater plays an important role in many landslides. Generally, landslides occur after a few hours of torrential precipitation. Rainfall is the dominant factor in causing groundwater fluctuations (Hong & Wan 2011). The pore water pressure gradient increases due to increasing fine content and a decreased initial void ratio (Lourenco, Sassa & Fukuoka 2004).

Matsushi, Hattanji and Matsukura (2006) studied shallow landslides in Japan with permeable and impermeable bedrocks and found that slopes with permeable sandstone bedrocks where infiltrated rainwater flows through as unsaturated gravitational flow, this causes landslides at steep lower parts of the hill slopes whereas transient pore water pressure develops in the thin layer of soil overlying impermeable mudstone bedrock, creating saturated subsurface flow and causing landslides at the uppermost part of hollows.

In terms of slope angle, Bhandary et al. (2011) identified that topographies with a mean slope angle between 27 degrees and 36 degrees have higher tendencies to landslides whereas Toll (2001) discovered that slope failures occurred in sedimentary Jurong and granitic Bukit Timah formations in Singapore where the slope angle is greater than or equal to 27 degrees.

Failures are shallow if the boundary has more permeable material than the soil cover while they will be deeper if the boundary has less permeable material compared to the soil cover (Ali et al. 2014).

The soil in the slope is not homogenous and there are fractures, cracks, macropores of biotic origin and interaggregate pores (Novak, Simunek & Van Genuchten 2000; Li & Zhang 2010,

2011). The presence of cracks in the slope reduces the shear strength and advances hydraulic conductivity (Zhang et al. 2016).

2.4.1.3 Findings from previous studies on rainfall-induced slope failures

Based on detailed investigation of several rainfall-induced slope failures in Lantau Island, Hong Kong, the following points are concluded (Fuchu, Lee & Sijing 1999):

- Landslides are caused by severe rainfall on the weaker thin colluvium layer on the steep slopes.
- Failure of colluvium is induced by infiltrated water during the heavy rainfall.
- There is a strong relationship between a landslide and factors such as the bedrock geology, slope angle, vegetation cover and presence of hollows.

On the other hand, grain size and fine components have considerable impact on the initiation of rainfall-induced landslides. It was discovered from flume tests that pore pressure generation is less in coarser sands as opposed to finer sands. A pore pressure increase was noted with an increasing component of loess (Wang & Sassa 2007).

From the study of landslides in the Himalayas, it was found that the key factors contributing to rainfall-induced landslides there are (Dahal 2012):

- Soil characteristics
- Low internal friction angle of fines in the soil
- The presence of clay minerals
- Clay minerology of slope materials
- Bedrock hydrology
- Human intervention

Nian et al. (2013) conducted experiments on the shear strength behaviour of remoulded clay samples from the slip-zone area of a Daxishan reservoir landslide with varying water content and discovered that the maximum shear strength can be achieved at 15% water content. Therefore, to prevent landslides at this location, the water content should be maintained at 15% to provide the maximum shear strength.

Ali et al. (2014) conducted a study on the boundary effects of rainfall-induced landslides by comparing the hydraulic conductivity of soil cover and underlying rock. They discovered that boundary conditions affect gentle slopes more than steeper slopes. The following are concluded based on laboratory-controlled experiments on loose soil slopes under various artificial rainfall conditions (Wu et al. 2015a):

- Water infiltration causes slope deformation and induces cracks along the trailing edge of the slope.
- The rainfall infiltrates into cracks and increases moisture content and pore water pressure.
- The slope failure is closely related to slope gradient, rainfall intensity and initial matric suction condition.
- Low rainfall intensity and long duration lead to a larger scale landslide.
- When the slope is smaller, the wetting front develops more rapidly.
- When the rainwater infiltrates into a gentle slope easily, deeper landslides occur.

Yubonchit et al. (2017) found that a slope is stable during the infiltration stage if the rainfall intensity is less than the saturated permeability which is the infiltration capacity due to the remaining matric suction. On the other hand, if the rainfall intensity is equal to or higher than the infiltration capacity, then slope failure occurs during the infiltration stage.

A study conducted before and after typhoons in Taiwan revealed that locations with an elevation of 450 m to 750 m, a slope angle of 30 degrees to 55 degrees and within 300 m distance from a road or water are susceptible to large-scale rainfall-induced landslides (Tseng, Chen & Wu 2018).

2.4.1.4 Stability analysis

Collins and Znidarcic (2004) and Zhang et al. (2016) discovered two types of failure mechanism in rainfall-induced landslides. In the first, there is a considerable amount of build-up of positive pore water pressure at the lower side on the slope or the soil-bedrock interface, which ultimately paves the way to liquefaction and results in rapid movement and long run out distances (Wang & Sassa 2001; Zhang et al. 2016). In the second type, the soil is unsaturated and infiltration and a reduction of the matric suction leads to slope failure (Fredlund & Raharadjo 1993; Fourie, Rowe & Blight 1999; Zhang et al. 2016).

Two methods exist for analysing rainfall-induced landslides (Wu et al. 2015a):

- Exploring the statistical relationships between rainfall characteristics and the displacement of landslides
- Examining the physical mechanism of the rainfall infiltration process

Terlien (1998) revealed that when a large data set is available on rainfall and landslide occurrences, a statistical model for hydrological triggering thresholds can be developed whereas a deterministic model can be created if the data is limited.

In analysing rainfall-induced slope failures, the focus should be on the rainfall intensity and soil properties, in particular, the saturated coefficient of permeability k_t (Rahardjo et al. 2007). Stark and Hussain (2010) endorsed the proposal by Skempton (1964, 1985) that for remediation of reactivated landslides and comparison of back-calculated shear strength, drained residual strength should be used.

Quantification of the shear strength and hydraulic parameters is vital for evaluating the slope stability of rainfall-induced landslides (Suradi, Fourie & Saynor 2016). The stability of the slope is dominated by the shear strength of unsaturated soil and thereby the matric suction (Fredlund, Rahardjo & Fredlund 2012; Abdullah et al. 2013). The effect of suction is linearly proportional to the amount water content in the soils (Abdullah et al. 2013).

Cascini et al. (2010) concluded from modelling rainfall-induced shallow landslides of flow-type that triggering factors are local stratigraphy and initial and hydraulic boundary conditions; a flow-type landslide occurred due to a deformation mechanism caused by rainfall infiltration and springs from the bedrock.

Zhang et al. (2016) highlighted many uncertainties in the current approach to the stability analysis of rainfall-induced landslides such as geological formation, spatial variability of soil properties, uncertainty in boundary conditions and initial conditions, measurement error, statistical error due to a limited number of samples, uncertainties in the input parameters of the model and systematic error attached to the prediction model, concluding these can be overcome by applying a probabilistic approach.

The stability of a slope can be measured not only by the factor safety but also by the reliability index which is assigned to the probability of a satisfactory performance of slope (Sivakumar Babu & Murthy 2005; Penalba, Luo & Hsein Juang 2009; Park, Nikhil & Lee 2013b; Zhang et al. 2016).

The following sections deal with comparisons of prediction modelling in some detail, first reviewing variables, then types of models: statistical and physical.

2.4.2 Prediction of rainfall-induced shallow landslides

In this section, key variables in the prediction models of rainfall-induced shallow landslides such as the soil moisture content, pore pressure, deformation, rainfall and duration, as well as types of statistical and physical models are discussed. Evidence in Chapter 1 has established the vital nature of landslide prediction for humanitarian and material concerns, while Zydron et al. (2016) emphasised its importance from an economic viewpoint.

2.4.2.1 Key variables in the prediction models

Orense et al. (2004) reported that rainfall-induced slope failure can be predicted by monitoring the soil moisture content of slopes and measuring displacements. The increasing soil moisture content associated with rainwater infiltration is significant in creating slope failure. Slope failure can be predicted by monitoring changes in soil moisture content, deformation and pore water pressure.

When performing rainfall simulation tests on sandy slopes, Orense et al. (2004) and Huang et al. (2008) concluded that saturation around the toe and the associated unstable zone are indicators of retrogressive slope failures (Ching-Chuan et al. 2009).

Monitoring soil water content and pore water pressure in unsaturated soil is widely used in slope stability analysis. When the pore water pressure is less than or equal to zero, landslide prediction can be made. This prediction is based on the factor of safety calculated using the moisture content only. However, when the pore water is positive, landslide prediction can be undertaken by a factor of safety that incorporates the pore water pressure (Bordoni et al. 2015a).

Nishigaki, Tohari and Komatsu (1999) carried out rainfall tests on sandy slope models and found two phases in the soil moisture content change: wetting front progress in a downward direction and ground water rise in an upward direction by rainfall infiltration. They concluded that the in-soil moisture content is better predictor of slope failure initiation than the pore water pressure. Based on local conditions, the duration of prolonged rain needs to be determined in predicting rainfall-induced landslides (Lee et al. 2014).

2.4.2.2 Types of models

There are two types of landslide vulnerability prediction methods. The first is qualitative, which is a statistical method incorporating various factors such as the soil type, soil cover, slope angle etc. and not the failure mechanism (Park, Lee & Woo 2013a; Zydron et al. 2016). On the other hand, the second method is quantitative and considers cause-and-effect relationship between physical and instability processes or physical models such as Stability Index Mapping (SINMAP) and Iverson's model. From these two physical models, it was revealed that the key factor influencing failure is seepage force within saturated soil cover (Zydron et al. 2016).

Bordoni et al. (2015a) discovered that shallow rainfall-induced landsides can either be predicted using a rainfall threshold based on the rainfall intensity-duration relationship or using stability models by monitoring the hydrological and mechanical properties of the soil. The most widely used method of predicting shallow rainfall-induced landslides is the rainfall threshold method.

Bordoni et al. (2015a) highlighted that stability models include closed form equations (Lu & Godt 2008, 2013), physically based models (Campbell 1975; Montgomery & Dietrich 1994; Iversion 2000; Baum, Savage & Godt 2002, 2008; Montrasio & Valentino 2008) and finite element models (Cuomo & Della Sala 2013; Springman et al. 2013).

In all these models, obtaining the main soil hydrological properties such as the soil water characteristics curve (SWCC) is paramount. Furthermore, in the SWCC, the drying path is considered; the effect of the wetting path is not taken into account in most of these stability models (Bordoni et al. 2015a).

Different approaches are taken in various stability models. Ali et al. (2014) reported that infinite slope modelling is used for most stability models for rainfall-induced landslides. Selby (1993) explained that the infinite stability model is suitable for the analysis of shallow rainfall-induced landslides as the failure planes of such landslides are normally parallel to the slope surface. Wu et al. (2016) recommended limit equilibrium as effective in analysing landslides with a small depth while Rahardjo et al. (2007) reported that the limit equilibrium method provides high accuracy (Ran et al. 2018).

Gutierrez-Martin (2020), in reviewing past research, found that most widely used methods in predicting rainfall-induced shallow landslides are constructed from the principles of physics and mechanics as opposed to the approaches from empirical and statistical methods.

2.4.2.3 Physical models

Table 2.4 highlights some examples of physical models in predicting shallow landslides with references.

Table 2.4: Some examples of physical models

No.	Name of physical model	Reference
1	dSLAM	Wu and Sidle (1995); Dhakal and Sidle (2003)
2	SINMAP	Pack, Tarboton and Goodwin (2001); Morrissey, Wieczorak and Morgan (2001); Calcaterra, Riso and Di Martire (2004)
3	SHE-TRAN	Ewen, Parkin and O'Connell (2000)
4	TRIGRS	Baum, Savage and Godt (2002); Iversion (2000)
5	SLIP	Montrasio, Valentino and Quintavalla (2010); Montrasio, Valentino and Losi (2011, 2012)
6	PG_TRIGRS	Salciarini, Fanelli and Tamagnini (2017)
7	SLIDE	Liao et al. (2010)
8	SIMTOP	Kee and Ho (2009)
9	TOPMODEL	Kirkby (1997)
10	SHIA_Landslide	Aristizabal et al. (2016)

11	SHALSTAB	Dietrich and Montgomery (1998); Montgomery and Dietrich (1994)
12	HIRESSS	Salvatici et al. (2018)
13	Model proposed by Balzano et al. (2018)	Balzano et al. (2018)
14	Model proposed by Park et al. (2013a)	Park et al. (2013a)
15	Model proposed by Luo et al. (2015)	Luo et al. (2015)
16	Model proposed by Rosso et al. (2006)	Rosso et al. (2006)
17	Model proposed by Borga et al. (2002)	Borga et al. (2002)

Some of the examples of physical models in predicting shallow rainfall-induced landslides from Table 2.4 are described below.

Physically based models such as dSLAM (Wu & Sidle 1995; Dhakal & Sidle 2003), SINMAP (Pack, Tarboton & Goodwin 2001; Morrissey, Wieczorak & Morgan 2001; Calcaterra, Riso & Di Martire 2004), SHE-TRAN (Ewen, Parkin & O'Connell 2000), TRIGRS (Baum, Savage & Godt 2002; Iversion 2000) and SLIP (Montrasio, Valentino & Quintavalla 2010; Montrasio, Valentino & Losi 2011, 2012) can determine the hazard of shallow landslides using physical stability equations and rainfall. Montrasio, Valentino and Losi (2011) disclosed that these models have different levels of complexity and their quality depends on the quality of input parameters (Ono, Kazama & Ekkawatpanit 2014).

Montrasio (2000), Montrasio and Valentino (2008) and Montrasio, Valentino and Losi (2009, 2011), Montrasio, Valentino and Terrone (2014) developed the shallow landslide instability prediction model (SLIP) to analyse shallow rainfall-induced landslides (Montrasio, Valentino & Meisina 2018). SLIP dynamically considers the stability conditions of the slope, soil characteristics and rainfall amount. The SLIP model can assess the stability of shallow landslides dynamically based on rainfall and stability equations (Ono, Kazama & Ekkawatpanit 2014). SLIP is a mathematical model developed to predict rainfall-induced shallow landslides.

Factor of safety is calculated using amount of rain, slope geometry and the state, mechanical and hydrological properties of soil (Montrasio, Valentino and Terrone 2014). SLIP simplifies the concept of shallow landslides and produces a factor of safety using a limited number of geotechnical parameters (Ono, Kazama & Ekkawatpanit 2014).

On the other hand, Baum, Savage and Godt (2002) developed a transient rainfall infiltration and grid-based regional slope stability model (TRIGRS) to predict shallow landslides caused by rainfall. Baum, Godt and Savage (2010) advised that TRIGRS can be used to identify a landslide hazard zone, analyse actual rainfall and calculate the factor of safety of slopes (Zhuang et al. 2017). The TRIGRS model can be implemented to calculate the pore water pressure and factor of safety during a rainfall event (Bordoni et al. 2015b).

Lu and Godt (2008) developed a model for analysing stability using suction stress (Bordoni et al. 2015a) whereas Martinovic, Reale and Gavin (2018) introduced fragility curves based on a probabilistic approach to predict the damage by rainfall and assess the risk of landslides in a large transport network.

Mercogliano et al. (2013) developed a prototype forecasting chain of three models to predict rainfall-induced shallow landslides over a larger area comprising a physically based weather prediction model, a statistical tool for the downscaling of the rainfall maps and an advanced tool for a slope stability model consisting of hydrological and geotechnical components. Concurrently, Olivares et al. (2014) followed a similar approach and developed software for a simulation chain for predicting rainfall-induced landslides which consists of three modules: weather forecasting, drilling-down weather data to basin level and infiltration and slope stability analysis.

Tsai, Tsai and Yang (2015) discovered that uncertainty in soil parameters is not incorporated into the physical stability models and so developed a probabilistic modelling of rainfall-induced shallow landslides using a point estimate method. In this modelling, a modified Iversion model and Rosenblueth point estimate method are integrated while considering uncertainty and the correlation of soil parameters. The simulated results showed that the Rosenblueth point estimate method can accurately and efficiently predict rainfall-induced shallow landslides better than the Monte Carlo simulation method.

Salciarini, Fanelli and Tamagnini (2017) developed new probabilistic physically based computational model called PG_TRIGRS to predict landslides at a regional scale based on the deterministic approach used in the original TRIGRS model. This considers the spatial variability of probability density function (PDF) soil properties over the region and evaluates the probability of failure (PoF). It is efficient, affordable and reliable, providing excellent predictive capabilities.

Yang et al. (2012) developed a logistic regression model to predict the probability of rainfall-induced landslides in Taiwan using parameters such as the slope angle, normalised difference vegetation index (NDVI), slope roughness, total curvature, maximum elevation, total slope height, maximum hourly rainfall and total accumulated rainfall.

Zhang et al. (2018) advised that the calculation of factor of safety using a physics-based model is affected by a high degree of uncertainty at a regional scale and therefore introduced the use of the Monte Carlo method to quantitatively express uncertainties by nominating random values to physical variables (for example, cohesion, friction angle etc.) in defined interval. Zhang et al. (2016) highlighted the range of the coefficient of variation (COV) from the literature as follows:

- COV of unit weight of soil varies from 5% to 10%
- COV of water content varies from 10% to 25%
- COV of porosity varies from 10% to 30%
- COV of shear strength parameters varies from 5% to 50%

Gutierrez-Martin (2020) developed a GIS physically based emergency methodology for predicting rainfall-induced shallow landslides via zonation maps (similar to the approach used by SINMAP) by considering key landslide variables such as the critical slope angle, depth of shear plane and infiltration factor (which is the depth of the saturated portion). This can produce hazard maps with zonation based on the factor of safety with respect to shallow landslides.

Montrasio, Valentino and Losi (2012) developed both SLIP and TRIGRS models for the Emilia Romagna region in northern Italy and discovered that the SLIP model predicts better than TRIGRS model (Ono, Kazama & Ekkawatpanit 2014).

2.4.3 Risk reduction of rainfall-induced landslides

As landslides occur regularly, it is necessary to consider risk reduction measures to reduce the impacts of rainfall-induced landslides. Wang (2005) and Zhang and Tang (2006) reported that the drainage system is an effective tool in preventing rising ground water below an unstable slope during heavy rain (Sun et al. 2010). By installing a suitable drainage system, ground water rise and surface runoff can be decreased and thereby the stability of the slope can be increased (Moayedi et al. 2011).

Orense et al. (2004) revealed two approaches to minimise the damage caused by rainfall-induced landslides which they called the hard and the soft approach. The hard approach includes slope treatments like the use of retaining walls, dewatering, anchor pile walls etc. The soft approach includes the implementation of alarm and warning systems. The hard approach is not always possible due to financial and environmental constraints.

Horizontal drains and capillary barrier systems can be used as preventive and remedial techniques to reduce slope failures in residual soil while vetiver grass and the orange jasmine shrub are effective in minimising infiltration and maintaining suction during the rainfall event (Rahardjo, Satyanaga & Leong 2012).

To maintain matric suction, the common practice in Hong Kong is to provide a layer of soil-cement-lime plaster cover called chunam on the soil slopes. Another way of maintaining matric suction is to reduce the saturated permeability of the surface soil by removing the loose soil up to 3 m depth vertically and recompacting to 95% standard compaction density, as used in Hong Kong (Zhang et al. 2016).

2.4.4 Summary of literature review

A summary of the previous research in rainfall-induced shallow landslides is as follows:

- Rainfall-induced landslides require an interdisciplinary approach from the fields of engineering geology, soil mechanics, hydrology and geomorphology.

- It is clear that both intense rainfall during a short period of time and continuous or antecedent rainfall for a long period of time can initiate or activate landslides.

- Shallow landslides are initiated by the loss of suction whereas deep-seated landslides occur due to increasing pore pressure by rising ground water.

- Rainfall intensity and duration, infiltration, slope angle, type of soil (whether fine-grained or coarse-grained; or whether colluvium, residual soils or filled material), type of rock (weathered or unweathered), hydraulic conductivity, suction, presence of clay minerals and initial moisture content are the dominant factors influencing rainfall-induced shallow landslides.

- The saturated permeability of soil is an important parameter as it determines the stability of the slope during rainfall. When the rainfall intensity is less than the saturated permeability which is the infiltration capacity, then the slope will be stable. On the other hand, when the rainfall is equal to or more than the saturated permeability, then slope failure will occur during the rainfall. Koizumi et al. (2019) have developed a structural health monitoring system of slope against rainfall-induced landslides, using rainfall intensity and unsaturated hydraulic conductivity.

- The wetting front develops in two directions: the infiltration of rainfall through the surface of the slope in the downward direction and the rise of ground water through the slope in the upward direction.

- The matric suction and net normal stress are the key parameters in the characterisation of unsaturated soil. Water affects the shear strength of unsaturated soils and a better indicator of the moisture state of unsaturated soil is matric suction. Houston (2014) reported that clayey soil will have a higher matric suction compared to silt and sand at a particular degree of saturation. The SWCC plays a crucial role in the suction distribution of soil and hydraulic conductivity is also one of unsaturated soils' important properties (Admadi-Adli, Huvaj & Toker 2014).

- There is a linear relationship between the shear strength and matric suction; shear strength decreases with the increasing degree of saturation. The shear strength of

unsaturated soils is higher than that of saturated soils due to matric suction. Based on centrifuge simulation modelling on a slope consisting of a sand-clay mix, it was found that increasing the degree of saturation reduces cohesion. At 80% of the degree of saturation, the cohesion is nearly zero. But the internal friction remains nearly the same at different water contents. The rule of thumb is that the friction angle due to matric suction of a soil is half of the friction angle of that soil.

- The shear strengths of soil under drying process and wetting process are different and the shear strength under wetting process is vital in terms of slope stability. During rainfall, the water content increases and matric suction decreases while the soil state changes from a drying path to a wetting path. During wetting, the reduction of shear strength occurs and thus, wetting shear strength triggers shear deformation. The water content of soil in a drying path is higher than that in a wetting path at a given matric suction. At the onset of rainfall-induced landslides, a low suction range (0 to 50 kPa) or positive pore pressure is anticipated.

- At a low suction range, fine-grained soils show substantial hysteresis which is the difference between the drying SWCC and wetting SWCC. The unsaturated shear strength is affected by hysteresis. The pore water pressure gradient increases due to increasing fine content and decreased initial void ratio.

- Garven (2009) reported there are 25 empirical equations available to predict the shear strength of unsaturated soil. Thirteen equations use the SWCC and saturated shear strength parameters while other equations are developed using mathematical fitting models and empirical relationships. Certain equations are suitable for particular type of soils.

- Kim and Borden (2011) have used three models: Fredlund et al.'s approach, Vanapalli et al.'s approach and Khalili and Khabbaz's approach and reported that these models predict reasonably well for tested soils.

- Zhang et al. (2016) revealed that there are many uncertainties in the current approach to the stability analysis of rainfall-induced landslides. These uncertainties derive from the geological formation, spatial variability of soil properties, uncertainty in boundary

conditions and initial conditions, measurement error, statistical error due to a limited number of samples, uncertainties in the input parameters of the model and systematic error attached to the prediction model, all of which can be overcome by applying a probabilistic approach. The stability of slope can be measured not only by factor safety but also by a reliability index which is assigned to the probability of satisfactory performance of the slope.

- The key parameters in the prediction models for rainfall-induced shallow landslides are moisture content, pore pressure, deformation, rainfall intensity and rainfall duration. However, in-soil moisture content is a better predictor of slope failure. Rainfall-induced landslides can be predicted using a rainfall threshold, rainfall index or stability modelling.

- Bordoni et al. (2015a) disclosed that stability models include closed form equations, physically based models and finite element models. In all these models, obtaining the main soil hydrological properties such as the SWCC is paramount. Furthermore, in the SWCC, the drying path is considered; the effect of the wetting path is not taken into account in most of these stability models.

- Examples of physically based models are SLIP, TRIGRS and SINMAP. The SLIP model is better a predictor than TRIGRS, according to Montrasio, Valentino and Losi (2012).

2.4.5 Gaps in the previous research

In this section, gaps in the previous research are discussed. From the literature review, it is evident that the following areas remain to be addressed:

- Improved relationship of rainfall vs. landslides by regions
- Using hysteresis and addressing more factors affecting shear strength behaviour in the SWCC
- Hydrological response of soil slopes to rainfall

Research studies are needed to address the uncertainty of data, the quality of geotechnical analysis and the application of these studies in relation to natural hazard. There are unknown

parameters such as the unsaturated soil hydrology, distribution of soil thickness and initial water content. The application of 3D stability analysis, developing a complete soil failure model and modelling the return period of rainfall responsible for triggering a landslide are recommended (Crosta & Frattini 2008).

According to Finlay, Fell and Maguire (1997), the correlation between landslides and rainfall can be improved if more data on landslide occurrences and rainfall records become available (Dai & Lee 2001).

The exact relationship between landslides and rainfall characteristics is not clear and studies on mountainous terrain are needed for different regions (Jan et al. 2016). Tohari (2018) reviewed rainfall-induced landslide studies and concluded that hillslope hydrology is difficult to understand and the response to rainfall in terms of transient and spatial variations cannot be clarified by a simplified hydrological model.

To analyse rainfall-induced shallow landslides, the effects of low suction and hysteresis of the SWCC on unsaturated shear strength parameters need to be known. Limited research has been done on the effects of low suction and hysteresis on unsaturated shear strength parameters (Gallage & Uchimura 2016). Further research is needed in estimating suction using the SWCC to obtain reliable values for suction for application in engineering practices (Gallage & Uchimura 2010).

Using the SWCC to predict in-situ suction has not been promoted due to the hysteresis linked with the SWCC. Generally, the drying SWCC is obtained using laboratory tests whereas the wetting SWCC is assessed from soil classification. Further research is needed in estimating suction using the SWCC to obtain reliable values for suction for the practical application in engineering (Fredlund, Sheng & Zhao 2011).

Shear strength behaviour is affected by soil structure, density, stress history, compaction energy and volume change and published equations for predicting shear strength using SWCC do not consider these factors. To understand the behaviour of unsaturated soils, testing a wide range of soils using different test procedures is recommended (Garven 2009). In addition, a comparison of published equations with respect to soil types is needed.

Strength characteristics and hydraulic characteristics need to be investigated as both of them influence the failure depth of rainfall-induced landslides (Collins & Znidarcic 2004). To understand the hydrological response of soil slopes, the influence of different types of vegetation and geomorphological factors need to be studied (Tohari 2018).

A comparison of physically based stability models for the prediction of rainfall-induced landslides is needed, by area subject to landslides.

Chapter 3: Methodology, Materials and Testing Methods

To achieve the goals of this study, the following major steps were conceived and implemented as part of the research methodology:

1. Review literature on rainfall-induced shallow landslides and related areas such as landslides in general, rainfall characteristics, slope characteristics and soil characteristics; failure mechanism of shallow landslides, prediction of shear strength of unsaturated soils and prediction of rainfall-induced shallow landslides and identify the gaps in the research.
2. Contact public authorities in northern NSW and obtain data on rainfall-induced landslides such as location and year in which landslides occurred. Collect information on rainfall data prior to landslides and when possible, review geotechnical investigation reports conducted at the landslide site.
3. Conduct field surveys to inspect the past landslide sites and obtain soil samples from the landslide mass for detailed laboratory examination.
4. Conduct laboratory investigation on soil properties on the soil samples collected from the past landslide sites at Geotechnical Laboratory, Griffith University, Gold Coast. Determine the shear strength of soil at different values of water content and establish empirical correlations between the soil strength and its water content.
5. Conduct numerical analysis of the obtained results to modify/refine the existing methods on estimation of soil strength in regard to water content.
6. Modify the existing method of the landslide prediction based on rainfall data and applied this method to the site conditions of northern NSW.

3.1 Testing plan

The following sections describe the testing plan and experimental procedures. Note that all tests were conducted at Griffith University. All tests were performed according to the reverent standard as shown in Table 3.1. Around 3 kg of soil samples were collected during site surveys from each of 18 landslide sites in northern NSW. The following laboratory work was performed:

1. Soil classification tests: Atterberg limits and particle size distribution;

2. Direct shear test at different moisture contents such as 10%, 15%, 20%, 25% and 30% on nine soil samples consolidated to a vertical stress of either 28.52, 55.77 and 83.02 kPa;
3. Suction tests using a filter paper method at different moisture content: 10%, 15%, 20%, 25% and 30%;
4. Consolidated undrained triaxial tests on soil samples at a consolidation stress of 28.52, 55.77 and 83.02 kPa;
5. Hydraulic conductivity tests.

Table 3.1: Testing program

No.	Description of test	Test standards
1	Atterberg limits	AS 1289 3.1.1 (LL), 3.2.1 (PL) & 3.3.1 (PI) - 2009
2	Particle size distribution	AS 1289 3.6.1 - 2009
3	Direct shear test	AS 1289 6.2.2 - 1998
4	Suction test	ASTM D 5298 - 2003
5	Consolidated undrained triaxial test	ASTM D 4767 - 1995
6	Hydraulic conductivity test	AS1289.6.7.3 - 2016

3.2 Direct shear test

Figure 3.1 shows the photo of direct shear box equipment. The data logger was used to record vertical displacement, horizontal displacement and shear force at every 10 seconds. Shear stress vs. horizontal displacement was plotted.

For shear box tests, oven dried soil samples were first sieved through the 4.75 mm sieve following Australian Standard (AS 1289 6.2.2 - 1998). To prepare moist samples, the oven-dried soil was mixed with distilled water and kept for 24 hours in a sealed bag for better moisture distribution. The water content from 10% to 30% was targeted for most of soils to provide a larger range of water content. The same procedure was used to prepare all shear box specimens; that is, the soil sample was placed in the shear box in 6 layers, and each layer was

gently compacted up to 30 times to assure the specimen uniformity. Before the shearing stage, all specimens were consolidated to a vertical stress of either 28.5 kPa, 55.7 kPa or 83.02 kPa. The testing procedure and typical results of shear box tests are presented and discussed in the following chapters (published papers). The results of all shear box tests are given in Appendix E.

Figure 3.1: Direct shear test equipment

3.3 Suction tests using filter paper

The suction tests were carried out in accord with ASTM Standard (ASTM D 5298 - 2003) using a plastic O-ring, air-tight container and cling wrap. A special hand gloves was used to prepare the specimen to avoid oils from the hand to the filter paper. The soil used for suction tests was first sieved through the 2.36 mm sieve to meet the standard requirement. The moist samples were prepared by adding 10%, 20% and 30% of distilled water by weight. A set of 4 larger size filter papers and a smaller size filter paper were dried for 16 hours in the oven prior to testing. A sensitive balance (that can measure up to four decimals) was used to measure the weight of the filter paper.

The O-ring was placed on top of a cling wrap and sample was hand-compacted up to the middle of O-ring. Two large filter papers were placed on the top and bottom to measure total suction, while a smaller-sized filter paper was placed in between the soil sample to measure the matric suction. The sample with the O-ring was placed in an airtight container which was kept in a cooler box for a week. After 7 days, the weight of wet filter papers was measured. They were placed in the oven at 105°C for 2 hours, and the weight of dried filter papers was measured

after drying. This process was made as quickly as possible to avoid any change in moisture of the filter paper which could occur when the filter paper was exposed to air.
Results of suction tests are discussed in the following sections while the summary of all suction tests in given in in Appendix E.

3.4 Consolidated undrained triaxial tests

Triaxial tests were carried out on specimens from three landslides sites (more details are given in the following chapters). The triaxial tests were carried out using GDS Triaxial Automated System which has a load frame, a triaxial cell, pressure controllers and a computer with specialised software. The test was conducted according to ASTM D 4767 – 1995. Soil samples passing 2.36 mm sieve were dried in the oven for at least 24 h, then mixed with distilled water to achieve 10% moisture content and left in a sealed bag for 24 hours. This was done for better moisture distribution in the soil. The cylindrical soil specimen (100 mm height and 50 mm diameter) was prepared using a membrane tube which was placed at the base of the triaxial chamber with a filter paper and a porous stone. The soil specimen was gently compacted in 3 layers.
The triaxial chamber was filled with distilled water, placed on axial loading device with computer-based pressure controllers for cell pressure and back pressure. The triaxial tests was carried out on the specimen consolidated to a confining pressure of either 28.52, 55.77 or 83.02 kPa. The maximum strain during the test was set to 10%. The test control and data recording were performed by means of a computer. Figures 3.2 to 3.4 show photos of membrane stretcher, preparation of specimen for triaxial test and specimen after shearing. The results of all triaxial tests are given in Appendix E.

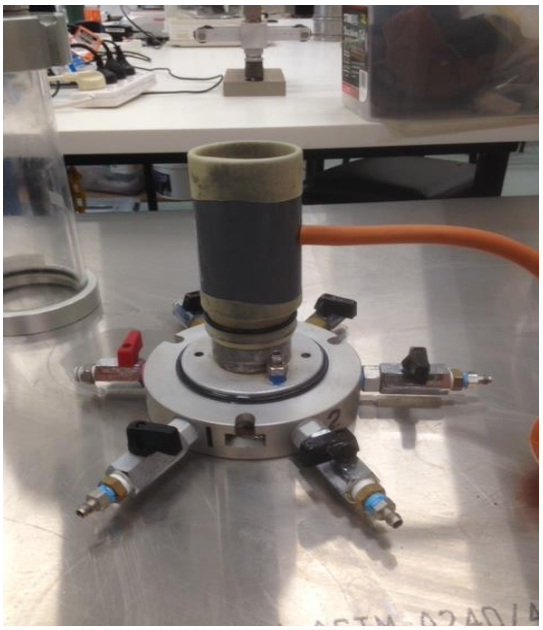

Figure 3.2: Membrane stretcher used to prepare specimen for triaxial test

Figure 3.3: Specimen prepared for triaxial test

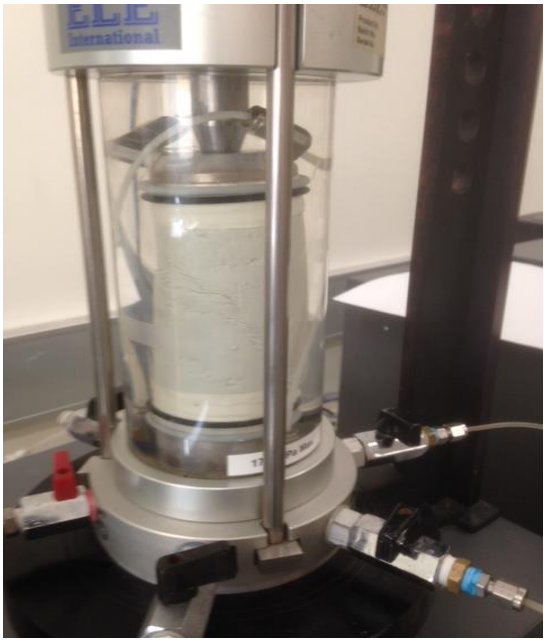

Figure 3.4: Specimen after shearing on the triaxial chamber

3.5 Hydraulic conductivity test

The hydraulic conductivity test was conducted using a constant head method (AS1289.6.7.3 – 2016). The was placed in a rigid permeameter and saturated until a steady state water flow conditions were established. The test was repeated several times and an average value of the coefficient of permeability was obtained for each tested soil.

3.6 Summary of properties of soils from landslide sites

The following chapters (4-6) consist of research papers published during this candidature, and they will discuss the lab results in detail. Table 3.2 summarizes all experimental data, including the test results which were not used in the published papers.

Table 3.2: Summary of properties of soils from landslide sites

Mountain pass/terrain where landslide occurred	Soil No.	Location/Site Name	Common bedrock type	Gravel (%)	Sand (%)	Fines (%)	Field water content	Saturated shear strength from triaxial test (kPa)		Unsaturated shear strength from shear box test			LL	PL	PI
								Cohesion (kPa)	Friction angle (degrees)	Water content	Apparent cohesion (kPa)	Friction angle (degrees)			
Mt Seaview	10	Culvert 416	sandstone	50.9	41.7	7.4	0.19								
	3	Culvert 475		38.6	57.6	3.7	0.32			0.00	18	39			
										0.10	13	36			
										0.20	12	31			
										0.30	10	27			
										0.40	5	26			
	12	Culvert 428		44.4	51.9	3.7									
	16	Culvert 489		52.3	39.9	7.8									
Dorrigo Mountain	13	Gordonville	Sandstone	40.6	55.6	3.8									
	7	Newell Fall3	granite	50.2	46.8	3.0	0.10			0.00	13	40			
										0.10	10	38			
										0.20	9	31			
										0.25	5	28			
Gibraltar Range	1	Culvert 10	sandstone	31.1	66.5	2.4	0.21	0	35	0.00	25	38			
										0.10	16	38			
										0.20	9	38			
										0.30	0	35			
	2	Culvert 32		52.3	42.1	5.6	0.17	0	31	0.00	24	37			
										0.10	16	37			
										0.20	11	36			

									0.25	0	33				
Mallanganee Range	6	Mallanganee West	Sandstone	66.1	31.6	2.3	0.17	0	29	0.00	26	34	20.17	16.41	3.80
										0.10	21	34			
										0.15	12	33			
										0.20	0	30			
Mt Lindsay	11	Tick Gate	Sandstone	54.3	42.2	3.5	0.29								
	8	Montgomerys		70.5	25.7	3.8				0.00	21	40			
										0.10	11	38			
										0.20	6	33			
										0.25	1	25			
	9	Rankin		85.8	13.0	1.2				0.00	18	40			
										0.10	8	40			
										0.20	6	35			
										0.25	4	29			
Ramornie - Cangai Range	5	Hill Ck	Sandstone	23.8	64.5	11.6	0.22			0.00	26	39	42.60	27.80	14.80
										0.10	16	39			
										0.20	5	36			
										0.30	0	34			
Rolling terrain	4	Piora	Sandstone	6.9	89.3	3.8				0.00	11	37			
										0.10	7	34			
										0.15	4	31			
										0.20	0	29			
	14	Cooredulla	Sandstone	10.3	80.0	9.7									
	15	Cherrydale	Granite	21.7	61.4	16.8									

	17	Fairymount Ck	Road fill material and Sandstone	55.9	40.7	3.5									
	18	Possum Ck	Basalt	59.2	38.7	2.1									

STATEMENT OF CONTRIBUTION OF CO-AUTHORED PUBLISHED PAPER

This chapter includes a co-authored paper. The bibliographic details for this paper including all the authors are:

Ravindran, S, Gratchev, I & Jeng, D-S 2019, 'Analysis of rainfall-induced landslides in northern New South Wales, Australia', *Australian Geomechanics,* vol. 54, no. 4, pp. 83–97.

My contribution to the paper involved:
Defining the scope and the structure of the paper, performing relevant experiment and collectiong data from relevant sources, categorising and analysisng data and writing the manuscript.

(Signed)_____ Date:
Sinnappoo Ravindran

(Countersigned)_____ Date:
Co-author1 of the paper: Dr Ivan Gratchev

(Countersigned)_____ Date:
Co-author2 of the paper: Prof Dong-Sheng Jeng

(Countersigned)_____ Date:
Suppervisor Dr Ivan Gratchev

Chapter 4: Analysis of rainfall-induced landslides in northern New South Wales, Australia

4.1 Abstract

Although rainfall-induced landslides are common phenomena in Northern New South Wales (NSW), no systematic studies have been performed to date to better understand this natural disaster. This study seeks to determine the common characteristics of these landslides, including geology, slope geometry, rainfall distribution, and soil properties. The study area includes mountain passes such as Mt Lindesay, Mallanganee Range, Ramornie–Cangai Bluff, Gibraltar Range, Dorrigo Mountain and Mt Seaview; and riverbanks, embankments and cuttings where more than 100 landslides occurred between 2009 and 2017. Field survey of sixteen landslide sites was carried out to collect soil samples, which were tested in a shear box apparatus. This study reveals that many natural slopes affected by landslides consist of weathered sedimentary rocks (mostly sandstone) while the soil from the landslide mass contains a significant amount of coarse material. In addition, landslides tend to occur every two years on natural slopes which are inclined at about 35°. Analysis of rainfall characteristics enabled the development of an indicative rainfall threshold associated with landslide occurrence in the studied area. Rainfall index studies show that landslides could occur at Mt. Lindesay and Dorrigo Mountain if daily rainfall reaches 88 mm and 136 mm respectively.

Keywords**:** landslides, rainfall, shear strength, mountain passes

4.2 Introduction

Rainfall-induced shallow landslides cause significant damage to infrastructure worldwide, including Italy (Donnini et al. 2017), Japan (Yang et al. 2015), Thailand (Ono et al. 2014), Nepal (Dahal 2012), and India (Chandrasekaran et al. 2012). This natural disaster also occurs in Australia where it commonly affects transportation routes (Michael-Leiba et al. 1997). Flentje et al. (2005) noted that more than 142 landslides were triggered in Wollongong (NSW) by rainfall events in 1998 while Cogan et al. (2018) reported several shallow landslides triggered by the cyclone Debbie in South-East Queensland in 2017.

There are several factors including rainfall characteristics, slope geometry and geological settings that can cause shallow landslides. Ma et al. (2015) reported that about 70% of 1500 shallow landslides that were recorded in Zhejiang Province (China) from 1990 to 2013 occurred within one day of the rainfall event. Trigo et al. (2005) reported that high-intensity short-duration rainfalls (greater than 130 mm/day) are commonly associated with shallow landslides in Lisbon, whereas low-intensity but prolonged rainfall tend to trigger deep-seated landslides (Lee et al. 2014). The type of slope material also contributes to the landslide formation. Yang et al. (2015) noted that shallow landslides generally occur in weathered debris or loose soils on steep slopes while Wu et al. (2015) emphasised the important role of mountain terrains in the initiation of shallow landslides.

Shallow landslides regularly occur in Northern NSW, Australia where more than 100 landslides were reported from 2009 to 2017. A good deal of these failures (78%) was caused by high levels of precipitation in northern NSW where annual rainfall varied from 791 mm (as per rain gauge station No. 58016 at Mt Lindesay in 2014) to 3238 mm (as per at rain gauge station No. 60085 at Mt Seaview in 2013), according to the Bureau of Meteorology. The rest of the landslides (22%) were caused by human activities, loose fill and seepage. Sixty percent (49 No.) of rainfall-induced landslides occurred in mountainous terrains, whereas forty percent (33 No.) happened in other terrains such as riverbanks, embankments and cuttings. The purpose of this study was to determine the common characteristics of rainfall-induced landslides that occurred in the mountain passes of Northern NSW; namely, Mt Lindesay, Mallanganee Range, Ramornie–Cangai Bluff, Gibraltar Range, Dorrigo Mountain and Mt Seaview (Figure 4.1) from 2009 to 2017. The analysis of rainfall distribution, geological context, slope geometry, and soil properties was conducted to better understand the mechanism of slope failures. The data on landslide distribution, geology and rainfall events was obtained from public domains and Bureau of Meteorology. In addition, a field survey of 20 landslide sites was conducted to investigate the landslide characteristics and to collect soil samples for laboratory examination and testing. Sieve analysis and shear box tests were performed at Griffith University, Queensland. This paper presents and discusses the obtained results.

Figure 4.1: Mountain passes in northern NSW

4.3. Characteristics of shallow landslides in the studied area

Figure 4.2 shows typical rainfall-induced landslides from Northern NSW while Table 4.1 summarizes their geometry. The cross-sections of these landslides are schematically illustrated in Figure 4.3. It can be seen that most of the slides are shallow, with a depth of landslide mass varying from 0.5 to 2 m and a relatively high slope inclination (>30°). The timeline of rainfall events that caused landslides in the studied area between 2009 and 2017 is shown in Figure 4.4. It appears that for most areas, landslides tend to occur every two years and correlates with heavy rainfall events.

Figure 4.2: Typical landslides in northern NSW

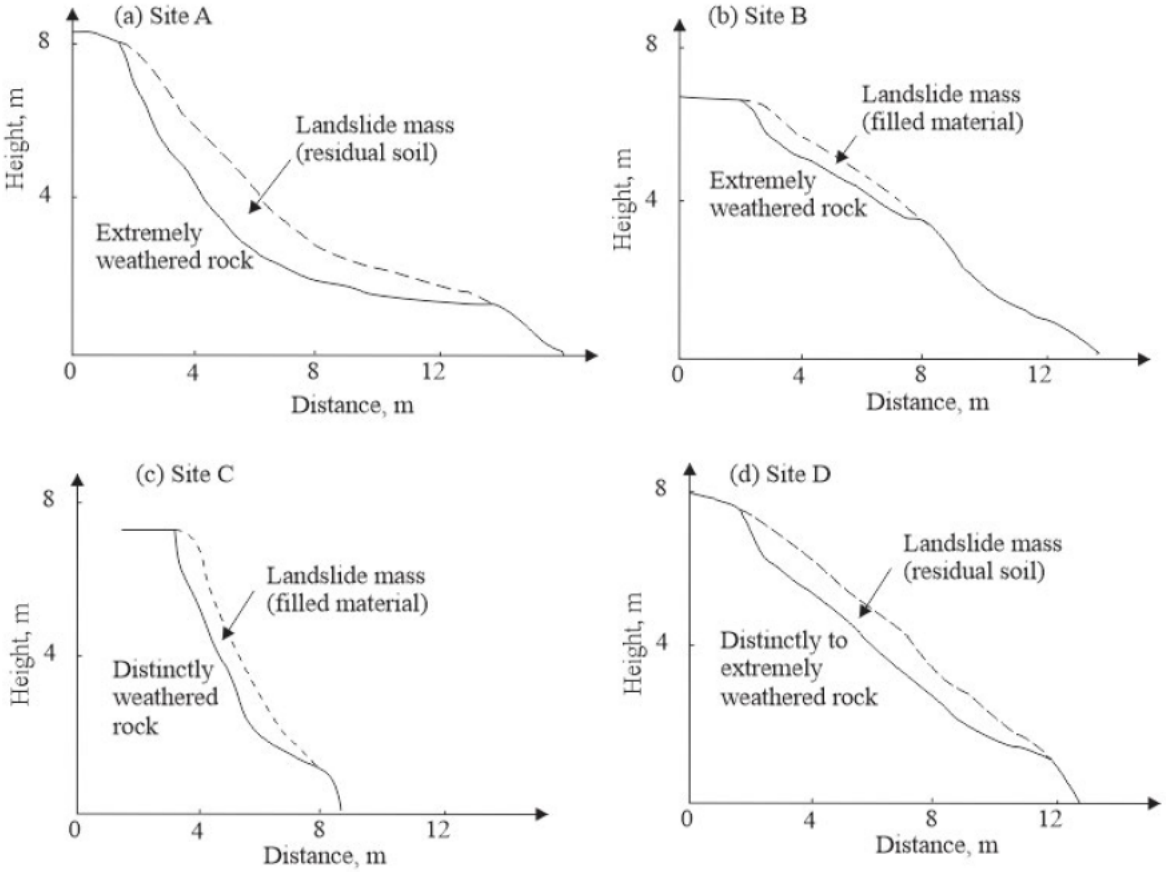

Figure 4.3: Schematic cross-sections of landslides from Figure 4.2

Table 4.1: Geometry of landslide sites from Figure 4.2

Location	Slope width (m)	Slope height (m)	Slope angle (°)	Depth of landslide mass (m)	Approximate volume of landslide (m^3)
Site A (Mt Seaview)	37	7	55	1 - 3	151
Site B (Mt Lindesay)	40	3	30	1 – 2	139
Site C (Dorrigo Mountain)	22	6	40	0.5 – 2	79
Site D (Gibraltar Range)	18	7	65	0.5 – 2	29

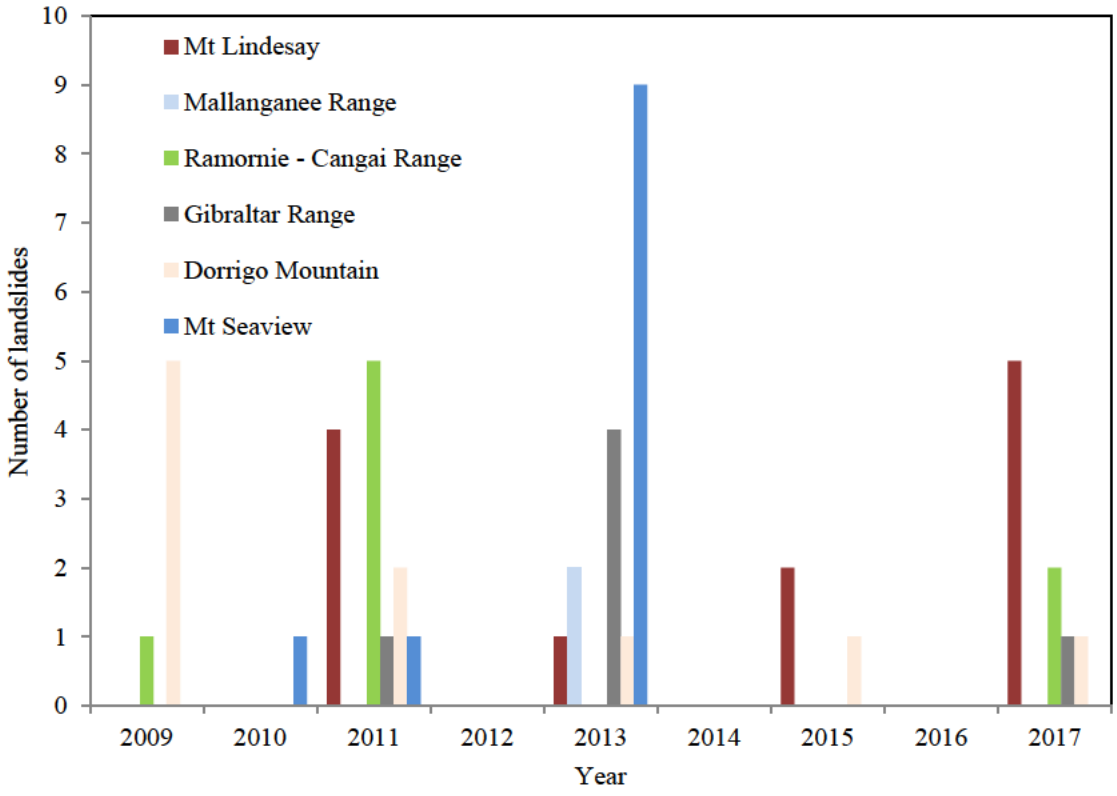

Figure 4.4: Timeline of landslides in the studied area

4.3.1 Geological context

Figures 4.5 to 4.8 give maps showing the main geological units and the location of rainfall-induced landslides. The geological setting of these areas includes sedimentary rocks (sandstone, siltstone, and mudstone) and igneous rocks (basalt and granite). Table 4.2 summarizes the number of rainfall-induced landslides at the mountain passes in Northern NSW by bedrock types. It is evident from this table that a large number of failures are related to sedimentary rocks (mostly sandstone); however, slope failures in weathered igneous rocks are also common. About 18 landslides that occurred in alluvium and fill in the studied area were recorded from 2009 - 2017.

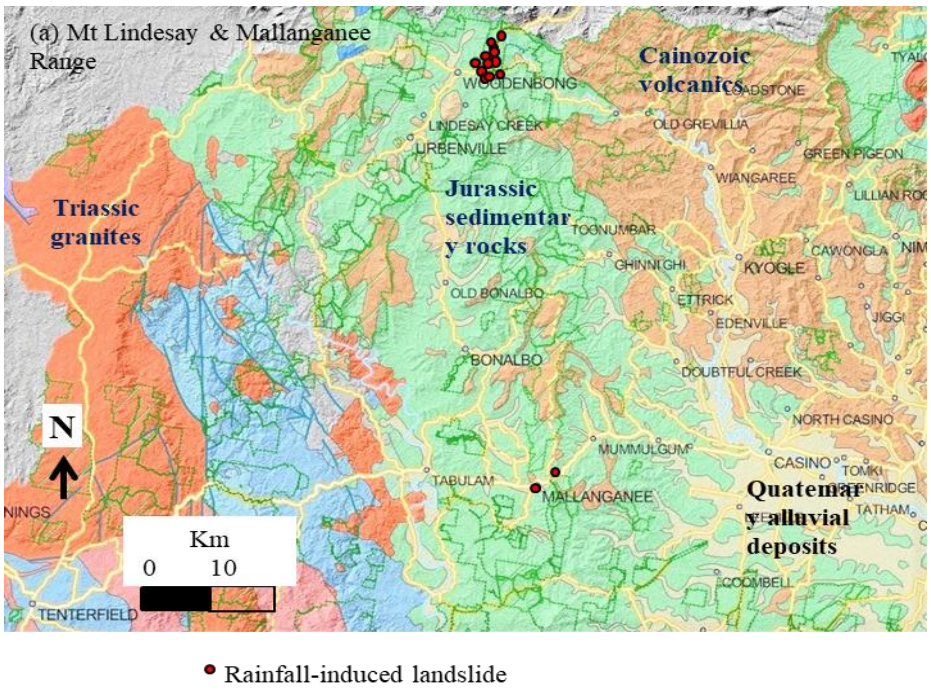

Figure 4.5: Mt Lindesay & Mallanganee Range

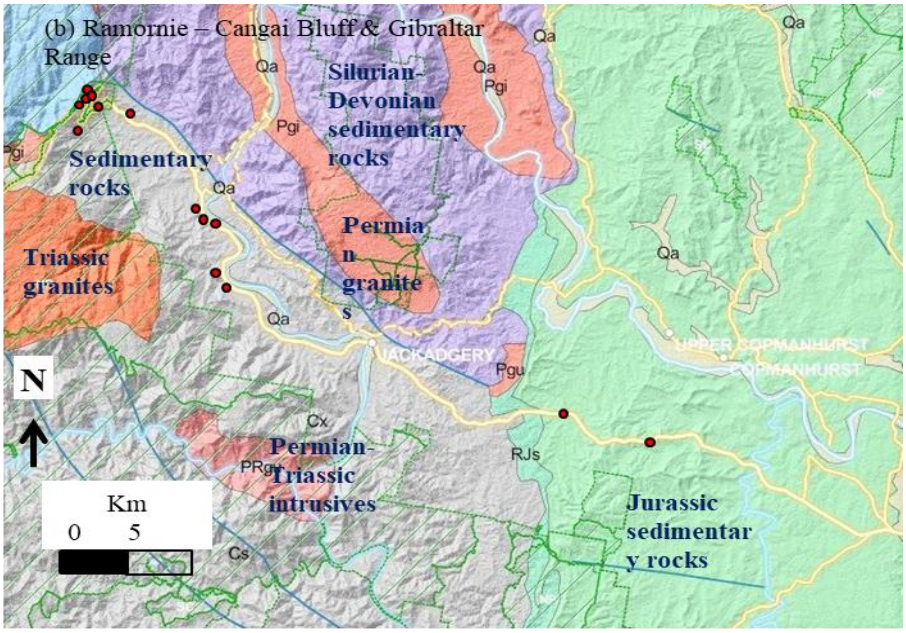

Figure 4.6: Ramornie – Cangai Bluff & Gibraltar Range

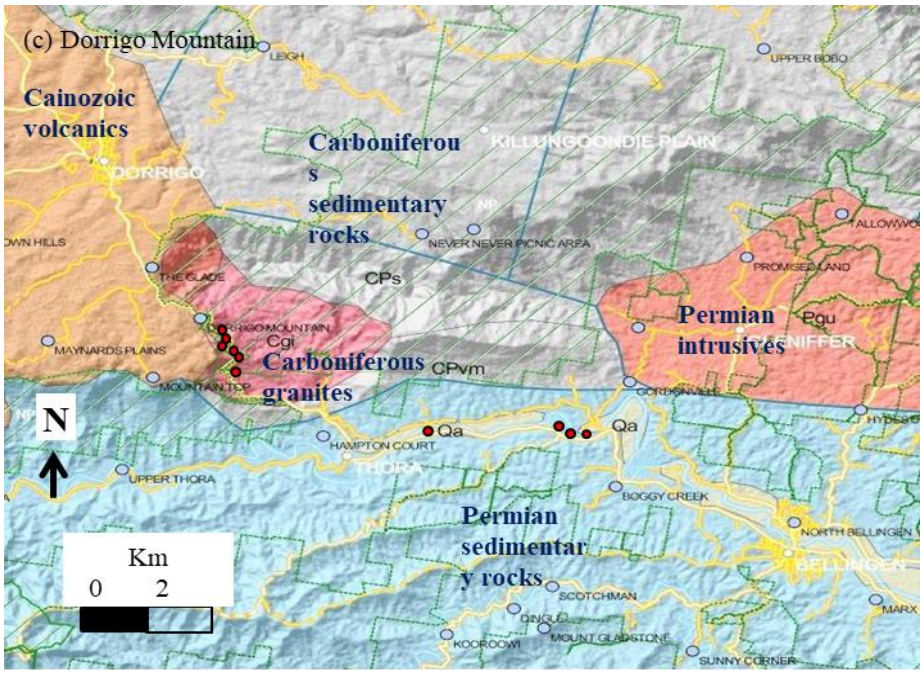

Figure 4.7: Dorrigo Mountain

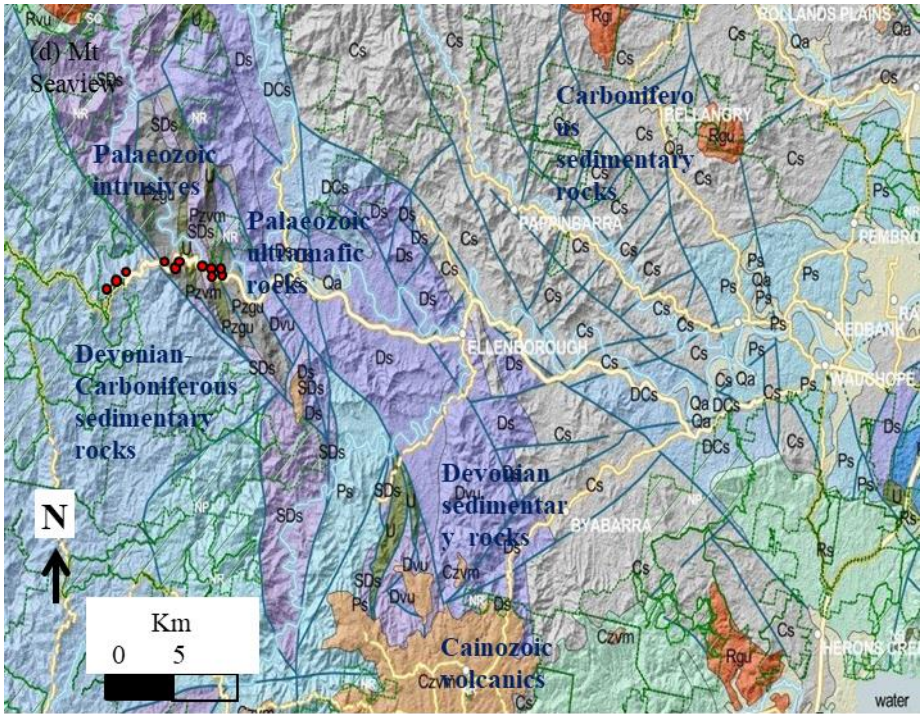

Figure 4.8: Mt Seaview

Table 4.2: Rainfall-induced landslides (2009 – 2017) by rock type

Geological units	Number of rainfall-induced landslides
Sedimentary rocks (mostly sandstone)	41
Volcanic rocks (mostly basalt)	13
Intrusive rocks (mostly granites)	10
Alluvium & filled material (riverbanks & embankments)	18

4.3.2 Slope characteristics

Analysis of slope geometry is given in Figure 4.9, where the number of landslides is plotted against the slope inclination. It is clear from this figure that most of landslides occurred on slopes inclined at 35 - 45°.

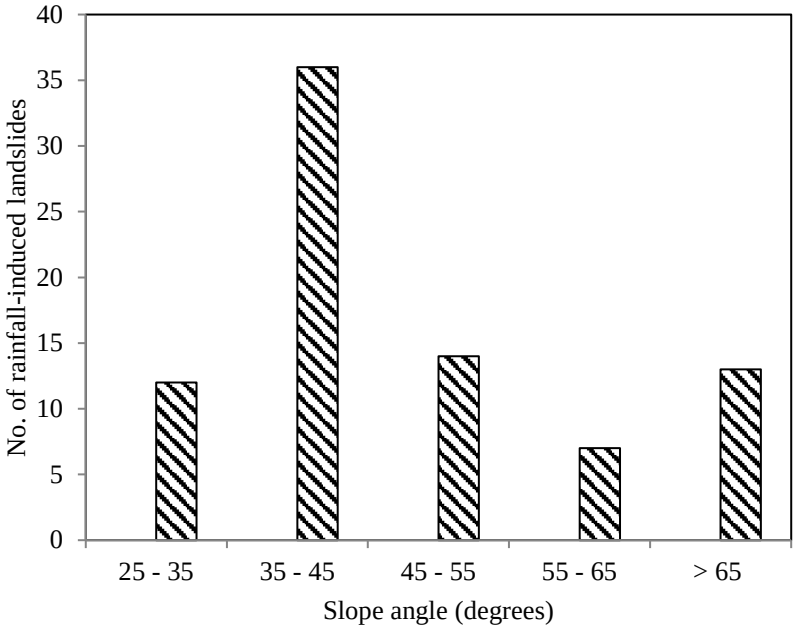

Figure 4.9: Slope angles of rainfall-induced landslides (2009 – 2017) in northern NSW

4.4 Rainfall characteristics

Bordoni et al. (2015) noted that landslide occurrence can be related to rainfall thresholds, and thus it is important to determine the average rainfall duration and intensity that can result in slope failures. The rainfall data for the time period of 2009 to 2017 is summarized in Table 4.3 in terms of the annual rainfall, cumulative rainfall causing landslides, and the number of landslides that occurred at the mountain passes in Northern NSW. It can be inferred from this table that the cumulative rainfall triggering landslides varied from 38 mm to 790 mm and most rainfall-induced landslides (87.5%) occurred when cumulative rainfall was between 100 mm and 600 mm.

Table 4.3: Characteristics of rainfall-induced landslides sites at mountain passes

Mountain passes in Northern NSW	Annual rainfall from 2009 to 2017 (mm)	Cumulative rainfall preceding landslides (mm)	Number of rainfall-induced landslides from 2009 to 2017
Mt Lindesay	791- 1249	113 – 386	12
Mallanganee Range	845 - 1285	152	2

Ramornie – Cangai Bluff	790 - 1351	38 – 444	8
Gibraltar Range	864 - 1664	438 – 515	6
Dorrigo Mountain	1220 - 2970	136 – 584	10
Mt Seaview	2160 - 3238	156 – 790	11

Data on daily rainfall precipitation prior to the landslide occurrence is presented in Figure 4.10 for Mt Lindesay (a), Gibraltar Range (b), Dorrigo Mountain (c), and Mt Seaview (d). As can be seen in this figure, the rainfall event generally continues for 5 or 6 days, producing the cumulative rainfall sufficient to trigger landslides.

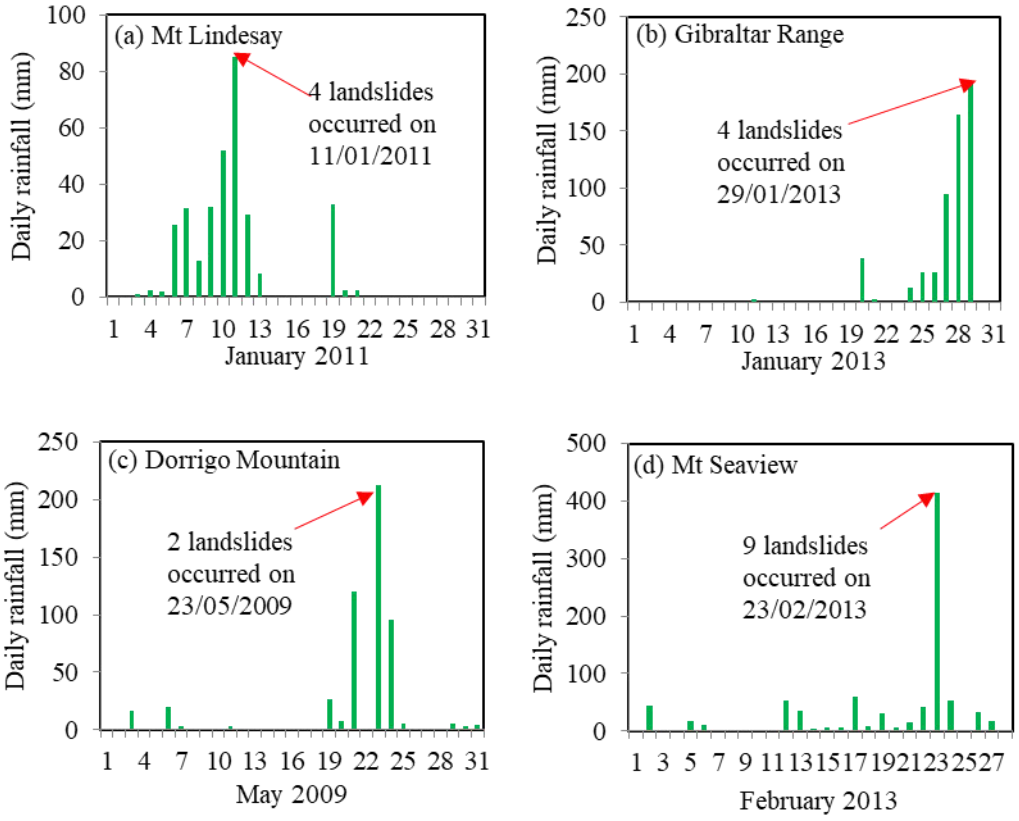

Figure 4.10: Rainfall data preceding landslide occurrence

4.4.1 Rainfall threshold

Many studies have developed rainfall thresholds for landslide initiation using empirical correlations between rainfall intensity and its duration (Caine 1980; Guzzetti et al. 2008; Saito

et al. 2010). It is noted that such thresholds are mostly applicable to the areas which they were developed for; and they may vary depending on site topography, geologic conditions, and human activities.

An attempt was made to develop a regional rainfall threshold for the studied area. The average rainfall intensity (which was defined as the cumulative rainfall divided by the rainfall duration) was calculated for each landslide event. If the rainfall event had the same duration in a particular year, the lowest of the average rainfall intensity was taken into account. Analysis of the obtained results are given in Figure 4.11, with the rainfall threshold is described as shown in Eq. (21):

$$I = 22.6\, D^{-0.554} \qquad (48<D<432 \text{ hr}) \qquad (21)$$

where, I is the rainfall intensity (mm/hr); D is the duration of rainfall (hr). The results from Figure 4.11 indicates that when the rainfall duration increases, the intensity that is likely to initiate shallow landslides decreases. From the data to date, it appears that when the intensity varies from 2.8 mm/hr to 0.8 mm/hr for the duration of 48 hr to 432 hr, respectively, there is an approximately 50% chance that rainfall-induced landslides may occur in northern NSW. It is anticipated that in later studies, further differentiation of landslides by, say, geology or geometry, will result in a more accurate correlation formulation of the rainfall threshold.

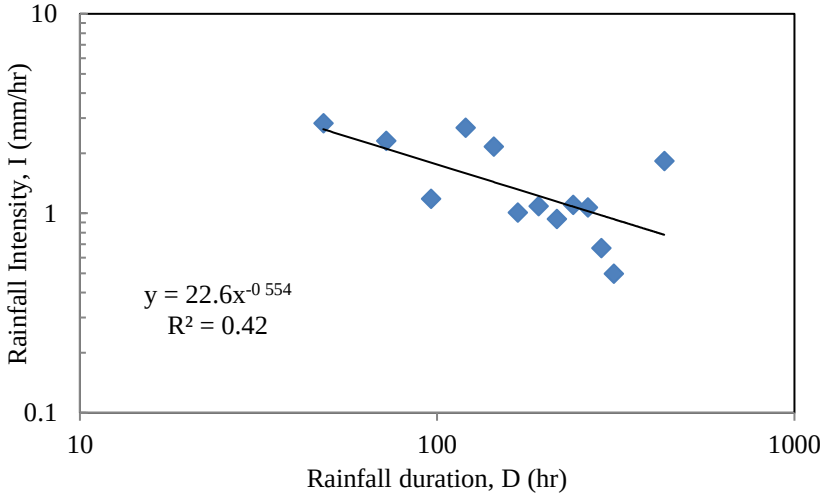

Figure 4.11: Landslide-triggering rainfall threshold for northern NSW

4.4.2 Rainfall index

Nakai et al. (2006) introduced a newly modified rainfall index (R') concept to take into account the decreasing effect of preceding rainfall and the passage of time. R′ is defined as shown in Equations (22) and (23) and schematically illustrated in Figure 4.12:

$$R' = R_{fw0} - R_{fw} \tag{22}$$

$$R_{fw} = ((R_1 - R_w)^2 + a^2(r_1 - r_w)^2)^{0.5} \tag{23}$$

where, R_1 is the highest long-term effective rainfall, r_1 is the highest short-term effective rainfall; R_w and r_w are the long-term and short-term effective rainfalls (in mm) during any rainfall event, and a is a constant. R_{fwo} is the distance from origin (0, 0) to reference point (R_1 , r_1) as shown in Figure 4.12.

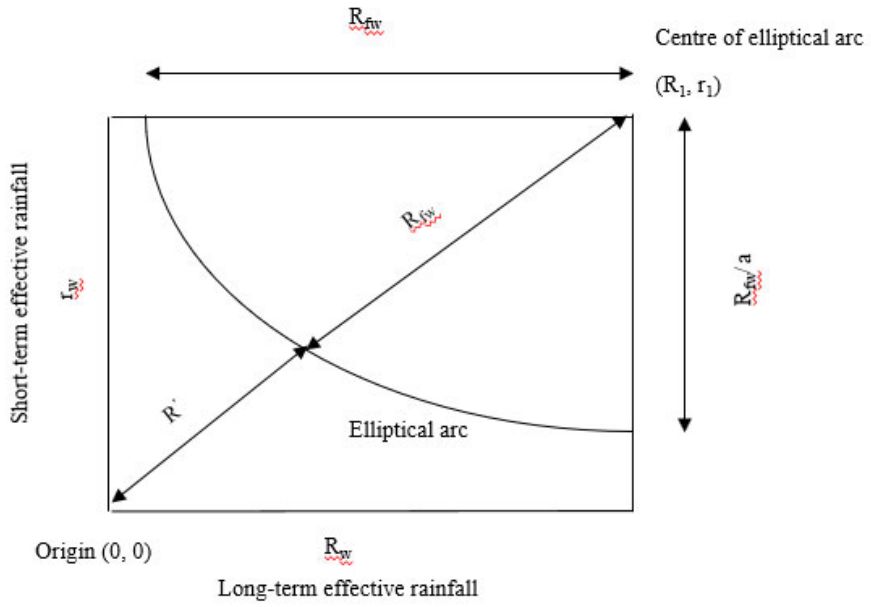

Figure 4.12: Modified rainfall index (R') concept (Source: Nakai et al. 2006)

A similar approach was applied to rainfall-induced landslides at Mt. Lindesay and Dorrigo Mountain to calculate modified rainfall index (R') using rainfall data from BOM. Every rainfall event has a distribution with a peak and lows. Long-term effective rainfall is considered as accumulated rainfall over a period (for example, a week) prior to an arbitrary time whereas

short-term effective rainfall is assumed as rainfall during a short duration (for example an hour) prior to an arbitrary time.

In this study, it was assumed that the long-term effective rainfall was the cumulative rainfall up to the peak during a rainfall event while the short-term effective rainfall was the peak rainfall during 24 hours (r_1=24 h) of the same rainfall event. All rainfall events were analysed for Mt. Lindesay and Dorrigo Mountain and the results are presented in Table 4.4. The assumptions regarding R_1 and r_1 (Table 4.4) were made on the basis of the past rainfall record which exists for Mt. Lindesay and Dorrigo Mountain passes (Table 4.5). Figures 4.13 and 4.14 present the obtained rainfall index R' for the studied areas. In this figure, the rainfall events that triggered landslides are depicted above the R′-curve while the points below the R′-curve correspond to rainfall events that did not trigger landslides.

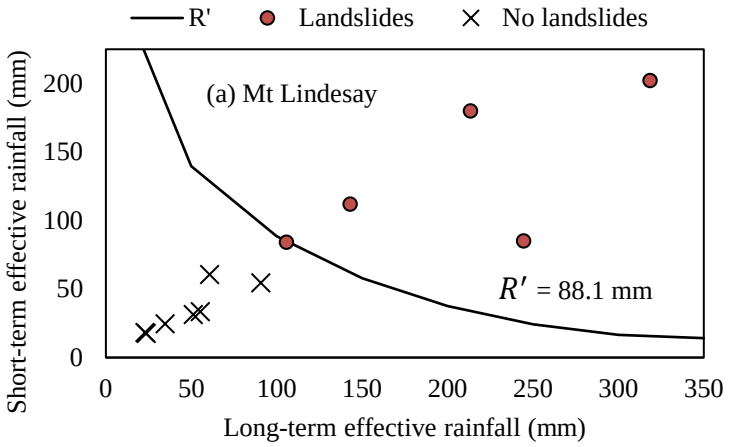

Figure 4.13: Rainfall index obtained for Mt Lindesay

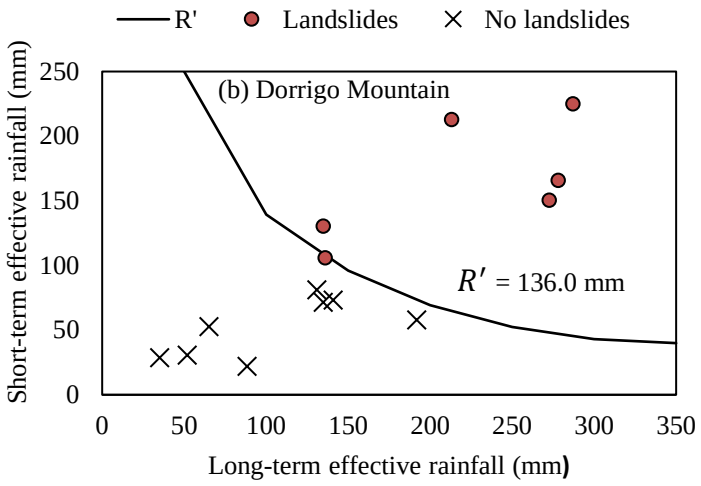

Figure 4.14: Rainfall index obtained for Dorrigo Mountain

Table 4.4: Calculation of rainfall index for Mt Lindesay and Dorrigo Mountain

Name of mountain pass	Parameters used to calculate R'				Minimum R' to cause landslides (mm)
	R_1 (mm)	Duration of R_1 (hr)	r_1 (mm)	Duration of r_1 (hr)	
Mt Lindesay	350	144	225	24	88.1
Dorrigo Mountain	350	72	250	24	136.0

Table 4.5: Highest historical rainfall data for Mt Lindesay and Dorrigo Mountain

Name of mountain pass	Rain gauge station No. from BOM	Year landslide occurred	R_1 (mm)	Duration of R_1 (hr)	r_1 (mm)	Duration of r_1 (hr)
Mt Lindesay	58194	2013	318.4	120	202.2	24
Dorrigo Mountain	59033	2011	325.6	48	225	24

The analysis of rainfall index R' shows that landslides are likely to occur at Mt. Lindesay and Dorrigo Mountain if the rainfall index reaches 88.1 mm and 136.0 mm, respectively.

4.5 Soil characteristics

Soil samples were taken from 16 landslide sites for laboratory testing. Sieve analysis (AS1289.3.6.1 - 2009) was conducted to determine grain-sized distribution of soil and the obtained results are summarized in Table 4.6. The majority of soils samples were coarse-grained material with a relatively small fine content, which can be attributed to the fact that most of landslides occurred in weathered sandstone.

Table 4.6: Grading of soil samples from landslides

Terrain	Soil No.	Gravel (%)	Sand (%)	Fines (%)	USCS Classification
Mt Seaview	1	50.9	41.7	7.4	GW
	2	38.6	57.6	3.7	SW
	3	44.4	51.9	3.7	SW
	4	52.3	39.9	7.8	GW
Dorrigo Mountain	5	40.6	55.6	3.8	SW
	6	50.2	46.8	3.0	GW
Gibraltar Range	7	31.1	66.5	2.4	SW
	8	52.3	42.1	5.6	GW
	9	71.8	26.5	1.8	GW
Mallanganee Range	10	66.1	31.6	2.3	GP
	11	80.1	18.6	1.4	GW
	12	87.3	12.6	0.1	GW
Mt Lindsay	13	54.3	42.2	3.5	GP
	14	70.5	25.7	3.8	GP
	15	85.8	13.0	1.2	GP
Ramornie - Cangai Range	16	23.8	64.5	11.6	SP

Riverbanks, embankments & cuttings	17	6.9	89.3	3.8	SP
	18	10.3	80.0	9.7	SW
	19	55.9	40.7	3.5	GW
	20	59.2	38.7	2.1	GW

4.5.1 Direct shear test

Understanding of the failure mechanisms of rainfall-induced landslides is important for prediction and assessment of this natural disaster. During rainfall, infiltration of water occurs in the slope, resulting in greater moisture content, lower soil suction, and decreased shear strength of soil (Yoshida et al. 1991; Bishop and Morgenstern 1960; Blight 2002; Springman et al. 2003; Rahardjo et al. 2005). To investigate the effect of moisture content on soil strength, a series of shear box tests on dry and moist soil samples were conducted, following Australian Standard AS1289.6.2.2-1998. Large gravel components were removed from each sample and the soil material passing 4.75 mm sieve was used for a series of direct shear tests. Pore water pressure was not measured. Direct shear tests were conducted on nine samples only.

For each soil sample, shear-box tests were performed on soil specimens with various moisture contents ranging from 0 to 40%. To allow comparisons of the obtained results, all shear box specimens for each soil were prepared to the same dry density. The moist specimens were prepared by mixing the oven-dried soil with distilled water. They were allowed to rest in a sealed bag for 24 hours for better moisture distribution. The soil was then compacted in the shear box (the shear box size was 60 x 60 mm) in thin layers to achieve the desirable dry density. Direct shear tests were carried out with at least four different moisture contents.

The soil specimens were sheared under three effective vertical stresses of either: 28.5, 55.8 or 83.0 kPa. The peak shear stress was recorded and used to determine the strength characteristics of the soil, according to the Mohr-Coulomb strength criterion. The relationship between landslide sites and soil samples tested is shown in Table 4.7.

Table 4.7: Landslide sites vs. soil samples taken and used in the direct shear tests

Terrain	No. of rainfall-induced Landslides	Sample Identification No.	Soil ID No. used in direct shear tests
Mt Seaview	11	1, 2, 3, 4	2
Dorrigo Mountain	10	5, 6	6
Gibraltar Range	6	7, 8, 9	7, 8
Mallanganee	2	10, 11, 12 (2 samples from the larger site)	10
Mt Lindesay	12	13, 14, 15	14, 15
Ramornie - Cangai	8	16	16
Riverbanks, embankments & cuttings	33	17, 18, 19, 20	17

4.5.2 Shear strength of soil from landslide sites

Results of shear box tests are given in Figures 4.15 to 4.17. Figure 4.15 shows the shear stress-displacement curves of moist specimens prepared from Soil 7 and consolidated under an effective vertical stress of 28.5 kPa. The effect of moisture can be seen in the greater peak shear strength obtained for the soil specimens with lower moisture content. All test results are summarized in Figure 4.16 in terms of shear strength and shear strength reduction against the moisture content is shown in Figure 4.17. In this study, to better demonstrate the effect of water content on shear strength, the shear strength of specimens at different water content was compared to the one of the dry specimens using a parameter called the shear strength reduction. It is clear from this figure that the shear strength decreases with increasing moisture content. When the moisture content increased to 20%, the shear strength reduction varied from 22.2% to 46.8% while for the moisture content of 30%, the shear reduction of some coarse-grained

soils could reach more than 60%. The laboratory data shows that the decrease in shear strength of some coarse-grained soils due to higher moisture content can be significant. The shear strength reduction is a warning sign for landslide occurrence. For example, field moisture content of Soil 7 was 23.1% (which will vary between summer and winter) whereas saturated moisture content of Soil 7 from the direct shear test was 39.3% at failure.

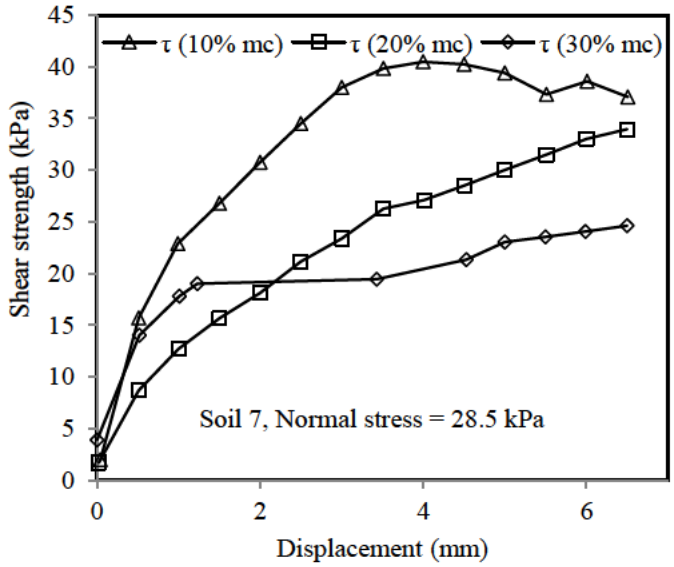

Figure 4.15: Typical shear stress-displacement behaviour observed for Soil 7 at 10%, 20% & 30% moisture content

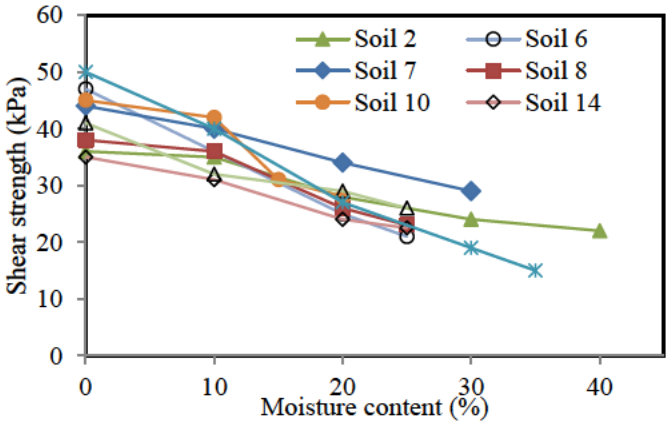

Figure 4.16: Shear strength against moisture content for all tested soils

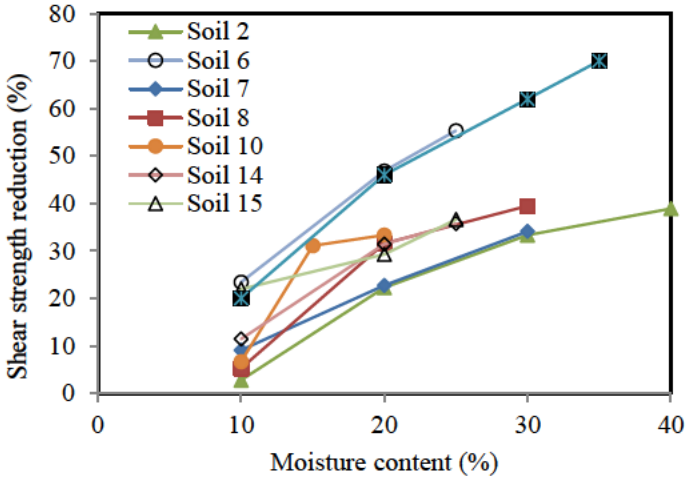

Figure 4.17: Shear strength reduction due to changes in moisture content

4.6 Conclusions

This study was performed to determine common characteristics of several shallow landslides triggered by rainfall events in mountain passes of northern NSW (namely, Mt Lindesay, Mallanganee Range, Ramornie–Cangai Bluff, Gibraltar Range, Dorrigo Mountain and Mt Seaview) from 2009 to 2017. Based on the field surveys, laboratory data and public information, the following major conclusions can be drawn:

- A good deal of shallow rainfall-induced landslides in the studied area occurred in weathered sandstone, in which the landslide mass consisted of coarse-grained material. Weathered igneous rocks such as basalt and granite were affected by the landslide phenomenon as well.
- The majority of landslides initiated on slope terrains which were inclined at 35-45°. Landslides tend to occur every two years and correlates with major rainfall events.
- Based on the historical rainfall data from 2009 to 2017, the rainfall intensity-duration threshold that triggers shallow landslides in the studied area can be indicatively described as $I = 22.6\ D^{-0.554}$, where I is the rainfall intensity (mm/hr); D is the duration of rainfall (hr).
- Analysis using the rainfall index (R′) concept reveals that landslides may occur at Mt. Lindesay and Dorrigo Mountain when R′ reaches 88 mm and 136 mm, respectively.

- Results of shear box tests indicated that for most soils samples, an increase in moisture content could decrease the shear strength by more than 30%, and such a change would contribute to the slope instability during rainfall events.

4.7 Acknowledgements

The comments and views expressed in this paper are those of the authors. The data was obtained from many public authorities including the Bureau of Meteorology, the Disaster Assist unit of the Department of Home Affairs and NSW Department of Planning and Environment, Division of Resources and Geoscience.

STATEMENT OF CONTRIBUTION OF CO-AUTHORED PUBLISHED PAPER

This chapter includes a co-authored paper. The bibliographic details for this paper including all the authors are:

Ravindran, S and Gratchev, I 2020, 'Estimation of shear strength of gravelly and sandy soils from shallow landslides', *International Journal of GEOMATE*, vol. 18, no. 70, pp. 130-137.

My contribution to the paper involved:
Defining the scope and the structure of the paper, performing relevant experiment and collectiong data from relevant sources, categorising and analysisng data and writing the manuscript.

(Signed)_____ Date:
Sinnappoo Ravindran

(Countersigned)_____ Date:
Co-author1 of the paper: Dr Ivan Gratchev

(Countersigned)_____ Date:
Suppervisor Dr Ivan Gratchev

Chapter 5: Estimation of shear strength of gravelly and sandy soils from shallow landslides

5.1 Abstract

This study seeks to investigate the unsaturated shear strength of six gravelly and sandy soils collected from shallow landslides in New South Wales, Australia. Results from a series of shear box tests on unsaturated soil specimens revealed that changes in water content (from 0% to 30%) could significantly reduce the shear strength of soil (by 34% to 43%). The observed increases in soil's apparent cohesion and friction angle were attributed to more pronounced effects of suction at low values of water content. The obtained laboratory data were compared with the shear strength estimates obtained by two published models for estimating shear strength. One of the methods was refined to provide a more simplified approach to obtain the air entry value (AEV) using the soil basic parameters. In addition, a new simplified method was proposed to predict the shear strength of unsaturated gravelly and sandy soils using the soil gradation characteristics. Comparisons made between the laboratory data and numerical methods showed a good agreement between the predicted and experimental values across a large range of matric suction which was within 35%.

Keywords: Apparent cohesion, Friction angle, Suction, Shear strength, Prediction

5.2 Introduction

It is already well-known that the shear strength of soil can be affected by changes in moisture content. Guan et al [1], Farooq et al [2], Cogan et al [3] reported that during rainfall, as moisture content increases, the matric suction decreases, reducing the shear strength of soil. Thus, the knowledge of shear strength of unsaturated soil provides vital information for slope stability analysis, especially shallow landslides [4,5]. Laboratory studies conducted in the past several years have revealed that although the shear strength generally decreases with increasing moisture, the response patterns may be somewhat different. For example, Hossain and Yin [6], Gallage and Uchimura [7], Patil et al [8] showed that a decrease in water content can significantly increase the apparent cohesion of soil, however, the friction angle may remain almost the same. On the contrary, Kong and Tan [9], Tilgen [10] reported that the apparent

cohesion may first increase with increasing moisture content and then significantly decrease as the amount of moisture in soil keeps increasing. In addition, the friction angle decreases as well [11]. Such difference may be attributed to the different structure, plasticity and origin of soil samples used in the aforementioned studies. It was also recognized that such laboratory studies can be extremely costly and time-consuming, which makes the available up-to-date experimental data rather limited. In addition, special equipment is typically required to perform suction-controlled tests, which may continue for a long period of time [8]. This can be seen as an obstacle in engineering practice where such special testing equipment is often not available, and the time allotted for laboratory investigation is generally constrained by project deadlines. Another approach that can minimize the use of experimental data is related to numerical studies. Several methods including Fredlund et al [12], Vanapalli et al [13], Khalili and Khabbaz [14], Vilar [15], Naghadeh and Toker [16] have been proposed to predict shear strength of unsaturated soils using soil-water characteristic curves (SWCC). However, these methods generally work well only for the soils for which they were developed, while they tend to yield relatively large errors (about 20% or even more) when applied to different soil conditions [14]. There is a lack of prediction models for gravelly and sandy soils from landslide-prone areas.

It is clear that more experimental data is needed to better understand the properties of unsaturated soils while a proven alternative technique for shear strength prediction that does not require special laboratory equipment would be of great benefit to engineers. This study seeks to investigate the unsaturated shear strength of six gravelly and sandy soils collected from shallow landslides in New South Wales (NSW), Australia [17], and proposes a simplified procedure to estimate the shear strength of such soils using the soil basic properties. This paper briefly introduces the theoretical considerations utilized to estimate the soil-water interaction and shear strength of unsaturated soil and discusses a new simplified procedure to obtain the air entry value. It continues with the discussion of the laboratory data in respect to the effect of suction on shear strength of soil. Finally, it compares the measured shear strength with its estimates using the already existing methods as well as the newly-proposed technique.

5.3 Theoretical considerations

5.3.1 Soil-Water Characteristic Curves

Soil-water characteristic curves (SWCC) show the relationship between suction and water content, and they are commonly used to estimate the effect of suction on soil properties, including shear strength and permeability. Fredlund and Xing [14] suggested Equation (24) to describe the entire SWCC using volumetric water content (θ) and suction (ψ).

$$\theta = \theta_s \left[1 - \frac{\ln\left(1+\frac{\psi}{\psi_r}\right)}{\ln\left(1+\frac{1000000}{\psi_r}\right)}\right]\left\{\frac{1}{\ln\left[e+\left(\frac{\psi}{a}\right)^n\right]}\right\}^m \quad (24)$$

where, θ_s is the saturated volumetric water content, ψ_r is the suction value corresponding to the residual volumetric water content θ_r. The fitting parameters (a, n and m values) can be determined using a nonlinear regression procedure as outlined by Fredlund and Xing [14]. As suction depends on soil moisture content, the normalized volumetric water content Θ is frequently used to define the amount of water contained in the pores of soil in Equation (25).

$$\Theta = \frac{\theta}{\theta_s} = \left[1 - \frac{\ln\left(1+\frac{\psi}{\psi_r}\right)}{\ln\left(1+\frac{1000000}{\psi_r}\right)}\right]\left\{\frac{1}{\ln\left[e+\left(\frac{\psi}{a}\right)^n\right]}\right\}^m \quad (25)$$

5.3.2 Shear Strength of Unsaturated Soils

Kim and Borden [14] discussed the most commonly used methods of shear strength prediction, including Fredlund et al; Vanapalli et al and Khalili and Khabbaz, and concluded that the Khalili and Khabbaz's method tends to provide more accurate estimates of shear strength of unsaturated coarse-grained soils. As the tested soils in this study are coarse-grained material, this method will be discussed in detail. In addition, a recent model proposed by Naghadeh and Toker [16] will be reviewed and discussed for comparisons.

5.3.2.1 Khalili and Khabbaz's (1998) method

According to Khalili and Khabbaz's method, the shear strength of unsaturated soil is estimated as shown in Equations (26) to (28):

$$\tau_f = c' + (\sigma_n - u_a)\tan\phi' + (u_a - u_w)_f[\chi(\tan\phi')] \quad (26)$$

where,

$$\chi = \left[\frac{(u_a - u_w)_f}{(u_a - u_w)_b}\right]^{0.55}, \text{ when } (u_a - u_w) > (u_a - u_w)_b \quad (27)$$

$$\text{where, } \chi = 1, \text{ when } (u_a - u_w) < (u_a - u_w)_b \quad (28)$$

where, $(u_a - u_w)_f$ is the matric suction of specimen at failure condition; $(u_a - u_w)_b$ is the air entry value (AEV, in kPa). It is commonly assumed that $(u_a - u_w)$ is 100,000 kPa when the moisture content is zero as the total suction is the same as the matric suction for any type of soil [12].

When there is no sufficient lab data, it may be rather difficult to accurately obtain AEV values for SWCC. Zapata [18] analysed SWCC of 120 non-plastic soils and suggested that D_{60} can be a key parameter to represent coarse-grained soils. Drawing on Zapata's findings, this study proposes Equation (29) to estimate the AEV value using D_{60}.

$$AEV = R \cdot \gamma \cdot D_{60} \quad (29)$$

where, R is the model parameter; γ is the unit weight of water (9.81 kN/m^3), and D_{60} is the 60% particles are finer than this size (in m). In this study, Eq. (27) to Eq. (29) will be used to estimate the shear strength of the studied soils using the Khalili and Khabbaz's method.

5.3.2.2 Naghadeh and Toker (2019) method

Naghadeh and Toker [16] proposed a relatively new approach that considers changes in the apparent cohesion of soil with different moisture content using the transition suction (ψ_t). Equations (30) and (31) describe the mathematical relationships used to estimate the unsaturated shear strength:

$$\tau = c' + (\sigma - u_a) \text{ x } \tan\phi' + [1 - e^{\left(-\frac{\psi}{\psi_t}\right)}] \text{ x } \psi_t \text{ x } tan\phi' \quad (30)$$

where, c' is the effective cohesion; ϕ' is the effective angle of internal friction; σ is the normal stress; u_a is the pore air pressure; ψ is the matric suction; ψ_t is the matric suction at transition. To estimate the transition suction (ψ_t), Naghadeh and Toker [16] suggested Eq. (31) which involves the maximum capillary cohesion (c''_{max}).

$$c''_{max} = (\tan\phi' \times \psi_t) \quad (31)$$

Naghadeh and Toker [16] also reported the relationship between the apparent cohesion, c_a effective cohesion (c') of saturated soil, and capillary cohesion (c") as shown in Equation (32):

$$c'' = c_a - c' \quad (32)$$

According to Lu and Likos [19], the capillary cohesion is proportional to matric suction, and the value of matric suction becomes very high when the moisture content is close to zero [20]. Thus, it can be assumed that the maximum capillary cohesion (c''_{max}) occurs when the moisture content is close to zero. Eq. (32) was proposed by Naghadeh and Toker [16] for all types of soil, including plastic soils with the effective cohesion. When applied to coarse-grained soils, it can be simplified using the assumption that the effective cohesion (c') of fully saturated coarse-grained soil is 0.

5.3.2.3 A new model to estimate the shear strength of unsaturated

This study proposes a new approach as shown in Equation (33) to estimate the shear strength of coarse-grained soil under low normal stress conditions using soil basic parameters such as the coefficient of uniformity (C_u) and shear box and suction test results.

$$\tau = c' + (\sigma_n - u_a) \text{ x } tan\phi' + \psi \text{ x } (\frac{1}{C_u})^M \text{ x } tan\phi' \quad (33)$$

where, c' is apparent cohesion at a particular moisture content; σ_n is normal stress which is 28.5 kPa at shear box tests which reflects low normal stress or shallow depth conditions; u_a is

pore air pressure which is assumed to be zero; ϕ' is friction angle at a particular moisture content; ψ is the matric suction at a particular moisture content; M is the model parameter.
Eq. (33) was developed using measured shear strength at a normal stress of 28.5 kPa at various moisture contents from shear box tests. The matric suctions at the corresponding moisture contents were obtained from the best fit curve of SWCC. The model parameter M was calculated by applying optimization technique by minimizing the squared sum of normalized residuals between measured shear strength and estimated shear strength using Eq. (33).
As suction is related to soil porosity [20] which is a reflection of soil grading, C_u can be selected as a key parameter to predict the matric suction of coarse-grained soils [21], Eq. (33) will be tested in this work to estimate the shear strength of six gravelly and sandy soils, and the obtained results will be compared with the laboratory data and estimates of shear strength using the Khalili and Khabbaz's and Naghadeh and Toker's methods.

5.4 Experimental Program

For this study, six soil samples of gravelly and sandy soils were collected in the northern New South Wales (NSW) from landslide-prone areas [17], Table 5.1 provides the particle size distribution, coefficients of uniformity (C_u) and curvature (C_c) as well as USCS classification for each soil. It is evident from this table that all soils were non-plastic coarse-grained soils, varying from gravel to sand with different degree of gradation. A series of laboratory tests including direct shear and suction tests were conducted on each soil in Griffith University, Gold Coast, Australia. The following section details the experimental procedures.

Table 5.1: Particle size distribution and classification of tested soils

Soil No.	%Passing 4.75 mm sieve	Fines (%)	Cu	Cc	USCS
1	89.4	2.4	8.6	1.2	SW
2	70.5	5.6	13.2	1.7	SW
3	78.9	3.7	15.7	1.1	SW
4	94.4	3.8	2.7	1.2	SP

5	70.7	3.0	13.1	1.4	SW
6	40.0	3.8	43.2	2.9	GW

5.4.1 Direct Shear Tests

Direct shear tests (the size of the shear box was 60 mm x 60 mm) were performed according to the AS1289.6.2.2 - 1998 procedure. Soil samples were oven-dried at 105^0C for 24 hours, and then passed through the 4.75 mm sieve. For each soil type, shear box tests were performed on specimens at various moisture contents, ranging from 0 to 40%. To allow comparisons of the obtained results, all specimens for each soil sample were prepared to the same dry density. The moist specimens were prepared by mixing the oven-dried soil with certain amount of water. They were allowed to rest in a sealed bag for 24 hours for more even saturation. Then, the soil specimen was compacted in the shear box in six layers to achieve the desirable value of dry density. The soil specimens were sheared under the effective vertical stress of either 28.5, 55.8 or 83.0 kPa. The peak shear stress was recorded and used to determine the strength characteristics of each soil specimen.

5.4.2 Suction Test using Filter Paper Technique

Suction tests were performed using the standard Whatman No. 42 filter paper, following the ASTM D5298 – 2016 procedure. The soil specimens were prepared with at least four different moisture contents, after which the individual SWCC could be obtained. For suction tests, material passing through a 2.36 mm sieve from the oven-dried samples was used. The suction tests were carried out using an O-ring, air-tight glass container and cling wrap. Special hand gloves and forceps were used to prepare the specimen to avoid any oil transferring from the hand to the filter paper. The wet samples were prepared by adding 10%, 20%, 30% and 40% of distilled water by weight. A set of four larger size filter papers and a smaller size filter paper were dried for 16 hours in the oven prior to use.

The plastic O-ring (a hollow tube of 51 mm diameter and 25 mm height) was placed on top of the cling wrap and the sample was hand-compacted up to the middle of O-ring. Two large filter papers with one small filter paper in between were then placed at the middle of O-ring. The purpose of the small filter paper was to measure matric suction. Then the sample was hand-compacted up to the top and a wire separator and another two large filter papers were placed at the top. The total suction was measured using the top two filter papers.

The soil sample with the O-ring was placed in a small glass bottle (of 62 mm opening diameter and 88 mm height) with the top two filter papers exposed within the bottle. Then, the bottle was tightly closed with a lid and placed in a cooler box for at least a week. After 7 days, the weight of the wet filter papers (the top two filter papers for total suction and the small filter paper for matric suction) were measured using a sensitive balance with four decimal points. Immediately, they were placed in the oven at 105^0C for 2 hours. After this drying, the weight of the filter papers was measured at once. This process was completed as quickly as possible to avoid any change due to the moisture in the air. The total suction and matric suction were calculated using Whatman No.42 calibration curves.

5.5 Results of Laboratory Tests

This section presents the lab data from shear box and suction tests. It also discusses the data on the apparent cohesion, friction angle, best fit models of SWCC, and AEV values.

5.5.1 Shear Strength of Unsaturated Soils

The shear strength at various moisture contents were obtained for each soil through a series of shear box tests and presented as the shear strength vs. displacement plots. To demonstrate typical behaviour of soil under shear, Figure 5.1 presents the lab data for Soil 1 at different normal stresses (28.52 kPa, 55.77 kPa, and 83.02 kPa). Figures 5.2 and 5.3 provide the apparent cohesion and friction angles of the tested soils plotted against the volumetric moisture content.

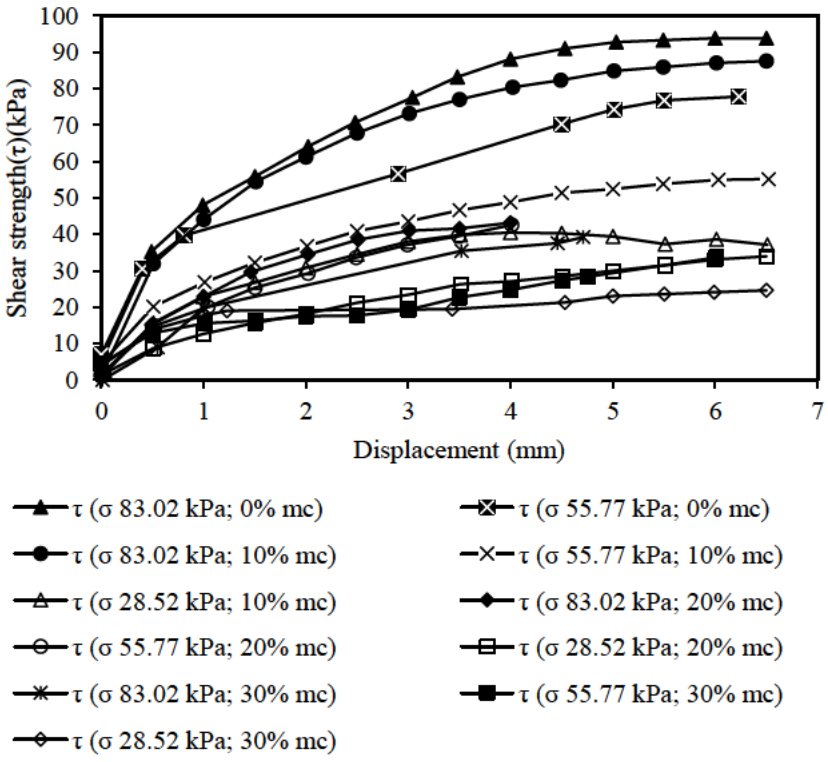

Figure 5.1: Shear stress vs. shear displacement at different normal stresses and moisture content (mc, in %)

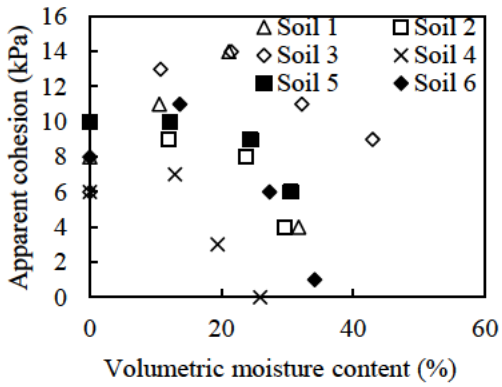

Figure 5.2: Test results from shear box test plotted as the apparent cohesion vs. volumetric moisture content

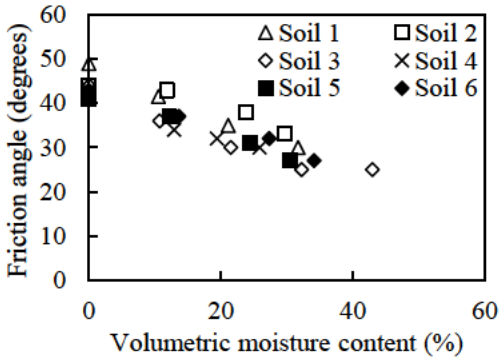

Figure 5.3: Test results from shear box tests plotted as the friction angle vs. volumetric moisture content

From Fig. 5.2, it can be noted that for four soils (Soil 1, 3, 4 and 6) the apparent cohesion increases up to a certain extent and then decreases with increasing amount of moisture. However, for all tested soils, the friction angle tends to decrease with increasing moisture content, as shown in Fig.5.3.

Based on the shear test results, Equations (34) and (35) can be obtained. These equations show the relationship for the cohesion ratio (c/c_0) and the friction angle ratio (ϕ/ϕ_0) with the moisture content, respectively, using an optimization technique by minimising the squared sum of the normalized residuals (SSNR):

$$c/c_o = 1 - 7.23\,\theta^2 \tag{34}$$

where, c is the cohesion at any volumetric moisture content; c_0 is the cohesion at zero volumetric moisture content; and θ is the volumetric moisture content.

$$\phi/\phi_0 = e^{-1.38\theta} \tag{35}$$

where, ϕ is the angle of internal friction at any volumetric moisture content; ϕ_0 is the angle of internal friction at zero volumetric moisture content.

Eq. (34) and Eq. (35) provide the relationship between the shear strength parameters of gravelly and sandy soils and moisture content that can be used to estimate the change of shear strength for similar types of gravelly and sandy soil.

5.5.2 SWCC of Tested Soils

The suction tests produced a series of data plotted as the volumetric moisture content against matric suction, as shown in Figure 5.4. To build SWCC for a wider range of moisture content, the lab data from Fig. 5.4 and Eq. 24 were used. According to Vanapalli et al [13], the suction value at the residual water content (ψ_r) can be assumed to be around 3000 kPa as it produced good estimates of shear strength. The saturated volumetric water content θ_s was obtained from the SWCC plot (Fig. 5.4). The fitting parameters (a, n, and m) from Eq. (24) were estimated by applying the optimization technique. To estimate the range of these parameters, the data on 30 coarse-grained soils provided by Chin et al [22] was considered. The following ranges were assumed: a (from 0.1 to 5), n (from 0.1 to 15), and m (from 0.1 to 2). The estimated fitting parameters are reported in Table 5.2.

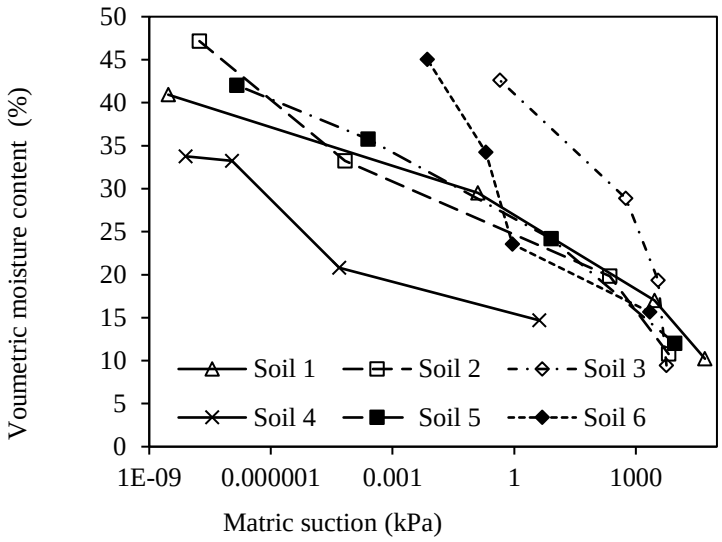

Figure 5.4: Volumetric moisture content vs. matric suction (measured SWCC)

Table 5.2: Model parameters used to estimate used to estimate shear strength

Soil No.	SWCC fitting parameters			D_{60} (m)	AEV (kPa)	M
	a	n	m			
1	0.1	0.1	1.2	1.9E-03	6.5E-09	5.9
2	0.2	0.1	2.0	3.3E-03	1.1E-08	5.6
3	5.0	0.5	0.9	5.8E-04	2.0E-09	4.7
4	0.6	9.6	0.3	2.7E-04	9.3E-10	7.0
5	2.2	8.4	0.2	3.4E-03	1.2E-08	7.0
6	0.2	15.0	0.2	2.8E-03	9.6E-09	3.9

Figures 5.5 to 5.7 show an example of comparisons between the laboratory data and the best fit SWCC models for Soils 1, 2 and 6, respectively, which will be used later for shear strength prediction.

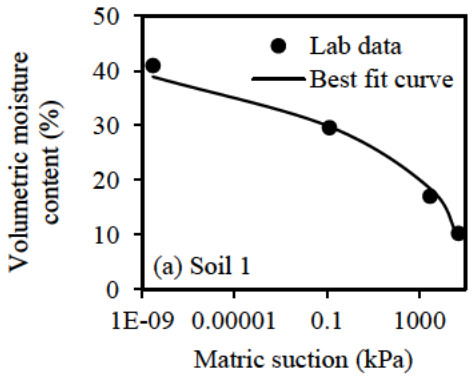

Figure 5.5: Comparison of the best fit SWCC models with the measured lab data – Soil 1

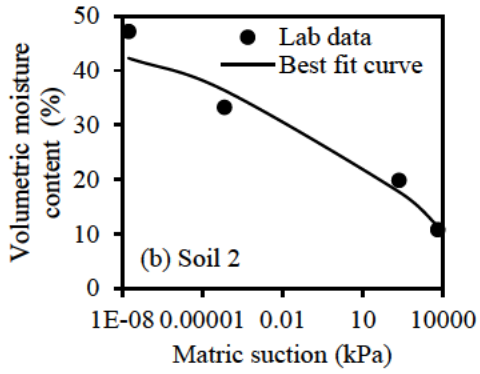

Figure 5.6: Comparison of the best fit SWCC models with the measured lab data – Soil 2

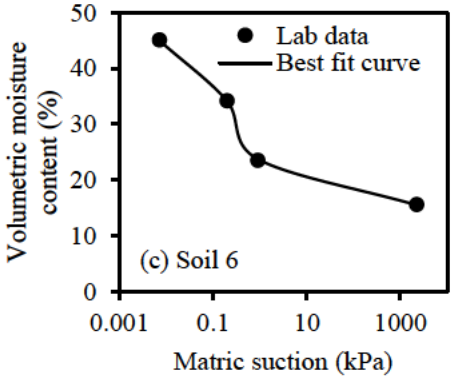

Figure 5.7: Comparison of the best fit SWCC models with the measured lab data – Soil 6

5.6 Estimation of Shear Strength

Vanapalli et al [23] and Kim et al [24] noted that the effect of vertical stress on the SWCC is negligible under relatively low confining pressures. Therefore, it can be assumed that the SWCC obtained using the filter paper technique can represent the SWCC of soils that are subjected to low vertical stresses. For this reason, only the shear box data obtained for the lowest normal stress of 28.5 kPa was used to for comparisons.

The suction value (u_a - u_w) for each moisture content was obtained from the relevant best fit SWCC models using the data from Table 5.2. The model parameter R used in Eq. (29) was calculated using the Excel Solver option by applying the optimization technique. In this study, R was estimated for all six soils as 0.35×10^{-6}. The estimated values of AEV for each soil were obtained using Eq. 29 and summarized in Table 5.2.

The shear strength for six soils was estimated using the Khalili and Khabbaz's method in Eq. (26) to Eq. (28) and the AEV value from Table 5.2. Eq. (30) to Eq. (32) were used to estimate the shear strength by the Naghadeh and Toker's method. For the newly-proposed method, the

parameter M from Eq. (33) was calculated using the Excel Solver by applying the optimization technique. The range for parameter M was assumed to be between 1 and 7. The obtained values of M for each soil are presented in Table 5.2. Figures 5.8 to 5.13 provide comparisons of the predicted shear strength using three models with the measured shear strength from the shear box tests.

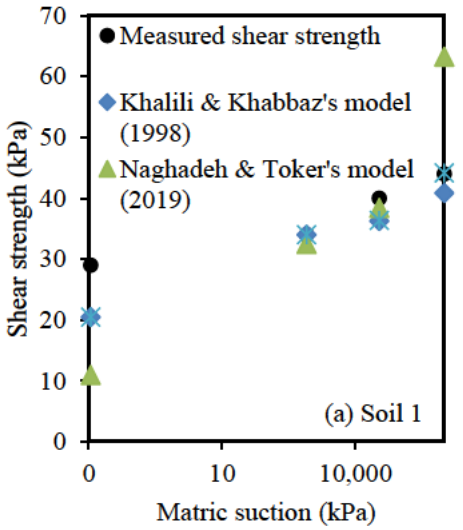

Figure 5.8: Comparison of predicted shear strength with measured shear strength of Soil 1

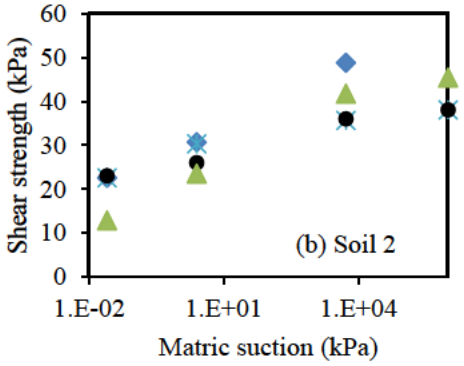

Figure 5.9: Comparison of predicted shear strength with measured shear strength of Soil 2

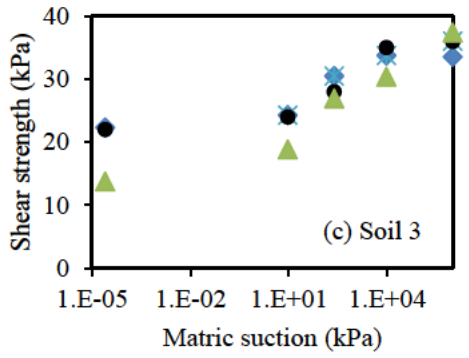

Figure 5.10: Comparison of predicted shear strength with measured shear strength of Soil 3

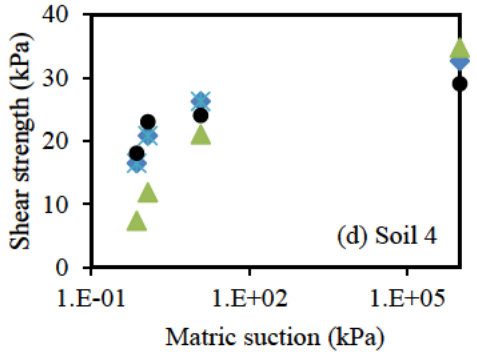

Figure 5.11: Comparison of predicted shear strength with measured shear strength of Soil 4

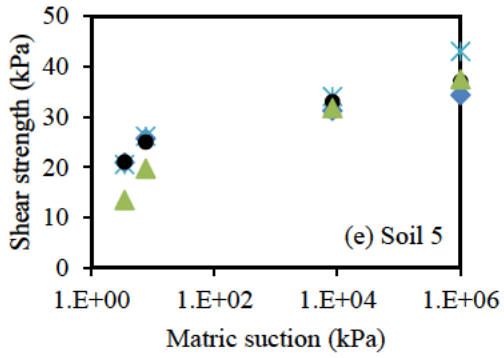

Figure 5.12: Comparison of predicted shear strength with measured shear strength of Soil 5

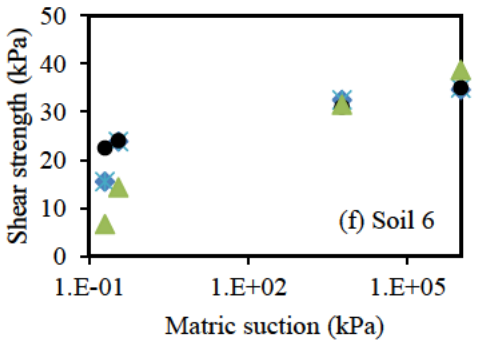

Figure 5.13: Comparison of predicted shear strength with measured shear strength of Soil 6

It is evident from Figures 5.8 to 5.13 that the three models predict the shear strengths of unsaturated soils within reasonable limits. However, both the Khalili and Khabbaz's model and the newly-proposed model provide closer values to the measured shear strength in the lab. The Khalili and Khabbaz's model predicts within 35% of the measured shear strength, while the Naghadeh and Toker's method tends to overestimate (44 - 71%). The proposed method predicts within 31% of the measured shear strength. The overestimation obtained for the Naghadeh and Toker's method can be attributed to the fact that this approach was developed using fine-grained plastic soils.

5.7 Conclusion

A series of shear box and suction test were performed on six coarse-grained soils at different water content and based on the obtained results the following major conclusions can be drawn:

- The shear strength of the studied soils decreased from 34% to 43% when the water content increased from 0% to 30%.
- It was found that the apparent cohesion slightly increased up to a certain extent and then significantly decreased with increasing water content. On the other hand, the friction angle continuously decreased with increasing water content.

  The Khalili and Khabbaz's model predicts within 35% of the measured shear strength, while the Naghadeh and Toker's method overestimate within 71%. The proposed method predicts using the soil gradation characteristics within 31% of the measured shear strength. Although being limited to gravelly and sandy soils, the proposed method can predict the shear strength

of soil at low normal stress conditions in respect to changes in moisture content with reasonable accuracy.

5.8 Acknowledgements

The comments and views expressed in this paper are those of the authors and not necessarily of others. It is acknowledged that soil samples were obtained from public authorities.

5.9 References

[1] Guan, G.S., Rahardjo, H., & Choon, L.E. Shear strength equations for unsaturated soils under drying and wetting. Journal of Geotechnical and Geoenvironmental Engineering, Vol. 136, No.4, 2010, pp.594-606.

[2] Farooq, K., Rogers, J.D., & Ahmed, M.F. Effect of densification on the shear strength of landslide material: A case study from Salt Range, Pakistan. Earth Science, Vol. 4, No. 1, 2015, p.113.

[3] Cogan, J., Gratchev, I., & Wang, W. Rainfall-induced shallow landslides caused by ex-tropical cyclone Debbie, 31st March 2017. Landslides, Vol. 15, No.6, 2018, pp.1215-1221.

[4] Krahn, J., Fredlund, D.G., & Klassen, M.J. Effect of soil suction on slope stability at Notch Hill. Canadian Geotechnical Journal, Vol. 26, 1989, pp.269-278.

[5] Yoshida, Y., Kuwano, J., & Kuwano, R. Rain-induced slope failures caused by reduction in soil strength. Soils and Foundations, Vol. 31, No. 4, 1991, pp.187-193.

[6] Hossain, M.A., & Yin, J.H. Shear strength and dilative characteristics of an unsaturated compacted completely decomposed granite soil. Canadian Geotechnical Journal, Vol. 47, No. 10, 2010, pp.1112-1126.

[7] Gallage, C., & Uchimura, T. Direct shear testing on unsaturated silty soils to investigate the effects of drying and wetting on shear strength parameters at low suction. Journal of Geotechnical and Geoenvironmental Engineering, Vol. 142, No. 3, 2016, p. 04015081.

[8] Patil, U.D., Puppala, A.J., Hoyos, L.R., & Pedarla, A. Modeling critical-state shear strength behavior of compacted silty sand via suction-controlled triaxial testing. Engineering Geology, Vol. 231, 2017, pp.21-33.

[9] Kong, L.W, & Tan, L.R. Study on shear strength and swelling – Shrinkage characteristic of compacted expansive soil. In Unsaturated soils for Asia, Singapore edited by Rahardjo, H., Toll, D.G., & Leong, E.C., 2000, pp.515-519.

[10] Tilgen, H.P. Relationship between suction and shear strength parameters of compacted metu campus clay. Masters of Science thesis, The Middle East Technical University, Ankara, Turkey. 2003.

[11] Qi, J., Song, X., & Liu, J. A study on the effects of water content on strength parameters of landslide soil. Applied Mechanics and Materials, Vol. 170-173, 2012, pp.785–788.

[12] Fredlund, D.G., Xing, A., Fredlund, M.D., & Barbour, S.L. The relationship of the unsaturated soil shear strength to the soil water characteristics curve. Canadian Geotechnical Journal, Vol. 32, No. 3, 1996, pp.440-448.

[13] Vanapalli, S.K., Fredlund, D.G., Pufahl, D.E., & Clifton, A.W. Model for the prediction of shear strength with respect to soil suction. Canadian Geotechnical Journal, Vol. 33, 1996, pp.379-392.

[14] Kim, W.S., & Borden, R.H. Influence of soil type and stress state on predicting the shear strength of unsaturated soil using the soil-water characteristics curve. Canadian Geotechnical Journal, Vol. 48, 2011, pp.1886-1900.

[15] Vilar, O.M. A simplified procedure to estimate the shear strength envelope of unsaturated soils. Canadian Geotechnical Journal, Vol 43, No. 10, 2006, pp.1088-1095.

[16] Naghadeh, R.A., & Toker, N.K. Exponential equation for Predicting Shear Strength Envelope of Unsatuated Soils. International Journal of Geomechanics, Vol. 19, No. 7, 2019, pp.04019061-1-04019061-12

[17] Ravindran, S., Gratchev, I., & Jeng, D-S. Analysis of rainfall-induced landslides in northern New South Wales, Australia. Australian Geomechanics, Vol. 54, No. 4, 2019, pp.85-99.

[18] Zapata, C.E. Uncertainty in soil water characteristics curve and impacts on unsaturated shear strength predictions. PhD Dissertation, Arizona State University, Tempe, 1999.

[19] Lu, N., & Likos, W.J. Unsaturated soil mehanics. Hoboken, NJ, Wiley, 2004.

[20] Fredlund, D.G., Rahardjo, H., & Fredlund, M.D. Unsaturated soil mechanics in engineering practice. New Jersey, USA and Canada, John Wiley & Sons, Inc., 2012.

[21] Ravindran, S., Gratchev, I., & Jeng, D-S. Prediction of shear strength of unsatuarated soils in landslide-prone areas using direct shear and suction tests under low normal stress condition. In Proceedings of UNSAT2018, The 7th International Conference on unsaturated soils, Hong Kong, Vol. 2, 2018, pp. 947-952.

[22] Chin, K.B., Leong, E.C., & Rahardjo, H. A simplified method to estimate the soil-water characteristics curve. Canadian Geotechnical Journal, Vol. 47, 2010, pp.1382-1400.

[23] Vanapalli, S.K., Fredlund, D.G., & Pufahl, D.E. The influence of soil structure and stress history on the soil-water characteristics of a compacted till. Geotechnique, Vol. 49, No. 2, 1999, pp.143-159.

[24] Kim, B.S., Shibuya, S., Park, S.W., & Kato, S. Application of suction stress for estimating unsaturated shear strength of soils using direct shear testing under low confining pressure. Canadian Geotechnical Journal, Vol. 47, 2010, pp.955-970.

STATEMENT OF CONTRIBUTION OF CO-AUTHORED PUBLISHED PAPER

This chapter includes a co-authored paper. The bibliographic details for this paper including all the authors are:

Ravindran, S and Gratchev, I 2021, 'Prediction of shallow rainfall-induced landslides using shear strength of unsaturated soil', *Indian Geotechnical Journal*, pp. 1-12.

My contribution to the paper involved:
Defining the scope and the structure of the paper, performing relevant experiment and collectiong data from relevant sources, categorising and analysisng data and writing the manuscript.

(Signed)_____ Date:
Sinnappoo Ravindran

(Countersigned)_____ Date:
Co-author1 of the paper: Dr Ivan Gratchev

(Countersigned)_____ Date:
Suppervisor Dr Ivan Gratchev

Chapter 6: Prediction of shallow rainfall-induced landslides using shear strength of unsaturated soil

This chapter has been accepted by Indian Geotechnical Journal.

6.1 Abstract

Rainfall-induced landslides occur more often with climate change, resulting in destruction and loss of lives in many parts of the world. Predicting such landslides is paramount to maintain local infrastructure and the well-being of communities. Several models have been proposed in the past years; however, most of them only work well when being applied to local site conditions for which they were developed. This work describes a new approach to estimate a model parameter related to shear strength conditions of local soils. To validate the theoretical concepts of a model, a series of shear box and undrained triaxial tests were conducted on soil specimens prepared at different values of water content. The refined model was then applied to three landslide sites to estimate the stability of slopes against past rainfall events. The obtained results showed more accurate predictions of landslide occurrence compared to the existing models. This paper presents and discusses field and laboratory data as well as the outcomes of numerical analysis.

Keywords: slope stability, factor of safety, cohesion, shear strength

6.2 Introduction

As rainfall-induced landslides cause significant casualties and destruction across the world (Cascini et al. 2008; Montrasio and Valentino 2008; Springman et al. 2013, Park et al. 2013; Ono et al. 2014; Bordoni et al. 2015a; Yang et al. 2015; Donnini et al. 2017), there have been several studies aimed at improving the existing methods and procedures for slope stability analysis. It has been shown that the stability of slopes can be affected by different factors such as rainfall characteristics (i.e., rainfall duration and intensity), slope geometry and soil properties (Cuomo and Della Sala 2013, 2015; Ali et al. 2014). To consider the aforementioned factors in slope stability analysis, different numerical methods including closed form equations (Lu and Godt 2008, 2013), physically based models (Campbell 1975; Montgomery and Dietrich 1994; Iversion 2000; Baum et al. 2002, 2008; Montrasio and Valentino 2008) and

finite element models (Cuomo and Della Sala 2013; Springman et al. 2013) have been proposed and tested in the literature. These methods have also indicated that the soil hydrological properties related to the soil water characteristics curve (SWCC) can be successfully used for the prediction of rainfall-induced landslides (Montgomery and Dietrich 1994; Iversion; 2000, Baum et al. 2002, 2008; Bathurst et al. 2005; Askarinejad et al. 2012; Park et al. 2013; Lu et al. 2013; Bordoni et al. 2015a). In addition, a few empirical relationships between the rainfall characteristics and landslide occurrence have been reported in the literature (Caine 1980; Guzzetti et al. 2007, 2008; Dahal and Hasegawa 2008; Saito et al. 2010, Ravindran et al. 2019; Cogan and Gratchev 2019) for different parts of the world that can be used to estimate the potential damage from landslide disaster.

From an engineering point of view, a simplified method for slope stability analysis under different rainfall conditions will provide a quick and effective solution to estimate the landslide hazard prior to construction (Ali et al. 2014). Selby (1993), Rahardjo et al. (2007), Wu et al. (2016), and Ran et al. (2018) noted that an infinite slope model can be suitable for the analysis of shallow rainfall-induced landslides as the failure planes of such landslides are normally parallel to the slope surface. In recent years, Baum et al. (2002; 2010) developed a transient rainfall infiltration and grid-based regional slope stability model (TRIGRS) to predict shallow rainfall-induced landslides and identify landslide hazard zones (Zhuang et al. 2017). Concurrently, Montrasio (2000), Montrasio and Valentino (2008) and Montrasio et al. (2009, 2011, 2016, 2018) developed a shallow landslide instability model (SLIP) that can assess the stability of shallow landslides using rainfall data (Ono et al. 2014).

Although these models provide a powerful tool to estimate landslide hazard, there were mostly tested and validated for local site conditions for which they were designed. It is not clear whether these models shall work for different parts of the world, particularly for the northern New South Wales, Australia where rainfall-induced shallow landslides cause significant economic loss to local communities on a regular basis (Ravindran et al. 2019). This study adopts the existing models to predict the occurrence of shallow landslides and proposes a new and more universal approach to estimate the model parameters related to local conditions. The new approach is verified against three case studies in which shallow landslides were triggered by rainfall events. This paper presents and discusses the obtained results.

6.3 Theoretical background

6.3.1 SLIP model to estimate the stability of unsaturated soil mass

This study adopts the SLIP model (Montrasio 2000), which employs a limit equilibrium method to estimate the factor of safety (*FS*) for an infinite slope. In this model, the potential landslide mass is divided into two parts (layers): a saturated layer at the bottom and an unsaturated layer near the surface as shown in Fig. 6.1 where *N* is the normal force; *W* is the weight of soil mass; *S* is the shear strength of soil along the failure plane; *H* is the height of slope and *m* is the boundary between the unsaturated and saturated layers.

The boundary between these two layers is defined by a parameter, which can vary in time depending on the amount and intensity of a rainfall event. The saturated layer is represented by *mH*, where 0<*m*<1 and *H* is the height of the slice as shown in Fig. 6.1. The unsaturated layer thickness is given as *(1 - m)H*. The parameter *mH* depends on the total amount of rainfall (*h*), and it is linked to the soil degree of saturation (S_r) (Montrasio and Valentino 2008) as shown in Eq. 36. Montrasio et al. (2010) noted that S_r is influenced by climatic conditions and seasonal weather, and it can vary from 0.6 in summer to 0.9 in winter (Ono et al. 2014).

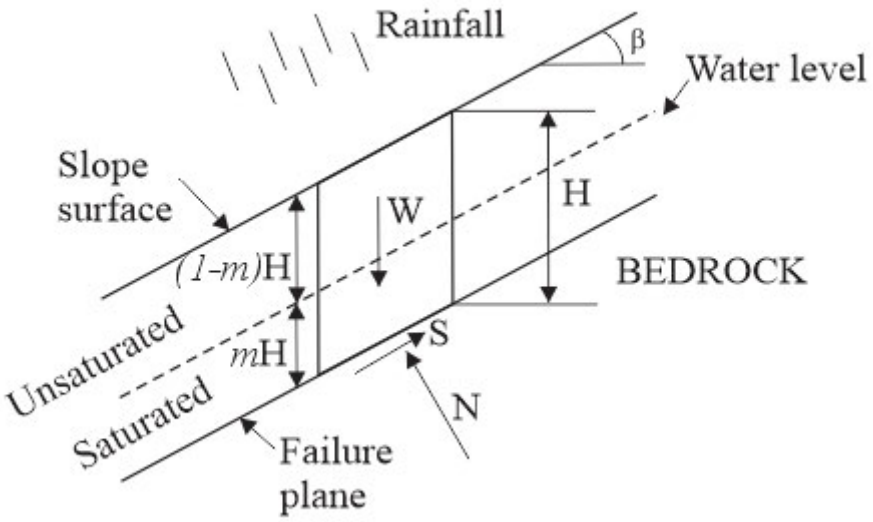

Figure 6.1: Forces acting on soil mass in an infinite slope (after Montrasio and Valentino, 2016)

$$mH = (\beta^* x\ h)/n(1 - S_r) \quad (36)$$

where, h is the rainfall amount as a function of time; H is the thickness of soil layer; β^* is the percentage of rainfall that infiltrates into the soil; n is the soil porosity; S_r is the degree of saturation, and m is the portion of saturated layer of H.

To estimate the shear strength of soil, Eq. 37 which describes the Mohr-Coulomb failure criterion for unsaturated soils (Fredlund and Rahardjo 1993; Montrasio et al. 2018) is used.

$$\tau = c' + \sigma' tan\emptyset' + c_\psi = \sigma' tan\emptyset' + C \quad (37a)$$

$$C = c' + c_\psi \quad (37b)$$

where, τ is the shear strength of soil; c' is the effective cohesion; σ' is the effective normal stress, and c_ψ is the apparent cohesion. The apparent cohesion (c_ψ) , which typically exists in unsaturated soil, depends on matric suction, and can be estimated using the degree of saturation (S_r) (Fredlund et al. 1996). Previous studies suggested that for saturated conditions, the amount of matric suction in soil drops to 0, and so does the apparent cohesion. To account for changes in the soil strength during a rainfall event when the soil mass gradually becomes saturated, Montrasio et al. (2018) proposed Eqs. 38 and 39. These equations can be used to estimate the variation in apparent cohesion of soil mass (Fig. 6.1) in respect to *m*.

$$c_\psi^* = A\, S_r(1 - S_r)^\lambda \quad (38)$$

where, c_ψ^* is the ancillary parameter, *A* is the model parameter which depends the type of soil; and λ is the constant for a wide range of soil. It is noted that for saturated soil (when $S_r=1$) c_ψ^* becomes zero.

$$c_\psi = c_\psi^*(1 - m)^\propto \quad (39)$$

where, $\propto$ is the model parameter equals to 3.4 (Montrasio and Valentino 2008). To estimate the Factor of Safety (*FS*), the limit equilibrium method is used as described in Eqs. 40-45.

$$FS = (cot\beta\ x\ tan\emptyset'\big(\Gamma + m(n_w - 1)\big) + C' x\ \Omega)/(\Gamma + m\ x\ n_w) \quad (40)$$

$$\Gamma = G_s \, x \, (1 - n) + n \, x \, S_r \tag{41}$$

$$C' = (c' + c_\psi) \, x \, L \tag{42}$$

$$m = \left(\frac{\beta^*}{nH(1-S_r)}\right) x \sum_{i=1}^{w} h_i \, x \exp\left(-k_t(t - t_i)\right) \tag{43}$$

$$n_w = n \, x \, (1 - S_r) \tag{44}$$

$$\Omega = 2/(\sin 2\beta \, x \, H \, x \, \gamma_w) \tag{45}$$

where, β is the slope angle; L is the width of a slice; k_t is the drainage capability of the slope (i.e., the coefficient of permeability), and γ_w is the unit weight of water.

Out of three model parameters ($\propto$, A, λ), the parameter A is the most difficult to estimate. Montrasio and Valentino (2008) proposed to use the following values: 40, 80, and 100 for sand, mud, and clay, respectively. However, it appears to suit only local conditions for which the parameter A was designed, and thus its use for different regions may be questionable. In addition, no guidelines on how to estimate the parameter A for different types of soil have been provided so far. This makes it rather difficult to apply the aforementioned SLIP model to a wider range of geotechnical conditions and different regions.

6.3.2 New procedure to estimate the parameter A

This study proposes a new procedure to estimate the parameter A on the basis of laboratory tests. A recent study on the initiation of shallow rainfall-induced landslides, which was conducted by Cogan and Gratchev (2019) using a series of flume tests, indicated that during a rainfall event, water infiltrates into the soil mass and accumulates at the bottom, making the soil saturated. Thus, for soil mass as shown in Fig. 6.1, the shear strength of soil varies from unsaturated (top of the slice) to saturated (bottom of the slice), and the parameter m is used to draw a boundary between the saturated and unsaturated conditions. To estimate the variation in soil strength within a soil slice (Fig. 6.1) during a rainfall event, the difference between the unsaturated and saturated shear strength will be considered as shown in Eq. 46. It is noted that this relationship is primarily used for coarse-grained material in which the difference between the saturated (τ_{sat}) and unsaturated (τ_{unsat}) shear strength is typically related to the apparent

cohesion. This assumption is supported by previous laboratory studies (Fredlund and Rahardjo 1993; Jotisankasa and Mairaing 2010; Montrasio et al. 2018; Naghadeh and Toker 2019) which indicated that changes in water content greatly affect the apparent cohesion of soil while the effect on soil's friction angle is rather limited. The validity of Eq. 46 will be examined in this study by testing the strength of three different soil under saturated and unsaturated conditions.

$$c_\psi \approx \tau_{unsat} - \tau_{sat} \tag{46}$$

Using conventional laboratory experiments such as triaxial and/or shear box tests, the saturated and unsaturated shear strength of soil can be readily obtained. It is widely accepted that for coarse-grained sandy material, the effective cohesion (c') is generally equal to 0. Therefore, the parameter *C* from Eq. 37a, b will be equal to c_ψ when the soil is unsaturated ($S_r<1$). From Eq. 39 it can be inferred that for unsaturated soil (when $m=0$) the ancillary parameter c_ψ^* is equal to c_ψ and, thus it can be estimated from lab tests on unsaturated soil sheared under drained conditions. In this study, a series of drained shear box tests on moist soil specimens were conducted to obtain c_ψ^*.

Following the curve fitting process, Excel Solver provides a means of estimating model parameters of any non-linear equations by minimising the residuals (*R*) which is the difference between the measured and estimated value – this is called optimisation. It is usual practice to normalise the residuals by dividing the difference between measured value and estimated value by the measured value – this is referred to as the normalised residual (*NR)*. As *NR* can be positive or negative it is normally squared – this is referred to as the squared normalised residual (*SNR)*. Following the optimisation process, the total of squared sum of normalised residuals (*SSNR*) as shown in Eq. (47) is minimised to calculate model parameters.

$$SSNR = \sum\left(\frac{measured - estimated}{measured}\right)^2 \tag{47}$$

To estimate the model parameter *A*, curve fitting process is applied using Excel Solver by minimising *SSNR* between measured c_ψ and estimated c_ψ. Measured c_ψ is calculated by applying Mohr-Coulomb theory on the plot of shear stress vs. water content obtained from the shear box test at the vertical stress of 28.5 kPa. Water content (*w*) is converted to S_r by using

specific gravity (G) and void ratio (e) and estimated c_ψ is obtained from Eq. 38 at corresponding S_r.

By first assuming different values of A in Eq. 38 (between 1 and 100) and using an optimisation technique of the *SSNR* (by means of Excel Solver) the calculation process will continue (Eq. 47) until the *SSNR* between the measured apparent cohesion values from shear box test and the estimated values using Eq. 38 is minimised. A sample calculation of the parameter A is shown in Appendix 6A which includes input parameters in calculating model parameter A for Site 1 (Table A1.1) and the results after optimisation (Table A1.2).

The following sections will provide experimental verifications of the proposed procedure and demonstrate how it can be employed to predict shallow slope failures using examples of three rainfall-induced landslides from New South Wales, Australia.

6.4 Experimental program

Soil samples were collected from the failure plane of three landslide sites (Sites 1, 2 and 3) in northern NSW, Australia. Fig. 6.2 presents cross-sections of the landslide sites. As shown by Ravindran et al. (2019), most of landslides in NSW are relatively shallow failures that occur in colluvium or filled material after a prolonged rainfall event. The field water content and unit weight for each soil were estimated and average values are given in Table 6.1. It is noted that for each site, the landslide occurred in coarse-grained sandy material.

A series of laboratory tests comprising particle size distribution, direct shear tests, undrained triaxial tests, and hydraulic conductivity tests were conducted on each soil sample at Griffith University, Gold Coast, Australia.

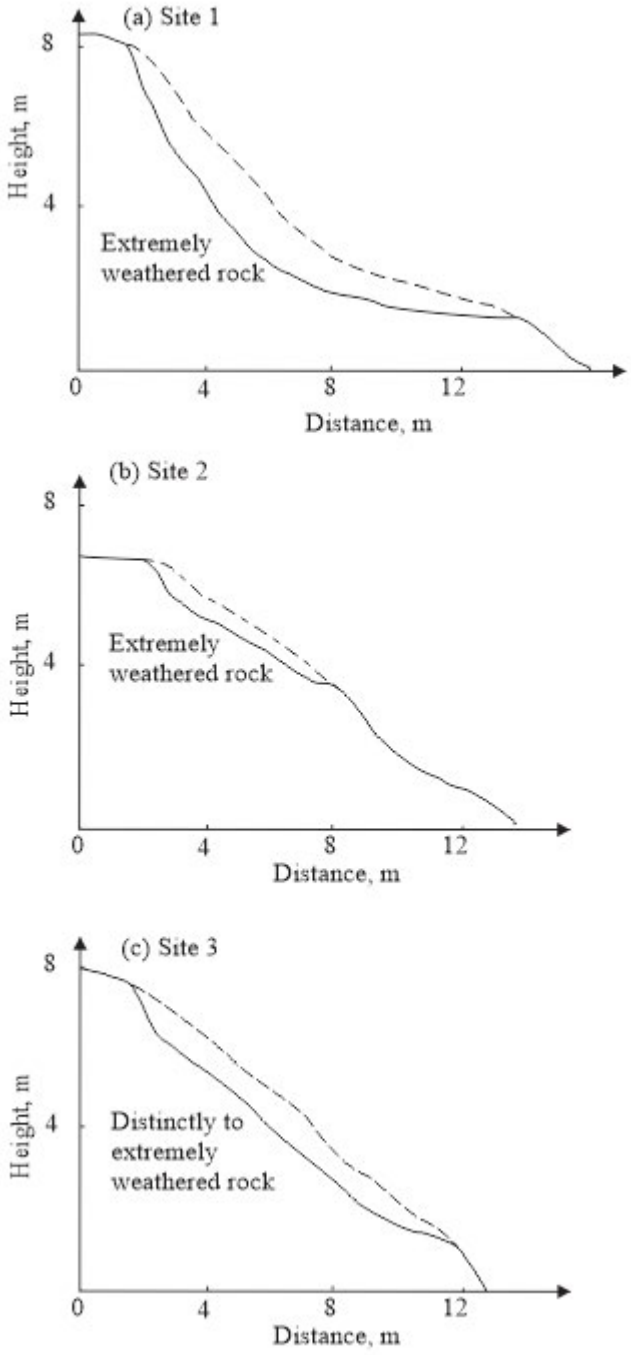

Figure 6.2: Cross-sections of the studied landslides

Table 6.1: Properties of soil samples collected from landslide sites

Landslide site	Field water content (%)	Field unit weight (kN/m^3)	Dry unit weight (kN/m^3)	Specific gravity	Voids ratio	Degree of saturation (%)	USCS classification	Hydraulic conductivity (m/s)
1	21	15.1	12.5	2.72	1.14	50	*SW*	9.1E-06
2	17	15.0	12.5	2.76	1.11	42	*SW*	1.2E-06
3	17	15.6	13.3	2.73	1.01	46	*SP*	4.2E-06

6.4.1 Direct shear tests

Direct shear tests (the size of the shear box was 60 mm x 60 mm) were performed according to the AS1289.6.2.2 - 1998. The soil samples were oven-dried at 105°C for 24 hours, and then passed through a 4.75 mm sieve. For each soil type, shear box tests were performed on specimens at various moisture contents, ranging from 0% to 40%. To allow comparisons of the obtained results, all specimens for each soil were prepared to the same dry unit weight as the one which was recorded in the field (Table 6.1).

The moist specimens were prepared by mixing the oven-dried soil with a certain amount of water. They were allowed to rest in a sealed bag for 24 hours for more even saturation. Each soil specimen was compacted in the shear box in six layers to achieve the desirable value of dry density. The soil specimens were sheared under the effective vertical stress of either 28.5, 55.8 or 83.0 kPa. The peak shear stress was recorded and used to determine the strength characteristics of each soil. For each value of water content, at least three tests with different vertical stresses were performed in order to obtain the shear strength of soil.

6.4.2 Undrained triaxial tests

Consolidated undrained triaxial tests were carried out in accordance with D4767 – 1995. The tests were performed using the GDS Triaxial Automated System which had a load frame, a triaxial cell, pressure controllers and a computer with specialised software. Soil samples passed through a 2.36 mm sieve were first dried in the oven for 24 h and the cylindrical soil specimen (100 mm height and 50 mm diameter) was then prepared. The specimen was saturated using a

back pressure control to achieve a *B-value* of at least 97%. All specimens were normally consolidated to one of the following pressure values (σ_3'): 28.5, 55.8 and 83.0 kPa. The specimen was loaded axially with a constant axial strain rate of 0.02%/min to ensure the uniform distribution of pore-water pressure in the specimen. The experiment was terminated when the axial strain reached a value of 10%.

6.4.3 Hydraulic conductivity test

A series of hydraulic conductivity tests were performed on soil samples using the constant head method, following AS 1289.6.7.3 (2016). The specimens were prepared to the same dry density as the ones used in shear box and triaxial tests. The flow rate was measured when steady state water flow conditions were established. The test was repeated at least three times and the average hydraulic conductivity was calculated and used in a numerical analysis.

6.5 Results and discussion

Typical results of shear box tests conducted on soil samples at different water contents (given in %) from three different landslide sites (1-3) are plotted in Fig. 6.3 as the shear stress vs. displacement. For each series of tests, the soil specimens with different water content were applied with the vertical stress of 28.5 kPa and sheared till the peak strength was obtained. As can be seen in Fig. 6.3, for all soil samples, an increase in the water content was generally correlated with a decrease in shear strength; that is, the maximum shear strength was observed for soil specimens with 0% and 10% water content while the lowest strength was observed for specimens with the greatest water content. It is believed that the higher shear strength at lower water content was due to the effect of suction. Table 6.2 summarizes the shear box test data for three soils from different landslide sites (1-3).

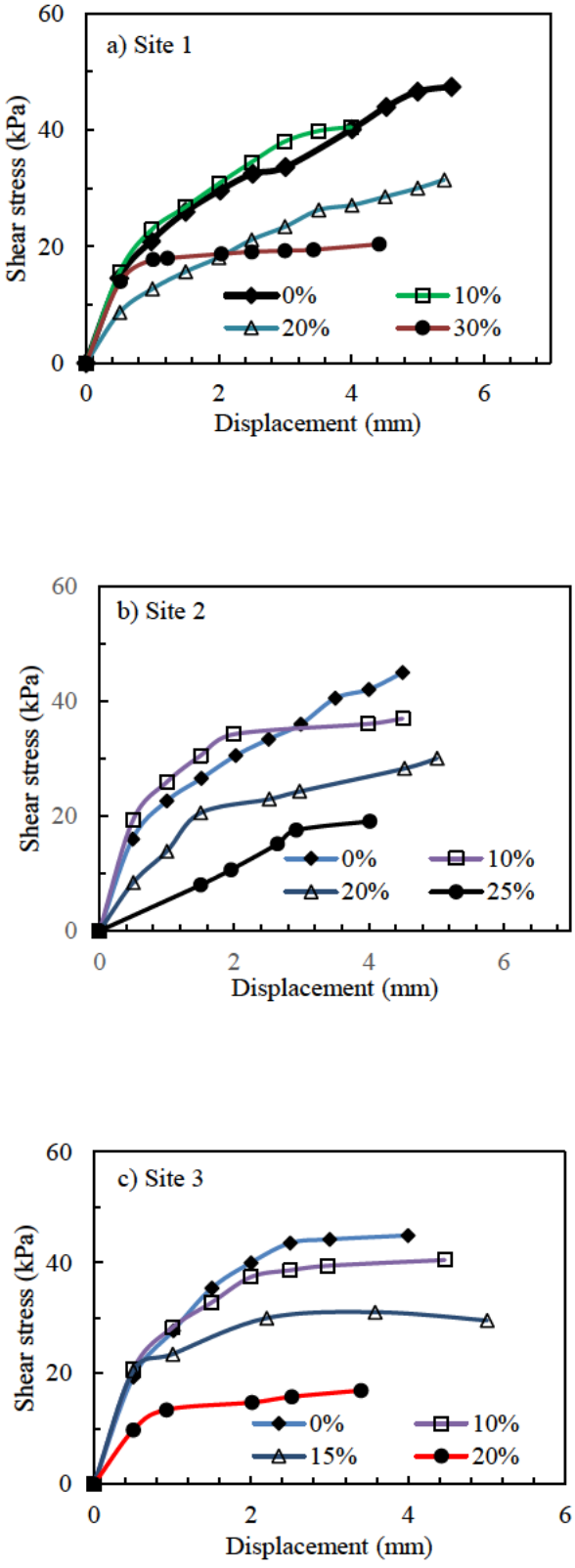

Figure 6.3: Results of shear box tests on soils from landslide sites (1 - 3) at different water content (given in %)

Table 6.2: Results of shear box and triaxial tests

Landslide site	Shear box test			Consolidated undrained triaxial test		
	Water content (%)	Apparent cohesion (kPa)	Friction angle (°)	Water content (%)	Effective cohesion, c'(kPa)	Effective friction angle, ϕ' (°)
1	0	25	38	39.3	0	35
	10	16	38			
	20	9	38			
	30	0	35			
2	0	24	37	29.1	0	31
	10	16	37			
	20	11	36			
	25	0	33			
3	0	26	34	25.5	0	29
	10	21	34			
	15	11	33			
	20	0	30			

Fig. 6.4 presents the lab data from a series of triaxial tests plotted as a change of the deviator stress against the axial strain at a confining pressure (σ'_3) of 28.5 kPa. Fig. 6.4a shows the variation of deviator stress with increasing axial strain while Fig. 6.4b gives the generation of excess pore water pressure during loading. The effective stress paths are recorded in Fig. 6.4c where $q'=q/2$, and $p'= (\sigma'_1+\sigma'_3)/2$. The saturated shear strength parameters c′and ∅′ (Table 6.2) were obtained from the analysis of undrained triaxial tests performed on the same soil at different confining stresses of 28.5, 56.0, and 84.0 kPa.

Fig. 6.5 shows the variation of the apparent cohesion (c_ψ) against the increasing degree of saturation. On the y-axis of Fig. 6.5, both the difference between unsaturated shear strength and saturated shear strength (τ_{unsat}-τ_{sat}) and apparent cohesion are plotted in kPa. It is clear from this figure that as the degree of saturation increases the value of apparent cohesion tends to decrease and it can drop to almost 0 when the degree of saturation is relatively high. It is believed that before a rainfall event the soil is partially saturated while the slope is typically under drained conditions. However, a prolonged rainfall can lead to soil saturation while the slope conditions can change to somewhat undrained, which may result in landslide. Therefore, the difference in soil strength before and after a rainfall event will have a significant impact on slope stability. It is interesting to note that for all tested soils, the change in soil strength (τ_{unsat}-

τ_{sat}) is closely related to the change in the apparent cohesion of soil (Fig. 6.5), which provides experimental evidence to the theoretical assumption in Eq. 45.

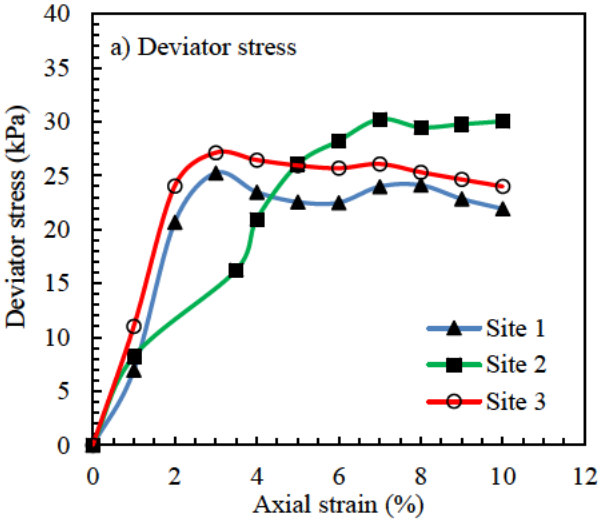

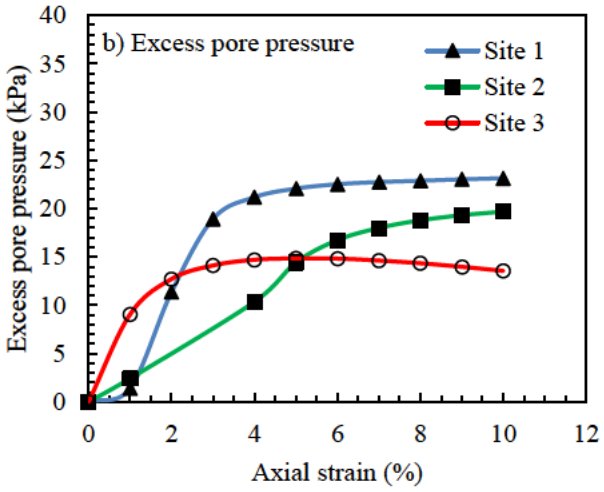

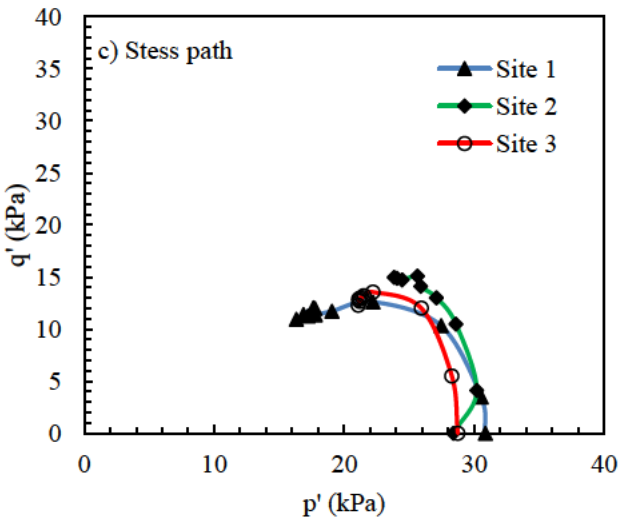

Figure 6.4: Results of undrained triaxial tests on three soils from landslide sites (1 - 3)

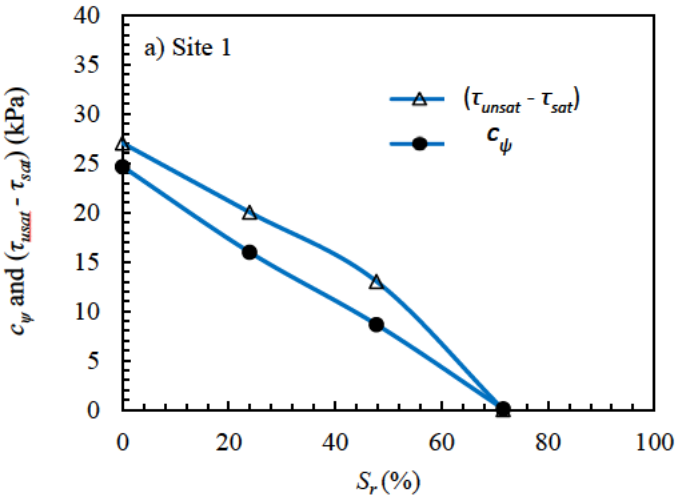

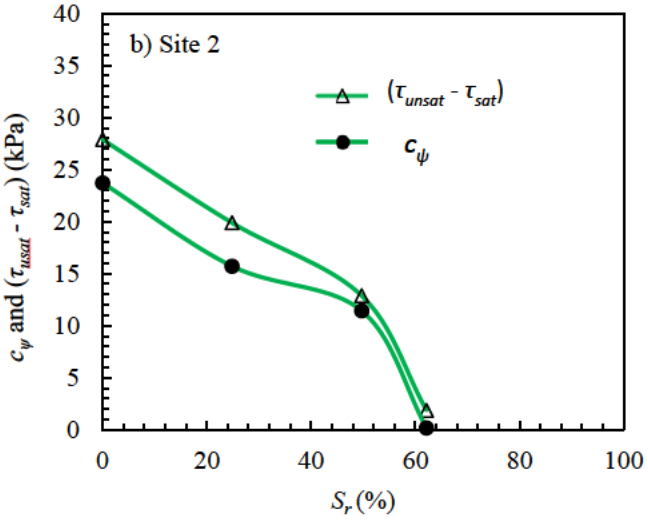

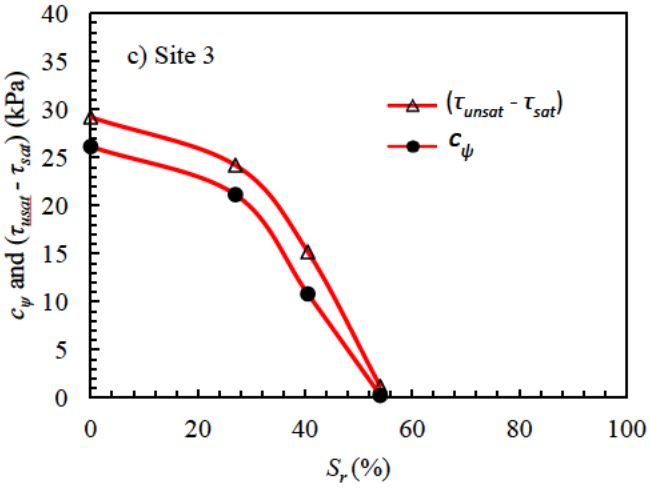

Figure 6.5: Difference between the unsaturated and saturated shear strength and the variation of apparent cohesion against the degree of saturation

6.6 Numerical analysis

To estimate the slope stability of three sites using the SLIP Model during the past rainfall evens, the following input data (Tables 6.1-6.3) were collected and analysed. The shear strength of unsaturated soil at different water content was obtained from a series of shear box tests (Table 6.2). The undrained triaxial tests provided the strength characteristics of saturated soil such as effective cohesion and effective friction angle. The coefficient of permeability was obtained

from a series of constant head tests. The degree of saturation, soil unit weight, and porosity were estimated from the field samples collected during site visits (Table 6.1).

The rainfall data was obtained from the nearest rain gauge stations from Bureau of Metrology (BOM) (Table 6.3) and shown in Figs. 6.6 to 6.8. The slope characteristics such as a depth of slip, slope angle and length were obtained during site visits (Table 6.3). It was assumed that 95% of the rainfall infiltrated the soil at these three sites (1 to 3).

Table 6.3: Input data and numerical analysis outcome

Landslide sites	Slope characteristics		Rainfall characteristics		Numerical analysis			
					Suggested by Montrasio and Valentino (2008)		This study	
	Slope angle (°)	Average slope height (m)	Duration (days)	Cumulative rainfall (mm)	*A*	Factor of Safety	*A*	Factor of Safety
1	33	2.2	6	515.4	40.0	1.02	28.2	0.96
2	28	2.8	8	378.8	40.0	1.01	36.5	0.99
3	32	2.6	5	260.4	40.0	1.05	32.7	0.99

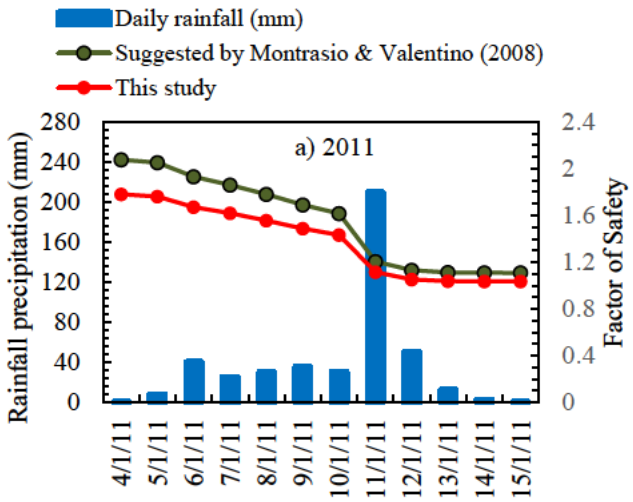

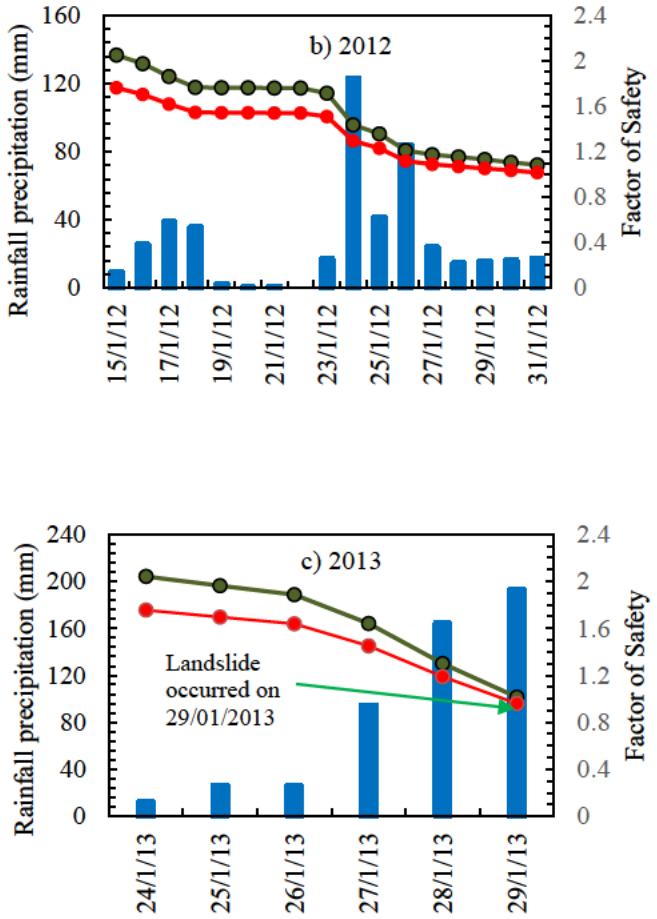

Figure 6.6: Estimation of the Factor of Safety (*FS*) during rainfall events at Site 1

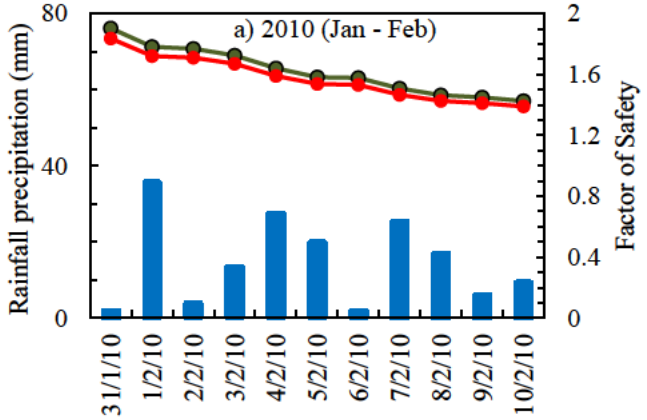

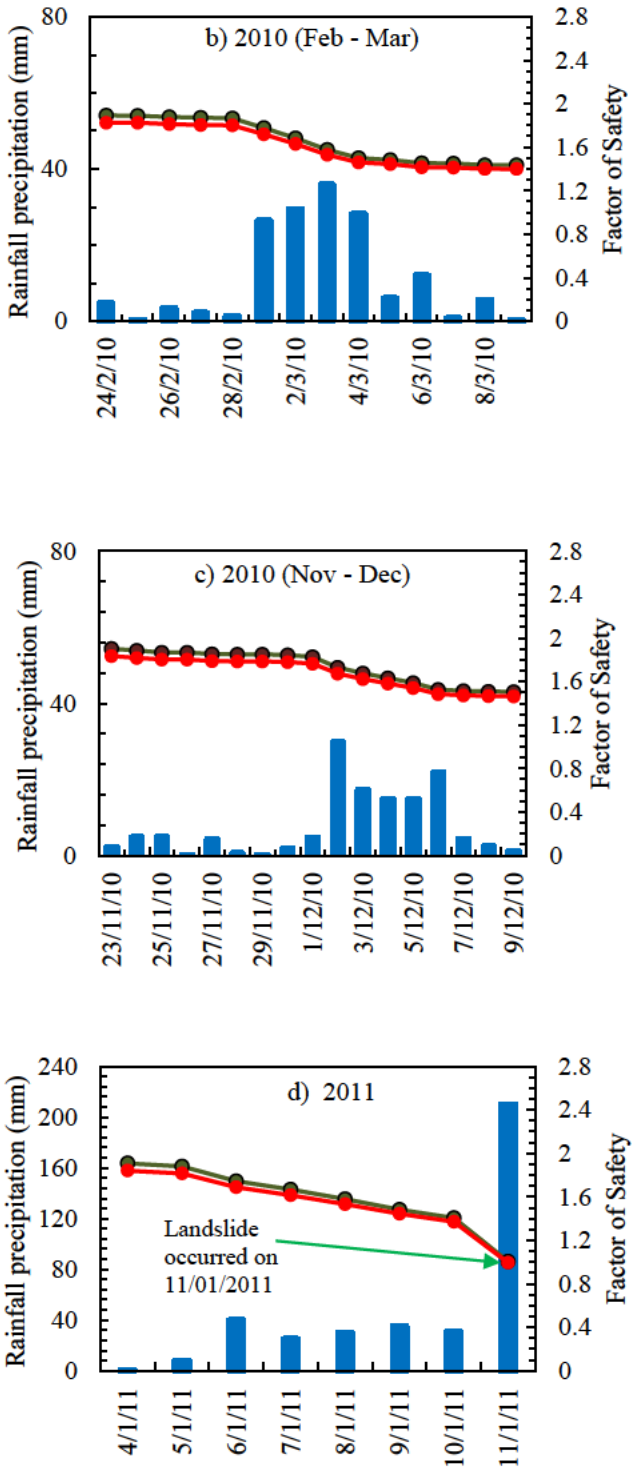

Figure 6.7: Estimation of the Factor of Safety (*FS*) during rainfall events at Site 2

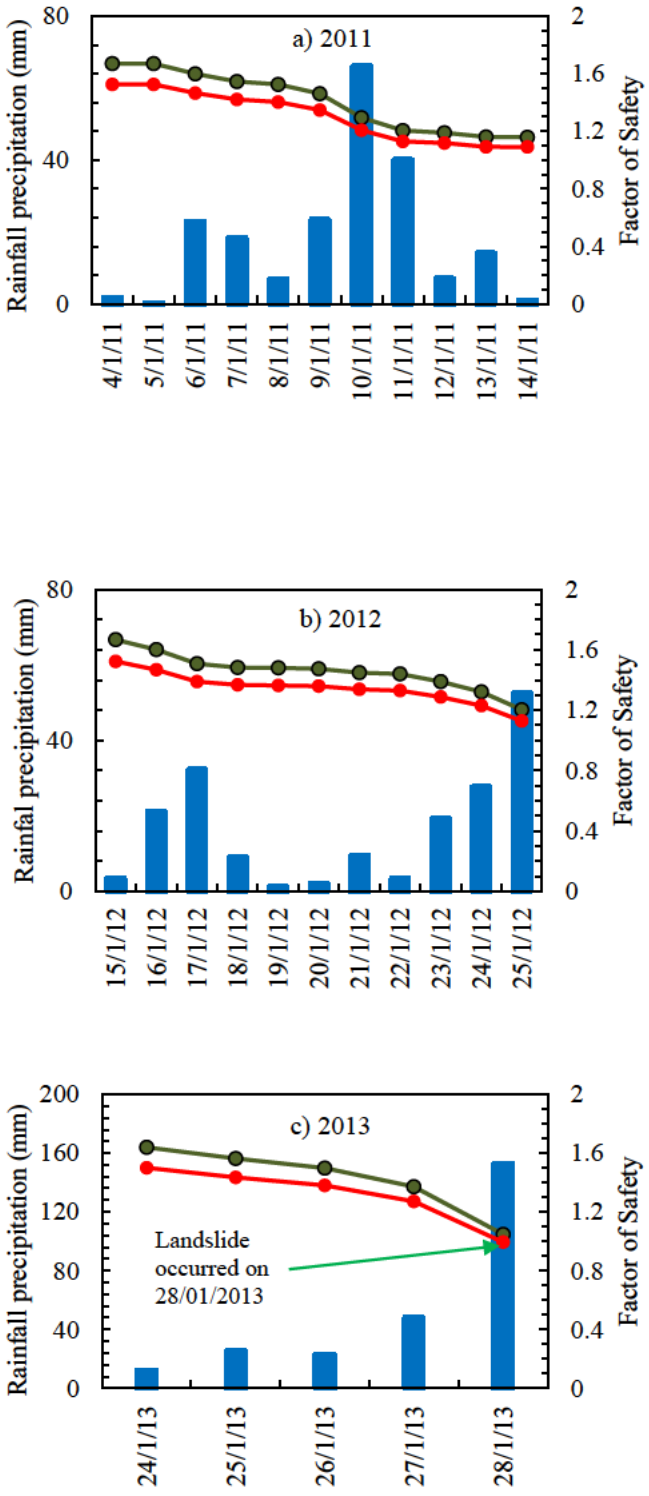

Figure 6.8: Estimation of the Factor of Safety (*FS*) during rainfall events at Site 3

The parameter *A* (in Eq. 38) was calculated using an optimisation technique without constraints (Eq. 47) by using the Excel solver function. Basically, the measured value of c_ψ from the shear box test and estimated value of c_ψ from Eq. 38 are utilised and *SSNR* is minimised to obtain model parameter *A*. The shear strength parameters obtained for the lowest normal stress of 28.5 kPa were considered in the analysis as this would better represent the stress conditions of relatively shallow landslides. The model parameters such as $\lambda = 0.4$ and $\alpha = 3.4$ were accepted following the recommendation of Montrasio and Valentino (2008) as they do not vary with the type of soil.

In the SLIP Model, the key variable is rainfall intensity (mm/day) for a particular site and thickness of saturated layer, *m* will vary per day depending on the cumulative amount of rainfall and as a result, apparent cohesion, c_ψ will also vary. The parameter *A*, which was estimated using the newly proposed procedure, was employed to calculate the factor of safety (*FS*) using the SLIP Model during rainfall events at Sites 1 to 3. For comparisons, *A=40*, as suggested by Montrasio and Valentino (2008) for sandy soils, was used in a numerical analysis for all three landslide sites as well. The calculated parameter *A* using newly proposed procedure is less than 40 which is the value suggested by Montrasio and Valentino (2008) at each site. An example of calculations is given in Appendix 6B showing input parameters to the SLIP Model (Table B1.1) and describing calculation of *FS*. (Table B1.2).

The results of numerical analysis such as rainfall precipitation vs. *FS* from the SLIP Model by using local model parameter *A* (by this study) and Italian model parameter *A* (suggested by Montrasio and Valentino 2008) are given in Figs. 6.6-6.8 and summarized in Table 6.3. Figs. 6.6-6.8 illustrate *FS* for rainfall events from 2011 to 2013 at Site 1; from 2010 to 2011 at Site 2 and from 2011 to 2013 at Site 3. For Site 1 (Fig. 6.6), at which the landslide occurred on 29th January, 2013, three different rainfall events in 2011, 2012, and 2013 were considered. According to the analysis, the slope was stable during the 2011 (Fig. 6.6a) and 2012 (Fig. 6.6b) events when the factor of safety (*FS*) was estimated to be greater than 1. For the 2013 rainfall event (Fig. 6.6c), the computed *FS* was less than 1, suggesting that the slope became unstable, which was indeed confirmed by the landslide occurrence. The model also correctly predicted the occurrence of landslide at Site 2 on 11th January, 2011 (Fig. 6.7d) and for Site 3 on 28th January, 2013 (Fig. 6.8c).

When employing the average value of *A* for sandy material (*A=40*) recommended by Montrasio and Valentino (2008), the model tends to overestimate *FS*, suggesting that the slope is still

stable (*FS>1*), despite the occurrence of landslide in the field. This contradiction indicates that the new approach to obtain *A* provides more accurate estimations of slope stability.

6.7 Conclusions

A series of shear box and triaxial tests on soil specimens prepared at different water content were conducted to study the change in shear strength of soil which typically occur in landslide mass during a rainfall event. A new approach to estimate site-specific parameters was proposed and validated against laboratory experiments and the field data from three landslide sites. Based on the obtained results, the following conclusions can be drawn:

- The experimental results obtained for three sandy soils indicated that the variation in the apparent cohesion of soil caused by increases in water content correlates with the difference between soil's unsaturated and saturated shear strength.
- A new approach to estimate the parameter *A* which is related to shear strength characteristics of local soils produced more accurate results in the prediction of landslide occurrence during rainfall. The currently recommended value of *A* (A=40) tends to overestimate the safety factor.
- In this study, the parameter A obtained for local sandy soils varied from 28.2 to 36.5.

6.8 Acknowledgements

The authors would like to thank Professor Lorella Montrasio for her assistance and discussion regarding the use of SLIP model and calculation of parameter *A*.

6.9 Declarations

Funding: Not applicable.
Conflicts of interest/competing interest: Not applicable.
Availability of data and material: Available.
Code availability: Not applicable.

6.10 Appendix 6A

Table A1.1 Input parameters for soil sample from Site 1

Notation	Description	From where it is obtained
σ	Normal stress (kPa)	Shear box tests
u_a	Pore air pressure (kPa)	u_a=0
c_ψ	Apparent cohesion (kPa)	Fig. 6.5(a) & Table 6.2
e	Voids ratio	Table 6.1
S_r	Degree of saturation	Eq. 48
G	Specific gravity	Table 6.1
w	Moisture content	Table 6.2
λ	Model parameter	λ =0.4

Table A1.1 provides the input values used to estimate the model parameter *A* for Site 1. The soil voids ratio (*e*) was 1.14 and specific gravity (*G*) was 2.72. The water content (*w*) was taken from Table 2 while the degree of saturation (S_r) was calculated using Eq. 48 (Gratchev et al. 2018). The values of *w* and S_r are summarized in Table A1.2. The data from a series of shear box tests (Fig. 5a and Table 6.2) with a normal stress of 28.5 kPa was used to measure the value of c_ψ for each water content used (Table A1.2). To find the *A* parameter, the following procedure was used: 1) it was assumed that *A* should be in the range from 1-100 (Montrasio & Valentino 2008); 2) for each assumed value of *A* from this range, c_ψ was estimated using Eq. 38; 3) the difference between the measured c_ψ (from the lab tests) and estimated c_ψ (using Eq. 3) was assessed using the normalised residual (*NR*) factor (Eq. 49); 4) the optimisation technique was then applied to calculate *SSNR* (Eq. 47); and the value of *A* that produced the lowest value of *SSNR* was selected as the *A* parameter. To expedite the calculation part, the Excel Solver function was used to estimate the *SSNR* for each assumed *A*. Table A1.2 shows the value of *A* (28.2) with the minimum value of *SSNR* (1.427), which was obtained using the above procedure by means of Excel Solver.

$$S_r = \frac{w \cdot G}{e} \tag{48}$$

$$NR = \frac{(measured - estimated)}{measured} \tag{49}$$

Table A1.2 The input values to estimate the *A* parameter using Excel Solver for Site 1

w (%)	S_r (%)	Measured c_ψ from shear box tests (kPa)	Model parameter *A* proposed by Excel Solver	Estimated c_ψ (kPa) using Eq. 38	Normalised residuals, *NR*	$SSNR_{min}$ using Eq. 47
0	0.0	24.7		0.0	1.000	
10	23.9	16.0		6.0	0.623	
20	47.7	8.7	28.2	10.4	-0.196	1.427

6.11 Appendix 6B

Table B1.1 Input parameters for the SLIP model for Site 1

Notation	Description	From where is obtained	Value
m	Portion of saturated layer (m)	Eq. 43	0 to 1
H	Height of slope (m)	Table 6.3	2.2
$ß^*$	Percentage of rainfall that infiltrates	Assumption	0.95
n	Porosity	Using void ratio from Table 6.1	0.53
S_r	Degree of Saturation at initial stage (%)	Table 6.1	50
c'	Effective cohesion (kPa)	Table 6.2	0
ϕ'	Effective friction angle (degrees)	Table 6.2	35
c_ψ	Apparent cohesion (kPa)	Eq. 39	
α	Model parameter	The original SLIP model	3.4
λ	Model parameter	The original SLIP model	0.4
A	Model Parameter	Table A1.2 (optimisation)	28.17
G	Specific gravity	Table 6.1	2.72
L	Length of soil slice (m)	The original SLIP model	1
e	Euler's number		2.72
k_t	Global drainage capability (1/s)	Table 6.1	9.14E-06
β	Slope angle (degrees)	Table 6.3	33
γ_w	Water density (kN/m^3)		9.81
h	Rainfall depth (mm/day)	BOM (Rain gauge station no. 57093) and Fig. 6.6c	
c^*_ψ	Ancillary parameter (kPa)	Eq. 38	10.67
n_w	Part of the SLIP model	Eq. 44	0.27
Ω	Part of the SLIP model	Eq. 45	0.10
Γ	Part of the SLIP model	Eq. 41	1.54

Table B1.2 Calculation of *FS* using the SLIP model for soils sample from Site 1 using model parameter *A*

Rainfall - h (mm)	Cumulative rainfall (mm)	t (day)	m from Eq. 43	c_ψ from Eq. 39	C' from Eq. 42	FS from Eq. 40
12.2	12.2	1	0.01	10.35	10.35	1.75
26.2	38.4	2	0.03	9.68	9.68	1.69
25.8	64.2	3	0.05	9.05	9.05	1.64
94.4	158.6	4	0.12	7.00	7.00	1.45
164.0	322.6	5	0.24	4.25	4.25	1.19
192.8	515.4	6	0.38	2.12	2.12	0.96

Chapter 7: Concluding remarks

Rainfall-induced shallow landslides are common in northern NSW, Australia, especially at mountain ranges such as Mt Lindesay, Mallanganee Range, Ramornie – Cangai Range, Gibraltar Range, Dorrigo Mountain and Mt Seaview. This research findings are related to the investigation and analysis of rainfall-induced shallow landslides in northern NSW. The major outcomes include the prediction of shear strength of coarse-grained soils obtained from landslide-prone areas in respect to changes in soil water content, and the prediction of rainfall-induced shallow landsides using rainfall threshold, rainfall index and slope stability models. The rainfall threshold for northern NSW and the rainfall index for Mt Lindesay and Dorrigo Mountain were developed as part of this work. A slope stability model has been developed and validated for past landslides that occurred at Gibraltar and Mallanganee Ranges.

It is also important to note some limitations of this study. Rainfall data has been obtained from the nearest rain gauge station to the landslide sites, which means that the actual rainfall amount at the sites where the landslides occurred may be slightly different. The rainfall data from BOM is daily-based and hourly rainfall data was not available. There were 108 rainfall-induced shallow landslides occurred in northern NSW and soil samples were collected from 18 sites only. This was due to the time and physical constraints as well as some landslide sites were already remediated before this study.

7.1 Concluding remarks

This study was performed to determine common characteristics of several shallow landslides triggered by rainfall events in mountain passes of northern NSW (Mt Lindesay, Mallanganee Range, Ramornie–Cangai Bluff, Gibraltar Range, Dorrigo Mountain and Mt Seaview) from 2009 to 2019. Based on the field surveys, laboratory data, collected public information, and numerical analysis, the following conclusions can be drawn:

- Rainfall-induced shallow landslides in northern NSW tend to occur every two years in the mountain ranges due to loss of suction in the colluvium and/or filled material. Out of 108 landslides, about 80% were related to large rainfall events, when the rainfall amount exceeds the average norm.
- About 64% landslides occurred in mountainous terrains whereas 36% slope failures were related to rolling terrains such as embankments and riverbanks. The majority of slope failures initiated on slope terrains inclined at 35-65°, or greater than 65°.

Geological characteristics of landslide sites include sedimentary and volcanic rocks. A good deal of shallow rainfall-induced landslides occurred in weathered sandstone, in which the landslide mass consisted of coarse-grained material.

- Based on the historical rainfall data from 2009 to 2017, the rainfall intensity-duration threshold that triggers shallow landslides in the studied area can be described as $I = 22.6\, D^{-0.554}$, where I is the rainfall intensity (mm/hr); D is the duration of rainfall (hr). Analysis using the rainfall index (R′) concept for the Mt. Lindesay and Dorrigo Mountain passes reveals that landslides may occur in those areas when R′ reaches 88 mm and 136 mm, respectively.
- Results of shear box tests indicated that for most soils samples, an increase in moisture content could decrease the shear strength by more than 30%, and such a change would contribute to the slope instability during rainfall events.
- The shear strength of the studied soils tends to increase when the water content decreases, a finding that is attributed to more pronounced effect of suction at lower values of water content. It was found that the apparent cohesion significantly decreased with increasing water content. On the other hand, the friction angle only slightly decreased with increasing water content.
- A new method to estimate the shear strength of coarse-grained soils using the soil gradation characteristics was proposed and validated against the laboratory data. Although being limited to coarse-grained soils, this method can predict the shear strength of soil in respect to changes in moisture content with a reasonable accuracy. This approach can provide a quick and effective alternative to existing methods that require special laboratory equipment. The proposed Eq. 33 for a suction range of 0 to 10,000 kPa can predict the shear strength of soil within 2% of the measured value. This study indicates that using a series of simple tests such as particle size distribution, direct shear and filter paper suction tests, it is possible to predict the shear strength of unsaturated soils within an acceptable range.
- The existing SLIP model was modified and adopted for northern NSW site conditions and validated against three different sites: Gibraltar Range (Sites 1 and 2) and Mallanganee Range (Site 3) using the past rainfall events. A new approach to estimate the parameter A using laboratory data was proposed to estimate the slope stability during rainfall. It was found that the currently recommended value of A (A=40) tends to

overestimate the safety factor. In this study, the parameter A obtained for the local soils varied from 28.2 to 36.5.

This study presents the major factors that lead to shallow rainfall-induced landslides in northern NSW, and proposes simple tools that can be used to predict this natural disaster. It is believed that these findings will be useful for the relevant industry including decision-makers who manage the slope assets and landslide hazard along the road corridors in northern NSW, Australia. These findings are also applicable to other parts of the world.

7.2 Future works

The following research is recommended:

- Prediction of rainfall-induced landslides using rainfall threshold or rainfall index in landslide-prone area can warn the public and authorities so that impacts can be minimized. But slope characteristics and soil characteristics are not taken into account in this type of prediction. On the other hand, locally developed SLIP model can consider rainfall, slope and soil characteristics and provide more confidence in predicting rainfall-induced shallow landslides as opposed to rainfall threshold or rainfall index. Therefore, locally developed SLIP models are needed for many landslide sites comprising different soil materials.
- The new equations and methods developed in this study are related to coarse-grained material. It is interesting to investigate whether they can also be used for fine-grained soils.

STATEMENT OF CONTRIBUTION OF CO-AUTHORED PUBLISHED PAPER

This Appendix A includes a co-authored paper. The bibliographic details for this paper including all the authors are:

Ravindran, S, Gratchev, I & Jeng, D-S 2018, 'Prediction of shear strength of unsaturated soils in landslides-prone areas using diect shear and suction tests under low normal stress condition', in *Proceedings of UNSAT 2018, The International Conference on Unsaturated Soil*, Hong Kong, August 3-5, vol. 2, pp. 947-952.

My contribution to the paper involved:
Defining the scope and the structure of the paper, performing relevant experiment and collectiong data from relevant sources, categorising and analysisng data and writing the manuscript.

(Signed)_____ Date:
Sinnappoo Ravindran

(Countersigned)_____ Date:
Co-author1 of the paper: Dr Ivan Gratchev

(Countersigned)_____ Date:
Co-author2 of the paper: Prof Dong-Sheng Jeng

(Countersigned)_____ Date:
Suppervisor Dr Ivan Gratchev

Appendix A: Conference Paper published at UNSAT 2018, Hong Kong - Prediction of shear strength of unsaturated soils in landslide-prone areas using direct shear and suction tests under low normal stress condition

Conference Paper:
Ravindran, S, Gratchev, I and Jeng, D-S (2018), *"Prediction of shear strength of unsaturated soils in landslide-prone areas using direct shear and suction tests under low normal stress condition",* Proceedings of UNSAT2018, The 7th International Conference on Unsaturated Soils". vol. 2, pp. 947–952.

A.1 Abstract

Rainfall has been recognised as the dominant trigger for most landslides in the world. Reduction of shear strength due to loss of suction is the main cause for shallow landslides where soil is in unsaturated state. The current research shows that the shear strength of unsaturated soil can be predicted by various soil parameters. The purpose of this research is to examine the influence of water in the shear strength of unsaturated soil and develop an effective model for the prediction of shear strength. Direct shear tests on the remoulded samples revealed that shear strength reduces as the moisture content increases. The soil behaviour in low suction range (0 to 500 kPa) is important for geotechnical structures. The suction test using filter paper technique indicated that tested soils exhibit low suction range, when the moisture content varies from 10% to 51%. Prediction of shear strength of unsaturated soils was carried out with two published equations and one proposed simpler equation.

A.2 Introduction

Landslides have caused massive destruction and numerous loss of life all over the world for many decades. Jotisankasa et al. (2008) reported that rainfall is one of the dominant triggers for landslides. It has been reported in the literature that the reduction of shear strength due to loss of suction is the main cause for rainfall-induced landslides where soil is in unsaturated state (Ali et al. 2014; Mohammad et al. 2014; Trandafir et al. 2007 and Chen et al. 2004).

In unsaturated soils, classification of properties plays a key role. The matric suction and soil water characteristics curve (SWCC) are the two key properties of unsaturated soil according to Fredlund et al. (2012). Matric suction is caused by environmental changes in the air and water phases in the vadose zone. Fredlund et al. (2012) outlined that matric suction increases with the reduction of pore size.

Unsaturated soils have higher shear strength than saturated soils according to Houston (2014). The shear strength increases with suction when the suction value is less than air entry value (AEV), as reported by Sheng et al. (2009). However, the rate of increase in shear strength declines, when the suction value reaches residual conditions according to Sheng et al. (2009).

Vanapalli et al. (1996) reported that during desaturation process, residual stage will be reached finally where little water left in the pores. The residual state occurs within the suction range of 0 to 200 kPa for gravels, sands, silts and their mixtures. This range for clays with low plasticity is between 500 to 1500 kPa. It will be greater than 1500 kPa for clays with medium to high plasticity.

Guan et al. (2010) found out from experiments that shear strength on the drying path is higher than that on the wetting path. None of the published equations for shear strength considers the strength on the wetting path according to Guan et al. (2010). Wetting shear strength behaviour is paramount in analysing rainfall-induced slope failures as reported by Guan et al. (2010).

Vanapalli et al. (1996) created a prediction model of shear strength of unsaturated soil using SWCC and shear strength parameters of saturated soil. Several prediction models of the shear strength of unsaturated soils are formulated recently according to Sheng et al. (2009). The main differences between these models (Vanapalli et al. 1996; Sheng et al. 2009) are mathematical formulations and material properties adopted.

A simplified version of shear strength prediction model is preferred due to high cost of material testing and considerable time involved in the laboratory testing according to Vanapalli et al. (1996).

In fact, practical engineers are interested in the suction range from 0 to 500 kPa due to the performance of geotechnical structures as reported by Vanapalli et al. (1996).

Gallage and Uchimura (2016) advised that effects of low suction and hysteresis of SWCC on unsaturated shear strength parameters are vital to analyse rainfall-induced shallow landslides.

This study focuses on simplified prediction models of shear strength of unsaturated soil under low normal stress.

In this paper, the results from direct shear test, suction test using filter paper method and particle size distribution test on the soil samples obtained from existing landslide sites were used. Both direct shear tests and suction tests were conducted at different water contents to identify the impact of moisture in the soil on the shear strength. SWCC has been prepared for tested soils. This paper presents three calibrated and validated prediction models of shear strength of unsaturated soils. Two of them are published models. The third one is proposed for the suction range of 0 to 10,000 kPa.

A.3 Materials and methods

A.3.1 Test setup and arrangement of instruments

Both direct shear and suction tests (using filter paper technique) were carried out on nine (9) soil specimens at 0%, 10%, 15%, 20%, 25%, 30%, 35% and 40% water contents. The soil samples were remoulded.

A.3.1.1 Direct shear test

Direct shear tests (the size of the shear box was 60mm length x 60mm width x 56mm depth) were performed according to AS1289.6.2.2 - 1998 procedure on soil specimens. Soil samples collected from each landslide site were oven-dried at 105^0C for 24 hours. Particle size distribution was carried out on each oven-dried sample and the soil material passing 4.75 mm sieve was used for a series of direct shear tests. For each soil sample, shear box tests were performed on soil specimen with various moisture contents, ranging from 0 to 40%. To allow comparisons of the obtained results, all specimens for each soil were prepared to the same dry density. The dry density values are given in Table A1.

The moist specimens were prepared by mixing the oven-dried soil with 10%, 20%, 30% or 40% distilled water. They were allowed to rest in a sealed bag for 24 hours for better and more even saturation. Then, the soil was compacted in the shear box in 6 layers to achieve the desirable dry density.

The wet samples were prepared by adding 10%, 20%, 30% and 40% of distilled water by weight to the dry sample and were kept at least for 24 hours in a sealed bag. Direct shear tests were carried out with at least 4 different moisture contents depending on soil behaviour with

water. However, some soil samples failed or became watery at 30% and 40% moisture contents during the preparation.

Direct shear testing equipment was set with the constant displacement rate of 0.2 mm/minute due to coarser materials tested. The data logger was organized to record vertical displacement, horizontal displacement and shear force at every 10 seconds. The maximum horizontal displacement was 7 mm.

The soil specimens were sheared under the effective vertical stress of 28.5, 55.8 and 83.0 kPa. The peak shear stress was recorded for different initial vertical stresses. It was used to determine the strength characteristics of soil (internal friction angle and cohesion), according to Mohr-Coulomb strength criterion. Shear stress vs. horizontal displacement was plotted for each test.

A.3.1.2 Suction test using filter paper technique

A number of suction tests were performed using the standard Whatman No. 42 filter paper, following ASTM D5298 – 2016 procedure. The soil specimens were prepared with at least four (4) different moisture contents (gravimetric), and then individual SWCC can be obtained.

For suction tests, material passing 2.36 mm sieve from oven-dried samples (for 24 hours) was used. The suction tests were carried out using O-ring, air-tight glass container and cling wrap. A special hand gloves and forceps were used to prepare the specimen to avoid oils from the hand to the filter paper. The wet samples were prepared by adding 10%, 20%, 30% and 40% of distilled water by weight. A set of 4 larger size filter papers and a smaller size filter paper were dried for 16 hours in the oven prior to using it.

The plastic O-ring (a hollow tube of 51mm diameter and 25mm height) was placed on top of a cling wrap and sample was hand-compacted up to the middle of O-ring. Two large filter papers were placed, and a small filter paper was placed in between. The purpose of small filter paper is to measure matric suction. Then the sample was hand-compacted up to the top and a wire separator and two large filter papers were placed. The total suction was measured using the top two filter papers.

The soil sample with the O-ring was placed in a small glass bottle (of 62mm opening diameter and 88mm height) with top two filter papers exposed within the glass bottle. Then, the glass bottle was closed with lid tightly and placed in a cooler box for a week at least. After 7 days, the weight of wet filter papers such as the top two filter papers and the small filter paper were

measured using a sensitive balance with four decimal points. Immediately, they were placed in the oven at 105^0C for 2 hours. The weight of dried filter papers was measured after drying. This process was completed as quickly as possible to avoid change of moisture in the air. The total suction and matric suction were calculated using Whatman No.42 calibration curves.

A.3.2 Soil type and index properties

A series of laboratory experiments were conducted on nine soil samples collected from landslide sites in the northern region of New South Wales (Australia). These shallow landslides (depth 1-3 m) occurred in the past few years during the rainfall events. The highest rainfall causing landslides varies from 45.4 mm/day to 415.2 mm/day according to the data from Bureau of Metrology from 2009 to 2017 in the northern region. The particle size distribution test results and dry densities are shown in Table A1.

Table A1: Particle size distribution and dry density

Soil No.	Gravel (%)	Sand (%)	Fines (%)	C_u	C_c	Dry density (kg/m^3)
Soil 1	31.1	66.5	2.4	8.64	1.17	1057.1
Soil 2	52.3	42.1	5.6	13.20	1.75	1186.5
Soil 3	38.6	57.6	3.7	15.71	1.09	1074.4
Soil 4	6.9	89.3	3.8	2.70	1.20	1294.6
Soil 5	23.8	64.5	11.6	13.85	0.83	1152.9
Soil 6	66.1	31.6	2.3	12.44	3.23	1359.8
Soil 7	50.2	46.8	3.0	13.08	1.37	1221.2
Soil 8	70.5	25.7	3.8	43.20	2.90	1366.0
Soil 9	85.8	13.0	1.2	3.81	1.61	1366.0

Table A1 shows that the tested soils were mainly coarse-grained soils because more than 50% of the soil particles are larger than 0.075 mm sieve size. The Atterberg limits are tabulated in Table A2.

Table A2: Atterberg limits.

Soil No.	LL (%)	PI (%)
Soil 5	42.6	24.8
Soil 6	20.2	3.8
Soil 9	37.9	9.2

A.4 Test results and analysis

The plot of shear strength (kPa) versus moisture content (%) under normal stress of 28.5 kPa from direct shear test is presented in Figure A1. It shows that shear strength of unsaturated soil reduces with increasing moisture content. The shear strength reduction was calculated as change in shear strength divided by original shear strength at 0% moisture content. Figure A2 depicts the reduction of shear strength versus moisture content. It is clear from Figure A2 that the shear strength reduction is increasing when the moisture content is increased. SWCC of the tested soils obtained using suction test using filter paper technique are shown in Figure A3.

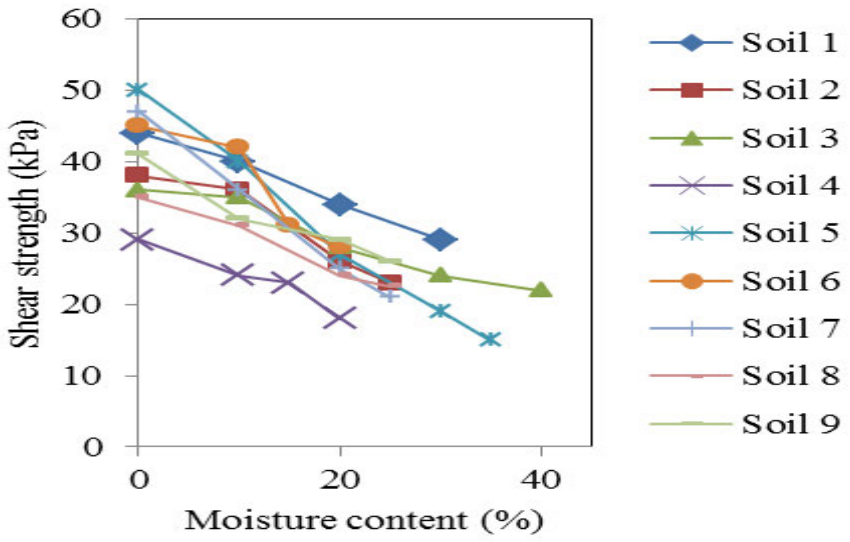

Figure A1: Shear strength vs. Moisture content plot from direct shear test on 9 soil specimens

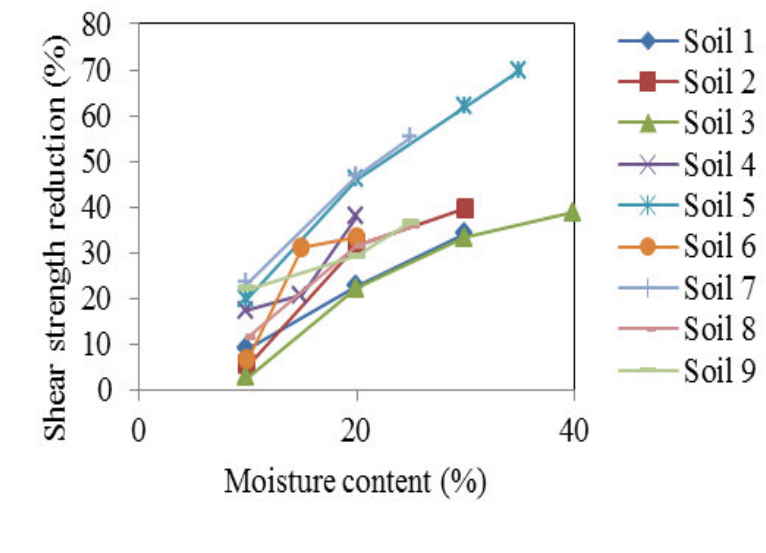

Figure A2: Shear strength reduction vs. Moisture content plot

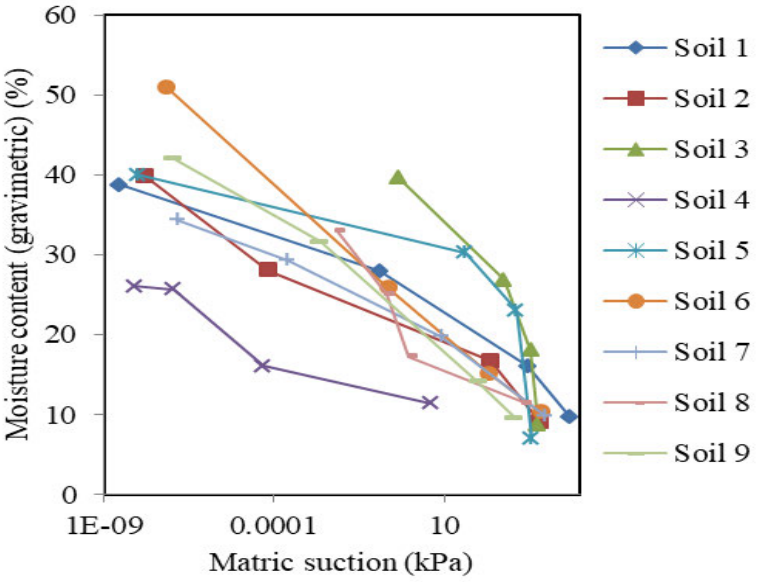

Figure A3: SWCC of the tested soils.

It is evident from Figure A3 that AEV of tested soils is under 10 kPa. The tested soils had matric suction in the range of 0 to 500 kPa when their moisture content varies between 10% and 51%.

A.5 Prediction of shear strength

A couple of approaches were used in this study to predict shear strength of unsaturated soils. One is the prediction of shear strength using direct shear test results and suction test results including SWCC. The other one is prediction of cohesive shear strength using direct shear test results only.

A.5.1 SWCC equation

Fredlund and Xing (1994) algorithm for SWCC equation is shown below as highlighted by Vanapalli et al. (1996):

$$\theta = C(\psi)[\theta_s / \ln[(e + (\psi / a)^n)]^m] \quad \text{(A1)}$$

$$C(\psi) = [1 - \ln(1 + \psi / \psi_r) / \ln(1 + 1000000 / \psi_r)] \quad \text{(A2)}$$

where θ = the volumetric water content at any suction; θ_s = the saturated volumetric water content; $C(\psi)$ = correction factor; ψ = soil suction; ψ_r = suction value at residual water content; e is natural number, 2.71828…; a = a suction related to the air entry value of the soil; n = a soil parameter related to the slope at the inflection point on the SWCC; m = a soil parameter related to the residual water content.

Leong and Rahardjo (1997) recommended the above Fredlund and Xing (1994)'s Model, i.e., Equation (A1) for SWCC after reviewing many equations as it provided best fit to the measured values.

The soil parameters of Equation (A1) such as a, n and m for the tested soils were estimated using EXCEL SOLVER by applying optimization technique. The squared sum of normalized residuals (SSNR1) as noted below is minimized:

$$SSNR1 = \sum_{i=1}^{n} ((\theta m - \theta e) / \theta m)^2 \quad \text{(A3)}$$

where θ_m is measured water content; θ_e is estimated water content. Chin et al. (2010) published the results of a, n and m for 30 coarse-grained soil samples. Based on these results, the following range for a, n and m is assumed for this study: a from 0.1 to 5; n from 0.1 to 15 and m from 0.1 to 2.

The suction value at residual water content ψ_r is assumed to be 100 kPa according to Chin et al. (2010). Based on the above assumptions, the soil parameters a, n and m for the tested soils were calculated and tabulated in Table A3.

Vanapalli et al. (1999) and Kim et al. (2010) pointed out that SWCC moves to the right when vertical stress is increased. However, the effect of vertical stress on SWCC is minimal under low confining pressure conditions. Fine content and structural retention of soils have more significant effect on SWCC at low confining pressure conditions.

Based on the above argument, it was assumed that SWCC obtained using the filter paper measurement technique (where is zero normal stress) will be the same as the SWCC under the vertical stress of 28.5 kPa at the direct shear test during this study. This is because the vertical stress is low. This SWCC was used for the prediction of shear strength of unsaturated soils.

Table A3: Soil parameters of SWCC of tested soils

Soil No.	θ_s	a (kPa)	n	m	SSNR1
Soil 1	39	0.10	0.10	0.69	0.05049
Soil 2	40	0.10	0.10	1.61	0.02560
Soil 3	39.5	5.00	0.47	0.55	0.25342
Soil 4	26	3.41	8.64	1.13	0.38097
Soil 5	40	5.00	0.53	0.82	0.34271
Soil 6	51	0.10	15.00	0.22	0.03867
Soil 7	34.5	0.10	15.00	0.12	0.03487
Soil 8	33	0.12	15.00	0.15	0.03279
Soil 9	42	2.73	8.78	0.29	0.10891

A.5.2 Shear strength equation

To predict shear strength of unsaturated soils, three equations were used. The first equation is from Vanapalli et al. (1996) for calculating shear strength at any suction value as noted below:

$$\tau = c' + (\sigma_n - u_a)\tan\phi + (u_a - u_w)((\theta^K)(\tan\phi')) \quad \text{(A4)}$$

where τ = shear strength of unsaturated soil; c' = effective cohesion; ϕ' = effective internal friction angle; σ_n = normal stress; u_a = pore air pressure; u_w = pore water pressure; θ =normalized water content; K = model parameter.

Guan et al. (2010) studied 13 prediction equations for the prediction of shear strength and recommended a new equation for prediction of drying and wetting shear strength. However, this particular equation involves a model parameter related to plasticity index of soils.

Garven and Vanapalli (2006) used the Equation (A4) for prediction of shear strength with K as a function of plasticity index. Equation (A4) has also predicted shear strength close to measured values according to Guan et al. (2010).

Using Equation (A4), the model parameter K is calculated for tested soils by minimizing squared sum of normalised residuals. The results are tabulated in Table A4. It was assumed that u_a is zero. Another assumption is that matric suction, $(u_a - u_w)$ = 100,000 kPa when the moisture content is zero for all the tested soils.

Each tested soil has four sets of data of measured shear strength and measured suction. Measured shear strength τ_m was obtained at 0%, 10%, 20% and 25% (or 30%) from the direct shear test with normal stress of 28.5 kPa. The corresponding suction value $(u_a - u_w)$ or ψ at 0%, 10%, 20% and 25% (or 30%) was obtained from SWCC. Three sets of data of each soil tested were used for curve-fitting and K was calculated. With respect to the range for K values, it was presumed that K should be between 1 and 9 for coarse soils.

The last set of data was used for prediction by comparing estimated shear strength and measured shear strength. The squared sum of normalized residuals between measured shear strength and estimated shear strength (SSNR2) is included Table A4. The low values of SSNR2 indicate that the curve-fitting is better.

Table A4: K values for shear strength prediction of tested soils

Soil No.	K	SSNR2
Soil 1	6.83	0.006242
Soil 2	6.92	0.010902
Soil 3	9.00	0.077215
Soil 4	9.00	0.033225
Soil 5	8.75	0.005477
Soil 6	9.00	0.010367
Soil 7	6.54	0.010093
Soil 8	9.00	0.004320
Soil 9	3.91	0.001811

Matsushi and Matsukura (2006) recommended the following Equation (A5) for predicting cohesion of unsaturated soils from moisture content:

$$\tau_c = \sigma' \tan\phi' + Ce^{-\mu w} \quad \text{(A5)}$$

where τ_c = cohesive shear strength of unsaturated soil; σ' = net normal stress; ϕ' = effective internal friction angle; C = maximum cohesion (kPa); w = volumetric water content; μ = susceptibility coefficient.

Equation (A5) is the second equation for predicting shear strength used in this paper. The model parameters of Equation (A5) such as ϕ', C and μ are calculated using EXCEL SOLVER using optimization technique. Instead of volumetric water content, gravimetric water content was used. It was assumed that pore air pressure is zero. The model parameters of Equation (A5) are shown in Table A5.

Table A5: Model parameters ϕ', C and μ of tested soils

Φ’	C - Ultimate cohesion (kPa)	μ	SSNR3
20.89	45.91	1.19	0.000830
24.99	56.45	1.32	0.010778
19.79	44.39	1.15	0.007009
17.59	47.06	0.94	0.000915
20.99	64.84	2.30	0.003438
24.99	66.25	1.59	0.018573
24.99	70.47	1.90	0.000614
16.12	35.33	1.93	0.002975
16.50	42.59	1.59	0.003925

The curve-fitting is better due to the low values of squared sum of normalized residuals between measured shear strength and estimated cohesive shear strength (SSNR3).

The predicted shear strengths using Equations (A4) and (A5) are presented in Table A6. Prediction accuracy ρ is defined as follows:

$$\rho = \tau_e / \tau_m \tag{A6}$$

where τ_m is measured shear strength; τ_e is estimated shear strength.

Table A6: Predicted shear strengths of tested soils

Soil No.	τ_m (kPa)	τ_e from Equation (A4) (kPa)	ρ from Equation (A4)	τ_e from Equation (A5) (kPa)	ρ from Equation (A5)
Soil 1	29.00	30.48	1.05	30.61	1.06
Soil 2	23.00	24.16	1.05	23.94	1.04

Soil 3	22.00	22.48	1.02	20.71	0.94
Soil 4	18.00	16.47	0.91	20.72	1.15
Soil 5	19.00	23.23	1.22	15.47	1.03
Soil 6	28.00	29.14	1.04	28.81	1.03
Soil 7	21.00	20.53	0.98	20.72	0.99
Soil 8	22.50	20.55	0.91	22.28	0.99
Soil 9	20.00	24.71	1.24	25.90	1.00

Table A6 demonstrates that both Equations (A4) and (A5) predict the shear strength within 0.9% to 1.2% of measured values. As engineers are interested in the low suction range, the following third equation is proposed to predict the shear strength in the low suction range:

$$\tau = c' + (\sigma_n - u_a)\tan\phi' + \psi(1/C_u)^M \tan\phi' \quad \text{(A7)}$$

where τ = shear strength of unsaturated soil; c' = effective cohesion; ϕ' = effective internal friction angle; σ_n = normal stress; u_a = pore air pressure; ψ = matric suction; C_u = coefficient of uniformity; M = model parameter.

In Equation (A7), C_u was considered as a parameter because the matric suction is affected by porosity which in turn a reflection of grading of soils. It was assumed that u_a is zero. From direct shear test results c' and ϕ' are obtained at various moisture contents when σ_n is 28.5 kPa. From SWCC, ψ is worked out at the corresponding moisture contents. The model parameter M is calculated from EXCEL SOLVER using optimization technique. For curve-fitting Equation (A7), the values of ψ used were from the range of 0 to 10,000 kPa. The results are tabulated in Table A7. From Table A7, low values of squared sum of normalised residuals (SSNR4) show that the curve-fitting is robust. Prediction accuracy varies from 0.9 to 1.2 of measured strength.

Table A7: Predicted shear strengths at suction range of 0 to 10,000 kPa

Soil No.	M	SSNR4	τ_m (kPa)	τ_e from equation (A7) (kPa)	ρ
Soil 2	3.54	0.010623	23.00	24.17	1.05
Soil 3	5.00	0.009249	22.00	22.30	1.01
Soil 4	5.00	0.026498	18.00	16.47	0.91
Soil 5	2.53	0.002842	19.00	21.01	1.11
Soil 6	5.00	0.006878	28.00	29.14	1.04
Soil 7	3.13	0.002074	21.00	20.54	0.98
Soil 9	4.19	0.001670	20.00	24.76	1.24

A.6 Conclusions

Direct shear tests on the remoulded samples obtained from rainfall-induced landslide sites revealed that shear strength reduces when the moisture content increases. The reduction in shear strength increases when moisture content is increased. Prediction of shear strength of unsaturated soils using Equations (A4) and (A5) under low normal stress (28.5 kPa) was done within 0.9% to 1.2% of measured shear strength.

The proposed Equation (A7) for the suction range of 0 to 10,000 kPa was also predicted shear strength within 0.9% to 1.2% of the measured values. This proposed Equation (A7) is in a simple form. Using direct shear test results, suction tests using filter paper technique and particle size distribution tests, it is possible to predict the shear strength of unsaturated soils within an acceptable range under low normal stress conditions.

Appendix B: Inventory of landslides in northern region

No	Road	Landslide name	Cause of failure	Terrain	Upslope / Downslope
1	Oxley Highway	Doyles West1	Rainfall	Mountainous	Downslope
2		Doyles West2	Rainfall	Mountainous	Downslope
3		Mass bloc	Geological features	Mountainous	Downslope
4		Longview1	Rainfall	Mountainous	Upslope
5		Longview2	Rainfall	Mountainous	Upslope
6		Jasper Cut u/s	Rainfall	Mountainous	Upslope
7		Jasper Cut d/s	Rainfall	Mountainous	Downslope
8		Mt Seaview Hotel1	Rainfall	Mountainous	Downslope
9		Mt Seaview Hotel2	Rainfall	Mountainous	Downslope
10		Mt Seaview Hotel3	Rainfall	Mountainous	Downslope
11		Stopping Bay	Rainfall	Mountainous	Downslope
12		Stockyard Ck	Rainfall	Mountainous	Downslope
13		Jerrys Hut u/s	Geological features	Mountainous	Upslope
14		Ralfes Ck	Geological features	Mountainous	Downslope
15		Gordonville Cutting upslope 2015	Rainfall	Mountainous	Upslope
16		Gordonville Cutting downslope 2013	Rainfall	Riverbank	Downslope
17		Nut Farm1	Rainfall	Riverbank	Downslope
18		Nut Farm2	Rainfall	Riverbank	Downslope
19		Myers Bluff1 - Nat Dis	Rainfall	Mountainous	Downslope
20		Myers Bluff2	Geological features	Mountainous	Downslope

21	Waterfall Way	Myers Bluff3	Geological features	Mountainous	Downslope
22		Myers Bluff4	Geological features	Mountainous	Downslope
23		Newell Fall 1 and 2	Rainfall	Mountainous	Upslope
24		Newell Fall3	Rainfall	Mountainous	Downslope
25		Sherrard Fall1	Rainfall	Mountainous	Downslope
26		Sherrard Fall2	Rainfall	Mountainous	Downslope
27		Weeping Jenny	Man-made activities	Mountainous	Upslope
28		West of Culvert 80	Geological features	Mountainous	Downslope
29		East of Sherrard Fall1	Geological features	Mountainous	Upslope
30		Culvert54	Geological features	Mountainous	Downslope
31		Culvert26	Geological features	Mountainous	Downslope
32		East of Newell Fall	Rainfall	Mountainous	Upslope
33		West of Newell Fall	Geological features	Mountainous	Downslope
34		Gordonville downslope 2009	Rainfall	Riverbank	Downslope
35		Culvert 54 - Slope 14426	Rainfall	Mountainous	Upslope
36		Timber crib wall #14514	Rainfall	Mountainous	Downslope
37		Crystal Fall	Man-made activities	Mountainous	Downslope
38	Gwydir Highway	Smokey Haven	Rainfall	Mountainous	Downslope
39		Hills Ck	Rainfall	Mountainous	Upslope
40		Cangai Bluff1	Rainfall	Mountainous	Upslope
41		Cangai Bluff2	Rainfall	Mountainous	Upslope
42		Gib Range entrance slip	Rainfall	Mountainous	Upslope
43		Bottom slip	Rainfall	Mountainous	Upslope
44		Culvert 32	Rainfall	Mountainous	Downslope

45		Gabion wall	Rainfall	Mountainous	Upslope
46		Hills Lookout	Rainfall	Mountainous	Upslope
47		West of Hills Lookout	Rainfall	Mountainous	Upslope
48		Middle Slip u/s	Rainfall	Mountainous	Upslope
49		Middle Slip d/s	Rainfall	Mountainous	Downslope
50		Top slip	Rainfall	Mountainous	Downslope
51		Bakers Hills	Geological features	Mountainous	Downslope
52		Culvert 86	Rainfall	Mountainous	Downslope
53		McLennan's Quarry	Rainfall	Mountainous	Upslope
54		Bellbird cut	Rainfall	Mountainous	Upslope
55		Cangai Bluff	Rainfall	Mountainous	Upslope
56	Bruxner Highway	Piora1	Rainfall	Riverbank	Downslope
57		Piora2	Rainfall	Riverbank	Downslope
58		Gundarimba	Rainfall	Riverbank	Downslope
59		Mallanganee East	Rainfall	Mountainous	Downslope
60		Mallanganee West	Rainfall	Mountainous	Downslope
61		Richmond Range	Geological features	Mountainous	Downslope
62		Tabulam	Geological features	Rolling	Downslope
63		Ballina Cutting	Rainfall	Rolling	Upslope
64		Lindendale	Rainfall	Rolling	Upslope
65		Crib wall	Rainfall	Rolling	Upslope
66		Happy Springs	Rainfall	Riverbank	Downslope
67		Cooredulla	Rainfall	Riverbank	Downslope
68		Gundarimba2	Rainfall	Riverbank	Downslope

69		Tabulam	Rainfall	Riverbank	Downslope
70	Summerland Way	Tick gate	Geological features	Mountainous	Downslope
71		Border gate1	Rainfall	Mountainous	Downslope
72		Border gate2	Rainfall	Mountainous	Downslope
73		Hildebrand	Rainfall	Mountainous	Downslope
74		Rankins slip	Rainfall	Mountainous	Downslope
75		Dingo Gully d/s	Rainfall	Mountainous	Downslope
76		Imbreys Rd	Seepage	Mountainous	Downslope
77		Montgomerys Rd	Rainfall	Mountainous	Downslope
78		Unumgar	Geological features	Mountainous	Downslope
79		Fairymount Ck	Geological features	Rolling	Downslope
80		Glen Rd	Rainfall	Mountainous	Downslope
81		Donaldson1	Rainfall	Mountainous	Downslope
82		Hildebrand2	Rainfall	Mountainous	Upslope
83		North of Tick Gate3	Rainfall	Mountainous	Upslope
84		Tick gate 1A	Rainfall	Mountainous	Downslope
85		Tick gate 1B	Rainfall	Mountainous	Downslope
86	Pacific Highway	Byrons lane	Rainfall	Riverbank	Downslope
87		Boundary Ck	Rainfall	Riverbank	Downslope
88		Rattle Ck	Rainfall	Riverbank	Downslope
89		Clarenze	Rainfall	Rolling	Downslope
90		Lumsden lane	Rainfall	Riverbank	Downslope
91		McClares Hill	Rainfall	Rolling	Downslope
92		Cooperabung	Rainfall	Rolling	Downslope

93		Mingaletta	Seepage	Rolling	Downslope
94		McIntyre Rd1 #13901 -S5120	Rainfall	Riverbank	Downslope
95		North of McIntyres Lane - S5120	Rainfall	Riverbank	Downslope
96		McIntyre Ln to Tyndale - #13900 - S5080-5103	Rainfall	Riverbank	Downslope
97		Woodburn Town - S6300	Rainfall	Riverbank	Downslope
98		Woodburn North - S6340	Rainfall	Riverbank	Downslope
99		Woodburn to MacDonaldson Rd - S6340-6360	Rainfall	Riverbank	Downslope
100		Broadwater to Wardell-S6440-7010	Rainfall	Riverbank	Downslope
101	New England Highway	Cherrydale	Rainfall	Riverbank	Downslope
102		Middle Ck	Rainfall	Riverbank	Downslope
103		Bungulla	Rainfall	Riverbank	Downslope
104	Lismore - Bangalow Road	Possum Ck	Rainfall	Rolling	Downslope
105		Binna Burra	Man-made activities	Riverbank	Downslope
106		St Helena1	Rainfall	Rolling	Upslope
107		St Helena2	Rainfall	Rolling	Upslope
108		North of Possum Ck	Rainfall	Rolling	Upslope

Appendix C: Rainfall characteristics of rainfall-induced landslides in northern NSW

No.	Name of Road	Landslide site name	Nearest rain gauge station from Bureau of Metrology	Rainfall event causing landslide		Duration (Days)	Cumulative rainfall (mm)
1	Summerland Way	Border gate slip1	58016	3/01/2011	13/01/2011	11	282.2
2		Border gate slip2	58016	6/01/2011	12/01/2011	11	282.2
3		Glen Rd Slip	58016	6/01/2011	12/01/2011	11	282.2
4		Dingo Gully	58016	6/01/2011	12/01/2011	11	282.2
5		Hildebrand 1	58194	24/01/2013	29/01/2013	6	385.6
6		Montgomerys	58016	1/05/2015	4/05/2015	4	113.4
7		Rankins	58194	1/05/2015	6/05/2015	6	142.8
8		Hildebrand 2	58194	30/03/2017	31/03/2017	2	213.4
9		Donaldson 1	58194	30/03/2017	31/03/2017	2	213.4
10		Tickgate1 A	58194	30/03/2017	31/03/2017	2	213.4
11		Tickgate1B	58194	30/03/2017	31/03/2017	2	213.4
12		North of Tickgate3	58194	30/03/2017	31/03/2017	2	213.4
13	Bruxner Highway	Mallangan ee West	57019	24/01/2013	29/01/2013	6	310.8
14		Mallangan ee East (Site 1 and 2)	57019	24/01/2013	29/01/2013	6	310.8
15		Piora Swamp1	58004	6/01/2011	13/01/2011	8	209
16		Piora Swamp2	58208	1/05/2015	2/05/2015	2	188.8
17		Cooredulla	56202	2/01/2011	14/01/2011	13	393.8
18		Lindendale	58023	2/06/2016	5/06/2016	4	310.2
19		Crib wall	58023	2/06/2016	5/06/2016	4	310.2
20		Ballina Cutting	58198	2/06/2016	5/06/2016	4	278.4
21		Gundurimba1	58214	24/01/2013	29/01/2013	6	226.4

22		Gundurimba2	58214	30/03/2017	31/03/2017	2	398.8
23		Happy Springs	56202	25/01/2013	29/01/2013	5	279.8
24		Tabulam	57018	24/01/2013	29/01/2013	6	244.4
25	Gwydir Highway	Smokey Haven	57093	31/03/2009	6/04/2009	7	169.8
26		Gibraltar Range Northern Entrance Slip	57093	4/01/2011	15/01/2011	12	444.2
27		Hills Lookout	58102	5/01/2011	13/01/2011	9	202.6
28		Culvert 32	58102	5/01/2011	13/01/2011	9	202.6
29		West of Hills lookout	58102	5/01/2011	13/01/2011	9	202.6
30		Cangai Bluff1	58102	5/01/2011	13/01/2011	9	202.6
31		Cangai Bluff2	58102	5/01/2011	13/01/2011	9	202.6
32		Middle Bend Gabion Wall	57093	4/01/2011	15/01/2011	12	444.2
33		Gibraltar Range - Middle Slip - Above the road with rock fall fence	57093	24/01/2013	29/01/2013	6	515.4
34		Gibraltar Range - Middle Slip - Below the road with rock fill	57093	24/01/2013	29/01/2013	6	515.4
35		Gibraltar Range - Top Slip (Soil nail wall)	57093	24/01/2013	29/01/2013	6	515.4
36		Gibraltar Range - Bottom Slip	57093	24/01/2013	29/01/2013	6	515.4
37		Cangai Bluff	57093	14/03/2017	27/03/2017	13	438.4
38		Culvert 86	57093	14/03/2017	27/03/2017	13	438.4
39		McLennan's Quarry	57093	14/03/2017	27/03/2017	13	438.4
40		Bellbird Cut	57093	30/01/2018	30/01/2018		

41		Cangai Bluff	57093	12/10/2019	13/10/2019		
42	Waterfall Way	Myers Bluff - Eastern zone	59033	30/03/2009	8/04/2009	10	489
43		Nut Farm Site 1	59033	5/11/2009	10/11/2009	6	316.9
44		Newell Falls 1 and 2	59140	28/03/2009	9/04/2009	13	584.4
45		Sherrard Falls 1 - Culvert 77	59140	23/05/2009	25/05/2009	3	313.8
46		Sherrard Falls 2 - Culvert 79	59140	23/05/2009	25/05/2009	3	313.8
47		Nut Farm Site 2	59033	12/06/2011	16/06/2011	5	322.4
48		Newell Falls 3	59140	12/06/2011	17/06/2011	6	435.6
49		Gordonville Cutting downslope 2013	59033	24/01/2013	29/01/2013	6	339
50		Gordonville Cutting upslope 2015	59033	30/04/2015	1/05/2015	2	135.9
51		Culvert 54	59140	18/03/2017	22/03/2017	5	473.6
52		East of Newell Fall	59140	12/06/2011	17/06/2011	6	435.6
53		Gordonville Cutting downslope 2009	59033	5/11/2009	10/11/2009	6	316.9
54		Timber crib wall	59140	16/12/2018	17/12/2018	2	228.2
55	Oxley Highway	Stockyard Ck	60085	11/02/2013	28/02/2013	18	790.2
56		Doyles West2	60085	11/02/2013	28/02/2013	18	790.2
57		Stopping Bay	60085	11/02/2013	28/02/2013	18	790.2
58		Longview1	60085	11/02/2013	28/02/2013	7	445.4
59		Longview2	60085	11/02/2013	28/02/2013	18	790.2
60		Jaspers Cut1	60085	11/02/2013	28/02/2013	18	790.2
61		Jaspers Cut2	60085	11/02/2013	28/02/2013	18	790.2
62		Mt Seaview Hotel1	60085	11/02/2013	28/02/2013	18	790.2

63		Mt Seaview Hotel2	60085	11/02/2013	28/02/2013	18	790.2
64		Mt Seaview Hotel3	60085	11/02/2013	28/02/2013	18	790.2
65		Doyles West1	60085	30/11/2010	12/12/2010	13	155.6
66	Pacific Highway	Byrons lane	58152	18/06/2009	29/06/2009	12	193
67		McClares Hill	58059	3/06/2016	5/06/2016	3	166.4
68		McIntyre Rd1 #13901 - S5120	58219	18/03/2017	21/03/2017	4	152.4
69		North of McIntyres Lane - S5120	58061	30/03/2017	31/03/2017	2	346
70		McIntyre Ln to Tyndale - #13900 - S5080-5103	58061	30/03/2017	31/03/2017	2	346
71		Woodburn Town - S6300	58061	30/03/2017	31/03/2017	2	346
72		Woodburn North - S6340	58061	30/03/2017	31/03/2017	2	346
73		Woodburn to MacDonaldson Rd - S6340-6360	58061	30/03/2017	31/03/2017	2	346
74		Broadwater to Wardell-S6440-7010	58061	30/03/2017	31/03/2017	2	346
75		Boundary Ck	58061	20/01/2013	29/01/2013	10	264.4
76		Rattle Ck	58061	20/01/2013	29/01/2013	10	264.4
77		Lumsdan lane	59150	5/11/2009	8/11/2009	4	285.8
78		Clarenza	58059	3/06/2016	5/06/2016	4	285.8
79		Cooperabung	59150	5/11/2009	8/11/2009	4	285.8
80	New England Highway	Cherry Dale Slip	56046	3/01/2011	12/01/2011	10	398.9
81		Middle Ck	55330	6/01/2011	6/01/2011	1	36.8
82		Bungulla	56046	3/01/2011	12/01/2011	10	398.9

83	Lismore - Bangalow Road	Possum Ck	58216	2/06/2016	6/06/2016	4	221.8
84		St Helena1	58216	2/06/2016	6/06/2016	4	221.8
85		St Helena2	58216	2/06/2016	6/06/2016	4	221.8
86		North of Possum Ck	58216	2/06/2016	6/06/2016	4	221.8

Appendix D: Slope characteristics of rainfall-induced landslides in northern NSW

No.	Name of Road	Slope site name	Terrain	Slope angle (degrees)	Rock type	Major rock group
1	Summerland Way	Border gate slip1	Mt Lindesay	45	Sandstone with minor conglomerate units and claystone	Sedimentary rocks
2		Border gate slip2		40		
3		Glen Rd Slip		40		
4		Dingo Gully		35		
5		Hildebrand1		38		
6		Montgomerys		35		
7		Rankins		36		
8		Hildebrand2		38		
9		Donaldson1		75		
10		Tickgate1A		40		
11		Tickgate1B		40		
12		North of Tickgate3		45		
13	Bruxner Highway	Mallanganee West	Mallanganee Range	32	Sandstone with minor conglomerate units and claystone	Sedimentary rocks
14		Mallanganee East (Site 1 and 2)		32		
15		Piora Swamp1	Rolling	25		
16		Piora Swamp2		25		
17		Cooredulla		40	Rhyolitic quartz feldspar to rhyodacitic quartz feldspar	Volcanic eruptive rocks
18		Lindendale		45	Basalt	Mafic volcanic rocks
19		Crib wall		80		
20		Ballina Cutting		65	Feldspar rich sandstone, siltstone, mudstone and conglomerate units	Sedimentary rocks
21		Gundurimba1		25	Mud, silt, sand and gravel deposited by alluvial system	Alluvium
22		Gundurimba2		25		
23		Happy Springs		40	Rhyolitic quartz feldspar to rhyodacitic quartz feldspar	Volcanic eruptive rocks
24		Tabulam		45	Mud, silt, sand and gravel deposited by alluvial system	Alluvium

25		Smokey Haven		38	Sandstone with minor conglomerate units and claystone	Sedimentary rocks
26		Gibraltar Range Northern Entrance Slip		60	Mix of chert, sandstone and mafic volcanic rocks	Mix of various rock types
27		Hills Ck	Ramornie - Cangai	50		
28		Hills Lookout		50		
29		Cangai Bluff1		60		
30		Cangai Bluff2		50		
31		Cangai Bluff 2018		60		
32		McLennans Quarry		50	Sandstone with minor conglomerate units and claystone	Sedimentary rocks
33	Gwydir Highway	Middle Bend Gabion Wall	Gibraltar Range	65	Mix of chert, sandstone and mafic volcanic rocks	Mix of various rock types
34		Cul 32		28		
35		Bellbird Cut		70		
36		West Hills Lookout		60		
37		Gibraltar Range - Middle Slip - Above the road with rock fall fence		50	Mafic and ultramafic rocks	Mafic and ultramafic rocks
38		Gibraltar Range - Middle Slip - Below the road with rock fill		35	Mix of chert, sandstone and mafic volcanic rocks	Mix of various rock types
39		Gibraltar Range - Top Slip (Soil nail wall)		80		
40		Gibraltar Range - Bottom Slip		35		
41		Culvert 86		40		
42	Waterfall Way	Myers Bluff - Eastern zone	Dorrigo Mountain	50	Sandstone, siltstone, mudstone	Sedimentary rocks
43		Newell Falls 1 and 2		60	I-type granite	Melting igneous rocks
44		Sherrard Falls 1 - Culvert 77		85		
45		Sherrard Falls 2 - Culvert 79		85		
46		Newell Falls 3		40	I-type granite	Melting igneous rocks

47		Gordonville Cutting downslope 2013		70	Sandstone, siltstone, mudstone	Sedimentary rocks
48		Gordonville Cutting upslope 2015		80		
49		Gordonville Cutting downslope 2009		40		
50		Culvert 54		80	I-type granite	Melting igneous rocks
51		Timber crib wall		40		
52		East of Newell Fall		65		
53		Nut Farm Site 1	Rolling	40	Mud, silt, sand and gravel deposited by alluvial system	Alluvium
54		Nut Farm Site 2		40		
55	Oxley Highway	Stockyard Ck	Mt Seaview	30	Quartz-rich pebbly sandstone and conglomerate units deposited in fluvial system and in siltstone, mudstone and sandstone with lithic fragments	Sedimentary rocks
56		Doyles West1		30		
57		Doyles West2		30		
58		Stopping Bay		40	A mix of plagioclase-rich rocks including trondhjemite, diorite and gabbro	Feldspar group and, intrusive igneous rocks
59		Longview1		70		
60		Longview2		70		
61		Jaspers Cut1		50	Mafic and ultramafic rocks	Mafic and ultramafic rocks
62		Jaspers Cut2		50		
63		Mt Seaview Hotel1		35		
64		Mt Seaview Hotel2		35		
65		Mt Seaview Hotel3		35		
66	Pacific Highway	Byrons lane	Rolling	30	Mud, silt, sand and gravel deposited by alluvial system	Alluvium
67		McClares Hill		35		
68		McIntyre Rd1 #13901 -S5120		35		
69		North of McIntyres Lane - S5120		35		

70		McIntyre Ln to Tyndale - #13900 - S5080-5103		35		
71		Woodburn Town - S6300		35		
72		Clarenza		35		
73		Lumsdan lane		40		
74		Woodburn North - S6340		35	Sand dune system	Sand dune system
75		Woodburn to MacDonaldson Rd - S6340-6360		35		
76		Broadwater to Wardell-S6440-7010		35		
77		Boundary Ck		35		
78		Rattle Ck		35		
79		Cooperabung		40	Sandstone, siltstone, mudstone	Sedimentary rocks
80	New England Highway	Cherry Dale Slip	Rolling	34	I-type granite	Melting igneous rocks
81		Middle Ck		45	Variable sedimentary rocks including conglomerate, sandstone, mudstone, siltstone	Sedimentary rocks
82		Bungulla		34	I-type granite	Melting igneous rocks
83	Lismore - Bangalow Road	Possum Ck	Rolling	45	Basalt	Mafic igneous rock
84		St Helena1		55		
85		St Helena2		55		
86		North of Possum Ck		55		

Appendix E: Test results

E.1 Direct shear test results

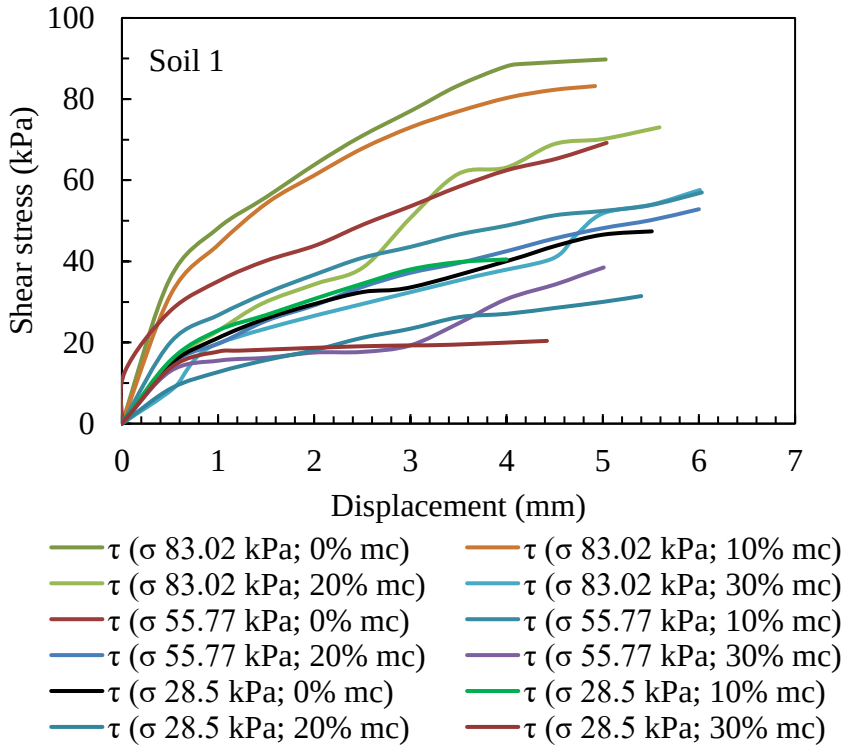

Figure E1.1: Shear strength vs. displacement of Soil 1

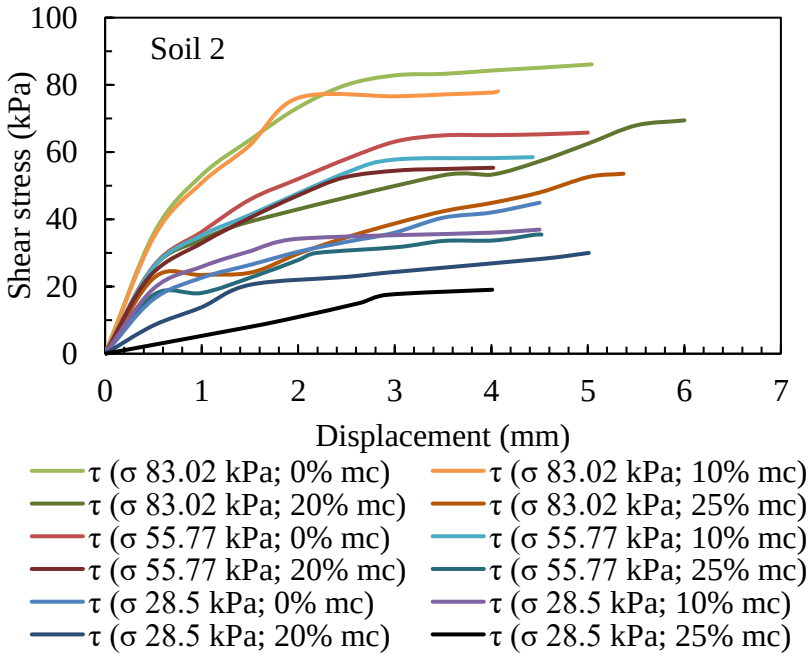

Figure E1.2: Shear strength vs. displacement of Soil 2

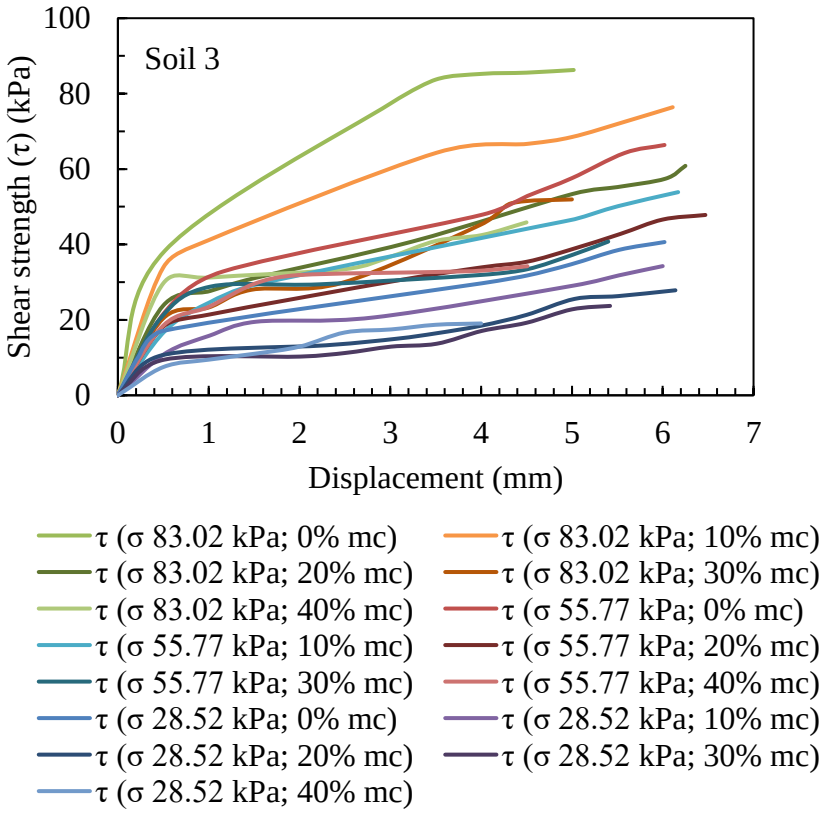

Figure E1.3: Shear strength vs. displacement of Soil 3

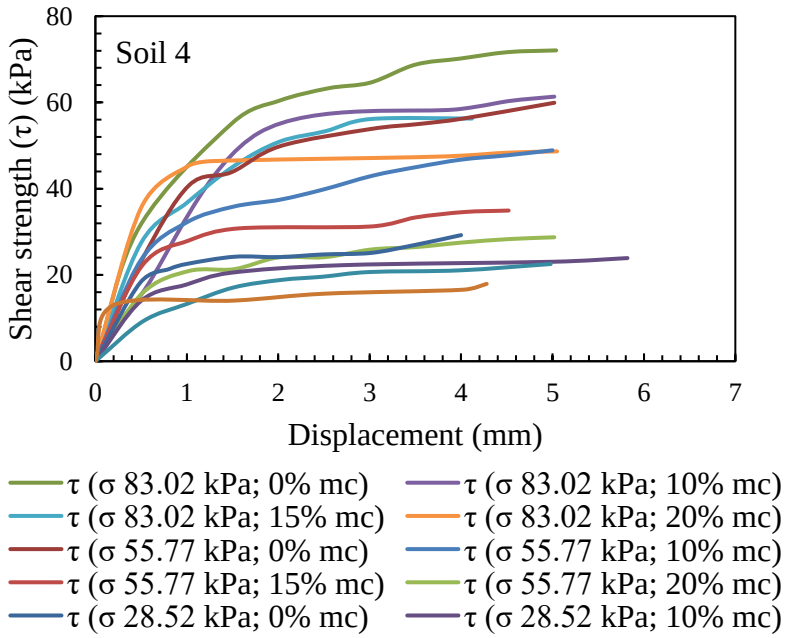

Figure E1.4: Shear strength vs. displacement of Soil 4

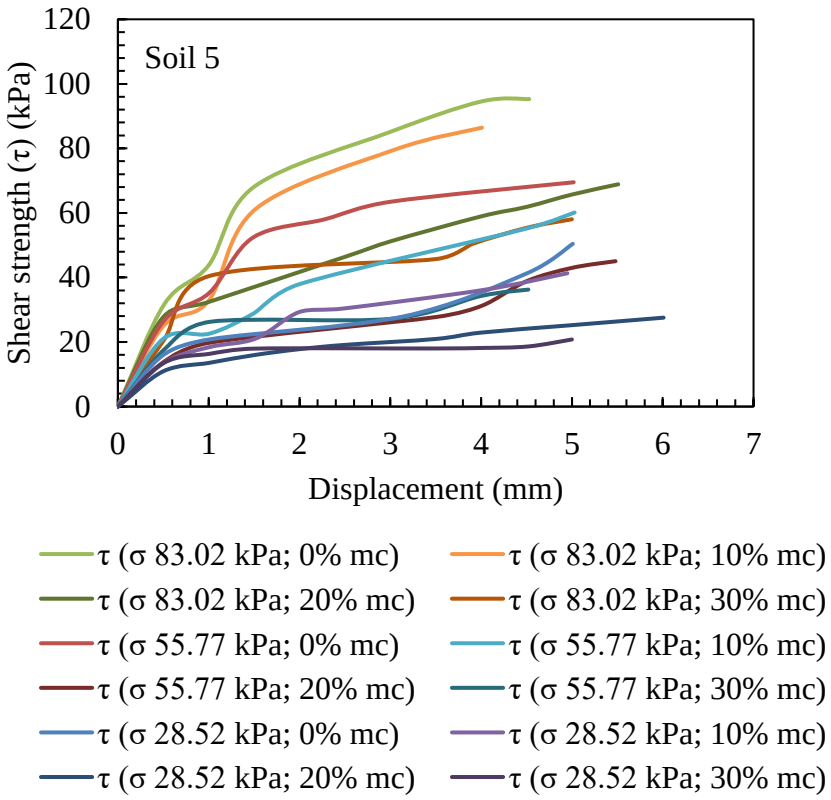

Figure E1.5: Shear strength vs. displacement of Soil 5

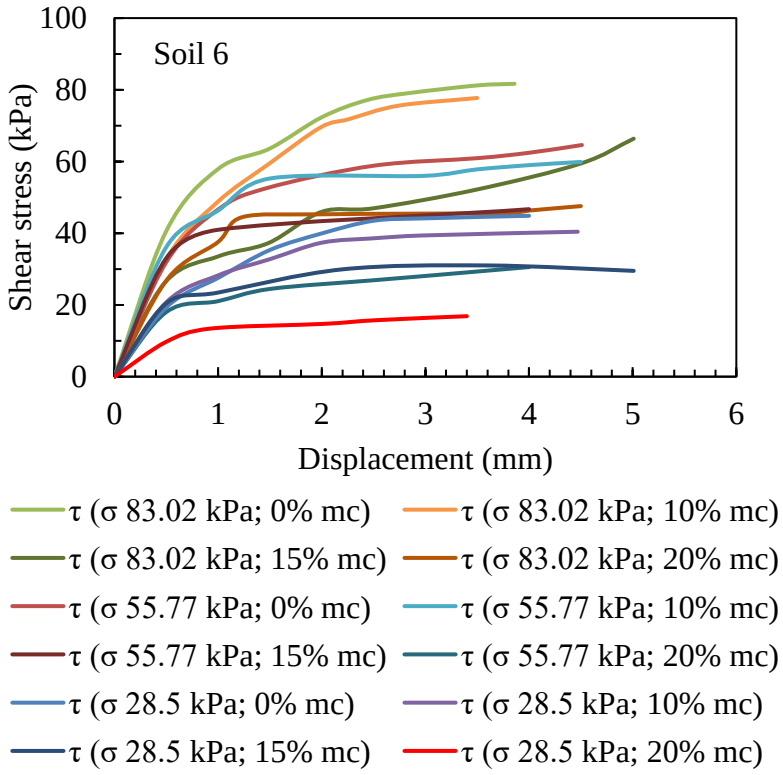

Figure E1.6: Shear strength vs. displacement of Soil 6

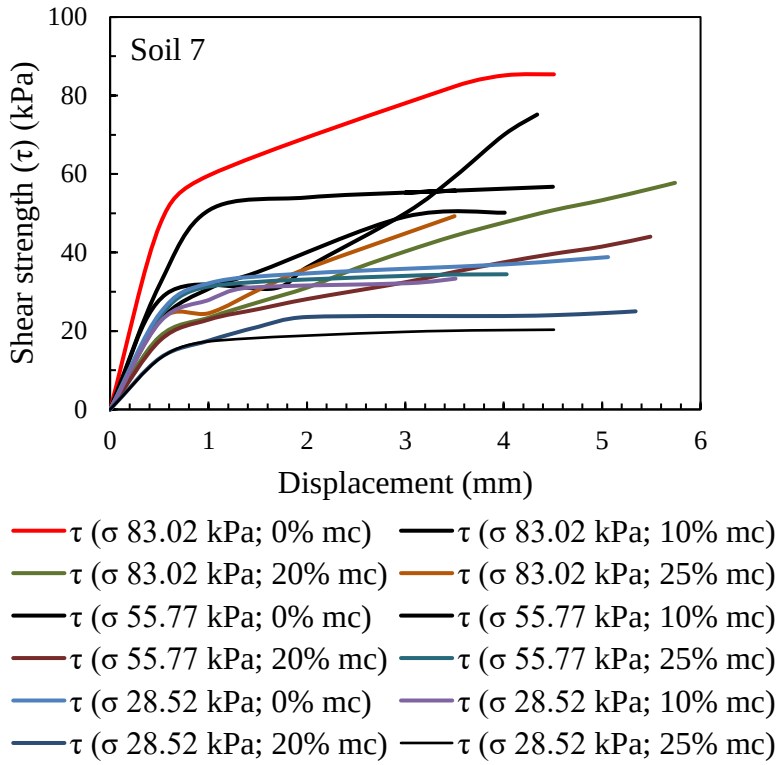

Figure E1.7: Shear strength vs. displacement of Soil 7

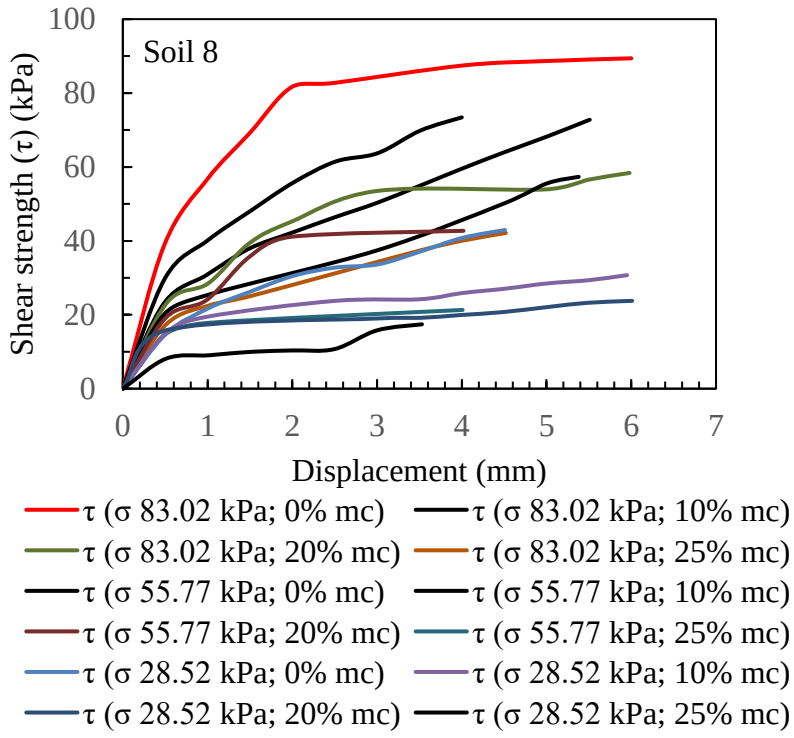

Figure E1.8: Shear strength vs. displacement of Soil 8

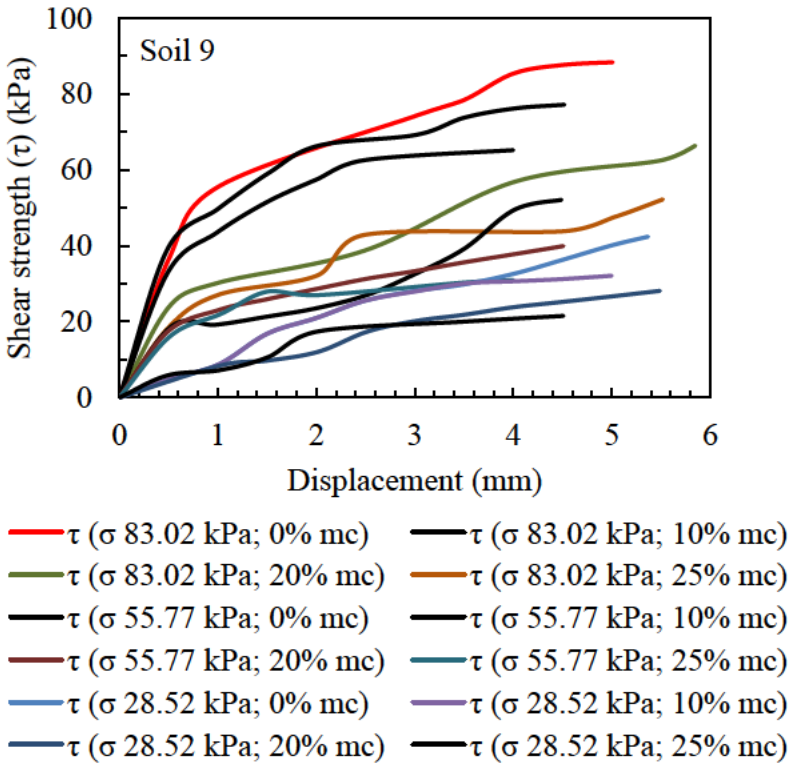

Figure E1.9: Shear strength vs. displacement of Soil 9

E.2 Suction test results

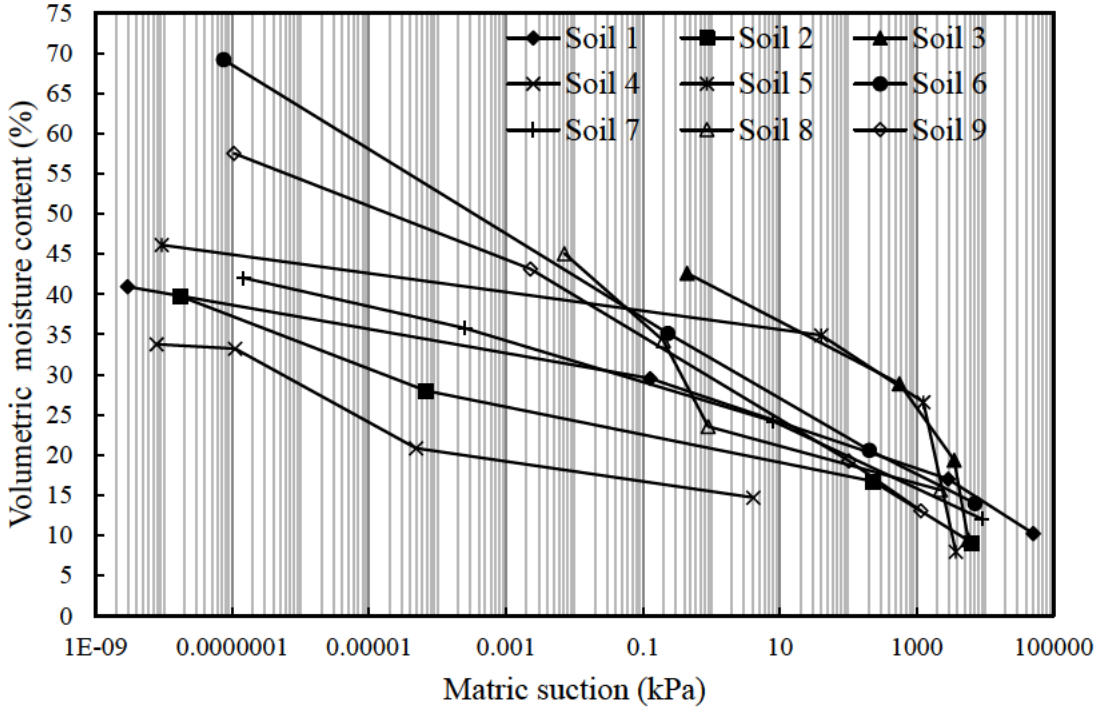

Figure E2.1: SWCC of soils from 9 landslides sites

Table E2.1: Total suction and matric suction obtained from suction test for soils from 9 landslide sites

Soil 1	Moisture content (gravimetric)	9.67	16.09	27.92	38.72
	Total Suction (kPa)	59508.49	8013.59	1636.25	1934.42
	Matric Suction (kPa)	50611.93	2883.87	0.13	0.00
Soil 2	Moisture content (gravimetric)	9.08	16.71	28.01	39.74
	Total Suction (kPa)	8327.76	1747.94	1621.67	1520.07
	Matric Suction (kPa)	6419.81	228.76	0.00	0.00
Soil 3	Moisture content (gravimetric)	8.80	18.01	26.87	39.66
	Total Suction (kPa)	7332.99	4623.97	1396.78	625.36
	Matric Suction (kPa)	5692.90	3530.23	561.71	0.44
Soil 4	Moisture content (gravimetric)	11.35	16.08	25.66	26.08
	Total Suction (kPa)	2974.71	1171.09	N/A	1122.19
	Matric Suction (kPa)	4.13	0.00	0.00	0.00
Soil 5	Moisture content (gravimetric)	6.91	23.04	30.25	40.00
	Total Suction (kPa)	4793.34	1770.10	1626.68	0.00
	Matric Suction (kPa)	3735.03	1257.67	40.43	0.00
Soil 6	Moisture content (gravimetric)	10.28	15.14	25.82	50.87
	Total Suction (kPa)	7877.20	1902.89	1179.03	1.62
	Matric Suction (kPa)	7164.02	204.23	0.23	0.00
Soil 7	Moisture content (gravimetric)	9.85	19.80	29.30	34.42
	Total Suction (kPa)	13080.32	3424.91	248.62	175.73
	Matric Suction (kPa)	9029.91	8.11	0.00	0.00
Soil 8	Moisture content (gravimetric)	11.46	17.23	25.05	32.98
	Total Suction (kPa)	2640.80	870.45	192.47	N/A
	Matric Suction (kPa)	2218.60	0.90	0.20	0.01
Soil 9	Moisture content (gravimetric)	9.55	14.11	31.58	42.11
	Total Suction (kPa)	4940.33	1868.51	1279.67	0.00
	Matric Suction (kPa)	1158.17	102.15	0.00	0.00

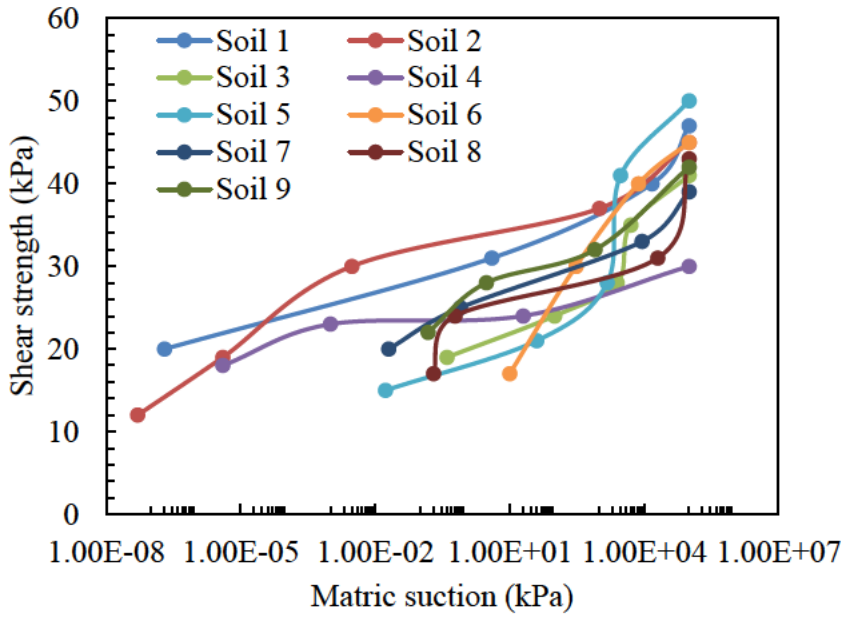

Figure E2.2: Shear strength vs. matric suction

E.3 Consolidated undrained (CU) triaxial test results

Table E3.1: Shear strength parameters from CU triaxial test

Soil No.	Effective stress parameters		Total stress parameters	
	Effective cohesion, c' (kPa)	Effective angle of internal friction, φ' (degrees)	Cohesion, c (kPa)	Angle of internal friction, φ (degrees)
Soil 1	0	35	10	6
Soil 2	0	31	0	11
Soil 6	0	29	0	6

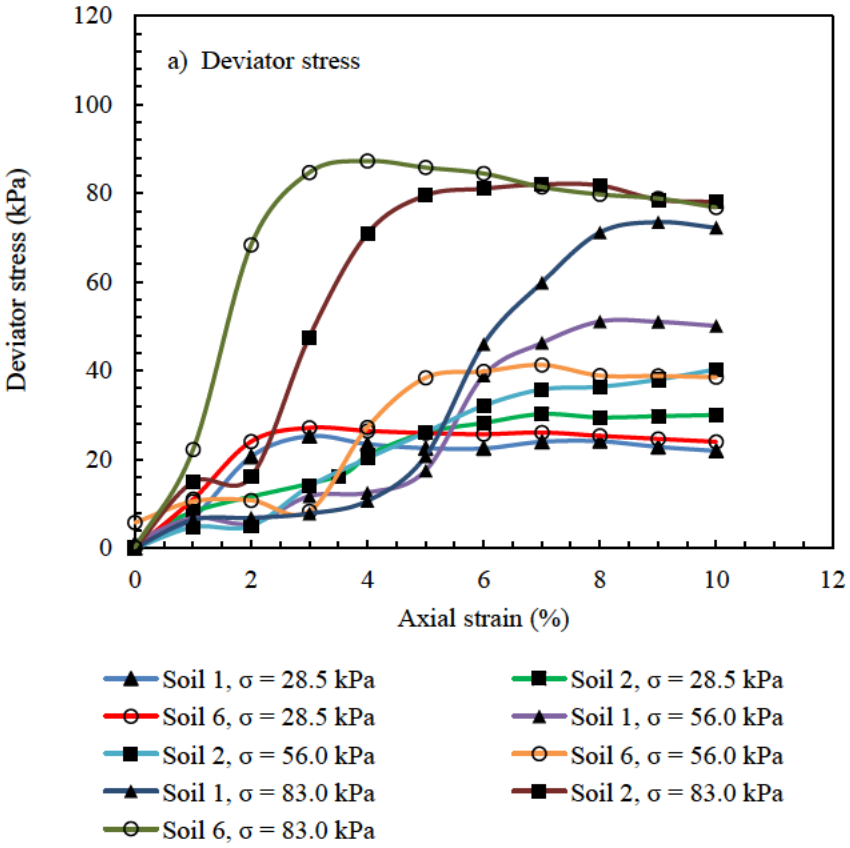

Figure E3.1: Deviator stress plot for Soils 1, 2 and 6

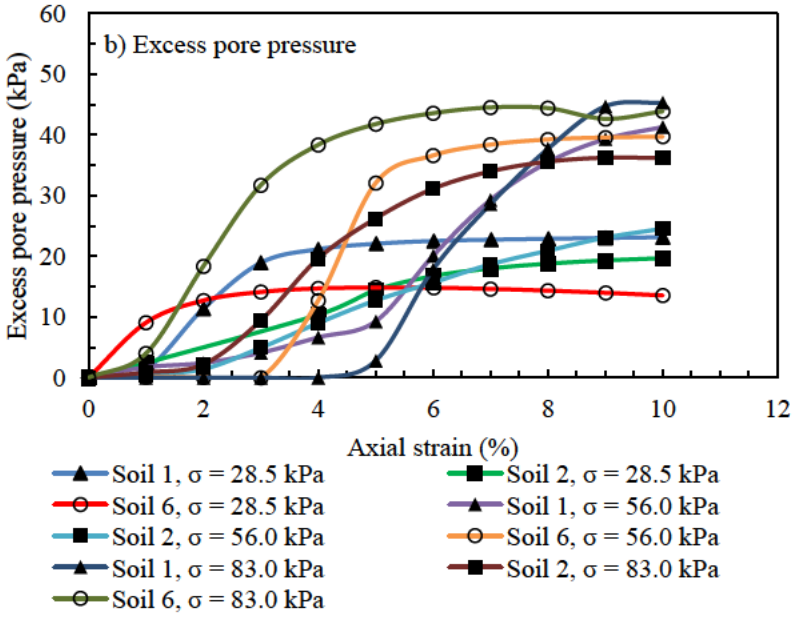

Figure E3.2: Excess pore pressure plot of Soils 1, 2 and 6

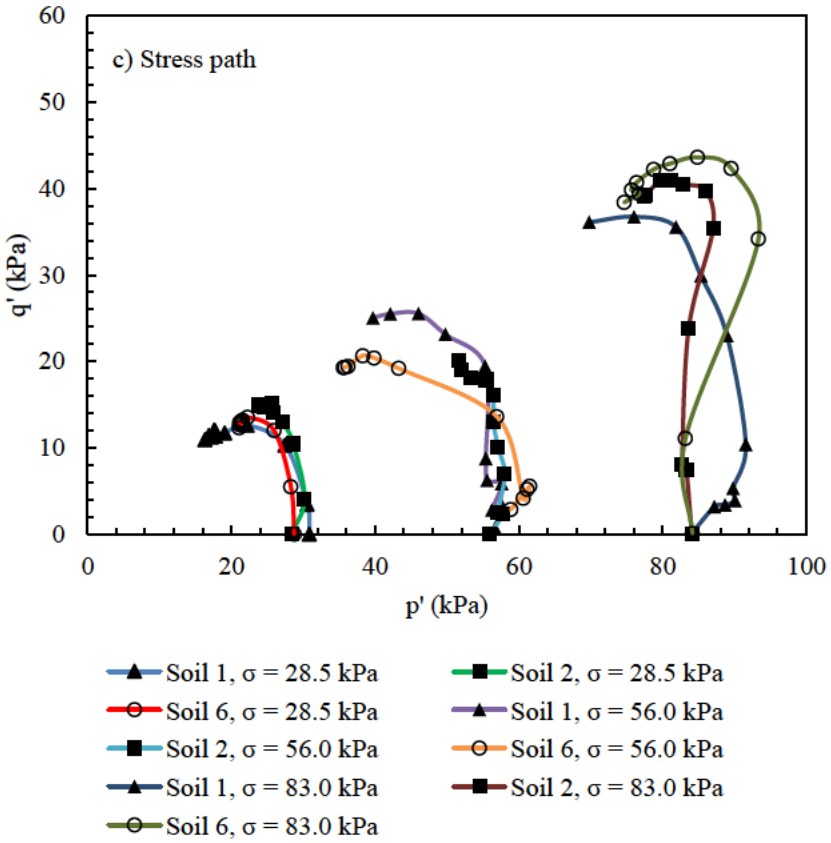

Figure E3.3: Stress path plot of Soils 1, 2 and 6

E.4 Hydraulic conductivity test results

Table E4.1: Hydraulic conductivity test results

Soil No	Average kt (m/s)
Soil 1	9.14E-06
Soil 2	1.15E-06
Soil 4	5.96E-06
Soil 6	4.19E-06
Soil 16	4.64E-07
Soil 17	5.79E-06

References

Abdullah, NHH, Gofar, N, Rahman, NAA & Roslan, SM 2013, 'Empirical correlation for estimation of unsaturated soil shear strength', in *Proceedings of 2013 IEEE Business Engineering and Industrial Applications Colloquium (BEIAC),* Langkawi, Malaysia, pp. 690-694.

Ahmadi-Adli, M, Huvaj, N & Toker, NK 2014, 'Effects of the size of particles on rainfall-induced slope instability in granular soils', in *Proceedings of the Geo-Congress 2014 Technical Papers*, GSP 234, Altanta, Georgia, pp. 4027-4036.

Al Aqtash, U & Bandini, P 2015, 'Prediction of unsaturated shear strength of an adobe soil from the soil-water characteristic curve', *Construction and Building Materials Journal*, vol. 98, pp. 892-899.

Ali, A, Huang, J, Lyamin, AV, Sloan, SW & Cassidy, MJ 2014, 'Boundary effects of rainfall-induced landslides', *Computers and Geotechnics,* vol. 61, pp. 341–354.

Aristizabal, E, Velez, JI, Martinez, HE & Jabojedoff, M 2016, 'SHIA_Landslide: a distributed conceptual and physically based model to forecast the temporal and spatial occurrence of shallow landslides triggerred by rainfall in tropical and mountainous basins', *Landslides*, vol. 13, pp. 497-517.

Askarinejad, A, Casini, F, Bischof, P, Beck, A & Springman SM 2012, 'Rainfall-induced instabilities: a field experiment on a silty sand slope in northern Switzerland', *Rivista Italiana di Geotecnica,* vol. 3 pp. 50-71.

Aydilek, AH & Ramanathan, RS 2013, *Slope failure investigation management system*, State Highway Administration Research Report, Maryland Department of Transportation, Baltimore, MD.

Balzano, B, Tarantino, A, Nicotera, MV, Forte, G, De Falco, M & Santo, A 2019, 'Building physically based models for assessing rainfall-induced shallow landslide hazard at catchment scale: case study of the Sorrento Peninsula (Italy)', *Canadian Geotechnical Journal*, vol. 56, pp. 1291-1303.

Bathurst, JC, Moretti, G, El-Hames, A, Moaven-Hashemi, A & Burton A 2005, 'Scenario modelling of basin-scale shallow landslide sediment yield, Valsassina, Italian Southern Alps', *Natural Hazards and Earth System Sciences,* vol. 5, no. 2, pp. 189-202.

Baum, RL, Godt, JW & Savage, WZ 2010, 'Estimating the timing and location of shallow rainfall-induced landslides using a model for transient, unsaturated infiltration', *Journal of Geophysical Research,* vol. 11, F03013, pp. 1-26.

Baum, RL, Savage, WZ & Godt, JW 2002, *TRIGRS – A Fortran program for transient rainfall infiltration and grid-based regional slope stability analysis*, US Geological Survey open-file report 02-424, Denver, CO.

Baum, RL, Savage, WZ & Godt, JW 2008, *TRIGRS – A Fortran program for transient rainfall infiltration and grid-based regional slope-stability analysis, Version 2.0,* US Geological Survey open-file report 2008-1159, Denver, CO.

Bell, FG 1993, *Engineering Geology*, Blackwell Scientific Publications, Oxford, UK.

Bernardie, S, Desramaut, N, Malet, J-P, Gourlay, M & Grandjean, G 2015, 'Prediction of changes in landslide rates induced by rainfall', *Landslides*, vol. 12, pp. 481-494.

Bhandary, NP, Yatabe, R, Dahal, RK, Hasegawa, S & Inagaki, H 2013, 'Areal distribution of large-scale landslides along highway corridors in central Nepal', *Georisk: Assessment and Management of Risk for Engineered Systems and Geohazards,* vol. 7, no. 1, pp. 1-20.

Bhandary, NP, Yatabe, R, Hasegawa, S & Dahal, RK 2011, 'Characteristic features of deep-seated landslides in Mid-Nepal Himalayas: Spatial distribution and Minerelogical evaluation', in *Proceedings of Geo-Frontiers Congress 2011, Advances in Geotechnical Engineering*, Dallas, Texas, pp. 1693-1702.

Bishop, AW & Blight, GE 1963, 'Some aspects of effective stress in saturated and partly saturated soils', *Geotechnique*, vol. 13, no. 3, pp. 177-197.

Bishop, AW & Morgenstern, N 1960, 'Stability coefficients for earth slopes', *Geotechnique*, vol. 10, no. 4, pp. 129-153.

Bishop, AW, Alpan, I, Blight, GE & Donald, IB 1960, 'Factors controlling the strength of partly saturated cohesive soils', in *Proceedings and Discussions of Research Conference on Shear Strength of Cohesive Soils,* American Society of Civil Engineers, Reston, VA, pp. 503-532 and 1027-1042.

Blight, GE 2002, 'Seasonal changes in the soil-moisture regime at shallow depth in an expansive soil in a semi-arid climate', in *Proceedings of the 3rd International Conference on Unsatuated Soils (UNSAT 2002)* (Eds. Juca, JFT, de Campos, TMP & Marinho, FAM), Lisse, the Netherlands: Swets & Zeitlinger, vol. 2. pp. 865-869.

Bordoni, M, Meisina, C, Valentino, R, Lu, N, Bittelli, M & Chersich, S 2015a, 'Hydrological factors affecting rainfall-induced shallow landslides: From the field monitoring to a simplified slope stability analysis, *Engineering Geology*, vol. 193, pp. 19-37.

Bordoni, M, Meisina, C, Valentino, R, Bittelli, M & Chersich, S 2015b, 'Site-specific to local –scale shallow landslides triggering zones assessment using TRIGRS. *Natural Hazards and Earth System Sciences,* vol.15, pp. 1025–1050.

Borga, M, Fontana, GD, Gregoretti, C & Marchi, L 2002, 'Assessment of shallow landsliding by using a physically based model of hillslope stability', *Hydrological Processes*, vol. 16, pp. 2833-2851.

Brand, EW 1995, 'Keynote paper: slope instability in tropical areas', in *Proceedings of International Symposium on Landslides,* AA Balkema, Rotterdam, The Netherlands, pp. 2031-2051.

Brand, EW, Premchitt, J & Phillipson, HB 1984, 'Relationship between Rainfall and Landslides in Hong Kong', in *Proceedings of 4th International Symposium on Landslides,* Toronto, Canada, pp. 374-384.

Brooks, RH & Corey, AT 1964, *Hydraulic properties of porous media,* Hydrology Papers, no. 3, Colorado State University, Fort Collins, Colorado, CO.

Cabellero, S 2014, 'Experimental model of rainfall induced slope failures in compacted clays', Masters thesis, California State University, Fullerton, California, CA.

Calcaterra, D, De Riso, R & Di Martire D 2004, 'Assessing shallow debris slide hazard in the Agnano Plain (Naples, Italy) using SINMAP, a physically based slope-stability model', in Lacerda et al. (eds), *Landslides: Evaluation and Stabilization*, Taylor & Francis Group, Rio de Janeiro, pp. 177-183.

Campbell, RH 1975, *Soil slips, debris flows and rainstorms in the Santa Monica Mountains and vicinity, Southern California*, Geological Survey Professional Paper 851, US Government Printing Office, Washington.

Caine, N 1980, 'The rainfall intensity-duration control of shallow landslides and debris flows', *Geografiska Annaler, Series A, Physical Geography,* vol. 62, no. 1-2, pp. 23-27.

Capra, L, Lugo-Hubp, J & Borselli, L 2003, 'Mass movements in tropical volcanic terrains: the case of Teziutlan (Mexico)', *Engineering Geology*, vol. 69, no. 3-4, pp. 359-379.

Caris, JPT & Van Asch, TWJ 1991, 'Geophysical, geotechnical and hydrological investigations of a small landslide in the French Alps', *Engineering Geology*, vol. 31, no. 3-4, pp. 249-276.

Cascini, L, Cuomo, S & Guida, D 2008, 'Typical source areas of May 1998 flow-like mass movements in the Campania region, Southern Italy', *Engineering Geology*, vol. 96, no. 3-4, pp. 107-125.

Cascini, L, Cuomo, S, Pastor, M & Sorbino, G 2010, 'Modelling of rainfall-induced shallow landslides of the flow-type', *Journal of Geotechnical and Geoenvironmetal Engineering*, vol. 136, no. 1, pp. 85-98.

Catani, F, Casagli, N, Ermini, L, Righini, G & Menduni G 2005, 'Landslide hazard and risk mapping at catchment scale in the Arno River basin', *Landslides*, vol. 2, pp. 329-342.

Chae, B-G & Kim, M-I 2012, 'Suggestion of a method for landslide early warning using the change in the volumetric water content gradient due to rainfall infiltration', *Environmental Earth Sciences*, vol. 66, pp. 1973-1986.

Chandrasekaran, SS, Sayed Owaise, R, Ashwin, S, Jain, RM, Prasanth, S & Venugopalan, RB 2013, 'Investigations on infrastructural damages by rainfall-induced landslides during November 2009 in Nilgris, India', *Natural Hazards*, vol. 65, pp. 1535-1557.

Chang, J-M, Chen, H, Jou, B-D, Tsou, N-C & Lin, G-W 2017, 'Characteristics of rainfall intensity, duration, and kinetic energy for landslide triggering in Taiwan', *Engineering Geology*, vol. 231, pp. 81-87.

Chen, H, Lee, CF & Law, KT 2004, 'Causative mechanisms of rainfall-induced fill slope failures', *Journal of Geotechnical and Geoenvironmental Engineering*, vol. 130, no. 6, pp. 593-602.

Chen, C-W, Oguchi, T, Hayakawa, YS, Saito, H & Chen, H 2017, 'Relationship between landslide size and rainfall conditions in Taiwan', *Landslides*, vol. 14, pp. 1235-1240.

Chen, HX & Zhang, LM 2014, 'A physically-based distributed cell model for predicting regional rainfall-induced slope failures', *Engineering Geology*, vol. 176, pp. 79-92.

Chen, S-C, Chou, H-T, Chen, S-C, Wu, C-H & Lin, B-S 2014, 'Characteristics of rainfall-induced landslides in Miocene formations: A case study of the Shenmu watershed, Central Taiwan', *Engineering Geology*, vol. 169, pp. 133-146.

Chen,Y-C, Chang, K-T, Chiu, Y-J, Lau, SM & Lee, H-Y 2013, 'Quantifying rainfall controls on catchment-scale landslide erosion in Taiwan', *Earth Surface Processes and Landforms*, vol. 38, no. 4, pp. 372-382.

Chin, K-B, Leong, E-C & Rahardjo, H 2010, 'A simplified method to estimate the soil charcteristics curve', *Canadian Geotechncial Journal*, vol. 47, no. 12, pp. 1382-1400.

Ching-Chuan, H, Yih-Jang, J, Lih-Kang, H & Jin-Long, L 2009, 'Internal soil moisture and piezometric responses to rainfall-induced shallow slope failures', *Journal of Hydrology*, vol. 370, no. 1-4, pp. 39-51.

Cho, SE 2009, 'Infiltration analysis to evaluate the surficial stability of two-layered slopes considering rainfall characteristics', *Engineering Geology*, vol. 105, no. 1-2, pp. 32-43.

Cho, SE 2017, 'Prediction of shallow landslide by surficial stability analysis considering rainfall infiltration', *Engineering Geology,* vol. 231, pp. 126–138.

Chou, J-S, Yang, K-H, Cheng, M-Y & Tu, W-T 2013, 'Identification and assessment of heavy rainfall-induced disaster potentials in Taipei City', *Natural Hazards*, vol. 66, pp. 167-190.

Cogan, J, Gratchev, I & Wang, G 2018, 'Rainfall-induced shallow landslides caused by ex-tropical cyclone Debbie, 31st March 2017, *Landslides*, vol. 15, pp. 1215-1221.

Collins, BD & Znidarcic, D 2004, 'Stability analyses of rainfall induced landslides', *Journal of Geotechnical and Geoenvironmental Engineering*, vol. 130, no. 4, pp. 362-372.

Conte, E & Troncone, A 2012, 'Simplified approach for the analysis of rainfall-induced shallow landslides', *Journal of Geotechnical and Geoenvironmental Engineering*, vol. 138, no. 3, pp. 398-406.

Costa, JE 1984, 'Physical geomorpholgy of debris flows', in JE Costa & PJ Fleisher (Eds), *Developments and Applications of Geomorphology*, Springer, Berlin, pp. 268-317.

Cornforth, D 2005, *Landslides in practice – Investigation, analysis and remedial/preventative options in soils*, John Wiley & Sons, Inc. Hoboken, New Jersey and Canada.

Crosta, G 1998, 'Regionalization of rainfall thresholds: an aid to landslide hazard evaluation', *Environmental Geology*, vol. 35, pp. 131 -145.

Crosta, GB & Frattini, P 2008, 'Rainfall-induced landslides and debris flows – Preface', *Hydrological Processes*, vol. 22, no. 4, pp. 473-477.

Crozier, MJ 1986, *Landslides: Causes, Consequences and Environment*, Croom Helm Ltd, London.

Cuomo, S & Della Sala, M 2013, 'Rainfall-induced infiltration, runoff and failure in steep unsaturated shallow soil deposits', *Engineering Geology*, vol. 162, pp. 118–127.

Cuomo, S & Della Sala, M 2015 'Large-area analysis of soil erosion and landslides induced by rainfall: A case of unsaturated shallow deposits', *Journal of Mountain Science*, vol. 12, pp. 783-796.

Cunningham, MR, Ridley, AM, Dineen, K & Burland, JB 2003, 'The mechanical behaviour of a reconstituted unsaturated silty clay', *Geotechnique*, vol. 53, no. 2, pp. 183-194.

Dahal, RK 2012, 'Rainfall-induced landslides in Nepal', *International Journal of Erosion Control Engineering*, vol. 5, no. 1, pp. 1-8.

Dahal, R & Hasegawa, S 2008, 'Representative rainfall thresholds for landslides in the Nepal Himalaya', *Geomorphology*, vol. 100, no. 3-4, pp. 429-443.

Dahal, R, Hasegawa, S, Nonomura, A, Yamanaka, M, Masuda, T & Nishino, K 2009, 'Failure characteristics of rainfall-induced shallow landslides in granitic terrains of Shikoku Island of Japan', *Environmental Geology*, vol. 56, pp. 1295-1310.

Dai, FC & Lee, CF 2001, 'Frequency-volume relation and prediction of rainfall-induced landslides', *Engineering Geology*, vol. 59, no. 3-4, pp. 253-266.

Dai, FC & Lee CF 2002, 'Landslide characteristics and slope instability modelling using GIS, Lantau Island, Hong Kong, *Geomorphology*, vol. 42, no. 3-4, pp. 213-228.

Dai, FC, Lee, CF, Li, J & Xu, ZW 2001, 'Assessment of landslide susceptibility on the natural terrain of Lantau Island, Hong Kong, *Environmental Geology,* vol. 40, pp. 381-391.

Dai, FC, Lee, CF, Tham, LG, Ng, KC & Shum, WL 2004, 'Logistic regression modelling of storm-induced shallow landsliding in time and space on natural terrain of Lantau Island, Hong Kong, *Bulletin of Engineering Geology and the Environment,* vol. 63, pp. 315-327.

Dev, KL, Pillai, RJ & Robinson, RG 2016, 'Drained angle of internal friction from direct shear and trixial compression tests', *International Journal of Geotechnical Engineering*, vol. 10, no. 3, pp. 283-287.

Dhakal, AS & Sidle, RC 2003, 'Long-term modelling of landslides for different forest management practices', *Earth Surface Processes and Landforms,* vol. 28, no. 8, pp. 853-868.

Dietrich, WE & Montgomery, DR 1998, *SHALSTAB: a digital terrain model for mapping shallow landslide potential,* National Council of the Paper Industry for Air and Stream Improvement.

Dominguez, JA 2007, 'Rainfall-induced pore pressure response in slopes: A case-study comparison of one- and two-dimensional analyses', Masters thesis, Tufts University, Medford, MA.

Donald, IB 1956, 'Shear strength measurements in unsaturated non-cohesive soils with negative pore pressures' in *Proceedings of the second Australia – New Zealand Conference in Soil Mechanics Foundation Engineering,* Adelaide, South Australia, pp. 41-46.

Donnini, M, Napolitano, E, Salvati, P, Ardizzone, F, Bucci, F, Fiorucci, F, Santangelo, M, Cardinali, M & Guzzetti, F 2017, 'Impact of event landslides on road networks: a statistical analysis of two Italian case studies', *Landslides*, vol. 14, pp. 1521-1535.

Duncan, JM & Wright SG 2005, *Soil strength and slope stability*, John Wiley & Sons, Inc., USA.

Escario, V & Saez, J 1986, 'The shear strength of partly saturated soils', *Geotechnique*, vol. 36, no. 3, pp. 453-456.

Ewen, J, Parkin, G & O'Connell, PE 2000, 'SHETRAN: Distributed river basin flow and transport modelling system', *Journal of Hydrologic Engineering*, vol. 5, no. 3, pp. 250-258.

Fan, C-C & Wang, H-Z 2014, 'The mechanism of soil moisture contents in a slope gully during rainfall', in *Proceedings of UNSAT2014 - Unsaturated Soils: Research & Applications,* Sydney, Australia, vol. 2, pp. 1257-1264.

Farisham, AS 2007, *Landslides in the hillside development in the Hulu Klang, Klang Valley*, Post-graduate seminar, Skudai, UTM, Malaysia, 6 Mar 2007.

Farooq, K, Rogers, JD & Ahmed, MF 2015, 'Effect of densification on the shear strength of Landslide Material: A case study from Salt Range, Pakistan, *Earth Science Research*, vol. 4, no. 1, pp. 113-125.

Finlay, PJ, Fell, R & Maguire, PK 1997, 'The relationship between the probability of landslide occurrence and rainfall', *Canadian Geotechncial Journal*, vol. 34, no. 6, pp. 811-824.

Flentje, P & Chowdhury, RN 2005, 'Managing landslide hazards on the Illawarra escarpment', in *Proceedings of the GeoQuest Symposium on Planning for Natural Hazards*, GeoQuest Research Centre, University of Wollongong, Wollongong, pp. 65-78.

Flentje, P, Chowdhury, RN, Tobin, P & Brizga, V 2005, 'Towards real-time landslide risk management in an urban area', in *Proceedings of the International Conference on Landslide Risk Management /18th Annual Vancouver Geotechnical Society Symposium,* Vancouver, pp. 741-751.

Fourie, AB, Rowe, D & Blight, GE 1999, 'The effect of infiltration on the stability of the slopes of a dry ash dump', *Geotechnique,* vol. 49, no. 1, pp. 1-13.

Fredlund, DG 2000, 'The 1999 RM Hardy Lecture: The implementation of unsaturated soil mechanics into geotechnical engineering', *Canadian Geotechnical Journal,* vol. 37, no. 5, pp. 963-986.

Fredlund, DG, Morgenstern, NR & Widger, RA 1978, 'Shear strength of unsaturated soils', *Canadian Geotechnical Journal,* vol. 15, no. 3, pp. 313-321.

Fredlund, DG, Rahardjo, H & Gan, JK-M 1987, 'Non-linearity of strength envelope for unsatuaretd soils', in *Proceedings of 6th International Conference on Expansive Soils,* New Delhi, India, pp. 49-54.

Fredlund, DG & Rahardjo, H 1993, *Soil mechanics for unsaturated soils*, John Wiley & Sons Inc., New York & Canada.

Fredlund, DG, Rahardjo, H & Ng, T 1993, 'Effect of pore-air and negative pore-water pressures on stability at the end-of-construction', in *Proceedings of International Conference on Dam Engineering*, Johor Bahru, Malaysia.

Fredlund, DG, Rahardjo, H & Fredlund, MD 2012, *Unsaturated soil mechanics in engineering practice,* John Wiley & Sons, Inc., New Jersey, USA and Canada.

Fredlund, DG, Sheng, D & Zhao, J 2011, 'Estimation of soil suction from the soil-water characteristic curve', *Canadian Geotechnical Journal*, vol. 48, no. 2, pp. 186-198.

Fredlund, DG & Xing, A 1994, 'Equations for the soil-water characteristic curve', *Canadian Geotechnical Journal,* vol. 31. no. 4, pp. 521-532.

Fredlund, DG, Xing, A, Fredlund, MD & Barbour, SL 1996, 'The relationship of the unsaturated soil shear strength to the soil-water characteristics curve', *Canadian Geotechnical Journal*, vol. 33, no. 3, pp. 440-448.

Fuchu, D, Lee, CF & Sijing, W 1999, 'Analysis of rainstorm-induced slide-debris flow on natural terrain of Lantau Island, Hong Kong, *Engineering Geology*, vol. 51, no. 4. pp. 279-290.

Gallage, CPK & Uchimura, T 2010, 'Effects of dry density and grain size distribution on soil-water characteristic curves of sandy soils', *Soils and Foundations*, vol. 50, no. 1, pp. 161-172.

Gallage, C & Uchimura, T 2016, 'Direct shear testing on unsaturated silty soils to investigate the effects of drying and wetting on shear strength parameters at low suction', *Journal of Geotechnical and Geoenvironmental Engineering*, vol. 142, no. 3, 04015081, pp. 1-9.

Gariano, SL & Guzzetti F 2016, 'Landslides in a changing climate', *Earth-Science Reviews*, vol. 162, pp. 227-252.

Garland, GG & Olivier, MJ 1993, 'Predicting landslides from rainfall in a humid, sub-tropical region, *Geomorphology*, vol. 8, no. 2-3, pp. 165-173.

Garven, EA 2009, 'Review of the empirical equations for predicting the shear strength of unsaturated soils', Masters thesis, University of Ottawa, Canada.

Garven, EA & Vanapalli, SK 2006, 'Evaluation of empirical procedures for predicting the shear strength of unsaturated soils', in *Proceedings of 4th International Conference on Unsaturated Soils*, Carefree, Arizona, AZ, pp. 2570-2581.

Gavin, K & Xue, J 2008, 'A simple method to analyse infiltration into unsaturated soil slopes', *Computers and Geotechnics*, vol. 35, no. 2, pp. 223-230.

Gerrard, J 1994, 'The landslide hazard in the Himalayas: geological control and human action', *Geomorphology*, vol. 10, no. 1-4, pp. 221-230.

Gerscovich, DMS, Vargas Jr, EA & De Campos, TMP 2006, 'On the evaluation of unsaturated flow in a natural slope in Rio de Janeiro, Brazil', *Engineering Geology*, vol. 88, no. 1-2, pp. 23-40.

Ghiassian, H & Ghareh, S 2008, 'Stability of sandy slopes under seepage conditions', *Landslides*, vol. 5, pp. 397-406.

Giannecchini, R, Galanti, Y & D'Amato Avanzi, G 2012, 'Critical rainfall thresholds for triggering shallow landslides in the Serchio River Valley, (Tuscany, Italy)', *Natural Hazards and Earth Systems Sciences*, vol. 12, pp. 829-842.

Gilley, JE, Elliot, WJ, Laflen, JM & Simanton, JR 1993, 'Critical shear stress and critical flow rates for initation of rilling', *Journal of Hydrology*, vol. 142, no. 1-4, pp. 251-271.

Godt, JW, Baum, RL & Chleborad, AF 2006, 'Rainfall characteristics for shallow landsliding in Seattle, Washington, USA', *Earth Surface Processes and Landforms*, vol. 31, no. 1, pp. 97-110.

Godt, JW, Baum, RL & Lu, N 2009, 'Landsliding in partially saturated materials', *Geophysical Research Letters*, vol. 36, no. 2, L02403, pp. 1-5.

Gofar, N, Lee, LM & Kassim, A 2008, 'Response of suction distribution to rainfall infiltration in soil slope', *The Electronic Journal of Geotechnical Engineering*, vol. 13, pp. 1-13.

Government of Hong Kong, 1977, *Report on the slope failures at Sau Mau Ping, August, 1976*, Hong Kong Government, Hong Kong.

Gratchev, I, Jeng, D-S & Oh, E 2018, *Soil mechanics through project-based learning*, CRC Press, Taylor & Francis Group, London, UK.

Guan, GS, Rahardjo, H & Choon LE 2010, 'Shear strength equations for unsaturated soil under drying and wetting', *Journal of Geotechnical and Geoenvironmental Engineering*, vol. 136, no. 4, pp. 594-606.

Gue, SS & Liong, CH 2007, 'Is the ground in Ulu Kelang unstable?', *Jurutera*, pp. 32-33.

Gul, M 2015, 'Lithological properties and environmental importance of the Quaternary colluviums (Mugla, SW Turkey)', *Environmental Earth Sciences*, vol. 74, pp. 4089-4108.

Guns, M & Vanacker, V 2013, 'Forest cover change trajectories and their impact on landslide occurrence in the tropical Andes', *Environmental Earth Sciences*, vol. 70, pp. 2941-2952.

Gutierrez-Martin, A 2020, 'A GIS-physically-based emergency methodology for predicting rainfall-induced shallow landslide zonation', *Geomorphology*, vol. 359, 107121, pp. 1-14

Guzzetti, F, Peruccacci, S, Rossi, M & Stark, CP 2007, 'Rainfall thresholds for the initiation of landslides in central and southern Europe', *Meteorlogy and Atmospheric Physics*, vol. 98, pp. 239-267.

Guzzetti, F, Peruccacci, S, Rossi, M & Stark, C 2008, 'The rainfall intensity-duration control of shallow landslides and debris flows: an update', *Landslides,* vol. 5, pp. 3-17.

Heshmati, AA & Motahari, MR 2012, 'Identification of key parameters on soil water characteristic curve', *Life Science Journal*, vol. 9, no. 3, pp. 1532-1537.

Highland, LM & Bobrowsky, P 2008, *The landslide handbook – A guide to understanding landslide*, US Geological Survey, Reston, Virginia, USA.

Ho, DYF & Fredlund, DG 1982, 'A multistage triaxial test for unsatuarted soils', *Geotechnical Testing Journal*, March/June, pp. 18-25.

Hong, Y, Adler, R & Huffman, G 2006, 'Evaluation of the potential of NASA multi-satellite precipitation analysis in global landslide hazard assessment', *Geophysics Research Letters*, vol. 33, no. 22, L22402, pp. 1-5.

Hong, Y-M & Wan, S 2011, 'Forecasting groundwater level fluctuations for rainfall-induced landslide', *Natural Hazards*, vol. 57, no. 2, pp. 167-184.

Horn, R & Fleige, H 2003, 'A method for assessing the impact of load on mechanical stability and physical properties of soils', *Soil and Tillage Research*, vol. 73, no. 1-2, pp. 89-99.

Hossain, MA & Yin, J-H 2010, 'Shear strength and dilative characteristics of an unsaturated compacted completely decomposed granite soil', *Canadian Geotechnical Journal*, vol. 47, no. 10, pp. 1112-1126.

Houston, SL 2014, 'Characterisation of Unsaturated soils: The importance of response to wetting', in *Proceedings of the Geo-Congress 2014 Keynote Lectures: Geo-characterisation and Modelling for sustainability*, Atlanta, Georgia, GA.

Howard, TR, Baldwin, JE & Donley, HF 1982, 'Landslides in Pacifica California caused by the storm', in ED Ellen and GF Wieckzoreck (eds), *Landslides, Floods and Marine effects of the storm of January, 3–5, 1982 in the San Francisco Bay Region, California,* US Geological Survey Professional Paper 1434, Version 1, US Geological Survey, Denver, CO, pp. 163-183.

Hsu, S-C, Maldonado, J, Loehr, E, Bowders, J, Lindsey, E & Omatsone, W 2013, 'Model testing of precipitation-induced landslides', in *Proceedings of the Geo-Congress 2013*, San Diego, California, CA.

Huang, C-C, Lo, C-L, Jang, J-S & Hwu, L-K 2008, 'Internal soil moisture response to rainfall-induced slope failures and debris discharge', *Engineering Geology*, vol. 101, no. 3-4, pp. 134-145.

Igwe, O 2015a, 'The geological characteristics of landslides on the sedimentary and metamorphic terrains of South-East Nigeria, West Africa', *Geoenvironmental Disasters*, pp. 1-14.

Igwe, O 2015b, 'Analyses of the October 2013 fatal slope failures on the metamorphic terrains of Obudu tourist area, South-Southeast Nigeria', *Arabian Journal of Geosciences*, vol. 8, pp. 7425-7434.

Igwe, O & Una, CO 2019, 'Landslide impacts and management in Nanka area, Southeast Nigeria', *Geoenvironmental Disasters*, pp. 1-12.

Iversion, RM 2000, 'Landslide triggering by rain infiltration', *Water Resources Research*, vol. 36, no. 7, pp. 1897–1910.

Jan, C-D, Yang, S-Y, Su, Y-W & Huang, W-S 2016, 'Investigation about rainfall-induced shallow landslides in CYL and TWR watersheds, Taiwan', *Environmental Earth Sciences*, vol. 75, no. 10, pp. 1-15.

Jemec, M & Komac M 2013, 'Rainfall patterns for shallow landsliding perialpine Slovenia', *Natural Hazards*, vol. 67, pp. 1011-1023.

Jotisankasa, A, Kulsawan, B, Toll, DG & Rahardjo, H 2008, 'Studies of rainfall-induced landslides in Thailand and Singapore', in *Proceedings of 1st European Conference on Unsaturated Soils, E-UNSAT 2008*, Durham, UK, pp. 901-907.

Jotisankasa, A & Mairaing, W 2010, 'Suction-monitored direct shear testing of residual soils from landslide-prone areas', *Journal of Getechnical and Geoenvironmental Engineering*, vol. 136, no. 3, pp. 533-537.

Karthikeyan, M, Toll, DG & Phoon, KK 2008, 'Prediction of changes in pore-water pressure response due to rainfall events', in *Proceedings of 1st European Conference on Unsaturated Soils, E-UNSAT 2008*, Durham, UK, pp. 829-834.

Kenney, TC 1967, 'Slide behaviour and shear resistance of a quick clay determined from a study of the landslide at Selnes, Norway', in *Proceedings of Geotechnical Conference*, Oslo, Norway, vol. 1, pp. 57-64.

Khaboushan, EA, Emami, H, Mosaddeghi, MR & Astaraei, AR 2018, 'Estimation of unsaturated shear strength parameters using easily-available soil properties', *Soil and Tillage Research*, vol. 184, pp. 118-127.

Khalili, N & Zarbargashi, S 2010, 'Influence of hydraulic hysteresis on effective stress in unsaturated soils', *Geotechnique*, vol. 60, no. 9, pp. 729-735.

Khalilnejad, A, Hj Ali F, Hashim, R & Osman, N 2013, 'Finite-element simulation for contribution of matric suction and friction angle to stress distribution during pulling-out process', *International Journal of Geomechnics*, vol. 13, no. 5, pp. 527-532.

Kim, WS & Borden, RH 2011, 'Influence of soil type and stress state on predicting shear strength of unsaturated soil using the soil-water characteristics curve', *Canadian Geotechnical Journal*, vol. 48, no. 12, pp. 1886-1900.

Kim, H, Ganju, E, Tang, D, Prezzi, M & Salgado, R 2015, 'Matric suction measurements of compacted subgrade soils', *Road Materials and Pavement Design*, vol. 16, no. 2, pp. 358-378.

Kim, J, Jeong, S, Park, S & Sharma, J 2004, 'Influence of rainfall-induced wetting on the stability of slopes in weathered soils', *Engineering Geology*, vol. 75, no. 3-4, pp. 251-262.

Kim, B-S, Shibuya, S, Park, S-W & Kato, S 2010, 'Application of suction stress for estimating unsaturated shear strength of soils using direct shear testing under low confining pressure', *Canadian Geotechnical Journal*, vol. 47, no. 9, pp. 955-970.

Kirschbaum, DB, Adler, R, Hong, Y, Hill, S & Lerner-Lam, A 2009, 'A global landslide catalog for hazard applications: method, results, and limitations', *Natural Hazards*, vol. 52, pp. 561-575.

Kirkby, M 1997, 'TOPMODEL: a personal view', *Hydrological Processes*, vol. 11, pp. 1087-1097.

Kitamura, R & Sako, K 2010, 'Contribution of "Soils and Foundations" to studies on rainfall-induced slope failure', *Soils and Foundations*, vol. 50, no. 6, pp. 955-964.

Knapen, A, Poesen, J & De Baets, S 2007, 'Seasonal variations in soil erosion resistance during concentrated flow for a loess-derived soils under two contrasting tillage practices', *Soil and Tillage Research*, vol. 94, no. 2, pp. 425-440.

Koizumi, K, Oda, K, Komatsu, M, Ito, S & Tsutsumi, H 2019, 'Slope structural health monitoring method against rainfall-induced shallow landslide', in *Proceedings of IOP Conference Series: Materials Science and Engineering, 7th International Conference on Euro – Asia Civil Engineering Forum,* Stuttgart, Germany, vol. 615, pp. 1-8.

Kong, L-W & Tan, L-R 2000, 'Study on shear strength and swelling – shrinkage characteristics of compacted expansive soil', in *Proceedings of the Asian Conference on Unsaturated Soils, UNSAT-ASIA 2000*, Singapore, pp. 515-519.

Krahn, J, Fredlund, DG & Klassen, MJ 1989, 'Effect of soil suction on slope stability at Notch Hill', *Canadian Geotechnical Journal*, vol. 26, no. 2, pp. 269-278.

Kristo, C, Rahardjo, H & Satyanaga, A 2017, 'Effects of variations in rainfall intensity on slope stability in Singapore', *International Soil and Water Conservation Research*, vol. 5, no. 4, pp. 258-264.

Lee, Y-F & Chi, Y-Y 2011, 'Rainfall-induced landslide risk at Lushan, Taiwan', *Engineering Geology*, vol. 123, no. 1-2, pp. 113-121.

Lee, LM, Gofar, N & Rahardjo, H 2009. 'A simple model for preliminary evaluation of rainfall-induced slope instability', *Engineering Geology*, vol. 108, no. 3-4, pp. 272-285.

Lee, KT & Ho, J-Y 2009, 'Prediction of landslide occurrence based on slope instability and hydrological simulation', *Journal of Hydrology*, vol. 375, pp. 489-497.

Lee, ML, Ng, KY, Huang, YF and Li, WC 2014, 'Rainfall-induced landslides in Hulu Kelang area, Malaysia', *Natural Hazards*, vol. 70, pp. 353-375.

Leonarduzzi, E, Molnar, P & McArdell, BW 2017, 'Predictive performance of rainfall thresholds for shallow landslides in Switzerland from gridded daily data', *Water Resources Research,* vol. 53, no. 8, pp. 6612-6625.

Leong, EC & Rahardjo, H 1997, 'Review of soil-water chacteristics curve equations', *Journal of Geotechnical and Geoenvironmental Engineering*, vol. 123, no. 12, pp. 1106-1117.

Lepore, C, Kamal, SA, Shanahan, P & Bras, RL 2012, 'Rainfall-induced landslide susceptibility zonation of Puerto Rico', *Environmental Earth Sciences*, vol. 66, pp. 1667-1681.

Li, CJ 2004, *Remote sensing survey and integrated investigation of land and resources in Zhejiang Province*, Geological Publishing House, Beijing, China, pp. 39-82 (In Chinese with Abstract in English).

Li, C, Ma, T, Zhu, X & Li W 2011, 'The power-law relationship between landslide occurrence and rainfall level', *Geomorphology*, vol. 130, no. 3-4, pp. 221-229.

Li, YR, Wen, BP, Aydin, A & Ju, NP 2013, 'Ring shear tests on slip zone soils of three giant landslides in the Three Gorges Project area', *Engineering Geology*, vol. 154, pp. 106-115.

Li, AG, Yue, ZQ, Tham, LG, Lee, CF & Law, KT 2005, 'Field-monitored variations of soil moisture and matric suction in a saprolite slope', *Canadian Geotechnical Journal*, vol. 42, no.1, pp. 13-26.

Li, JH & Zhang, LM 2010, 'Geometric parameters and REV of a crack network in soil', *Computers and Geotechnics*, vol. 37, no. 4, pp. 466-475.

Li, JH & Zhang, LM 2011, 'Study of desiccation crack initiation and development at ground surface', *Engineering Geology*, vol. 123, no. 4, pp. 347-358.

Liao, Z, Hong, Y, Wang, Y, Fukuoka, H, Sassa, K, Karnawati, D & Fathani, F 2010, 'Prototyping an experimental early warning system for rainfall-induced landslides in Indonesia using satellite remote sensing and geospatial datasets', *Landslides*, vol. 7, no. 3, pp. 317-324.

Likos, WJ, Lu, N & Godt, JW 2014, 'Hysteresis and uncertainty in soil water-retention curve parameters, *Journal of Geotechnical and Geoenvironmental Engineering*, vol. 140, no. 4, 04013050, pp. 1-11.

Liming Engineering Consultants Co., Ltd, 2006, 'Final report to investigations, managements and planning projects of landslide area', *Soils and Water Conservation Bureau* (in Chinese).

Lin, G-W & Chen, H 2012, 'The relationship of rainfall energy with landslides and sediment delivery, *Engineering Geology*, vol. 125, pp. 108-118.

Ling, H & Ling, HI 2012, 'Centrifuge model simulations of rainfall-induced slope instability', *Journal of Geotechnical and Geoenvironmental Engineering*, vol. 138, no. 9, pp. 1151-1157.

Lo, H-C, Hsu, S-M, Chi, S-Y & Ku, C-Y 2010, 'Coupled stability analyses of rainfall induced landslide: A case study in Taiwan Piedmont area', in *Proceedings of the GeoShangai 2010 International Conference*, Shanghai, China.

Look, BG 2007, *Handbook of geotechnical investigation and design tables*, Balkema, Taylor and Francis Group, The Netherlands.

Lourenco, SDN, Sassa, K & Fukuoka, H 2004, 'An experimental study on the pore water pressure increase in rainfall-induced landslides', in *Proceedings of International Symposium on Landslides*, Rio de Janeiro, Brazil, pp. 716-716.

Low, TH, Ali, F & Ibrahim, AS 2012, 'An investigation on one of the rainfall-induced landslides in Malaysia', *Electronic Journal of Geotechnical Engineering*, vol. 17, no. D, pp. 435-449.

Lu, N & Godt, J 2008, 'Infinite slope stability under steady unsaturated seepage conditions', *Water Resources Research*, vol. 44, no. 11, W11404, pp. 1-13.

Lu, N, Godt, JW & Wu, DT 2010, 'A close-form equation for effective stress in unsaturated soil', *Water Resources Research*, vol. 46, no. 5, W05515, pp. 1-14.

Lu, N & Godt, J 2013, *Hillslope hydrology and stability*, Cambridge University Press, Cambridge, UK.

Lu N, Kaya, M, Collins, BD & Godt JW 2013, 'Hysteresis of unsaturated hydromechanical properties of a silty soil', *Journal of Geotechnical and Geoenvironmental Engineering*, vol. 139, no. 3, pp. 507-510.

Lu, N & Likos, WJ 2004, *Unsaturated soil mechanics*, Wiley, Hoboken, NJ.

Lu, N & Likos WJ 2006, 'Suction stress characteristic curve for unsaturated soil', *Journal of Geotechnical & Geoenvironmental Engineering*, vol. 132, no. 2, pp. 131-142.

Luo, Y, He, S-M, Chen, F-Z, Li, X-P & He, J-C 2015, 'A physical model considered the effect of overland water flow on rainfall-induced shallow landslides', *Geoenvironmental Disasters*, vol. 2, no. 8, pp. 1-11.

Ma, T, Li, C, Lu, Z & Bao, Q 2015, 'Rainfall intensity-duration thresholds for the initiation of landslides in Zhejiang Province, China', *Geomorphology*, vol. 245, pp. 193-206.

Maharaj, RJ 1993, ‘Landslide processes and landslide susceptibility analysis from an upland watershed: A case study from St. Andrew, Jamaica, West Indies’, *Engineering Geology*, vol. 34, no. 1-2, pp. 53-79.

Martinovic, K, Reale, C & Gavin, K 2017, ‘Fragility curves for rainfall-induced shallow landslides on transport networks’, *Canadian Geotechnical Journal*, vol. 55, no. 6, pp. 852-861.

Matsushi, Y, Hattanji, T & Matsukura, Y 2006, ‘Mechanisms of shallow landslides on soil-mantled hill slopes with permeable and impermeable bedrocks in the Boso Peninsula, Japan’, *Geomorphology*, vol. 76, no. 1-2, pp. 92-108.

Matsushi, Y & Matsukura, Y 2006, ‘Cohesion of unsaturated residual soils as a function of volumetric water content’, *Bulletin of Engineering Geology and the Environment*, vol. 65, pp. 449-455.

Matsuura, S, Asano, S & Okamoto, T 2008, ‘Relationship between rain and/or meltwater, pore-water pressure and displacment of a reactivated landslide’, *Engineering Geology*, vol. 101, no. 1-2, pp. 49-59.

Mercogliano, P, Segoni, S, Rossi, G, Sikorsky, B, Tofani, V, Schiano, P, Catani, F & Casagli, N 2013, ‘Brief communication: A prototype forecasting chain for rainfall induced shallow landslides’, *Natural Hazards and Earth System Sciences*, vol. 13, pp. 771-777.

Michael-Leiba, M, Andrews, K & Blong, R 1997, ‘The impact of landslides in Australia’, *Australian Journal of Emergency Management*, vol. 12, no. 1. pp. 23-25.

Michaels, AS 1959, ‘Discussion - Physical-chemical properties of soils: Soil - Water System’, *Journal of the Soil Mechanics and Foundation Engineering Division,* ASCE, vol. 85, no. SM-2, part 1, pp. 91-102.

Michiue, M 1985, ‘A method for predicting slope failures on cliff and mountain due to heavy rain’, *Natural Disaster Science*, vol. 7, no. 1, pp. 1-12.

Moayedi, H, Huat, BBK, Mohammad Ali, TA, Asadi, A, Moayedi, F & Mokhberi, M 2011, ‘Preventing landslides in times of rainfall: case study and FEM analyses’, *Disaster Prevention and Management*, vol. 20, no. 2, pp. 115-124.

Montgomery, DR & Dietrich, WE, 1994, ‘A physically based model for the topographic control on shallow landsliding’, *Water Resources Research,* vol. 30, no. 4, pp. 1153–1171.

Montgomery, DR, Sullivan, K & Greenberg, HM 1998, 'Regional test of a model for shallow landsliding', *Hydrological Processes*, vol. 12, no. 6, pp. 943-955.

Montrasio, L 2000, 'Stability analysis of soil slip', in *Proceedings of International Conference "Risk 2000"*, Southampton, pp. 357–366.

Montrasio, L & Valentino, R 2008, 'A model for triggering mechanisms of shallow landslides', *Natural Hazards and Earth System Sciences*, vol. 8, pp. 1149-1159.

Montrasio, L, Valentino, R & Losi, GL 2009, 'Rainfall-induced shallow landslides: A model for the triggering mechanism of some case studies in Northern Italy', *Landslides*, vol. 6, pp. 241–251.

Montrasio, L, Valentino, R & Quintavalla, C 2010, 'Estimation of the degree of saturation of shallow soils from satellite observations to model soil slips occurred in Emilia Romagna of Nothern Italy', *International Journal of Geosciences*, vol. 1, pp. 58-65.

Montrasio, L, Valentino, R & Losi, GL 2011, 'Towards a real-time susceptibility assessment of rainfall-induced shallow landslides on a regional scale', *Natural Hazards and Earth System Sciences*, vol. 11, pp. 1927–1947.

Montrasio, L, Valentino, R & Losi, GL 2012, 'Shallow landslides triggerred by rainfalls: modelling of some case histories in the Reggiano Apennine (Emilia Romagna Region, Northern Italy)', *Natural Hazards*, vol. 60, pp. 1231-1254.

Montrasio, L, Valentino, R & Terrone, A 2014, 'Application of the slip model', *Procedia Earth and Planetary Science*, vol. 9, pp. 206-213.

Montrasio, L & Valentino, R 2016, 'Modelling rainfall-induced shallow landslides at different scales using SLIP – Part 1', *Procedia Engineering*, vol. 158, pp. 476-481.

Montrasio, L, Valentino, R & Meisina, C 2018, 'Soil saturation and stability analysis of a test site slope using the Shallow Landslide Instability Prediction (SLIP) Model', *Geotechnical and Geological Engineering*, vol. 36, pp. 2331-2342.

Morrissey, MM, Wieczorek, GF & Morgan BA 2001, *A comparative analysis of hazard models for predicting debris flow in Madison County, VA*, USGS, Open-File Report 2001-67, Denver, CO.

Naghadeh, RA & Toker, NK 2019, 'Exponential equation for predicting shear strength envelope of unsaturated soils', *International Journal of Geomechanics*, vol. 19, no. 7, 04019061, pp. 1-12.

Nian, T-K, Feng, Z-K, Yu, P-C & Wu, H-J 2013, 'Strength behaviour of slip-zone soils of landslide subject to the change of water content', *Natural Hazards*, vol. 68, pp. 711-721.

Nishigaki, M, Tohari, A & Komatsu, M 1999, 'Predicting rainfall-induced slope failures from moisture content measurement', in *Proceedings of International Symposium on Slope Stability Engineering – IS-Shikoku*, Matsuyama, Shikoku, Japan, vol. 1, pp. 465-469.

Norris, JE, Stokes, A, Mickovski, SB, Cammeraat, E, Van Beek, R, Nicoll, BC & Achim, A 2008, *Slope stability and erosion control: Ecotechnological Solutions*, vol. 1, Springer, New York.

Novak, V, Simaunek, J & Van Genuchten, MT 2000, 'Infiltration of water into soils with cracks', *Journal of Irrigation and Drainage Engineering*, vol. 126, no. 1, pp. 41-47.

Oh, H-J, Lee, S, Chotikasathien W, Kim CH & Kwon JH 2008, 'Predictive landslide susceptibility mapping using spatial information in the Pechabun area of Thailand', *Environmental Geology*, vol. 57, pp. 641 - 651.

Olivares, L, Damiano, E, Mercogliano, P, Picarelli, L, Netti, N, Schiano, P, Savastano, V, Cotroneo, F & Manzi, MP 2014, 'A simulation chain for early prediction of rainfall-induced landslides', *Landslides*, vol. 11, pp. 765-777.

Ono, K, Kazama, S & Ekkawatpanit, C 2014, 'Assessment of rainfall-induced shallow landslides in Phetchabun and Krabi provinces, Thailand, *Natural Hazards*, vol. 74, pp. 2089-2107.

Orense, RP, Shimoma, S, Maeda, K & Towhata, I 2004, 'Instrumented model slope failure due to water seepage', *Journal of Natural Disaster Science*, vol. 26, no. 1, pp. 15-26.

Pack, RT, Tarboton, DG & Goodwin, CN 2001, 'Assessing terrain stability in a GIS using SINMAP', in *Proceedings of 15th annual GIS Conference, GIS 2001*, Vancouver, pp. 56-68.

Pando, MA, Ruiz, ME & Larsen, MC 2005, 'Rainfall-induced landslides in Puerto Rico: An overview, in *Proceedings of Geo-Frontiers Congress 2005, GSP 140 Slopes and Retaining structures under seismic and static conditions,* Austin, TX, pp. 1-15.

Park, HJ, Lee, JH & Woo, I 2013a, 'Assessment of rainfall-induced shallow landslide susceptibility using a GIS-based probabilistic approach', *Engineering Geology*, vol. 161, pp. 1-15.

Park, DW, Nikhil, NV & Lee SR 2013b, 'Landslide and debris flow susceptibility zonation using TRIGRS for the 2011 Seoul landslide event', *Natural Hazards Earth Sytsem Sciences*, vol. 13, pp. 2833-2849.

Parriaux, A 2009, *Geology – Basics for Engineers*, CRC press, Taylor and Francis Group, London, UK.

Patil, UD, Puppala, AJ, Hoyos, LR & Pedarla, A 2017, 'Modelling critical-state shear strength behaviour of comapcted silty sand via suction-controlled triaxial testing', *Engineering Geology*, vol. 231, pp. 21-33.

Pedrozzi, G 2004, 'Triggering of landslides in Canton Ticino (Switzerland) and prediction by the rainfall intensity and duration method', *Bulletin of Engineering Geology and the Environment*, vol. 63, pp. 281-291.

Penalba, RF, Luo, Z & Hsein Juang, C 2009, 'Framework for proabilistic assessment of landslide: a case study of El Berrinche', *Environmental Earth Sciences*, vol. 59, pp. 489-499.

Phoon, K-K & Kulhawy, FH 1999a, 'Characterisation of geotechnical variability', *Canadian Geotechnical Journal*, vol. 36, no. 4, pp. 612-624.

Phoon, K-K & Kulhawy, FH 1999b, 'Evaluation of geotechncial property variability', *Canadian Geotechnical Journal*, vol. 36, no. 4, pp. 625-639.

Pradhan, AMS, Lee, S-R & Kim, Y-T 2019, 'A shallow slide prediction model combining rainfall threshold warning and shallow slide susceptibility in Busan, Korea', *Landslides*, vol. 16, pp. 647-659.

Qi, JF, Song, XL & Liu, JC 2012, 'A study on the effects of water content on strength paramaters of landslide soil', *Applied Mechanics and Materials*, vol. 170-173, pp. 785-788.

Rahardjo, H, Lee, TT, Leong, EC & Rezaur, RB 2005, 'Response of a residual soil slope to rainfall', *Canadian Geotechnical Journal*, vol. 42, no. 2, pp. 340-351.

Rahardjo, H, Lim, TT, Chang, MF & Fredlund DG 1995, 'Shear strength characteristics of a residual soil', *Canadian Geotechnical Journal*, vol. 32, no. 1, pp. 60-77.

Rahardjo, H, Ong TH, Rezaur, RB & Leong, EC 2007, 'Factors controlling instability of homogenous soil slopes under rainfall', *Journal of Geotechnical and Geoenvironmental Engineering*, vol. 133, no. 12, pp. 1532-1543.

Rahardjo, H, Satyanaga, A & Leong, EC 2012, 'Unsaturated soil mechanics for slope stabilization', *Geotechnical Engineering Journal of the SEAGS and AGSSEA*, vol. 43, no. 1, pp. 48-58.

Rahimi, A, Rahardjo, H & Leong, E-C 2011, 'Effect of antecedent rainfall patterns on rainfall-induced slope failure', *Journal of Geotechnical and Geoenvironmental Engineering*, vol. 137, no. 5, pp. 483-491.

Ran, Q, Hong, Y, Li, W & Gao, J 2018, 'A modelling study of rainfall-induced shallow landslide mechanisms under different rainfall characteristics', *Journal of Hydrology*, vol. 563, pp. 790-801.

Ravindran, S, Gratchev, I & Jeng, D-S 2019, 'Analysis of rainfall-induced landslides in northern New South Wales, Australia', *Australian Geomechanics*, vol. 54, no. 4, pp. 83–97.

Ravindran, S, Gratchev, I & Jeng, D-S 2018, 'Prediction of shear strength of unsaturated soils in landslides-prone areas using direct shear and suction tests under low normal stress condition', in *Proceedings of UNSAT 2018, The 7th International Conference on Unsaturated Soils*, Hong Kong, vol. 2, pp. 947-952.

Regmi, AD, Yoshida, K, Dhital, MR & Devkota, K 2013, 'Effect of rock weathering, clay mineralogy, and geological structures in the formation of large landslide, a case study from Dumre Besei landslide, Lesser Himalaya Nepal', *Landslides*, vol. 10, pp. 1-13.

Regmi, RK, Nakagawa, H, Kawaike, K, Baba, Y & Zhang, H 2012, 'Three-dimensional analysis of rainfall-induced slope failure', *International Journal of Erosion Control Engineering*, vol. 5, no. 2, pp. 156-165.

Ren, D, Fu, R, Leslie, LM & Dickinson, RE 2011, 'Predicting storm-triggered landslides', *Bulletin of the American Meteorological Society*, vol. 92, no. 2, pp. 129-139.

Rosso, R, Rulli, MC & Vannucci, G 2006, 'A physically based model for the hydrologic control on shallow landsliding', *Water Resources Research*, vol. 42, no. 6, W06410, pp. 1-16.

Saito, H, Nakayama, D & Matsuyama, H 2010, 'Relationship between the initiation of a shallow landslide and rainfall intensity-duration thresholds in Japan', *Geomorphology*, vol. 118, no. 1-2, pp. 167-175.

Salciarini, D, Fanelli, G & Tamagnini, C 2017, 'A probabilistic model for rainfall-induced shallow landslide prediction at the regional scale', *Landslides,* vol. 14, pp. 1731-1746.

Salvatici, T, Tofani, V, Rossi, G, D'Ambrosio, M, Stefanelli, CT, Masi, EB, Rosi, A, Pazzi, V, Vannocci, P, Petrolo, M, Catani, F, Ratto, S, Stevenin, H & Casagli, N 2018, 'Application of a physically based model to forecast shallow landslides at a regional scale', *Natural Hazards and Earth System Sciences,* vol. 18, pp. 1919-1935.

Sassa, K 1988, 'Geotechnical model for the motion of landslides', in *Proceedings of 5th International Symposium on Landslides,* Lausanne, Switzerland, vol. 1, pp. 37-56.

Sassa, K, Rouhban, B, Briceno, S, McSaveney, M & He, B 2013, *Landslides: Global risk preparedness,* Springer-Verlag, Berlin Heidelberg, Germany.

Satyanaga, A & Rahardjo, H 2019, 'Unsaturated shear strength of soil with bimodal soil-water characteristics curve', *Geotechnique,* vol. 69, no. 9, pp. 828-832.

Schnellmann, R, Rahardjo, H & Schneider, HR 2015, 'Controlling parameter for unsaturated soil property functions: validated on the unsaturated shear strength', *Canadian Geotechnical Journal,* vol. 52, no. 3, pp. 374-381.

Selby, MJ 1993, *Hillslope materials and processes,* Oxford University Press, UK.

Shen, Z, Jiang, M & Thornton, C 2016, 'Shear strength of unsaturated granular soils: three dimensional discrete element analyses', *Granular Matter,* vol. 18, no. 3, pp. 1-13.

Sheng, D, Zhou, A & Fredlund, DG 2009, 'Shear strength criteria for unsaturated soils', *Geotechnical and Geological Engineering,* vol. 29, pp. 145-159.

Sivakumar Babu, GL & Murthy, DS 2005, 'Reliability analysis of unsaturated soil slopes', *Journal of Geotechnical and Geoenvironmental Engineering,* vol. 131, no. 11, pp. 1423-1428.

Skempton, AW 1964, 'The long-term stability of clay slopes', *Geotechnique,* vol. 14, no. 2, pp. 77-102.

Skempton, AW 1985, 'Residual strength of clays in landslides, folded strata and the laboratory', *Geotechnique,* vol. 35, no. 1, pp. 3-18.

Springman, SM, Jommi, C & Teysseire, P 2003, 'Instabilities on moraine slopes induced by loss of suction: a case history', *Geotechniqu*e, vol. 53, no. 1, pp. 3-10.

Springman, S, Kienzler, P, Casini, F & Askarinejad A 2009, 'Landslide triggering experiment in a steep forested slope in Switzerland', in *Proceedings of the 17th International Conference on soil mechanics and geotechnical engineering, ICSMGE 2009,* Alexandria, Egypt, vol. 2, pp. 1698-1701.

Springman, SM, Thielen, A, Kienzler, P & Friedel, S 2013, 'A long-term field study for the investigation of rainfall-induced landslides', *Geotechnique,* vol. 63, no. 14, pp. 1177-1193.

Sreedeep, S & Singh, DN 2011, 'Critical review of the methodologies employed for soil suction measurement', *International Journal of Geomechanics,* vol. 11, no. 2, pp. 99-104.

Stark, TD & Hussain, M 2010, 'Shear strength of preexisting landslides', *Journal of Geotechnical and Geoenvironmental Engineering,* vol. 136, no. 7, pp. 957-962.

Sun, H-Y, Wong, LNY, Shang, Y-Q, Shen, Y-J & Lu, Q 2010, 'Evaluation of drainage tunnel effectiveness in landslide control', *Landslides,* vol. 7, no. 4, pp. 445-454.

Suradi, M, Fourie, A, Beckett, C & Buzzi, O 2014, 'Rainfall-induced landslides: development of a simple screening tool based on rainfall data and unsaturated soil mechanics principles', in *Proceedings of the 6th International Conference on Unsaturated Soils, UNSAT 2014,* Sydney, Australia.

Suradi, M, Fourie AB & Saynor MJ 2016, 'An experimental and numerical study of a landslide triggered by an extreme rainfall event in northern Australia', *Landslides,* vol. 13, pp. 1125-1138.

Taha, MR, Hossain, MK & Mofiz, SA 2000, 'Effect of suction on the strength of unsaturated soil', in *Proceedings of Sessions at Geo-Denver 2000 - Advances in Unsaturated Geotechnics,* GSP 99, Denver, CO, pp. 210-221.

Terlien, MTJ 1998, 'The determination of statistical and deterministic hydrological landslide-triggering thresholds', *Environmental Geology,* vol. 35, pp. 124-130.

Tilgen, HP 2003, 'Relationship between suction and shear strength parameters of compacted METU Campus clay', Masters thesis, The Middle East Technical University, Ankara, Turkey.

Tofani, V, Dapporto, S, Vannocci, P & Casagli, N 2006, 'Infiltration, seepage and slope instability mechanisms during the 20-21 November 2000 rainstorm in Tuscany, central Italy', *Natural Hazards and Earth System Sciences,* vol. 6, no. 6, pp. 1025-1033.

Tohari, A 2018, ‘Study of rainfall-induced landslide: a review’, *Earth and Environmental Science*, vol. 118, 012036, pp. 1-6.

Toll, DG 2001, ‘Briefing: Rainfall-induced landslides in Singapore’, in *Proceedings of the Institution of Civil Engineers – Geotechnical Engineering*, vol. 149, no. 4, pp. 211-216.

Trandafir, AC, Sidle, RC, Gomi, T & Kamai, T 2007, ‘Monitored and simulated variations in matric suction during rainfall in a residual soil slope’, *Environmental Geology*, vol. 55, pp. 951-961.

Townsend, FC & Gilbert, PA 1973, ‘Tests to measure residual strengths of some clay shales’, *Geotechnique*, vol. 23, no. 2, pp. 267-271.

Trigo, RM, Zezere, RL, Rodriguez, ML & Trigo, IF 2005, ‘The influence of the North Atlantic oscillation on rainfall triggering of landslides near Lisbon’, *Natural Hazards*, vol. 36, pp. 331-354.

Tsai, T-L 2007, ‘The influence of rainstorm pattern on shallow landslide’, *Environmental Geology*, vol. 53, pp. 1563-1569.

Tsai, T-L 2010, ‘Influnces of soil water characteristics curve on rainfall-induced shallow landslides’, *Environmental Earth Sciences*, vol. 64, pp. 449-459.

Tsai T-L, Chen, H-E & Yang, J-C 2008, ‘Numerical modelling of rainstorm-induced shallow landslides in saturated and unsaturated soils’, *Environmental Geology*, vol. 55, pp. 1269-1277.

Tsai, T-L & Chen, H-F 2010, ‘Effects of degree of saturation on shallow landslides triggered by rainfall’, *Environmental Earth Sciences*, vol. 59, pp. 1285-1295.

Tsai, T-L, Tsai, P-Y & Yang, P-J 2015, ‘Probabilistic modelling of rainfall-induced shallow landslide using a point-estimate method’, *Environmental Earth Sciences*, vol. 73, pp. 4109-4117.

Tsai, T-L & Wang, J-K 2011, ‘Examination of influences of rainfall patterns on shallow landslides due to dissipation of matric suction’, *Environmental Earth Sciences*, vol. 63, no. 1, pp. 65-75.

Tsaparas, I, Rahardjo, H, Toll, DG & Leong, EC 2002, ‘Controlling parameters for rainfall-induced landslides’, *Computers and Geotechnics*, vol. 29, no. 1, pp. 1-27.

Tseng, C-M, Chen, Y-R & Wu, S-M 2018, 'Scale and spatial distribution assessment of rainfall-induced landslides in a catchment with mountain roads', *Natural Hazards and Earth System Sciences*, vol. 18, pp. 687-708.

Van Asch, TWJ, Buma, J & Van Beek, LPH 1999, 'A view on some hydrological triggering systems in landslides', *Geomorphology*, vol. 30, no. 1-2, pp. 25-32.

Van Genuchten, MT 1980, 'A closed-form equation for predicting the hydraulic conductivity of unsaturated soils', *Soil Science Society of America Journal*, vol. 44, no. 5, pp. 892-898.

Vanapalli, SK, Fredlund, DG, Pufahl, DE & Clifton AW 1996, 'Model for the prediction of shear strength with respect to soil suction', *Canadian Geotechnical Journal*, vol. 33, no. 3, pp. 379-392.

Vanapalli, SK, Fredlund, DG & Pufahl, DE 1999, 'The influence of soil structure and stress history on the soil-water characteristics of a compacted till', *Geotechnique*, vol. 49, no. 2, pp. 143-159.

Vanapalli, SK & Fredlund, DG 2000, 'Comparison of different procedures to predict unsaturated soil shear strength', in *Proceedings of Advances in Unsaturated Geotechnics, Geo-Denver 2000,* GSP 99, Denver, CO, pp. 195-209.

Vilar, OM 2006, 'A simplified procedure to estimate the shear strength envelope of unsaturated soils', *Canadian Geotechnical Journal*, vol. 43, no. 10, pp. 1088-1095.

Wang, GX 2005, 'Key technique in landslide control and its handling measures', *Chinese Journal of Rock Mechanics and Engineering*, vol. 24, no. 21, pp. 3818-3827 (in Chinese).

Wang, F & Sassa, K 2000, 'A modified geotechnical simulation model for the areal prediction of landslide motion', *Annuals of the Disaster Prevention Institute, Kyoto University*, vol. 43, B-1, pp. 129-139.

Wang, G & Sassa, K 2001, 'Factors affecting rainfall-induced flowslides in laboratory flume tests', *Geotechnique*, vol. 51, no. 7, pp. 587-599.

Wang, G & Sassa, K 2007, 'On the pore-pressure generation and movement of rainfall-induced landslides in laboratory flume tests', Chapter 12, in K Sassa, H Fukuoka, F Wang & G Wang (eds), *Progress in Landslide Science*, Springeronline.com, Berlin, Heildeberg, Germany, pp. 167 – 181.

Wang, D-J, Tang, H-M, Zhang, Y-H, Li, C-D & Huang, L 2017, 'An improved approach for evaluating the time-dependent stability of colluvial landslides during intense rainfall', *Environmental Earth Sciences*, vol. 76, no. 321, pp. 1-12.

Wang, F, Wu, Y-H, Yang, H, Tanida, Y & Kamei A 2015, 'Preliminary investigation of the 20 August 2014 debris flows triggerred by a severe rainstrom in Hiroshima City, Japan', *Geoenvironmental Disasters*, vol. 2, 17, pp. 1-16.

Wheeler, SJ & Sivakumar, V 2000, 'Influence of compaction procedure on the mechanical behaviour of an unsaturated compacted clay, Part 2 – Shearing and constitutive modelling', *Geotechnique,* vol. 50, no. 4, pp. 369-376.

Wieczorek, GF 1987, 'Effect of rainfall intensity and duration on debris flows in the central Santa Cruz Mountains, California', in JE Costa & GF Wieczorek (eds), *Debris flows/Avalanches: Processes, Recognition and Mitigation*, Geological Society of America, Boulder, Colorado, CO, vol. 7, pp. 93-104.

Wilson, RC & Wieczorek, GF 1995, 'Rainfall thresholds for the initiation of debris flows at La Honda, California', *Environmental and Engineering Geoscience*, vol. 1, no. 1, pp. 11-27.

Wu, LZ, Huang, RQ, Xu, Q, Zhang, LM & Li, HL 2015a, 'Analysis of physical testing of rainfall-induced soil slope failures', *Environmental Earth Sciences*, vol. 73, pp. 8519-8531.

Wu, Y-M, Lan, H-X, Gao, X, Li, L-P & Yang, Z-H 2015b, 'A simplified physically based coupled rainfall threshold model for triggering landslides', *Engineering Geology*, vol. 195, pp. 63-69.

Wu, LZ, Selvadurai, APS, Zhang, LM, Huang, RQ & Huang, J 2016, 'Poro-mechanical coupling influences on potential for rainfall-induced shallow landslides in unsaturated soils', *Advances in Water Resources*, vol. 98, pp. 114–121.

Wu, W & Sidle, RC 1995, 'A distributed slope stability model for steep forested basins', *Water Resources Research*, vol. 31, no. 8, pp. 2097-2110.

Yang, H, Wang, F, Vilimek, V, Araiba, K & Asano, S 2015, 'Investigation of rainfall-induced shallow landslides on the northeastern rim of Aso Caldera, Japan, in July 2012', *Geoenvironmental Disasters*, vol. 2, no. 20, pp. 1-14.

Yang, S-R, Shen, C-W, Huang, C-M, Lee, C-T, Cheng, C-T & Chen, C-Y 2012, 'Prediction of mountain road closure due to rainfall-induced landslides', *Journal of Performance of Constructed Facilities*, vol. 26, no. 2, pp. 197-202.

Yang, H, Rahardjo, H, Leong, E-C & Fredlund, DG 2004, 'Factors affecting drying and wetting soil-water characteristic curves of sandy soils', *Canadian Geotechnical Journal*, vol. 41, no. 5, pp. 908-920.

Yeh, HF, Lee CC & Lee CH 2008, 'A rainfall-infiltration model for unsaturated soil slope stability, *Sustainable Environment Research,* vol. 18 , no. 2, pp. 271-278.

Yoshida, Y, Kuwano, J & Kuwano, R 1991, 'Rain-induced slope failures caused by reduction in soil strength', *Soils and Foundations*, vol. 31, no. 4, pp. 187-193.

Yu, F-C, Chen, T-C, Lin, M-L, Chen, C-Y & Yu, W-H 2006, 'Landslides and rainfall characteristics analysis in Taipei City during the Typhoon Nari event', *Natural Hazards*, vol. 37, pp. 153-167.

Yubonchit, S, Chinkulkijniwat, A, Horipibulsuk, S, Jothityangkoon, C, Arulrajah, A & Suddeepong, A 2017, 'Influence factors involving rainfall-induced shallow slope failure: Numerical study', *International Journal of Geomechanics*, vol. 17, no. 7, 04016158, pp. 1-13.

Zapata, CE 1999, 'Uncertainty in soil-water-characteristics curve and impacts on unsaturated shear strength predictions', PhD thesis, Arizona State University, Tempe, TZ.

Zhai, Q, Rahardjo, H, Satyanaga, A & Dai, G 2019, 'Estimation of unsaturated shear strength from soil-water characteristics curve', *Acta Geotechnica,* vol. 14, pp. 1977-1990.

Zhang, LL, Fredlund, DG, Fredlund, MD & Wilson, GW 2014, 'Modelling the unsaturated soil zone in slope stability analysis', *Canadian Geotechnical Journal*, vol. 51, no. 12, pp. 1384-1398.

Zhang, J, Jiao, JJ & Yang, J 2000, 'In situ rainfall infiltration studies at a hillside in Hubei Province, China', *Engineering Geology*, vol. 57, no. 1-2, pp. 31-38.

Zhang, L, Li, J, Li, X, Zhang, J & Zhu, H 2016, *Rainfall-induced soil slope failure – Stability analysis and probabilistic assessment,* CRC Press, Taylor & Francis Group, Boca Raton, FL.

Zhang, PB & Tang, XW 2006, 'Application of ultra-long-range drainage pipe on the expressway landslide treatment', *Highway*, vol. 1, pp. 80-85 (in Chinese).

Zhang, LL, Zhang, J, Zhang, LM & Tang, WH 2011, 'Stability analysis of rainfall-induced slope failure: a review', in *Proceedings of the Institution of Civil Engineers – Geotechnical Engineering*, vol. 164, no. 5, pp. 299-316.

Zhang, B, Zhao, QG, Horn, R & Baumgartl, T 2001, 'Shear strength of surface soil as affected by soil bulk density and soil water content', *Soil and Tillage Research*, vol. 59, no. 3-4, pp. 97-106.

Zhang, S, Zhao, L, Delgado-Tellez, R & Bao, H 2018, 'A physics-based probabilistic forecasting model for rainfall-induced shallow landslides at regional scale', *Natural Hazards and Earth System Sciences*, vol. 18, pp. 969-982.

Zhou, W-H, Yuen, K-V & Tan, F 2014, 'Estimation of soil-water characteristics curve and relative permeability for granular soils with different initial dry densities', *Engineering Geology*, vol. 179, pp. 1-9.

Zhu , J-H & Anderson SA 1998, 'Determination of shear strength of Hawaiian residual soil subject to rainfall-induced landslides', *Geotechnique*, vol. 48. no. 1, pp. 73-82.

Zhuang, J, Peng, J, Wang, G, Igbal, J, Wang, Y, Li, W, Xu, Q & Zhu, X 2017, 'Prediction of rainfall-induced shallow landslides in the Loess Plateau, Yan'an, China, using the TRIGRS model', *Earth Surface Processes and Landforms*, vol. 42, no. 6, pp. 915–927.

Zydron, T, Bucala, A, Demczuk, P & Gruchot, A 2016, 'Analysis of rainfall-induced shallow landslides in Jamne and Jaszeze stream valleys (Polish Carpathians) - preliminary results', *Annals of Warsaw University of Life Sciences – SGGW Land Reclamation*, vol. 48, no. 1, pp. 27-40.